PHOSPHORESCENT PROPERTIES OF RIBOFLAVIN AND ITS POTENTIAL APPLICATIONS IN FOOD QUALITY AND FOOD SAFETY

by

Yan Wang

A dissertation submitted to the

Graduate School – New Brunswick

Rutgers, The State University of New Jersey

in partial fulfillment of the requirements

for the degree of

Doctor of Philosophy

Graduate Program in Food Science

Written under the direction of

Dr. Richard D. Ludescher

and approved by

_____

_____

_____

_____

New Brunswick, New Jersey

May 2016

ABSTRACT OF THE DISSERTATION

Phosphorescent Properties of Riboflavin and Its Potential Applications in Food Quality and Food Safety

by

YAN WANG

Dissertation Director:
Dr. Richard D. Ludescher

This project characterized the triplet properties of riboflavin and demonstrated that riboflavin, a widespread vitamin in foods, has the potential to be used as a phosphorescent sensor for food quality and as a photosensitizer for food safety.

Phosphorescence spectroscopy has been used as a sensitive tool to study molecular motions in supercooled liquid and glass. Since molecular level movements play a critical role in determining macroscopic quality attributes of amorphous foods, phosphorescence measurement thus can serve as an optical analytical tool that leads to a better understanding of macroscopic quality attributes from a molecular perspective. In this study, phosphorescence from riboflavin and its sensitivity to molecular motions was first characterized in 3:1 glycerol/water mixture (v/v) over the temperature range from 77K to 200K and in amorphous sucrose matrix from 243K to 373K. The results suggested that riboflavin phosphorescence is sensitive to the secondary relaxation processes below the glass transition temperature.

Riboflavin phosphorescence was then utilized to study the effects of molecular size and the addition of plasticizer in six malto-oligomers, three dextrans of different molecular weights, and four dextran films with different glycerol content. The results suggested that the molecular mobility increased with the increase in molecular size and that low added glycerol content (<10%) reduced mobility while high glycerol content (>22%) increased mobility.

Phosphorescence also provides direct information on excited triplet state properties of a molecule, including its interaction with oxygen. Triplet molecules collide with oxygen and form singlet oxygen, a reactive species that is detrimental to living cells and microorganisms. Riboflavin has shown efficacy for virus inactivation for blood disinfection and has the potential to photo-inactivate pathogens as an environmental-friendly photosensitizer. To better understand the mechanism between triplet riboflavin and oxygen, in this study, oxygen quenching rate of riboflavin was characterized in three amorphous carbohydrate films: 6k Da dextran, 5% glycerol-dextran, and methylcellulose. Additionally, the singlet oxygen generation efficacy of riboflavin was studied under various irradiation wavelengths.

Acknowledgement

I would like to first and foremost give my sincere thanks to my advisor, Dr. Richard D. Ludescher, for his support and guidance throughout my time at Rutgers University, academically, professionally, and personally. I am deeply grateful that he introduced me to this complicated yet extremely interesting research field. My research has broadened tremendously my understanding of photophysics, physical chemistry, and food science. It provided me with an alternative lens to look at scientific research. Moreover, his support and advice for my job as a graduate mentor and my leadership roles in the food science community has helped me grow professionally.

I would like to thank Dr. Maria G. Corradini. I could not have made so much progress and achievement without her help. Her role during my four years at Rutgers has been more than just an advisor; she has also been a mentor and an invaluable friend. She fostered a welcoming and supportive atmosphere in the lab, where I enjoyed every second. She also gave me the opportunity to mentor undergraduate students, which was an especially valuable experience.

I would like to thank Dr. Qingrong Huang, Dr. Paul Takhistov, and Dr. Joel Friedman for their effort and suggestions as my committee members. I greatly appreciate all their input and suggestions on my project.

I would like to thank my family, especially my parents Jie Jian and Tao Wang, for their constant love, continuous support, persistent patience, and never-ending trust.

I would like to thank my dear friends and my labmates, Lumeng Jin, Si Nian, Jie Xiao, Yaqi Lan, Tzu-min Wang, Xuechen Xu, Sarah Waxman, Alexia Ciarfella, Victoria Yeung, Nanxi Li, Karina Lewerissa, Ziqian Qu, Derrick Fondaco, and An Le for making my time at Rutgers and in the lab so pleasant despite of all the obstacles that research inevitably entails. Thank you all for sharing my joys and my tears and for bringing so much laughter into my life.

Lastly, I would like to thank my husband, Joshua Mauldin, for coming into my life and for giving me so much love and support. I greatly appreciated the dissertation writing tip (write 500 words everyday!) that he shared with me, which helped me finish my dissertation in time.

Table of Contents

List of Tables

List of Figures

Chapter I Introduction

General Properties of Riboflavin

Riboflavin (7,8-dimethyl-10-ribityl-iso-alloxazine), commonly known as Vitamin B_2, is a yellow-orange colored water-soluble compound readily available in nature. This compound was first isolated from cow milk back in the late 1800s (Blyth, 1879; Northrop-Clewes & Thurnham, 2012). Over the past 130 years since its discovery, various properties of riboflavin have been subjected to extensive study, for example, its biological functions, nutritional importance, and stability.

Riboflavin is the precursor of all biologically significant flavins. Flavins are a large family of molecules that participate in a number of photobiological and photochemical activities as cofactors and photoreceptors (Edwards, 2006). Riboflavin has a wide distribution in tissues in the form of cofactors flavin mononucleotide (FMN) and flavin adenine dinucleotide (FAD) participating in oxidation reactions (Edwards, 2006).

Unlike plants and microorganisms, animals and humans cannot synthesize this nutrient, but have to acquire it from their diet. Riboflavin is found in a variety of food sources including milk, cheese, leafy vegetables, liver, and whole grains. As an essential vitamin, riboflavin plays an important role in metabolism, growth and development of body, and regulation of hormones (Choe, Huang, & Min, 2005). Riboflavin deficiency still happens in today's developing world, but no fatal diseases or symptoms have been associated with Vitamin B_2 deficiency. Some minor

symptoms associated with riboflavin deficiency include cracked, swollen, and bright red lips, sensitivity of eyes to light, and scaling and itchy skin (Northrop-Clewes & Thurnham, 2012).

On a commercial level, riboflavin is produced mainly by microbial fermentation (Choe et al., 2005). In the food industry, riboflavin, due to its yellow color, is sometimes used as a coloring agent in mayonnaise, puddings, and candies. A riboflavin based flavoenzyme, glucose oxidase, is used to trap residual oxygen in food processing. Riboflavin is heat stable but susceptible to light. During normal food processing such as canning, cooking, dehydration, and γ-irradiation (Choe et al., 2005), riboflavin exhibits good stability towards most processing methods with only 10%-15% content loss. However, milk lost 30% of its riboflavin after being exposed to light for 30min (Wishner, 1964). Riboflavin also causes photo-oxidation in dairy goods, either via interaction between triplet-excited state riboflavin and proteins or via singlet oxygen mediated lipid oxidation (Cardoso, Libardi, & Skibsted, 2012). Photo-oxidation promotes degradation via oxidation of methionine, which results in the generation of methional contributing to the so-called sunlight flavor in milk (Cardoso et al., 2012).

Spectral and Photophysical Properties of Riboflavin

The light sensitivity of riboflavin is greatly due to its molecular structure and the light sensitivity is also the foundation of various biological reactions. Given its importance in photobiological processes and photochemical reactions, photophysical and photochemical properties of riboflavin have been subjected to

extensive studies during the past 50 years (Ahmad & Vaid, 2006). Riboflavin has strong and broad absorption in the UV-Vis region with four maxima located at 445, 375, 265, and 220 nm (Figure I-2) (Grodowski, Veyret, & Weiss, 1977; Moore, McDaniels, & Hen, 1977). The location and absorptivity of the peaks are dependent on physical properties of surrounding environment such as solvent polarity, pH, etc. (Moore et al., 1977). Neutral riboflavin has a strong neon green fluorescence emission with its peak located at 525nm. The location of this fluorescence peak varies depending on solvent polarity and H-bonding (Ahmad & Vaid, 2006). Riboflavin in its cationic and anionic forms does not fluoresce. Phosphorescence of riboflavin, on the other hand, is not readily detected in aqueous environment due to high probability of quenching of the triplet-excited state. When affixed in rigid media, such as, cellulose, starch film, or organic solvent at cryogenic temperature (77K) (Penzkofer, Tyagi, Slyusareva, & Sizykh, 2010; Penzkofer, 2012; Sikorski, 2002; Sun, Moore, & Song, 1972), phosphorescence of riboflavin exhibits a peak located at ~615nm and its triplet lifetime ranges from 0.1 to 0.2s.

Figure I-1

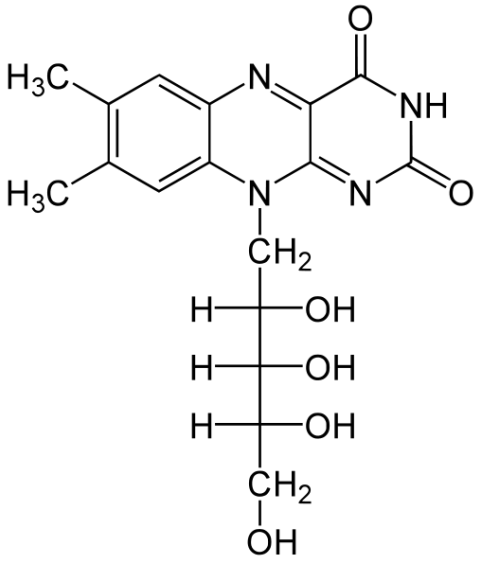

Figure I-1: Molecular Structure of Riboflavin

Figure I-2

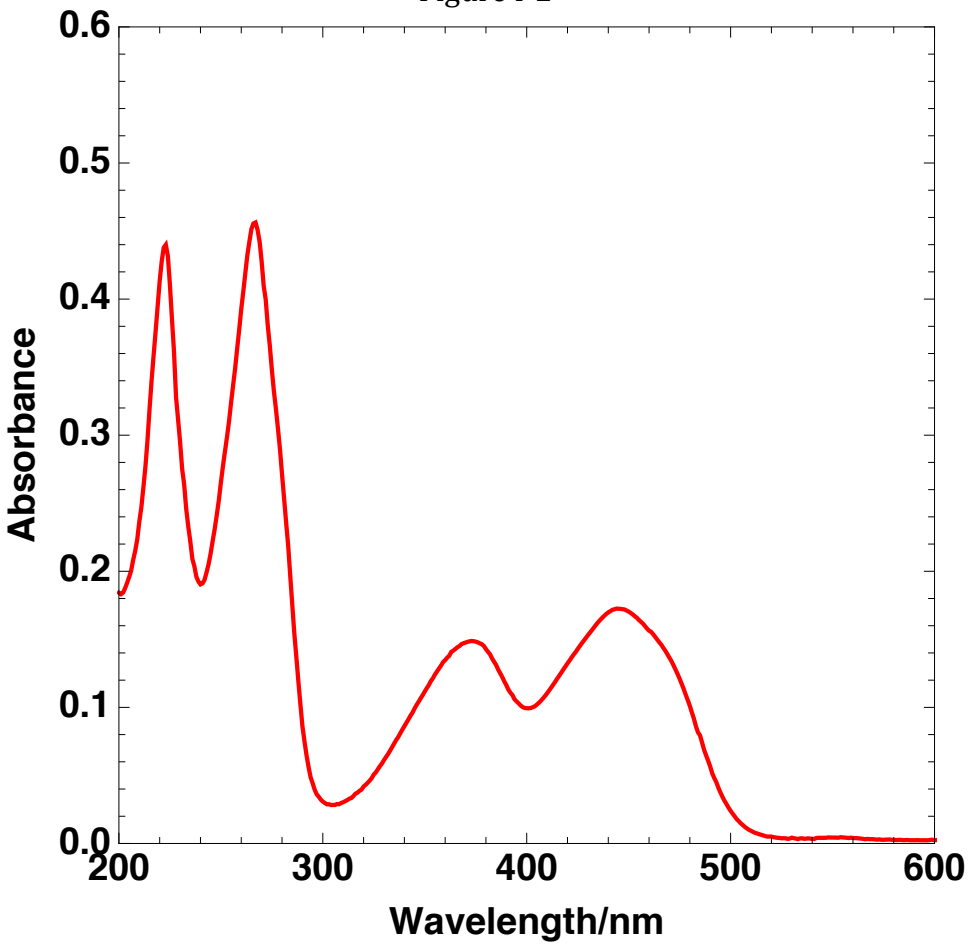

Figure I-2: The absorption spectrum of riboflavin in deionized water

Basic Photophysics- Jablonski Diagram

Figure I-3 is a Jablonski Diagram illustrating some basic photophysical processes described above, i.e., fluorescence, phosphorescence. Upon light excitation, ground state (S_0) molecules absorb photons and jump to excited singlet state (S_1), where they possess excessive energy and are energetically unfavorable. To dissipate the energy, they can de-excite via the following pathways: 1) radiative decay by emitting fluorescence (rate constant for fluorescence k_{RF}), 2) matrix-induced non-radiative decay (rate constant for non-radiative decay k_{SS0}), and 3) intersystem crossing to excited triplet state (T_1) for further de-excitation pathways (rate constant for intersystem crossing k_{ST1}). Similarly, excited triplet state molecules still possess an excess amount of energy and have to relax back to the ground state. De-excitation processes for triplet state molecules include: 1) radiative decay by emitting phosphorescence (rate constant for phosphorescence k_{RP}), 2) matrix-induced non-radiative decay (rate constant for non-radiative decay k_{TS0}), 3) collisional quenching with active quenchers such as oxygen and water (rate constant for oxygen quenching $k_Q[Q]$), and 4) thermally activated reverse intersystem crossing back to the excited singlet state followed by the emission of delayed fluorescence (rate constant for reverse intersystem crossing k_{TS1}).

Both k_{RF} and k_{RP} are intrinsic properties of the luminescent molecule, thus independent of environmental factors such as temperature, water activity, and oxygen content. Yet, other rate constants, especially k_{TS0}, k_{TS1} and $k_Q[Q]$, are

essentially determined by matrix properties, temperature, and the abundance of quenchers. Luminescence therefore provides direct information on molecular motions as well as indirect information on the environment surrounding the luminescent molecules. Luminescence spectroscopy, both fluorescence and phosphorescence, has been used as site-specific and sensitive analytical tools to study molecular structure and function and local microenvironment surrounding the chromophore (Corradini & Ludescher, 2015; Karoui & Blecker, 2011; Ludescher, Shah, McCaul, & Simon, 2001).

Figure I-3

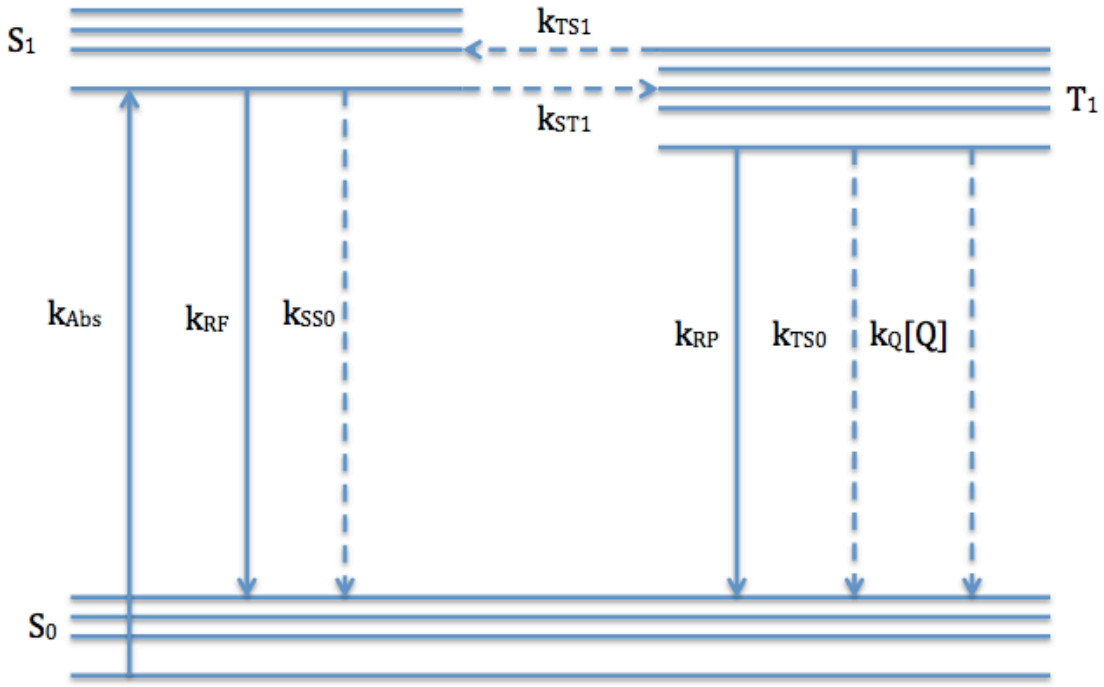

Figure I-3: A modified Jablonski diagram illustrating the electronic states of a molecule and the transitions between them. The ground state, singlet excited state and triplet excited state are marked as S_0, S_1, and T_1, respectively. The rate constants for transitions are marked as k. From the excited singlet state, there are: the rate constant for fluorescence k_{RF}, rate constant for non-radiative decay k_{SS0}, rate constant for intersystem crossing k_{ST1}). From the excited triplet state, there are rate constant for phosphorescence k_{RP}, rate constant for non-radiative decay k_{TS0}, rate constant for oxygen quenching $k_Q[Q]$, and rate constant for reverse intersystem crossing k_{TS1}.

Riboflavin as a Fluorescent Probe in Food

Fluorescence spectroscopy is an intrinsic, non-invasive, and rapid analytical tool that has gained popularity in the field of food science (Corradini & Ludescher, 2015; Ludescher et al., 2001). Due to the widespread presence of riboflavin in foods, its fluorescence has been used in a number of food-related studies. For example, in dairy research, fluorescence of riboflavin has been used to study the heat treatment and Maillard browning reactions in milk, to discriminate milk and cheese based on geographical regions of origin, and to investigate oxidation and physiochemical modifications in milk (Karoui & Blecker, 2011). It has also been used in cereal studies to discriminate cereal flours, to differentiate botanical origin of flours, and to monitor flour refinement and milling efficiency (Karoui & Blecker, 2011).

Similar to fluorescence spectroscopy, phosphorescence spectroscopy also exhibits advantages for being a rapid and non-invasive method. Yet, few applications of riboflavin phosphorescence have been developed.

Phosphorescent Molecular Probes in Food

Both fluorescence and phosphorescence can provide indirect information about molecular mobility of local environments (Corradini & Ludescher, 2015; Ludescher et al., 2001). Phosphorescence decay happens on a slower time scale ranging from 10^{-4} to 1s, compared to that of fluorescence in the order of 10^{-8}s (Ludescher et al., 2001). The longer lifetime of triplet state thus makes phosphorescence more

sensitive to and suitable to study slow molecular motions characteristic of amorphous glasses (Ludescher et al., 2001).

A number of organic phosphorescence dyes of high phosphorescence quantum yields and long triplet lifetimes have been used to monitor such molecular motions. In the field of food amorphous solid research, Generally Recognized As Safe (GRAS) probes including erythrosine B, tryptophan, tyrosine, and vanillin have demonstrated sensitivity towards the mobility in a range of amorphous matrices (Draganski, 2014; Pravinata, You, & Ludescher, 2005; Tiwari & Ludescher, 2010).

Erythrosine B is one of the most widely applied phosphorescent probes. It is a cherry-red synthetic food coloring agent known as FD&C Red #3. It has a high quantum yield of triplet state and its triplet state lifetime ranges from 10^{-5} to 10^{-3} sec. Room temperature phosphorescence of erythrosine B in sol-gel silica has been applied as an optical sensor for oxygen (Kuan Lam, Namdas, & Lo, 1998; Lam, Chan, & Lo, 2001). Oxygen is an effective quencher of the excited triplet state; when present, phosphorescence emission intensity and lifetime will be significantly quenched. Erythrosine B was also used in a recent study as a phosphorescent probe to study oxygen depletion in wheat flour dough (Joye, Delcour, Draganski, & Ludescher, 2012). Erythrosine B has been incorporated in various amorphous protein films and a number of amorphous carbohydrate matrices as a luminescent probe to investigate molecular mobility, dynamic heterogeneity, the effects of salts and plasticizers on matrix structure, and the air permeability of the hosting matrices

(Lukasik & Ludescher, 2006; Pravinata, You, & Ludescher, 2005; You & Ludescher, 2007; You & Ludescher, 2010).

Tryptophan is an essential amino acid in the human diet. It exhibits strong room temperature phosphorescence and is the most widely applied intrinsic phosphorescent probe in the study of protein dynamics (Draganski, 2014). Phosphorescence of tryptophan has been reported as a sensitive tool to monitor local structural environment and protein dynamics in both liquid and solid environments. Its lifetime varies as the rigidity, conformation, and flexibility of protein changes (Schauerte, Steel, & Gafni, 1997; Steel, Subramaniam, & Gafni, 1996).

Vanillin is the key flavor compound for vanilla flavor. Recently, vanillin was reported as a phosphorescent probe of molecular mobility (Tiwari & Ludescher, 2010; Tiwari & Ludescher, 2012). It was found that phosphorescence of vanillin was especially sensitive to molecular mobility in glassy state of amorphous sugar matrices.

Numerous studies have demonstrated the validity of using phosphorescence as an optical sensor for molecular mobility. The use of phosphorescence spectroscopy also allows for rapid non-invasive real-time measurement. Yet, the different molecular structures and natural phosphorescence lifetimes of the phosphorescent molecules mentioned above give them different sensitivity to molecular motions of different timescales. There is a need to expand the pool and to explore other natural phosphorescent probes for future applications. Riboflavin, a GRAS water-soluble

vitamin whose phosphorescence has been observed, is thus of the potential as a phosphorescent probe for molecular mobility.

Physical Properties of Amorphous Solids

Amorphous solids are solids that lack ordered structure characteristic of a crystalline. Amorphous solids are hard, brittle, and rigid at low temperature, and rubbery, soft, and flexible at high temperature. Most low water content or frozen foods are partially or completely amorphous. Changes in molecular mobility of amorphous carbohydrates and proteins directly affect physical, chemical, and microbiological stability of the products, thus of great importance to the food and pharmaceutical industry.

Glass transition temperature (Tg) is a commonly used index temperature to predict macroscopic properties and stability of amorphous foods. Yet, research has shown that Tg was not an absolute indicator for stability, but one of the factors controlling the kinetics (Cicerone, Tellington, Trost, & Sokolov, 2003; Kaminski et al., 2012). At temperatures below Tg, although long-range rotational motions are restricted, vibrational movements and rearrangement of small side-chain groups and small molecules are still present, which affects food properties such as texture and oxidation (Ludescher et al., 2001; Slade & Levine, 1995). A thorough understanding of molecular mobility thus has a great impact on formulation design, quality control, and stability of food products.

Previous research has confirmed the sensitivity of using phosphorescence spectroscopy to study molecular mobility of various protein and carbohydrate

based amorphous materials. Studies have also verified riboflavin's high intersystem crossing quantum yield and prominent phosphorescence emission intensity either under cryogenic temperatures or when affixed in a solid matrix, suggesting its potential as a phosphorescent probe for molecular motions in amorphous solids. Yet, few of them have systematically investigated the applicability of riboflavin phosphorescence as an indicator for molecular mobility of the hosting matrices. Given its widespread presence in food sources and safe profile, I propose to do an in-depth study of phosphorescence from riboflavin and to explore its potential as a phosphorescent probe for molecular mobility in various amorphous food systems and food packaging materials.

Riboflavin as a Photosensitizer in Foods

According to the Jablonski scheme (Figure I-3), triplet excited state molecules can be quenched by oxygen molecules present in their vicinity ($k_Q[O_2]$. During this process, the energy is transferred from the triplet excited state molecules to the triplet ground state oxygen and the latter become singlet oxygen ($^1O_2$), a highly reactive oxygen species that can readily oxidize lipids and proteins and react with nucleic acids causing damage to RNAs and DNAs. This process is called photosensitization and the triplet excited state molecules are photosensitizers.

Riboflavin is known as a good sensitizer for the formation of singlet oxygen and its role in facilitating oxidation of various food components has attracted research attention (Choe et al., 2005; Choe & Min, 2006). Due to the universal presence of riboflavin in foods and the rapid reaction rate of singlet oxygen oxidation, riboflavin

mediated oxidation of unsaturated lipids, proteins, vitamins, phenolic compounds, and carotenoids was found to result in nutritional losses, the formation of undesirable flavor and color compounds, and the impairment of food quality and stability (Cardoso et al., 2012; Choe et al., 2005).

Photodynamic Inactivation

In addition to oxidizing food components, singlet oxygen has received wide attention in the field of medical research. Since singlet oxygen can react rapidly with lipids, proteins, and nucleic acids, it poses detrimental effects to living cells by damaging their cell membrane and cleaving DNAs and RNAs. Modern photodynamic therapy was developed over a hundreds of year ago utilizing this mechanism to combat cancers, macular degeneration, and some dermatological conditions (Wainwright, 2009). Taking the concept of photodynamic therapy, researchers have successfully applied this method on microbial photo-inactivation and utilized it as a therapeutic tool against bacterial infections.

Over the past few decades, researchers have demonstrated the potential of photosensitizers to inactivate a wide range of human pathogens, including both gram positive and gram negative organisms: *Escherichia coli*, *Streptococcus spp.*, *Helicobacter pylori, Staphylococcus aureus, Pseudomonas aeruginosa, Campylobacter rectus, Deinococcus radiodurans, Acinetobacter Baumannii*, and others (Alotaibi & Heaselgrave, 2011; Cardo, Salata, Mendez, Reddy, & Goodrich, 2007; Corbin, 2002; DeRosa & Crutchley, 2002; Kashiwabuchi et al., 2013; Kumar et al., 2004; Lang, 2008; López-Carballo, Hernández-Muñoz, Gavara, & Ocio, 2008; Martins et al., 2008).

Particularly, riboflavin has been used for virus inactivation in blood components, obtaining 4 to 7 log reduction (Corbin, 2002). It was also reported that riboflavin was able to inactivate *E*. *coli*, DH5 α strain, with irradiation of blue light by damaging nucleic acids (Liang et al., 2013).

Microbial Food Safety of Fresh Produce

Recent years have witnessed a remarkable trend of incorporating more fruits and vegetables as part of a healthy diet. Interestingly, fresh produce has been increasingly identified as the cause of foodborne illnesses (CDC, 2013). Thermal treatment to reduce the microbial load is not applicable for fresh and fresh-cut produce, while conventional sanitizing methods for these produce including chlorine, ozone, and organic acids suffer from insufficient microbial load reduction, the risk of development of drug resistance, and consumer concerns about mutagenic and carcinogenic residues (Fernandez, Noriega, & Thompson, 2013). The continuous consumer trends in the consumption of fresh fruits and vegetables and the unsatisfying conventional washing and sanitizing treatments thus call for novel disinfection methods for fresh produce. Several studies have evaluated the antimicrobial efficiency of photosensitization based on GRAS photosensitizers including erythrosine B, chlorophyll, and Na-chlorophyllin (López-Carballo et al., 2008; Luksiene & Brovko, 2013; Tsai, Yang, Wang, Chien, & Chen, 2009).

Since riboflavin has been recognized as an efficient photosensitizer in the respect of photo-oxidation in food, it also has the potential as an environmentally friendly photosensitizer to inactivate foodborne pathogens. I propose to study its triplet

state properties, particularly its interaction with oxygen ($k_Q[Q]$), by monitoring its phosphorescence in various matrices in the absence and presence of oxygen to assess its applicability as a photosensitizer.

Research Objectives

Overall, the purpose of this study is to assess and evaluate the use of riboflavin as an optical sensor for food quality and as a photosensitizer for food safety. I hypothesize that: 1) phosphorescence from riboflavin can be used as a non-invasive and sensitive analytical tool to monitor molecular motions in glassy amorphous solids, and 2) riboflavin can be used as a safe and consumer-friendly photosensitizer of singlet oxygen and has the efficacy to photo-inactivate foodborne pathogens.

The following objectives have been identified for this project:

Objective 1: Characterize the luminescence properties and photophysical events of riboflavin as a triplet probe in glycerol/water (v/v 3:1) mixture at 77K and during ballistic heating.

Objective 2: Characterize the luminescence properties and photophysical events of riboflavin as a triplet probe in amorphous sucrose solid films as a function of temperature and to understand the mechanism of environmental sensitivity of riboflavin to molecular motions.

Objective 3: Study the effect of molecular weight/size and glass transition temperature on molecular mobility in a series of glucose oligomers and a series of disaccharides using phosphorescence from riboflavin.

Objective 4: Investigate the molecular mobility of dextran of various molecular weights and the effect of glycerol as a plasticizer on molecular mobility using phosphorescence from riboflavin.

Objective 5: Calculate the rate constant for oxygen quenching of triplet state riboflavin when riboflavin is dispersed in various amorphous matrices.

Objective 6: Investigate singlet oxygen photosensitized by riboflavin under various environmental conditions and explore its application as a photosensitizer to enhance food safety.

References

Ahmad, I., & Vaid, F. H. M. (2006). Chapter 2 photochemistry of flavins in aqueous and organic solvents. (pp. 13-40) The Royal Society of Chemistry. doi:10.1039/9781847555397-00013

Alotaibi, M. A., & Heaselgrave, W. (2011). Solar disinfection of water for inactivation of enteric viruses and its enhancement by riboflavin. *Food and Environmental Virology, 3*(2), 70-73. doi:10.1007/s12560-011-9058-5

Blyth, A. W. (1879). LVI.-the composition of cows' milk in health and disease. *Journal of the Chemical Society, Transactions, 35*(0), 530-539. doi:10.1039/CT8793500530

Cardo, L. J., Salata, J., Mendez, J., Reddy, H., & Goodrich, R. (2007). Pathogen inactivation of trypanosoma cruzi in plasma and platelet concentrates using riboflavin and ultraviolet light. *Transfusion and Apheresis Science, 37*(2), 131-137. doi:10.1016/j.transci.2007.07.002

Cardoso, D. R., Libardi, S. H., & Skibsted, L. H. (2012). *Riboflavin as a photosensitizer. effects on human health and food quality*

CDC. (2013). *Estimating Foodborne Illness: An Overview.* http://www.cdc.gov/foodborneburden/estimates-overview.html. Last Updated April 16, 2014, Last Accessed February 22, 2016

Choe, E., Huang, R., & Min, D. (2005). Chemical reactions and stability of riboflavin in foods. *Journal of Food Science, 70*(1), R28-R36.

Choe, E., & Min, D. (2006). Chemistry and reactions of reactive oxygen species in foods. *Critical Reviews in Food Science & Nutrition, 46*(1), 1.

Cicerone, M. T., Tellington, A., Trost, L., & Sokolov, A. (2003). Substanstially improved stability of biological agents in dried form: The role of glassy dynamics in preservation of biopharmaceuticals. *BioProcess International, 1*, 1-9.

Corbin, F. (2002). Pathogen inactivation of blood components: Current status and introduction of an approach using riboflavin as a photosensitizer. *International Journal of Hematology, 76*, 253-257.

Corradini, M. G., & Ludescher, R. D. (2015). Making sense of luminescence from GRAS optical probes. *Current Opinion in Food Science, 4*, 25-31. doi:10.1016/j.cofs.2015.04.004

DeRosa, M. C., & Crutchley, R. J. (2002). Photosensitized singlet oxygen and its applications. *Coordination Chemistry Reviews, 233/234*(2), 351.

Edwards, A. M. (2006). Chapter 1 general properties of flavins. In E. Silva, & A. M. Edwards (Eds.), *Flavins: Photochemistry and photobiology* (). Cambridge, UK: The Royal Society of Chemistry. doi:10.1039/9781847555397-00001

Fernandez, A., Noriega, E., & Thompson, A. (2013). Inactivation of salmonella enterica serovar typhimurium on fresh produce by cold atmospheric gas plasma technology. *Food Microbiology, 33*(1), 24-29. doi:10.1016/j.fm.2012.08.007

Grodowski, M. S., Veyret, B., & Weiss, K. (1977). Photochemistry Of Flavins. Ii. Photophysical Properties Of Alloxazines And Isoalloxazines. *Photochemistry and Photobiology, 26*(4), 341-352. doi:10.1111/j.1751-1097.1977.tb07495.x

Joye, I. J., Delcour, J. A., Draganski, A., & Ludescher, R. D. (2012). Monitoring molecular oxygen depletion in wheat flour dough using erythrosin B phosphorescence: A biophysical approach. *Food Biophysics, 7*(2), 138-144. doi:10.1007/s11483-012-9251-6

Kaminski, K., Adrjanowicz, K., Zakowiecki, D., Kaminska, E., Wlodarczyk, P., Paluch, M., . . . Tarnacka, M. (2012). *Dielectric studies on molecular dynamics of two important disaccharides: Sucrose and trehalose*

Karoui, R., & Blecker, C. (2011). Fluorescence spectroscopy measurement for quality assessment of food systems-a review. *Food & Bioprocess Technology, 4*(3), 364.

Kashiwabuchi, R. T., Carvalho, F. R. S., Khan, Y. A., Hirai, F., Campos, M. S., & McDonnell, P. J. (2013). Assessment of fungal viability after long-wave ultraviolet light irradiation combined with riboflavin administration. *Graefes Archive for Clinical and Experimental Ophthalmology, 251*(2), 521-527. doi:10.1007/s00417-012-2209-z

Kuan Lam, S., Namdas, E., & Lo, D. (1998). Effects of oxygen and temperature on phosphorescence and delayed fluorescence of erythrosin B trapped in sol–gel silica. *Journal of Photochemistry and Photobiology A: Chemistry, 118*(1), 25-30. doi:http://dx.doi.org/10.1016/S1010-6030(98)00350-5

Kumar, V., Lockerbie, O., Keil, S. D., Ruane, P. H., Platz, M. S., Martin, C. B., Goodrich, R. P. (2004). Riboflavin and UV-light based pathogen reduction: Extent and consequence of DNA damage at the molecular level. *Photochemistry and Photobiology, 80*(1), 15-21. doi:10.1562/2003-12-23-RA-036.1

Lam, S. K., Chan, M. A., & Lo, D. (2001). Characterization of phosphorescence oxygen sensor based on erythrosin B in sol–gel silica in wide pressure and temperature ranges. *Sensors and Actuators B: Chemical, 73*(2–3), 135-141. doi:http://dx.doi.org/10.1016/S0925-4005(00)00695-X

Lang, A. (2008). In Lang A. (Ed.), *Dyes and pigments: New research* (1st ed.). New York: Nova Science Publishers, Inc.

Liang, J., Yuann, J. P., Cheng, C., Jian, H., Lin, C., & Chen, L. (2013). Blue light induced free radicals from riboflavin on E. coli DNA damage. *Journal of Photochemistry and Photobiology B-Biology, 119*, 60-64. doi:10.1016/j.jphotobiol.2012.12.007

López-Carballo, G., Hernández-Muñoz, P., Gavara, R., & Ocio, M. J. (2008). Photoactivated chlorophyllin-based gelatin films and coatings to prevent microbial contamination of food products. *International Journal of Food Microbiology, 126*(1–2), 65-70. doi:http://dx.doi.org/10.1016/j.ijfoodmicro.2008.05.002

Ludescher, R. D., Shah, N. K., McCaul, C. P., & Simon, K. V. (2001). Beyond tg: Optical luminescence measurements of molecular mobility in amorphous solid foods. *Food Hydrocolloids, 15*(4-6), 331-339. doi:10.1016/S0268-005X(01)00050-9

Lukasik, K. V., & Ludescher, R. D. (2006). Effect of plasticizer on dynamic site heterogeneity in cold-cast gelatin films. *Food Hydrocolloids, 20*(1), 88-95. doi:http://dx.doi.org/10.1016/j.foodhyd.2005.03.006

Luksiene, Z., & Brovko, L. (2013). Antibacterial photosensitization-based treatment for food safety. *Food Engineering Reviews, 5*(4), 185-199. doi:10.1007/s12393-013-9070-7

Martins, S. A. R., Combs, J. C., Noguera, G., Camacho, W., Wittmann, P., Walther, R., . . . Behrens, A. (2008). Antimicrobial efficacy of riboflavin/UVA combination (365 nm) in vitro for bacterial and fungal isolates: A potential new treatment for infectious keratitis. *Investigative Ophthalmology & Visual Science, 49*(8), 3402-3408. doi:10.1167/iovs.07-1592

Moore, W. M., McDaniels, J. C., & Hen, J. A. (1977). The photochemistry of riboflavin-vi. the photophysical properties of isoalloxazines. *Photochemistry & Photobiology, 25*(6), 505.

Northrop-Clewes, C., & Thurnham, D. I. (2012). The discovery and characterization of riboflavin. *Annals of Nutrition & Metabolism, 61*(3), 224-230. doi:10.1159/000343111

Penzkofer, A. (2012). Photoluminescence behavior of riboflavin and lumiflavin in liquid solutions and solid films. *Chemical Physics, 400*, 142-153. doi:10.1016/j.chemphys.2012.03.017

Penzkofer, A., Tyagi, A., Slyusareva, E., & Sizykh, A. (2010). Phosphorescence and delayed fluorescence properties of fluorone dyes in bio-related films. *Chemical Physics, 378*(1–3), 58-65. doi:http://dx.doi.org/10.1016/j.chemphys.2010.10.001

Pravinata, L. C., You, Y., & Ludescher, R. D. (2005). Erythrosin B phosphorescence monitors molecular mobility and dynamic site heterogeneity in amorphous sucrose. *Biophysical Journal, 88*(5), 3551-3561. doi:http://dx.doi.org/10.1529/biophysj.104.054825

Schauerte, J. A., Steel, D. G., & Gafni, A. (1997). Time-resolved room temperature tryptophan phosphorescence in proteins. *Methods in Enzymology, 278*, 49-71.

Sikorski, M. (2002). Photophysics of dimethyl-alloxazines and 1-methyllumichrome on cellulose. *Physical Chemistry Chemical Physics, 4*(2), 211-215. doi:10.1039/b106953e

Slade, L., & Levine, H. (1995). Glass transitions and water-food structure interactions. *Advances in Food and Nutrition Research, 38*, 103-269.

Steel, D. G., Subramaniam, V., & Gafni, A. (1996). Time-resolved tryptophan phosphorescence spectroscopy: A sensitive probe of protein folding and structure. *IEEE Journal on Selected Topics in Quantum Electronics, 2*(4), 1107-1114. doi:10.1109/2944.577341

Sun, M., Moore, T. A., & Song, P. (1972). Molecular luminescence studies of flavines. I. excited states of flavines. *Journal of American Chemical Society, 94*(5), 1730-1740.

Tiwari, R. S., & Ludescher, R. D. (2010). Vanillin phosphorescence as a probe of molecular mobility in amorphous sucrose. *Journal of Fluorescence, 20*(1), 125.

Tiwari, R. S., & Ludescher, R. D. (2012). *Molecular mobility in a homologous series of amorphous solid glucose oligomers* Elsevier Ltd. doi:10.1016/j.foodchem.2011.12.011

Tsai, T., Yang, Y., Wang, T., Chien, H., & Chen, C. (2009). Improved photodynamic inactivation of gram-positive bacteria using hematoporphyrin encapsulated in liposomes and micelles. *Lasers in Surgery and Medicine, 41*(4), 316-322. doi:10.1002/lsm.20754

Wainwright, M. (2009). *Photosensitizers in biomedicine* (1st ed.). Oxford ; Hoboken, N.J: Wiley-Blackwell.

Wishner, L. A. (1964). Light-induced oxidations in milk.*47*(2), 216-221.

You, Y., & Ludescher, R. D. (2007). The effect of glycerol on molecular mobility in amorphous sucrose detected by phosphorescence of erythrosin B. *Food Biophysics, 2*(4), 133-145. doi:10.1007/s11483-007-9030-y

You, Y., & Ludescher, R. D. (2010). The effect of molecular size on molecular mobility in amorphous oligosaccharides. *Food Biophysics, 5*(2), 82-93. doi:10.1007/s11483-010-9148-1

Chapter II Characterization of Phosphorescence from Riboflavin in Glycerol/Water, Ethanol/Water, Sucrose/Water, and Dextran/Water under 77K and during Ballistic Heating

Introduction

Research over the past couple of decades has identified the critical role of amorphous carbohydrate in preserving the bioactivity of delicate biomaterials such as enzymes, bioactive compounds, volatile flavor compounds, and active drug ingredients. Despite the importance of using amorphous solids in preserving labile biomaterials and decades of practical applications in pharmaceutical and food industries, the mechanism of how these rigid amorphous matrices retard the degradation processes of labile biological agents is not fully understood. Historically, researchers speculated that a high glass transition temperature, Tg, of the excipient would result in long preservation time and that storage below Tg would be sufficient to maintain the stability of biomaterials (Bhattacharya & Suryanarayanan, 2011). Yet, recent studies have shown that degradation processes could happen at temperatures as low as 50K below Tg and suggested that Tg, as well as α relaxation (structural relaxation), was not sufficient to predict the preservation stability (Cicerone & Douglas, 2012; Kaminski et al., 2008). It was also proposed that fast secondary relaxations (β- and γ- relaxations) played an important role in stabilizing proteins, although the mechanism of this stabilization is still not clear (Bhattacharya & Suryanarayanan, 2011; Cicerone, Tellington, Trost, & Sokolov, 2003; Cicerone & Douglas, 2012).

Techniques including dielectric relaxation spectroscopy (DRS), nuclear magnetic resonance spectroscopy (NMR), neutron scattering and differential scanning calorimetry (DSC) have all been used to study the molecular mobility of amorphous solids. Yet, each measurement method has certain drawbacks: for example, DRS cannot provide reliable data for freeze-dried samples due to the deceptive signals from high surface area, neutron scattering is not readily available for routine testing (Cicerone & Douglas, 2012), and DSC, which although has been used to study β relaxation (Dranca, Bhattacharya, Vyazovkin, & Suryanarayanan, 2009), is less sensitive to secondary relaxations than to α relaxation.

Phosphorescence from molecules including erythrosine B (Daganski et al., 2010; Pravinata, You, & Ludescher, 2005; You & Ludescher, 2010), vanillin (Tiwari & Ludescher, 2010), tryptophan (Draganski, 2014), tyrosine (Draganski, 2014), and eosin Y (Rodriguez, San Roman, Duarte, Machado, & Ferreira, 2012) have been used as a spectroscopic indicator to study molecular mobility and heterogeneity in various amorphous matrices. These studies have shown that phosphorescent probes can perform as sensitive and site-specific optical indicators to study the molecular mobility of their surrounding environment (Corradini & Ludescher, 2015; Ludescher, Shah, McCaul, & Simon, 2001). The change in phosphorescence emission spectra and the fashion of phosphorescence decay sensitively reflect changes in local molecular mobility and environment dynamics of the hosting matrix. Strong phosphorescence emission and long phosphorescence lifetime suggest constrained packing and rigid local environment, while weak emission intensity and short

lifetime indicate mobile and disorganized local environment. Therefore, phosphorescence from molecules entrapped in amorphous solid matrix can provide information on the molecular motions of the matrix through a different lens, thus allowing us to further understand how molecular motions and relaxation processes in the matrix affect the preservation and stabilization of labile biomaterials. However, the current status of using phosphorescent probes as optical sensors to study molecular mobility has heavily centered on the use of the two amino acids mentioned above: tryptophan and tyrosine. The synthetic nature of erythrosine B makes it less desirable for food applications. There is thus a need to expand the pool of phosphorescent probes and to find suitable candidates from natural phosphorescent molecules.

In this research, we aimed to explore the feasibility, potential, and limitations of using riboflavin as a phosphorescent probe. Riboflavin is a Generally Recognized As Safe (GRAS) molecule, which makes it extremely desirable for food and pharmaceutical applications. Riboflavin has been shown to have relatively high intersystem crossing quantum yield and to exhibit phosphorescence emission at cryogenic temperature in organic solvents and at room temperature when fixed in rigid media such as cellulose and starch films (Penzkofer, Tyagi, Slyusareva, & Sizykh, 2010; Penzkofer, 2012; Sun, Moore, & Song, 1972). Yet, no study has systematically investigated how its phosphorescence responded to molecular mobility changes in an amorphous matrix.

This research is aimed to characterize the triplet-state photophysical properties of riboflavin dispersed in 3:1(v/v) glycerol/water mixture under 77K and during ballistic heating process. Phosphorescence decays from riboflavin in three additional solvent systems: 1:2 (v/v) ethanol/water mixture, 30%wt sucrose/water mixture, and 30%wt dextran/water mixture, were also characterized. The glycerol/water mixture was chosen because it is a well-characterized glass-forming system and has been used in another study to characterize four phosphorescent probes (Draganski, 2014). This will allow for the comparison between different probes, which thus can provide insight into how probes respond differently to the same dynamic change. Glycerol is a typical glass former, while water, on the other hand, crystalizes very easily. Glycerol-water mixture with high glycerol content is known as an excellent glass former and is widely used as cryoprotectant (Trejo González, Longinotti, & Corti, 2011). Not only has the properties of glycerol/water mixtures are of practical interest to biopharmaceutical applications, but the complicated dynamics of this system has also attracted great attention in the field of soft condensed matter physics (Hayashi, Puzenko, & Feldman, 2006). This extensively studied system and limited possible interactions between glycerol/water mixture and riboflavin thus make it a great starting point to characterize riboflavin as a phosphorescent probe. In addition to glycerol/water mixture, the ethanol/water mixture (1:2 v/v) was selected as another glass-forming system with a known glass transition temperature of 125K reported in the literature (Menzel, 2001). The sucrose/water and dextran/water mixtures were included in the research because attention has been given to the ability of sugar molecules to

lower water mobility as cryoprotectants (He, Fowler, & Toner, 2006), although the relaxation processes of these two mixtures were less studied under cryogenic temperature range.

Riboflavin dispersed in four solvent mixtures was introduced to liquid nitrogen to first rapidly cool the systems into rigid glass. A systematic characterization was carried out and phosphorescence decays from riboflavin were analyzed to assess its sensitivity to temperature induced molecular motions and mobility change in different matrices.

Materials and Methods

Sample Preparation: A stock solution of 400μM riboflavin was prepared by dissolving riboflavin (Sigma-Aldrich, St Louis, MO, USA) in deionized water. The solution stirred overnight while kept in the dark and then stored at 4˚C in an amber Nalgene bottle until it was used. To make riboflavin in glycerol-water mixture, 250μL of the riboflavin stock solution was mixed with 750μL ultrapure, spectrophotometric grade glycerol (Alfa Aesar, Ward Hill, MA, USA) to yield a final ratio of glycerol/water (3:1 v/v) mixture. The ratio of riboflavin to solvent (glycerol + water) was approximately $1:2\times10^5$, which is an essentially small probe-solvent ratio to avoid probe-probe collisional quenching (Richert, 1998). Riboflavin in the ethanol/water (1:2 v/v) mixture was prepared by mixing 300μL ethanol (Sigma-Aldrich, St Louis, MO, USA) with 600μL riboflavin solution (400μM). The final riboflavin to solvent (ethanol + water) molar ratio of the ethanol/water (1:2 v/v) mixture was approximately $1:10^5$.

Riboflavin in two carbohydrate solutions was prepared by mixing 0.3g of sugar (sucrose or dextran), both purchased from Sigma-Aldrich (St. Louis, MO, USA) and used without further purification (St Louis, MO, USA) with 1mL riboflavin solution (400μM). The final riboflavin to solvent (water + monomer sugar unit) was about $1:10^5$. All mixtures were gently heated in a water bath to 30˚C for 10min followed by vigorous vortexing for 5min to achieve well-mixed solutions. Controls of these four solvent systems were prepared in the absence of riboflavin.

Before the phosphorescence measurements, custom-made copper sample holders were first thoroughly cleaned with 70% nitric acid (Sigma-Aldrich, St. Louis, MO, USA) to remove any remaining sample from previous experiments and the copper carbonate accumulated during storage, followed by rinsing with distilled water and drying.

Phosphorescence Measurement: The phosphorescence measurement at cryogenic temperature was conducted following the procedure described by Draganski (2014). An aliquot of 10μL riboflavin-solvent mixture was transferred into the recessed area of a cleaned and dried copper holder. A thin thermocouple wire was attached onto the bottom of the recessed area of the copper holder to monitor the temperature change during the ballistic heating of the sample. The copper holder was carefully slid into a dewar and the recessed area of the copper tip with the sample was positioned to the emission light path with front face geometry for phosphorescence lifetime measurement (Draganski, 2014). Liquid nitrogen was poured into the dewar and the temperature of the sample was maintained at 77K by insuring that the dewar was not depleted from liquid nitrogen. As the liquid nitrogen slowly evaporated, the temperature gradually increased. Phosphorescence decays from riboflavin were collected at 77K and during the ballistic heating process.

Phosphorescence decays were obtained by exciting the sample at 440nm and collecting the emission at 620nm with delay and gate times set to 0.2 and 5ms, respectively. A total decay time of 2000ms was collected. Each decay was collected

from one lamp flash and was an average of 5 cycles to improve the signal to noise ratio over a relatively small temperature fluctuation range. For all measurements, both monochromator slit widths were set to 20nm to maximize the signal. Phosphorescence from blank samples was also measured and the blank samples exhibited no phosphorescence signals but only noises. The phosphorescence decay data were analyzed without further subtracting the blank sample.

Analysis of Phosphorescence Decay: Since excited triplet riboflavin molecules resided in various unique micro-environments in the amorphous matrix, the phosphorescence from riboflavin decayed in a heterogeneous manner. Two fitting models that allow for a heterogeneous decay were used: the stretched exponential function and multi-exponential function. The stretched exponential function, or Kohlrausch-Williams-Watts (KWW) decay model (II-1):

	$I(t) = I(0)\times\exp\left[-(t/\tau)^{\beta} + c\right]$	(II-1)

has been widely used to describe heterogeneous decay processes of triplet probes in viscous liquids and glassy materials (Richert, 2000). In the stretched exponential decay model, I(0) is the initial intensity at t=0, τ is the fitted stretched lifetime, and β is the stretching exponent factor. The goodness of the fit was judged by the distribution of modified residuals ($(data - fit)/data^{1/2}$): if modified residuals varied randomly about zero, then the fit was determined as sufficient to characterize the data. The average lifetime was calculated using τ and β (II-2):

	$\tau_s = \frac{\tau}{\beta}\Gamma(\frac{1}{\beta})$	(II-2)

in which, Γ is the gamma function. In the stretched exponential model, the stretching exponent factor β is a measure of the width of lifetime distribution that varies from 0 to 1. A value of 1 indicates complete homogeneity, whereas a value close to 0 suggests great heterogeneity in the system. This parameter reflects the non-exponential nature of the decay and describes the distribution of dynamically distinct regions in the amorphous solid.

A multi-exponential function (II-3) was also employed in this study:

	$I(t) = I(0) * \sum_{i=1}^{n} \alpha_i \exp\left(-\frac{t}{\tau_i}\right)$	(II-3)

In this model, I(0) is the initial intensity at t=0, τ_i are the lifetimes, α_i are the fractional amplitudes of each lifetime component, and n is the number of lifetime components. The fractional amplitudes A_i describe the distribution of the lifetime components. The average lifetime derived from multi-exponential function was calculated using the population average (II-4):

	$\tau_m = \sum_{i}^{n} \alpha_i \tau_i$	(II-4)

Different from stretched exponential model, which is a model of continuous lifetime distribution, in this model, a discrete number of exponential decay components is

arbitrarily determined and justified by the goodness of the fit (Lee et al., 2001). Estimating the number of lifetime components can potentially introduce errors to the analysis, since the improvement of the fit can lead to physically meaningless values for α_i and τ_i. For example, a decay with two or three- exponential components can be well fitted by a five- or six- exponential function. However, the use of a five-exponential function not only complicates the interpretation of the parameters but also increases the possibility of having physically meaningless parameters. In our analysis, in addition to judging the fit by the distribution of modified residuals, the Akaike information criterion (AIC), an indicator of the trade-off between the goodness of the fit and the complexity of the model, was also used as a factor to determine how many components were needed to avoid overfitting the data.

The stretched exponential model enjoys the simplicity of only having two parameters but it sometimes is not sufficient enough to satisfactorily describe complex data. Multi-exponential model, on the other hand, can successfully fit the complex data but suffers from the difficulty to find a global overall minimum of the chi-squared function while minimizing the parameters used. Because the change in one parameter can be compensated for by changing other parameters, there thus are a large number of minima on a multi-dimensional probability surface (Fuhrmann, Brubach, & Dreizler, 2013; Steinbach, Ionescu, & Matthews, 2002).

In addition to the stretched exponential and multi-exponential models, the lifetime distribution was also determined using a hybrid analysis that combines the Maximum Entropy with Nonlinear Least Squares (NLS) methods (Steinbach et al.,

2002). The software MemExp version 4.0 was downloaded through the NIH center for molecular modeling site (http://cmm.cit.nih.gov/memexp/). This algorithm uses the MEM to guide a series of discrete NLS fits during the analysis process, which direct a continuous description to evolve and eventually result in an automated and objective approach to solve multiple-minimum problem (Steinbach et al., 2002). The goodness of the fits is judged by if modified residuals evenly distribute about zero, as well as the value of Ratio, *r*, and the image normalization, *I*, recorded along with the fit in the .out files.

Photophysical Rate Constants: The calculated average lifetimes provide a means to calculate the rate constant of triplet state de-excitation (k_P) and consequently the rate constant of non-radiative decay (k_{TS0}), which is a direct measure of matrix mobility-controlled quenching. Phosphorescence lifetime is determined by the rate constants of all possible de-excitation pathways as we discussed in Chapter I (II-5):

	$$\frac{1}{\tau} = k_P = k_{RP} + k_{TS1} + k_{TS0} + k_Q[O_2]$$	(II-5)

where k_{RP} is the rate constant of radiative decay, an intrinsic property of the phosphorescent probe; k_{TS1} is the rate constant of reverse intersystem crossing; k_{TS0} is the rate constant of non-radiative decay, a measure of matrix-induced quenching; and $k_Q[O_2]$ is the rate constant of collisional quenching with oxygen. Oxygen quenching was negligible in the liquid nitrogen environment where oxygen was absent. In this research, under cryogenic temperature, no delayed fluorescence was observed, therefore, the extremely low temperature and low thermal energy were

not enough to promote reverse intersystem crossing to emit delayed fluorescence (k_{TS1}=0). It was assumed that under 77K, the glassy solvent matrix was rigid enough and the collisional quenching between the solvent molecules and triplet riboflavin molecules was negligible. Yet, the different composition of each matrix exhibited slightly different rigidity. The different phosphorescence lifetime collected at 77K from four matrices allowed us to compare the matrix rigidity among the four matrices studied. As temperature gradually increased, rigid glassy system gradually became more flexible, and once the Tg was surpassed, the matrix turned into melt with full molecular motions activated. Consequently, the phosphorescence lifetime is shortened due to enhanced collisional quenching. (II-5 thus provided a way to quantitatively calculate the value of non-radiative decay rate to describe the molecular mobility change in the system. Additionally, an Arrhenius plot of the rate of non-radiative decay reveals the activation energy (E_A) of the non-radiative process, which also serves as a measure of the molecular mobility in the solvent matrix.

Results and Discussion

PART 1: Riboflavin Natural Phosphorescence Lifetime

Phosphorescence Decays at 77K: The phosphorescence decays from riboflavin were collected under 77K to estimate the phosphorescence natural lifetime of riboflavin and consequently to estimate the rate constant of radiative decay, an intrinsic property of riboflavin. In this study, both oxygen quenching and reverse intersystem crossing were negligible. Under 77K, the molecular mobility of the matrix was extremely low so there is little collisional quenching between the solvent molecules and the triplet excited riboflavin molecules, which allowed for the estimation of natural phosphorescence lifetime for riboflavin.

Phosphorescence intensity decays of riboflavin were collected at 77K in four different matrices: glycerol/water (3:1 v/v), ethanol/water (1:2 v/v), sucrose/water (30%wt), and dextran/water (30%wt). Figure II-1 shows the phosphorescence decays of riboflavin in the four solvent systems mentioned above. In all solvent systems studied here, as suggested by the curved log plot of the phosphorescence decays in Figure II-1, the decays of riboflavin were not single exponential. The decays were fitted using a stretched exponential model, a two-exponential model, and a three-exponential model, as well as the maximum entropy method (MEM). Figure II-2, Figure II-3 and Figure II-4 are examples of riboflavin phosphorescence decay in glycerol/water mixture at 77K, different fits, and corresponding modified residuals. As shown in Figure II-2, stretched exponential

model and the two multi-exponential models fitted the tail of the decay equally well, but stretched exponential overestimated the initial part of the decay while the two-exponential model underestimated the beginning part of the decay. Overall, the three-exponential model best characterized the decay behavior. Similarly, from the modified residuals for these fits shown in Figure II-3, only the residuals for the three-exponential model exhibited random distribution about zero, suggesting a satisfactory fit of the decay data. Figure II-4 depicts the fit from MEM and the modified residuals: as shown, the fit well described the decay data and the modified residuals distributed randomly about zero, suggesting a satisfactory fit of the decay data. Although both three-exponential function and MEM satisfactorily fitted the decay, MEM analysis was favored and used in the following analysis because: 1) it results in a continuous lifetime distribution and 2) it avoids the potentially physically meaningless parameters from multi-exponential model.

To characterize the phosphorescence intensity decays from riboflavin in four matrices at 77K, the decays were fitted using MEM and the lifetime distributions are plotted in Figure II-5. Take the riboflavin decay in glycerol/water mixture for example: the decay was best represented by a distribution of lifetime centered at $10^{2.2}$≈160ms. The longest lifetime in glycerol/water mixture was calculated as 170ms from 10 replicates, and the average was determined to be 161±3ms. The calculated average lifetime of triplet riboflavin in other matrices were: 140ms in ethanol/water mixture, 138ms in dextran/water mixture, and 127ms in sucrose/water mixture. The difference in lifetime values was likely caused by the

slightly different mobility in the hosting matrices introduced by the different compositions, consequently water content and intermolecular interactions. According to (II-5), the inverse of lifetime is determined by all possible de-excitation pathways. In the absence of delayed fluorescence and oxygen quenching, the magnitude of lifetime thus reflects the non-radiative decay rate, which provides a measure of molecular mobility. As indicated by the lifetime, the mobility was the lowest in glycerol/water mixture and highest in sucrose/water mixture. Further comparison on matrix mobility will be discussed in the following sections.

Riboflavin was reported to have a 170ms triplet lifetime in ethanol at 77K (Sun et al., 1972) and a140ms lifetime in both ethanol-methanol (9:1, v/v) and glycerol/water (1:1 v/v) (Moore, McDaniels, & Hen, 1977). All the riboflavin triplet lifetime in glycerol/water mixture calculated from the MEM fitting methods were in accordance to the values reported previously. Both studies mentioned earlier dated back to 1970s and the latter used electron spin resonance spectroscopy for measuring the phosphorescence lifetime. The differences in the measuring techniques and hosting matrices might be responsible for slight differences in lifetime values. Yet the improved sensitivity of the spectrophotometer and the data analysis method used in this study are expected to contribute to more reliable and accurate data. Therefore, the longest riboflavin phosphorescence lifetime, 170ms, measured at 77K, in glycerol/water mixture was used to approximate the intrinsic radiative decay rate. The inverse of 170ms, $5.88s^{-1}$, was used as the radiative decay rate and this value is used in the rest of the study. In principle, more accurate

estimations of radiative decay rate could be obtained by recording lifetime decays at an even lower temperature, such as 4K, when the molecular mobility is further restricted. However, such measurements require the use of alternative media such as liquid helium and special equipment during phosphorescence measurement that our lab does not currently possesses. Therefore, the 170ms lifetime measured at the lowest temperature that we could achieve was approximated as the natural phosphorescence lifetime.

Figure II-1

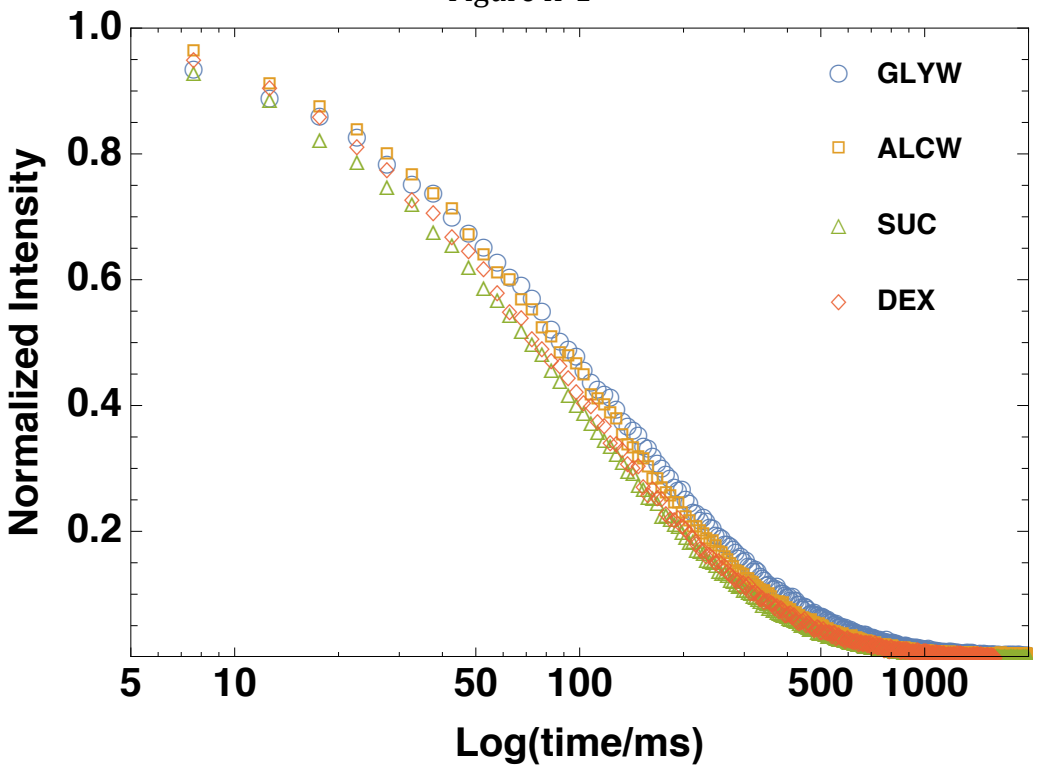

Figure II-1: Normalized phosphorescence decays of riboflavin dispersed in glycerol/water (3:1 v/v) (blue circle), ethanol/water (1:2 v/v) (orange square), sucrose/water (30%wt) (green triangle), and dextran/water (30%wt) (red diamond) at 77K.

Figure II-2

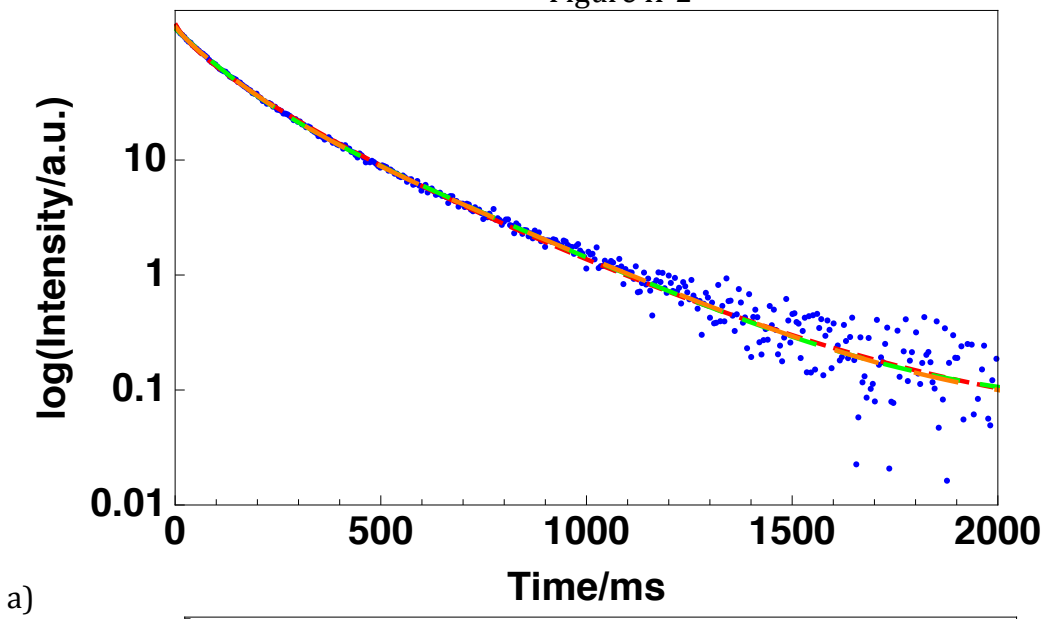

a)

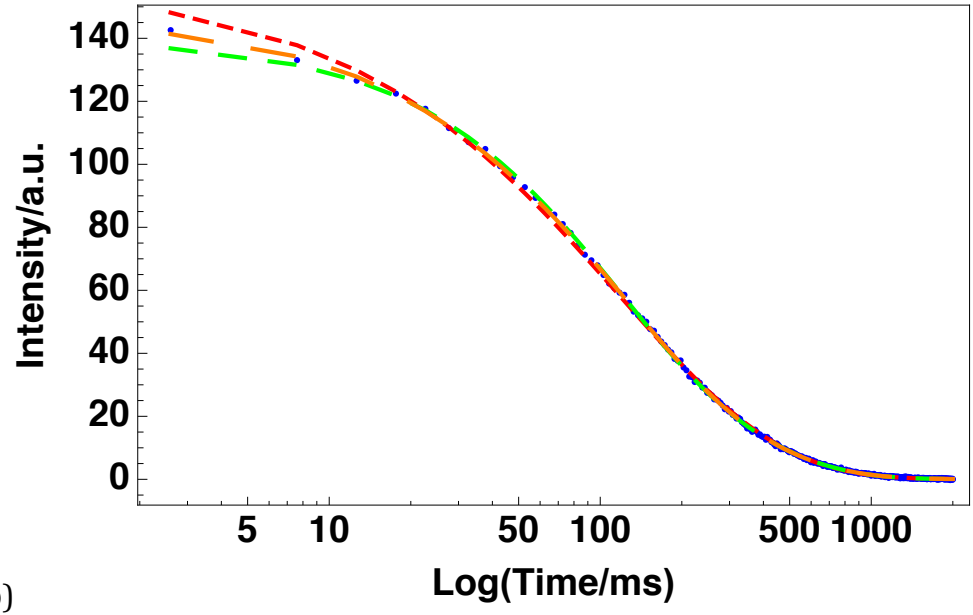

b)

Figure II-2: Phosphorescence decay of riboflavin in glycerol/water (3:1 v/v) mixture at 77K (blue circles) along with stretched exponential fit (red dashed line), 2-exponential fit (green dashed line), and 3-exponential fit (orange dashed line) plotted on linear-log (a) and log-linear (b) scale.

Figure II-3

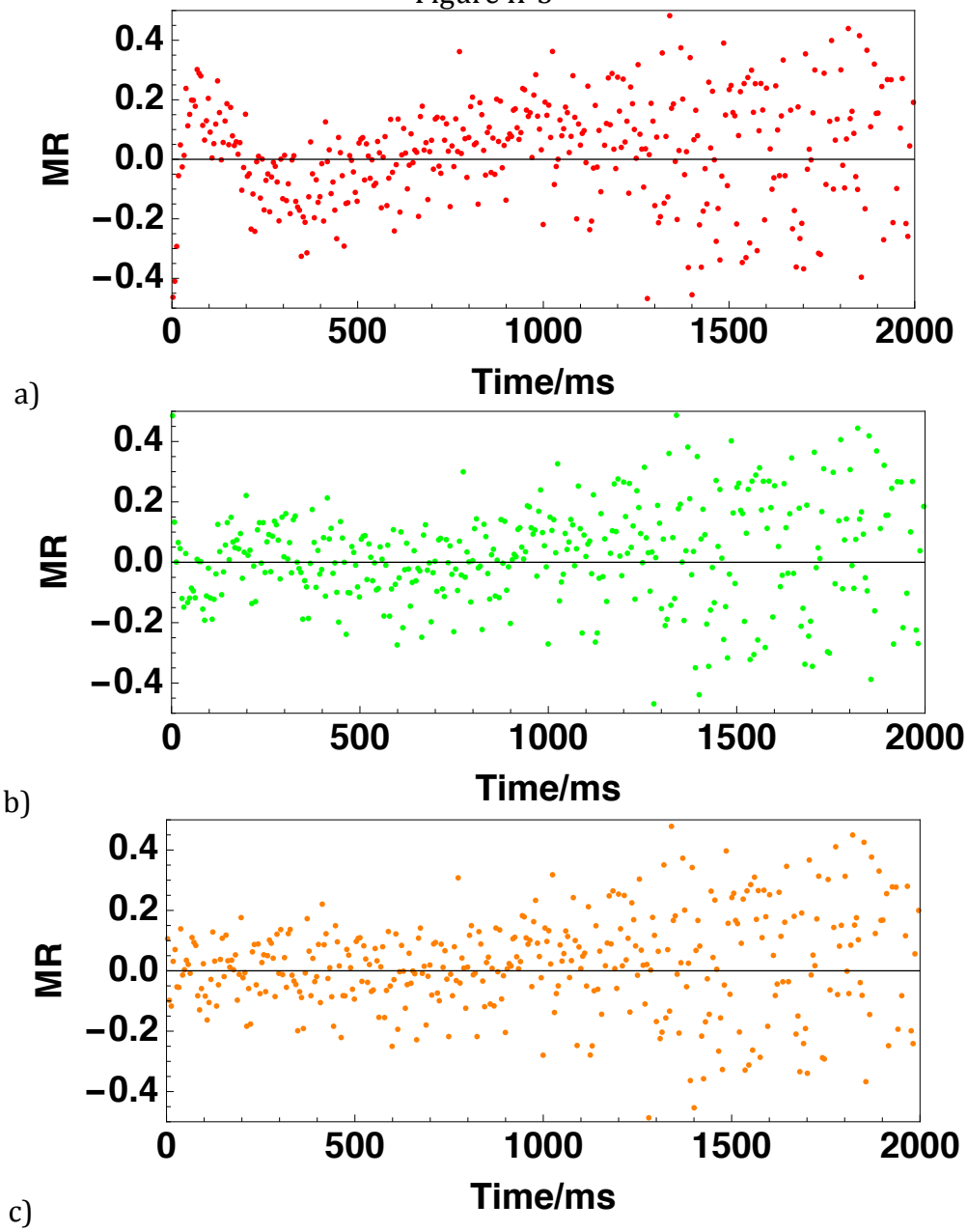

a)

b)

c)

Figure II-3: Modified residuals $\left({}^{(data-fit)}/_{data^{1/2}}\right)$ for stretched exponential fit (a), 2-exponential fit (b), and 3-exponential fit (c)

FigureII-4

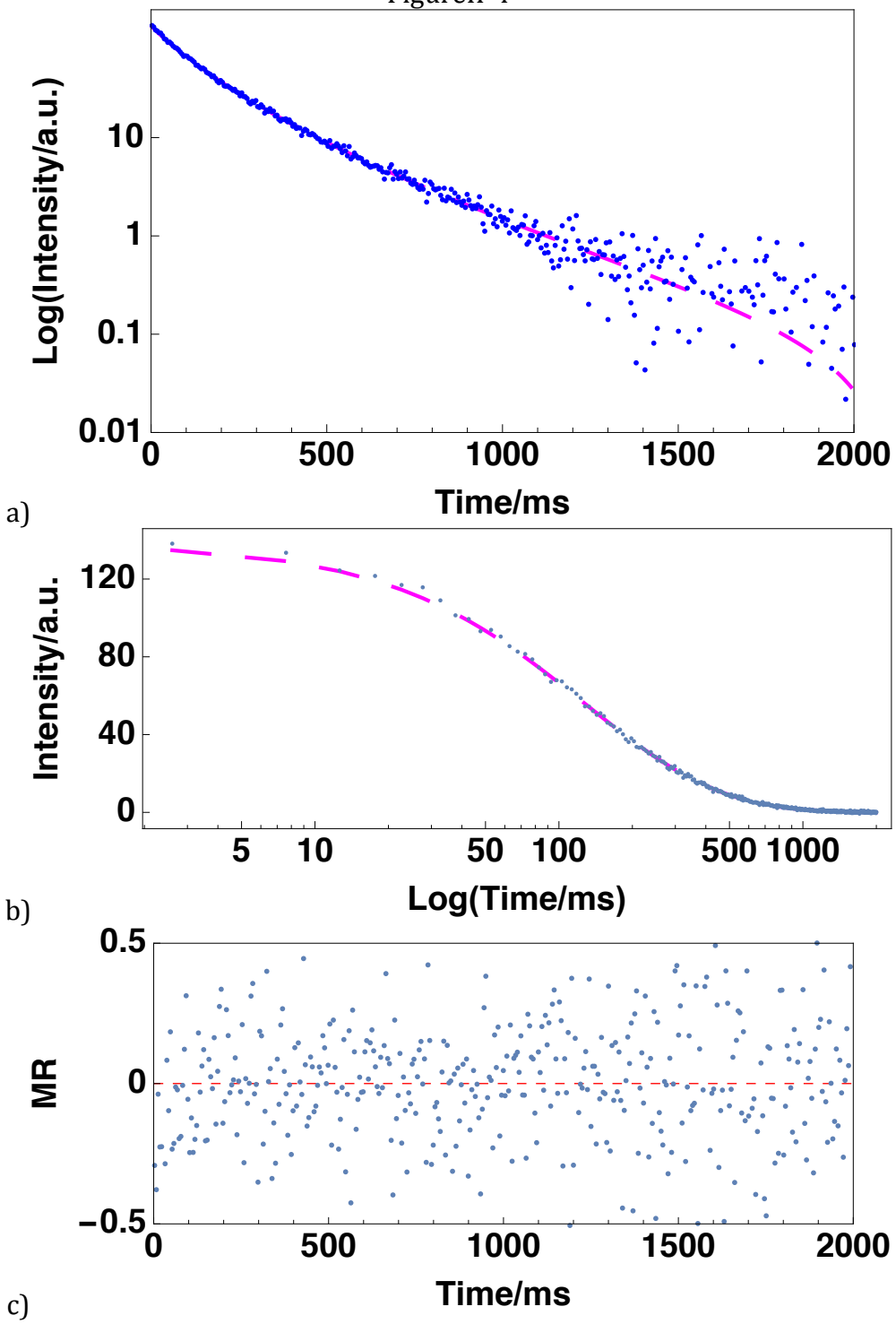

Figure II-4: Phosphorescence decay of riboflavin in glycerol/water (3:1 v/v) mixture at 77K (blue circle) and the fit using the maximum entropy method (MEM) (magenta dashed line) on linear-log (a) and log-linear (b) scale and a plot of modified residuals for this fit (c).

Figure II-5

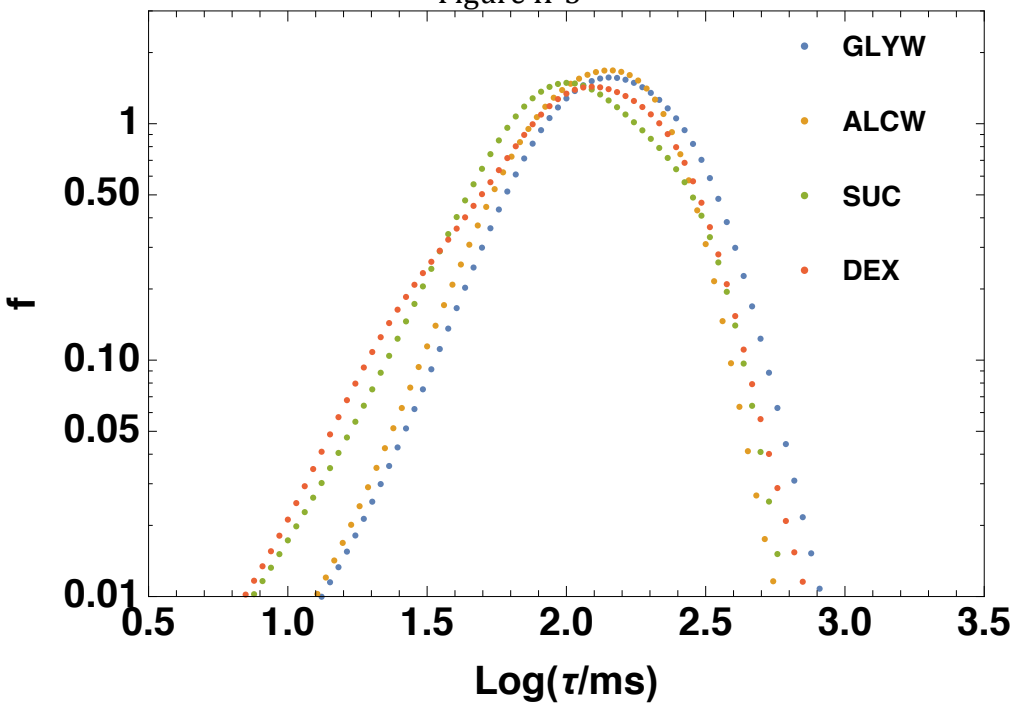

Figure II-5: The maximum entropy method (MEM) determined lifetime distribution of the phosphorescence intensity decays from riboflavin dispersed in glycerol/water mixture (blue), ethanol/water mixture (orange), sucrose/water mixture (green), and dextran/water mixture (red).

PART II: Glycerol/Water as the Matrix

Phosphorescence intensity decays of riboflavin in glycerol/water mixture were collected over the temperature range from 77 to 220K. The glass transition temperature, Tg, of the glycerol/water solvent system used in this study was reported to be ~178K (Sudo et al., 2002; Trejo González et al., 2011). The Tg was characterized in one study by the relaxation peak in the dielectric relaxation spectra (Sudo et al., 2002) and in another study by the estimated temperature at which the dynamic viscosity of the mixture reached $10^{12.5}$mPa*s (Trejo González et al., 2011).

The phosphorescence decays were fitted using MEM and Figure II-6 shows the MEM lifetime distribution as a function of temperature both below and above Tg. From 77 to 170K (Figure II-6a), the shape of the distribution barely changed while the distribution slightly shifted to shorter lifetime as temperature increased. Over the temperature range from 170K to 233K (Figure II-6b), both the shape and the center location of the lifetime distribution changed dramatically. The center of the distribution rapidly shifted to shorter lifetime, while the spread of the distribution changed in an irregular manner with broadening happening around 180~190K and sudden sharpening around 200~215K. The dramatic changes in riboflavin phosphorescence lifetime distribution corresponded to the onset of the glass transition in glycerol/water mixture around 170K.

The average lifetime τ was calculated from the center of gravity of the MEM lifetime distribution. The calculated riboflavin phosphorescence lifetime was plotted as a function of temperature in Figure II-7. From 77K to ~160K, the lifetimes only decreased gradually, decreasing from ~165ms to ~110ms. The decrease in lifetime became very steep when Tg was surpassed. From 160K to 180K, lifetimes drastically dropped from ~110ms to ~20ms. In the absence of quenching molecule oxygen ($k_Q[O_2]$) and reverse intersystem crossing (k_{TS1}), as discussed in Equation II-(II-5, the phosphorescence lifetimes reflected the changes in non-radiative decay rate, which provided a direct measurement of molecular mobility. The decrease in τ directly reflected an increase in k_{TS0}, thus an increase in matrix mobility.

The slight decrease in τ below Tg indicated that the glycerol/water mixture was slowly becoming more mobile as temperature increased. The sudden drop in lifetime between 160K and 180K, which coincided with the glass transition process, suggested that the probe was sensitive to the dynamic changes in the solvent system during glass transition. Over the temperature range from 180K to 230K, the rapid reduction in lifetime ceased; the lifetime remained constant around ~18ms over the first 20K, followed by a gradual reduction to 2ms. A similar trend was also observed when using erythrosine as a phosphorescent probe to study the molecular mobility in glycerol/water (3:1 v/v) mixture during ballistic heating from 77K and up (Draganski, 2014). It is not yet clear what was the cause of the plateau after the sudden drop in lifetime during glass transition. It was speculated that the probe might have lost its sensitivity to the changes in the softened matrix.

To better understand how the molecular mobility changed as the temperature increased from 77K to above Tg, the rate of non-radiative decay, k_{TS0}, was examined. According to(II-5, the inverse of the measured phosphorescence lifetime is only affected by the rates of radiative and non-radiative decays in the absence of oxygen quenching and reverse intersystem crossing. The rate of radiative decay was determined as $5.88s^{-1}$, as discussed before. The rate of non-radiative decay during the ballistic heating was calculated accordingly. The logarithm of the non-radiative decay rate is plotted versus the inversion of temperature in Figure II-8. The slope of the Arrhenius plot was used to determine the activation energy of the non-radiative decay process. Therefore, the activation energy to quench the triplet riboflavin was determined to be 1.7kJ/mol from 77 to 120K (red line), 4.1kJ/mol from 120 to 165K (magenta line), and 43.1 from 170 to 185K (green line). The very small activation energy, 1.7kJ/mol, over the temperature range from 77 to 120K suggested that there was little motion in the very rigid glassy solvent matrix and that the non-radiative quenching is likely due to normal mode of vibrations of the riboflavin molecule itself (Draganski, 2014). As temperature continued to increase, the Arrhenius plot exhibited a second regime with a slightly higher Ea~4.1kJ/mol. This slight increase in Ea was not evidence of a transition to a distinct process than the previous vibrational motions, but it was likely caused by the changes in heterogeneity in the glassy solvent system (Draganski, 2014).

The onset of the rapid change in non-radiative decay rate roughly marked the Tg of the solvent system, 178K, as indicated with the gray dashed line in Figure II-8. The activation energy, 43.1kJ/mol, is apparent much smaller than the activation energy for a typical α relaxation process. The apparent activation energy for α relaxation was calculated as 138.8 kJ/mol for 80%wt glycerol aqueous solution (Gao, Wang, Liu, Zhou, & Hua, 2007), compared to the mass fraction of glycerol (79%wt) in the glycerol/water mixture studied here. Additionally, at Tg, a typical time of α relaxation process is around 100s, which is 1000 times slower than the phosphorescence lifetime of riboflavin in the vicinity of glass transition process (~100ms). Therefore, until the α relaxation process becomes faster, approaching the same timescale of riboflavin phosphorescence lifetime, it is unlikely for triplet riboflavin to de-excite via non-radiative collisional quenching by the α relaxation. The phosphorescence from riboflavin will always be quenched first by the fastest motions in the matrix. It is thus reasonable to suggest that the phosphorescence from excited triplet riboflavin has little sensitivity towards the α relaxation within this temperature range but is more likely responding to the β relaxations in the matrix. Furthermore, the value of 43.1 kJ/mol is comparable to the activation energy for a universal secondary relaxation process of water in aqueous binary glass-forming systems (Capaccioli, Ngai, & Shinyashiki, 2007; Sjöström et al., 2010). A Johari-Goldstein secondary relaxation of water is omnipresent in a variety of glass-forming binary aqueous systems. This relaxation process was found to have a value of activation energy of 50kJ/mol independent of the binary aqeous composition (Capaccioli et al., 2007; Sjöström et al., 2010). Therefore, the rapid quenching of

triplet excited riboflavin molecules in the vicinity of glass transition temperature might be caused by the local relaxation process of the water component in the solvent system.

Hayashi et al (Hayashi et al., 2006) studied how the water molecules affect the relaxation dynamics in glycerol/water mixture with various water concentrations using broadband dielectric spectroscopy (BDS) and differential scanning calorimetry (DSC). It was found that the main relaxation process in glycerol rich mixtures followed Vogel-Flucher-Termann (VTF) law, but changed to the Arrhenius fashion when the glycerol content was below 40mol%. The change from a VTF dependence to the Arrhenius one suggested that water cooperative domain started to appear when the glycerol concentration falls below 40mol%. They also concluded that the existence of water pools would increase the heterogeneity of the system and consequently affects the syetem's static and dynamic properties. The glycerol concentration used in our study was approximately 42.5mol%, which was very close to the critical value when the water-water domain starts to appear mentioned in Hayashi *et al*'s study. In addition, according to their estimation, water-water interaction coexists with glycerol-water mixture when the glycerol content is between 55-40mol%. In the water-rich glycerol/water mixture (glycerol content less than 40mol%), two Arrhenius relaxation processes were identified: one due to the presence of ice crystal with an activation energy ~77kJ/mol and the relaxation process from interfacial water between ice and glycerol-water mixture with an activation energy quantified as ~33kJ/mol. The value of activation energy calculated

from our study, 43.1kJ/mol, falls in between these two values, suggesting that the relaxation processes that quenched triplet riboflavin might be attributed to both ice crystal and the interfacial water between ice and glycerol-water mixture.

As temperature further increased, the rapid increase of radiative decay rate ceased; instead, the radiative decay rate of triplet riboflavin molecule first remained almost constant and then increased rapidly again when temperature increased to 210K and above. A similar pattern has also been observed from erythrosine B phosphorescence decays in glycerol/water mixture, and it was concluded that such unusual trend was likely due to a temporary loss of sensitivity and conformational averaging (Draganski, 2014).

Interestingly, this unusual pause in the increase of non-radiative rate corresponded to an unexpected increase in stretching exponent factor β from the stretched exponential fit to the data, which also appeared around 170K. Similar behaviors were also observed from erythrosine B and tryptophan phosphorescence in glycerol/water mixture (Draganski, 2014). It was speculated that in the glassy state, probes resided in clusters and each probe decayed in a unique manner due to the difference from cluster to cluster. As temperature increased, all the sites became more mobile and the solvent molecules relaxed in a fast manner. The probes residing in these sites were able to adapt multiple conformations during the lifetime. This conformational averaging thus eventually exhibited a single exponential like decay.

Despite an extensive literature research, only one study gave some insightful explanation on our observation of proposed conformational averaging. This study used the time-resolved spectral dynamics of the eosin phosphorescence to examine the heterogeneity of glycerol/water mixture (94%wt, Tg~187K) and observed similar behaviors from the phosphorescent probe (Pastukhov, Khudyakov, Vogel, & Kotelnikov, 2001). In this study, the phosphorescence spectral dynamics of the probe changed as a function of temperature, reflecting the temperature-dependent changes in the rates of relaxation processes in the matrix. Around Tg, the peak frequency of eosin exhibited a time-dependent red shift, due to lowering the electronic energy level of the excited solute state because of solvation dynamics. At temperatures above 219K, eosin phosphorescence decays at different wavelength exhibited approximately equal decay times, suggesting that the thermal fluctuations of solvent molecules became 3-4 order of magnitude faster compare to the deactivation rate of triplet eosin molecules to create the thermal equilibrium distribution of solvent configurations around excited solutes prior to the emission. Therefore, the observed pause in the non-radiative decay rate and the increase in stretching parameter β from our study might be attributed to the solvent molecules creating a thermal equilibrium distribution of solvent configurations around the excited riboflavin molecules prior to the emission.

Figure II-6

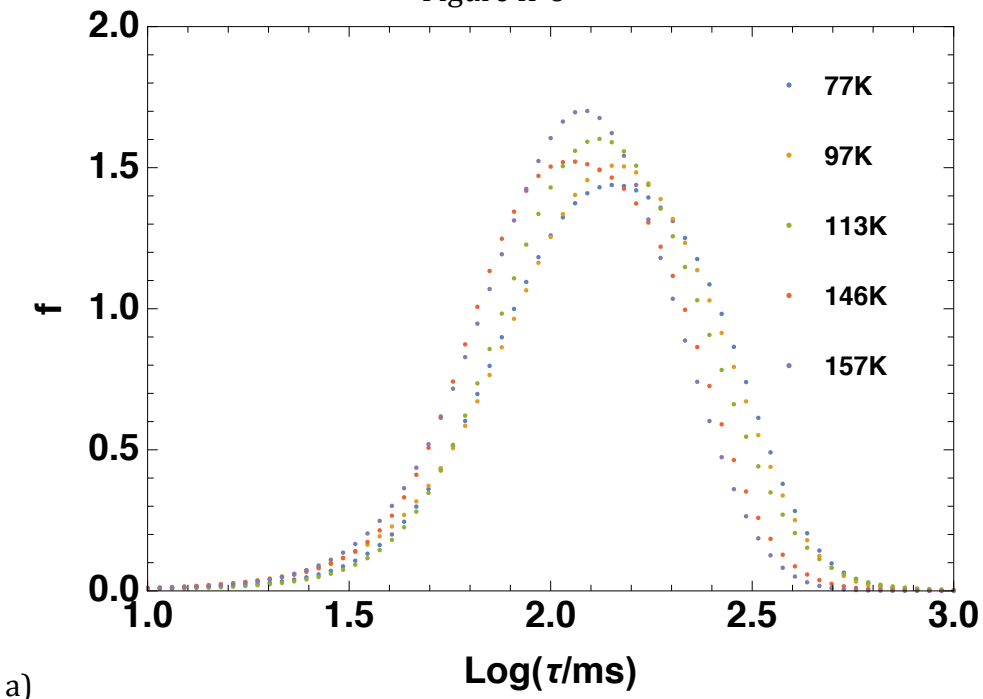

a)

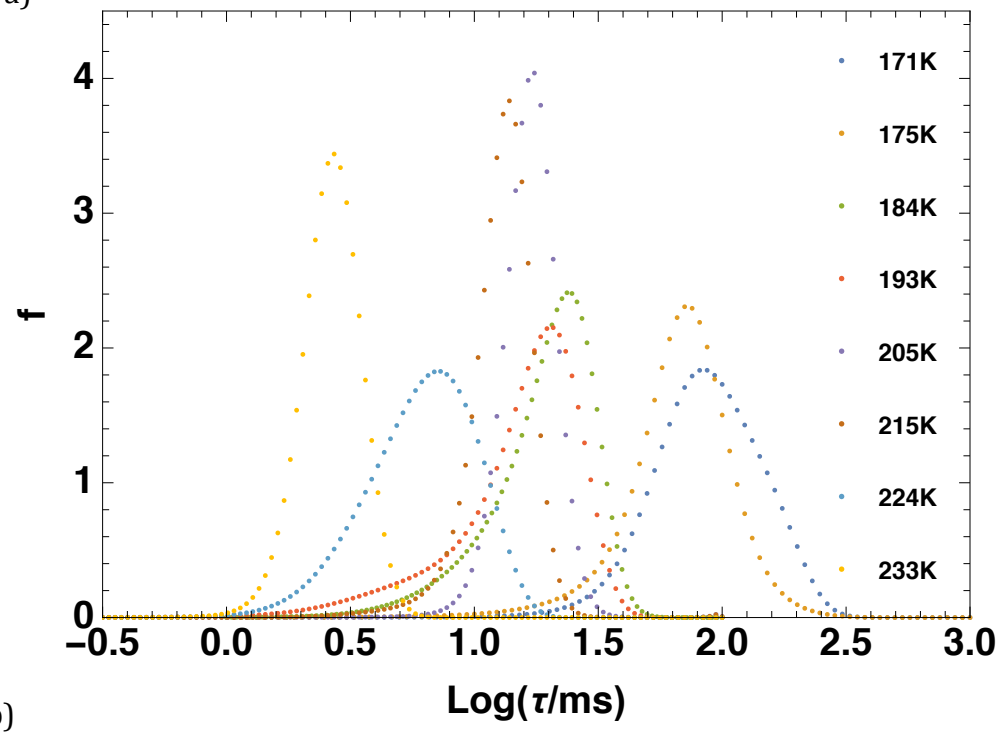

b)

Figure II-6: Plots of the MEM lifetime distribution of riboflavin phosphorescence in glycerol/water mixture at selected temperatures below Tg (a) and above Tg (b).

Figure II-7

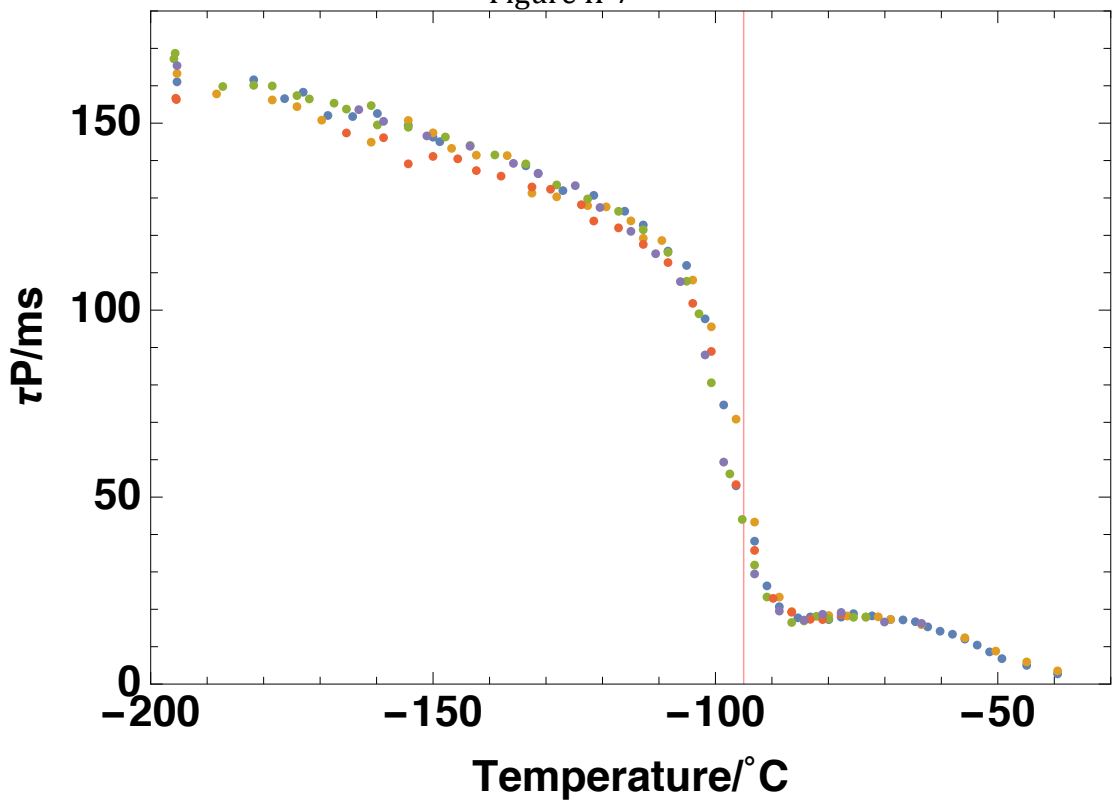

Figure II-7: Average phosphorescence lifetime from riboflavin in glycerol/water mixture as a function of temperature during ballistic heating from 77K onwards. Results from 5 replicates are shown here. The red thin line marks the estimated Tg of glycerol/water mixture.

Figure II-8

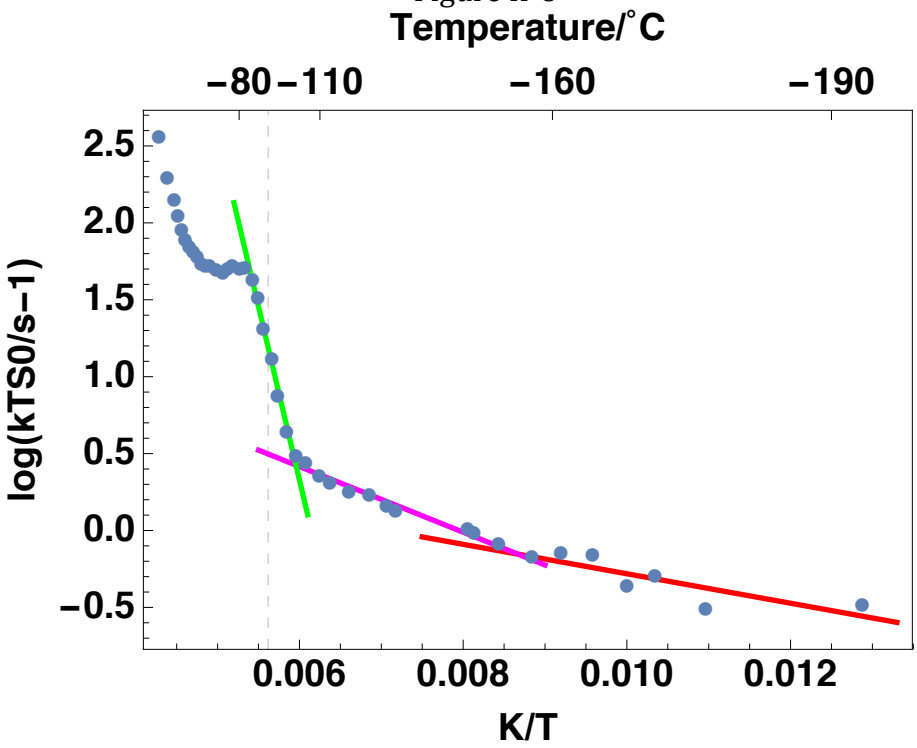

Figure II-8: Arrhenius plot of the rate of the non-radiative decay kTS0 for triplet riboflavin in glycerol/water mixture. The red, magenta, and green lines are Arrhenius fits to the data in different temperature ranges. The dashed grey line marks the Tg of glycerol/water mixture at 178K.

PART III: Ethanol/Water as the Matrix

The phosphorescence decays from riboflavin dispersed in ethanol/water (1:2 v/v) mixture were collected during ballistic heating. The decays were fitted using the MEM and the lifetime distributions obtained at selected temperatures are plotted in Figure II-9. As shown, the center of the lifetime distribution shifted from long lifetimes (~140ms) to short lifetimes (~40ms) as the temperature increased from 77K to 109K. From 109K to 197K, two distinct peaks were estimated from MEM: one centered at a longer lifetime (~40ms) and the other centered at a shorter lifetime (~5ms) (Figure II-9), suggesting a broadening in the lifetime distribution. As temperature increased, the centers of both peaks moved to short lifetime and the peak centered at short lifetime became more prominent than the one located at the long lifetime. The lifetimes at individual temperature point were calculated from the center of gravity of the lifetime distribution, as discussed before, and the calculated lifetimes are plotted as a function of temperature in Figure II-10. In comparison to the phosphorescence lifetime from riboflavin in glycerol/water mixture, which only slightly shortened from 160 to 110ms over the temperature range from 77 to 170K, riboflavin phosphorescence lifetime changed from 140 to 110ms within in very small temperature range, i.e. from 77 to 100K, and rapidly decreased from 110 to 40ms as the temperature further increased from 100 to 120K, prior to reaching the Tg of ethanol/water mixture. From 120K to 190K, the lifetime only gradually decreased from 40 to 25ms.

The non-radiative decay rate of triplet riboflavin was calculated based on (II-5, in which the radiative decay rate was approximated using the inverse of the longest phosphorescence lifetime of riboflavin measured in glycerol/water mixture. The logarithm of the non-radiative decay rate is plotted versus the inverse of the temperature in Figure II-11. As suggested by the solid lines in the plot, there were three distinct Arrhenius processes. The slope of the Arrhenius plot was used to estimate the activation energy of the non-radiative collisional quenching process. Over the temperature range from 77 to 97K, the fit of the non-radiative decay rate yielded an activation energy value of 1.2 kJ/mol. This small activation energy suggested that there was little motion in the glassy state of ethanol/water mixture over this temperature range. From 100 to 120K, the activation energy was increased to 12kJ/mol. This value was smaller than the typical activation energy for β relaxation. As reflected by the plateau in lifetime reduction at temperatures above 120K, the rate of non-radiative decay followed the same pattern as that of lifetime and the activation energy was calculated to be 2kJ/mol. Riboflavin phosphorescence lifetime exhibited distinct decay patterns in ethanol/water mixture. It was speculated that the low hydrogen bonding ability of ethanol compared to glycerol might be the cause of this phenomenon. As indicated by the molecular structure of ethanol, only the oxygen molecule of the hydroxyl group on ethanol is able to form hydrogen bonding with water. Additionally, research showed that the strength of hydrogen bond among clusters in the ethanol/water mixture was affected when the binary system was not well mixed on a molecular level (Dolenko, Burikov, Efitoriv, Plastinin, Patsaeva, & Dolenko, 2015). However, further research is needed to

understand the underlying mechanism of this very distinct behavior of riboflavin in ethanol/water mixture.

Figure II-9

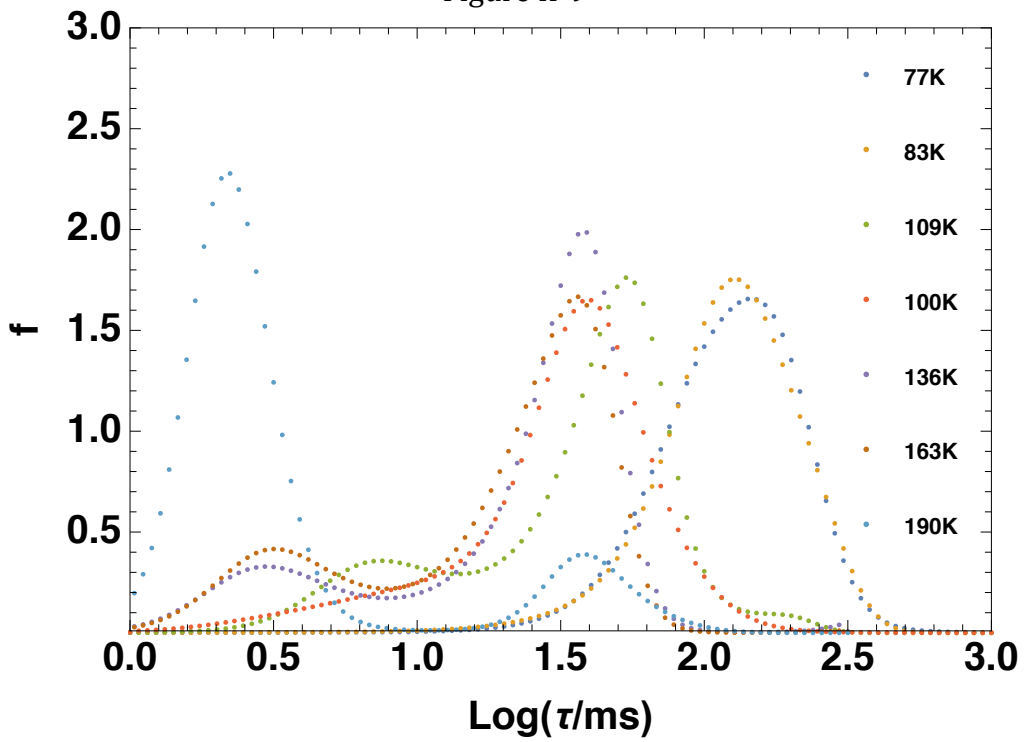

Figure II-9: Plots of the MEM lifetime distribution of riboflavin phosphorescence in ethanol/water mixture at selected temperatures.

FigureII-10

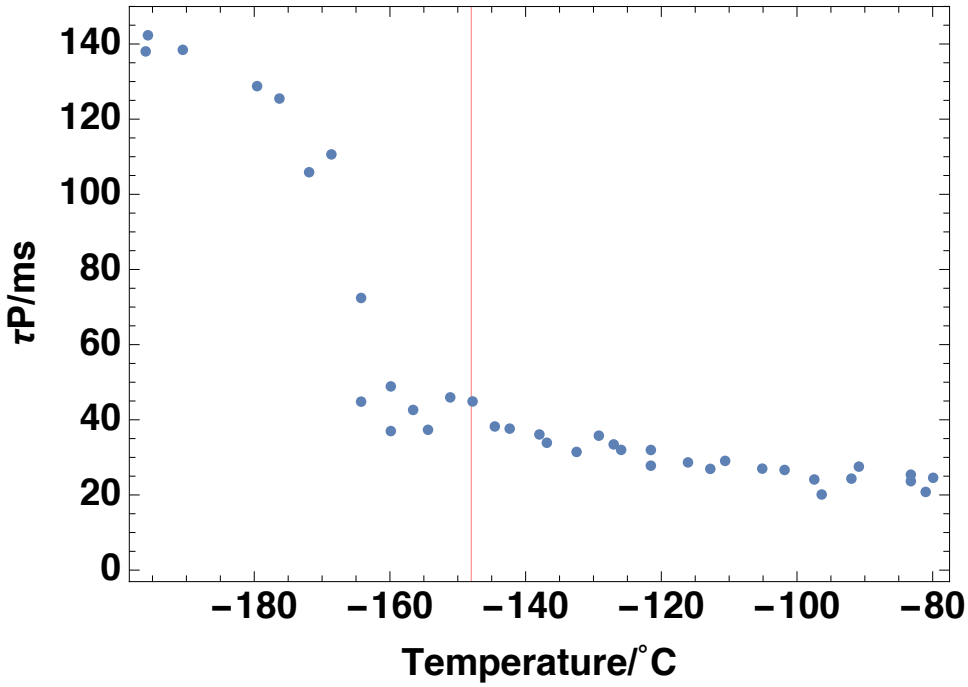

Figure II-10: Average phosphorescence lifetime from riboflavin in ethanol/water mixture as a function of temperature during ballistic heating from 77K upwards. The thin vertical red line marks the Tg of ethanol/water mixture.

Figure II-11

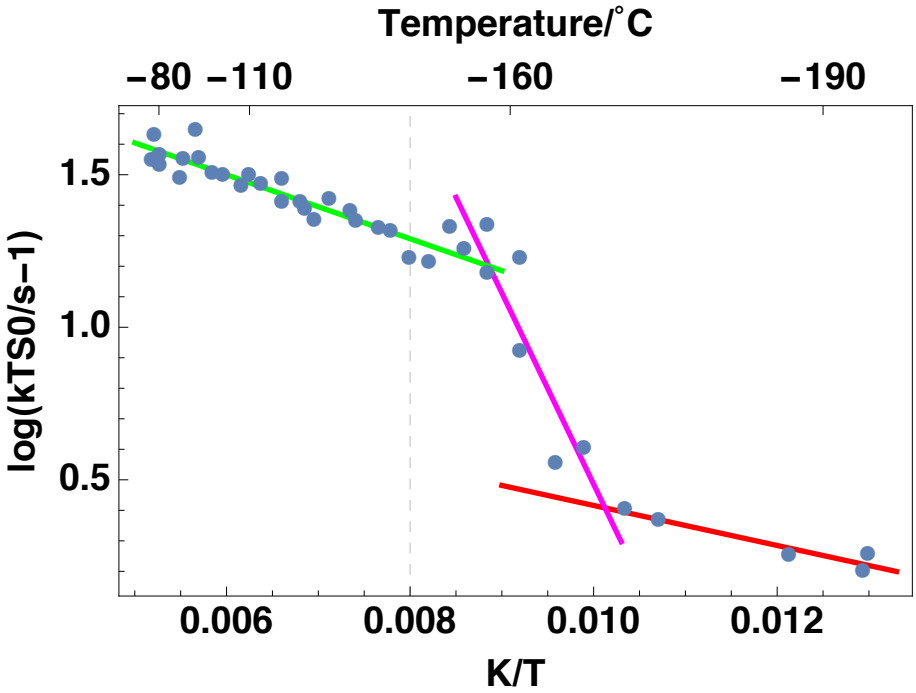

Figure II-11: Arrhenius plot of the rate of the non-radiative decay kTS0 for triplet riboflavin in ethanol/water mixture. The red, magenta, and green lines are Arrhenius fits to the data in different temperature ranges. The dashed grey line marks the Tg of ethanol/water mixture at 125K.

PART IV: Sucrose/Water as the Matrix

Phosphorescence decays of riboflavin in sucrose/water (30%wt) were collected over the temperature range from 77 to 240K. The Tg of the sucrose/water mixture used in our study was estimated to be 220K from an equilibrium temperature-composition phase diagram for water-sucrose mixtures (Chen, Sun, & Warncke, 2013). The lifetime distributions at selected temperatures obtained from fitting using MEM are plotted in Figure II-12: the center of lifetime distribution gradually moved to short lifetime as temperature increased, indicating that the riboflavin phosphorescence lifetime shortened as the temperature increased. The calculated lifetime from MEM is plotted against temperature in Figure II-13. The lifetime decreased monotonically with temperature. The decrease of riboflavin phosphorescence lifetime can be roughly divided into three regimes: 77~110K, 110~200K, and 200 ~240K. The decrease became steeper moving from one regime to another as temperature increased.

The rate of non-radiative decay of triplet riboflavin in sucrose/water mixture was calculated using (II-5) and the logarithm of k_{TS0} is plotted against 1/T to further estimate the activation energy of the non-radiative process in Figure II-14. The Arrhenius fits are presented by solid colored lines in the plot. As shown, from 77 to ~140K, the rate at which the rate of non-radiative decay increased was relatively small and the activation energy to quench the triplet riboflavin over this

temperature range was determined as 0.8kJ/mol. This extremely small value suggested that the molecular motions over this temperature range were highly prohibited and that triplet riboflavin was likely quenched by small amplitude of vibrational motions in the rigid glassy matrix. From 140 to 200K, the Arrhenius plot exhibited another regime with slightly higher activation energy of 3.2kJ/mol. Although two different behaviors were observed below Tg, this slight increase in Ea should not be interpreted as a transition to a distinct process, but it was possibly caused by the changes in heterogeneity in the glassy solvent system. Interestingly, the Tg of pure water is approximate 136K, which coincides with the starting point of the second regime. Therefore, the changes in the molecular interactions in the sucrose/water mixture above the Tg of pure water might be attributed to the slightly higher activation energy of this second regime. As temperature further increased from 200 to 230K, the activation energy over this range was determined to be 18.5kJ/mol- higher than the previous regime but still lower than a typical β relaxation process. Further investigation is needed to identify the molecular origin accounting for this regime. At temperatures above 230K, the slope increased rapidly and the non-radiative decay quickly transitioned to a high activation energy process. The activation energy for this process was estimated to be 116.5kJ/mol: this value is in par with the scale of α relaxation and this high activation energy process coincided with the estimated Tg of sucrose/water mixture. It is reasonable to speculate that the rapid de-excitation of triplet riboflavin is caused by the α relaxation process after Tg was surpassed.

Figure II-12

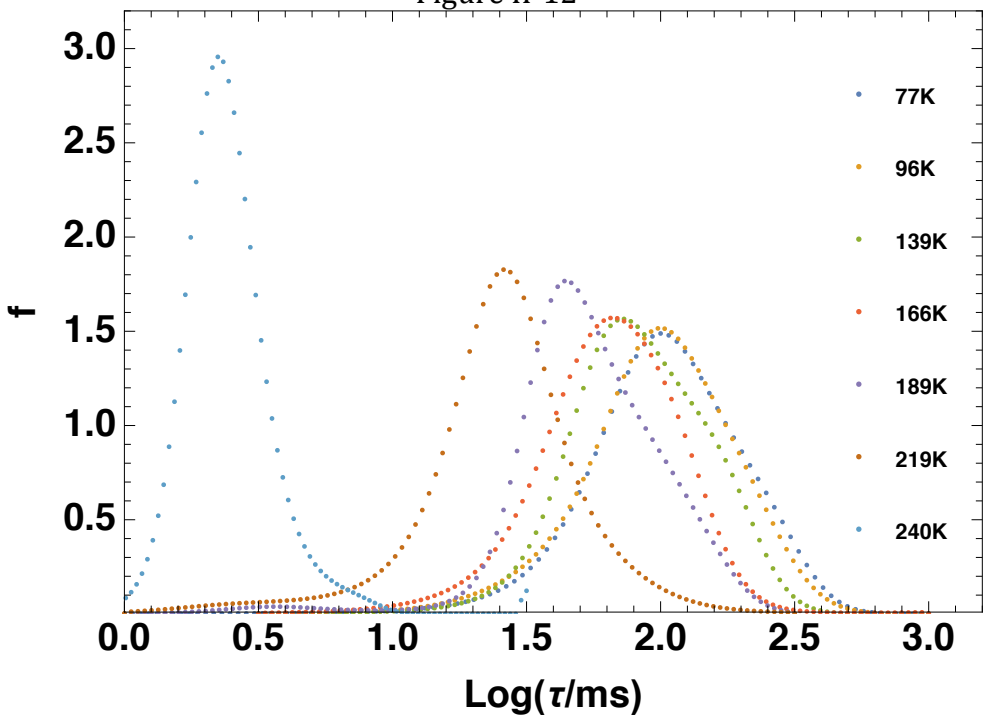

Figure II-12: Plots of the MEM lifetime distribution of riboflavin phosphorescence in sucrose/water mixture at selected temperatures.

Figure II-13

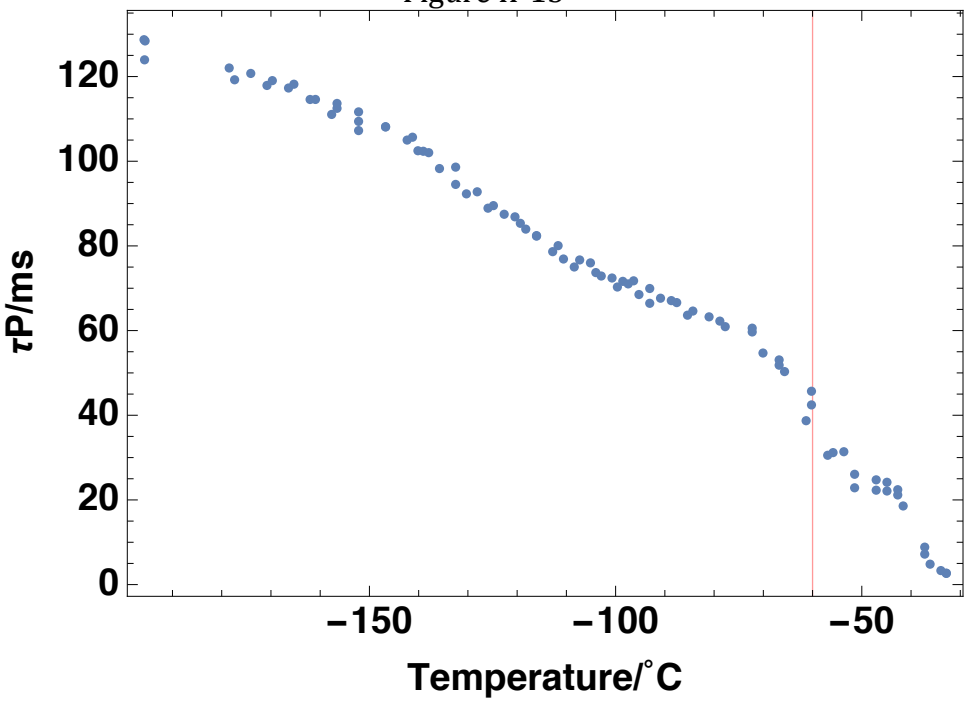

Figure II-13: Average phosphorescence lifetime from riboflavin in sucrose/water mixture as a function of temperature during ballistic heating from 77K upwards. The thin vertical red line marks the estimated Tg of sucrose/water mixture.

Figure II-14

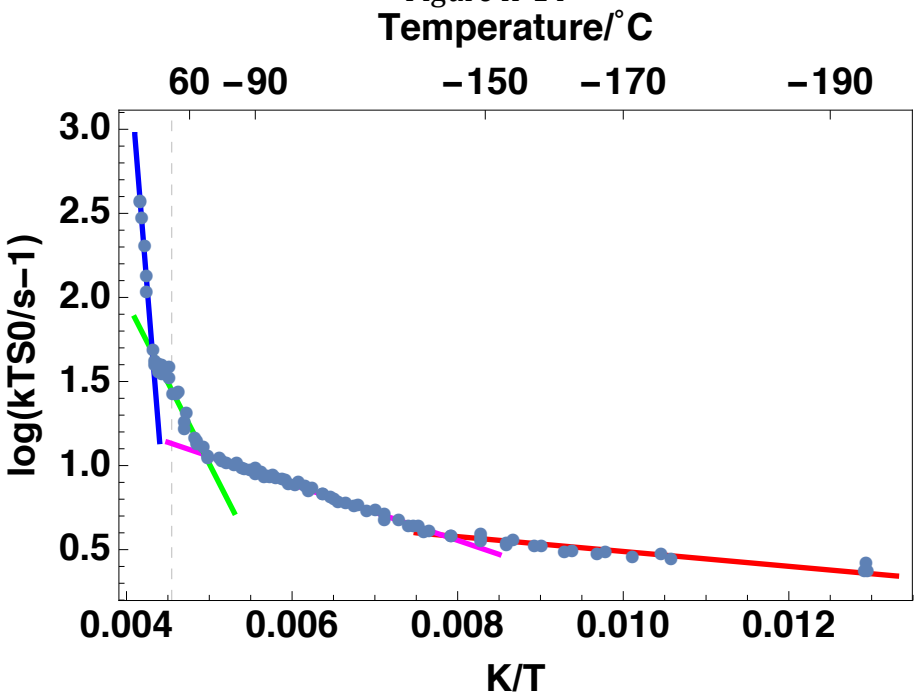

Figure II-14: Arrhenius plot of the rate of the non-radiative decay k_{TS0} for triplet riboflavin in sucrose/water mixture. The red, magenta, green, and blue lines are Arrhenius fits to the data in different temperature ranges. The dashed grey line marks the estimated Tg of sucrose/water mixture at 220K.

PART IV: Dextran/Water as the Matrix

Dextran/water mixture was rarely studied under cryogenic temperature, and no information is available in the literature on the Tg of this mixture. However, since the Tg of dextran is higher than that of sucrose, we speculate that the Tg of dextran/water mixture should be higher than that of sucrose/water mixture, thus above 220K. Phosphorescence intensity decays from riboflavin dispersed in dextran/water (30%wt) solution were collected over the temperature range from 77 to 230K. Selected MEM lifetime distributions are plotted in Figure II-15. As shown, the overall lifetime distribution moved towards a short lifetime regime as the temperature increased. Furthermore, two or more peaks appeared when temperature reached above 130K, which reflected a distinct change in lifetime distribution and indicated that the dextran/water mixture became more heterogeneous as the temperature increased. The MEM lifetime distributions also indicated greater heterogeneity in dextran/water binary system than the sucrose/water mixture.

As before, the average lifetime was calculated from the center of gravity of the MEM lifetime distribution. In Figure II-16, the calculated lifetime is plotted against temperature. As temperature increased from 77K to 230K, the phosphorescence lifetime decreased from 140ms to 5ms. The decrease in phosphorescence lifetime became slightly faster as the temperature reached 200K. In the absence of oxygen quenching and reverse intersystem crossing, the reduction in lifetime reflected the

increase in non-radiative decay, which provided a measure of molecular mobility of the local environment in the vicinity of the phosphorescent probe.

The rate of non-radiative decay at each temperature point was calculated based on (II-5 and the logarithm of the calculated non-radiative rate is plotted against the inverse of temperature in Figure II-17. Three distinct regimes marked in red, pink, and green can be observed in the logarithm plot of non-radiative decay rate. From 77 to 140K, the rate of non-radiative decay only slightly increased, and the fit of the data yielded an activation energy of 1.3kJ/mol. This small activation energy indicated that there is little molecular motion in the rigid glassy matrix over this temperature range. From 140 to 200K, the slope became steeper compared to the first regime, and the activation energy was calculated as 4.3kJ/mol. Again, this increase in activation energy was not indicative of any distinct relaxation process, but was possibly a result of the heterogeneity change in the matrix. Once more, the emergence of the second regime on the Arrhenius plot coincided with the estimated Tg of pure water is, i.e., 136K (Trejo González et al., 2011). This slightly higher activation energy process might be a result of the new dynamics with hydrogen bonding in dextran-dextran, dextran-water and water-water regimes after the Tg of pure water is surpassed. From 200 to 230K, the modified Arrhenius plot exhibited a third regime with the highest activation energy, 30kJ/mol, in the dextran/water mixture. This value of activation energy was roughly comparable to the activation energy of a typical β relaxation process, which suggested that over the temperature range from 200 to 230K, the prominent β relaxation process in dextran/water

mixture attributed to the de-excitation of triplet riboflavin. As discussed before, the Tg of dextran/water mixture used in this study is estimated to be above 220K, therefore from 200-230K, the phosphorescence from riboflavin is likely to be quenched primarily by the β relaxation in the dextran/water matrix.

Figure II-15

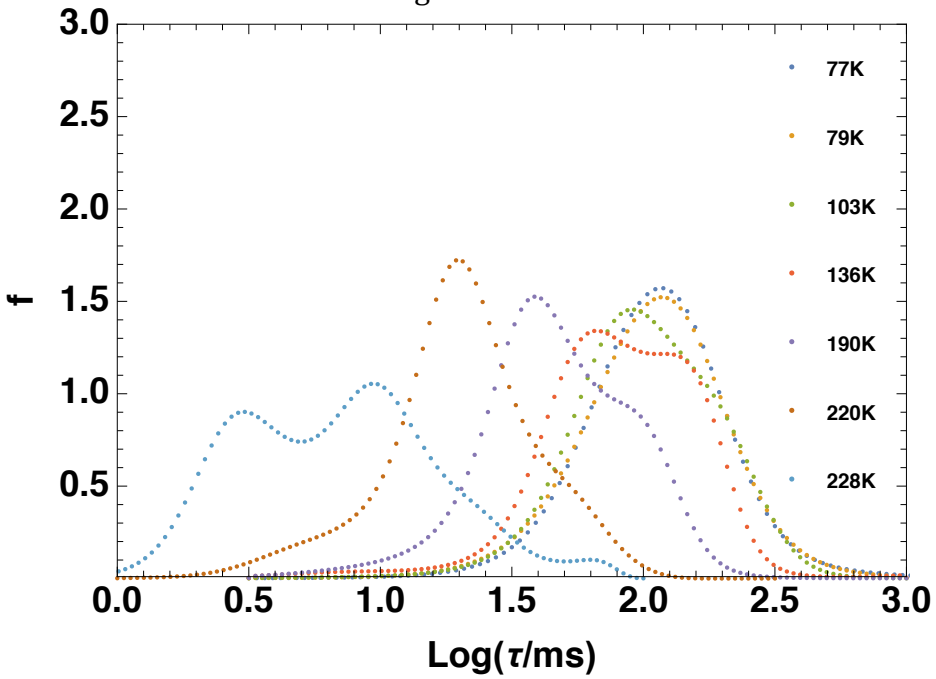

Figure II-15: Plots of the MEM lifetime distribution of riboflavin phosphorescence in dextran/water mixture at selected temperatures.

Figure II-16

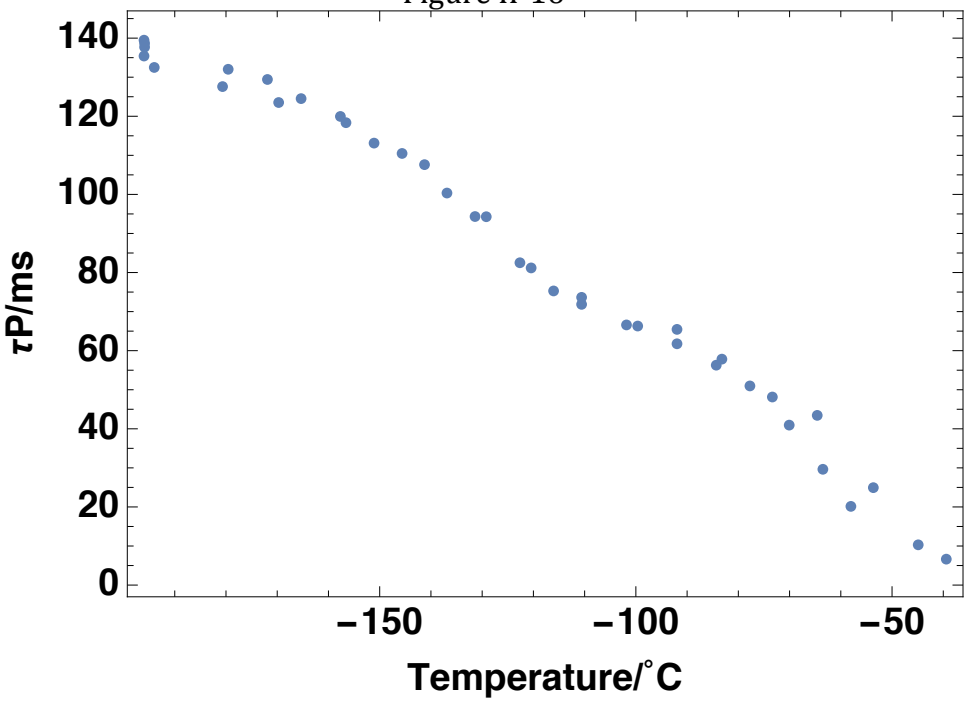

Figure II-16: Average phosphorescence lifetime from riboflavin in dextran/water mixture as a function of temperature during ballistic heating from 77K upwards.

Figure II-17

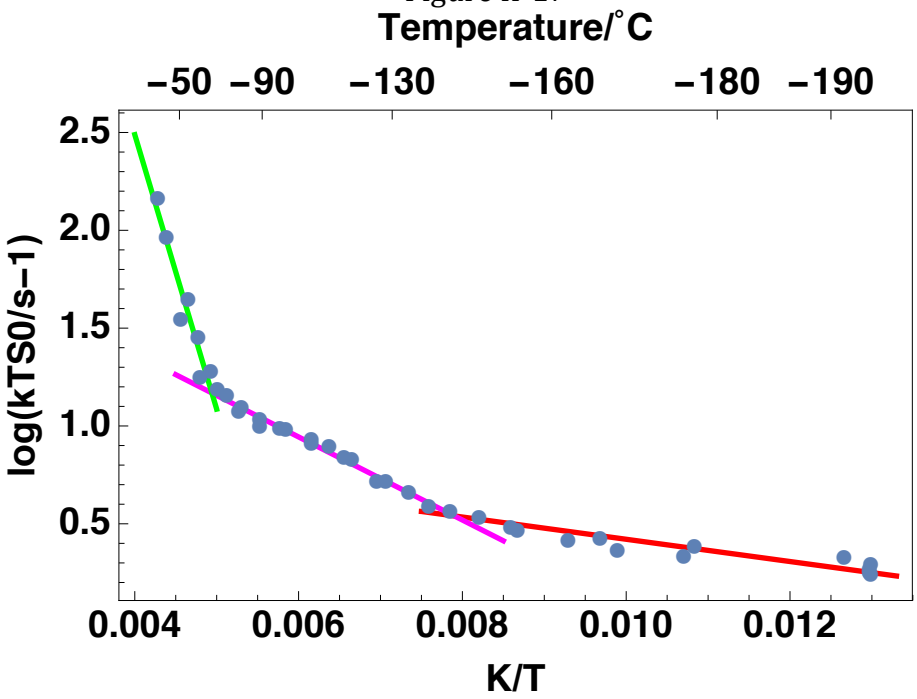

Figure II-17: Arrhenius plot of the rate of the non-radiative decay kTS0 for triplet riboflavin in dextran/water mixture. The red, magenta, and green lines are Arrhenius fits to the data in different temperature ranges.

Conclusions

Phosphorescence intensity decays of riboflavin were first characterized under 77K- the lowest temperature our current equipment allowed for in four matrices: glycerol/water (3:1 v/v), ethanol/water (1:2 v/v), sucrose/water (30%wt), and dextran/water (30%wt). Logarithmic plots of the riboflavin phosphorescence decays at 77K yielded curved lines, indicating that riboflavin phosphorescence decays were not single exponential. Stretched and multi-exponential models were used to fit the decays and the three-exponential function exhibited the most satisfactory fit for the data. Improves fits to the decays, however, were achieved using the MEM. The triplet lifetimes of riboflavin in glycerol/water, ethanol/water, sucrose/water, and dextran/water obtained using MEM were 170ms, 140ms, 138ms, and 127ms, respectively. The longest lifetime, 170ms, measured in our study matched the previous reported riboflavin natural phosphorescence lifetime, and its the inverse of it was thus used as the intrinsic radiative decay rate of riboflavin. The difference in measured phosphorescence lifetime at 77K in four matrices was attributed to the different matrix mobility due to different compositions.

The riboflavin phosphorescence decays in four matrices were also collected during ballistic heating from 77K upwards. The decays were fitted using MEM and the activation energy over different temperature regimes in different matrices were analyzed accordingly. Our results suggested that from the perspectives of timescale of relaxation processes and the activation energy of relaxation processes, riboflavin phosphorescence exhibited good sensitivity towards β relaxations in glycerol/water

mixture, a well characterized system whose dielectric spectra were readily available for comparison. Riboflavin phosphorescence decays exhibited different behaviors in the other three matrices. Further investigation is needed to fully understand the underlying mechanisms of our observations.

References

Bhattacharya, S., & Suryanarayanan, R. (2011). Molecular motions in sucrose-PVP and sucrose-sorbitol dispersions: I. implications of global and local mobility on stability. *Pharmaceutical Research, 28*(9), 2191-2203. doi:10.1007/s11095-011-0447-0

Capaccioli, S., Ngai, K. L., & Shinyashiki, N. (2007). The johari-goldstein ß-relaxation of water. *Journal of Physical Chemistry B, 111*(28), 8197-8209. doi:10.1021/jp071857m

Chen, H., Sun, L., & Warncke, K. (2013). Heterogeneous ordered-disordered structure of the mesodomain in frozen sucrose-water solutions revealed by multiple electron paramagnetic resonance spectroscopies. *Langmuir, 29*(13), 4357-4365. doi:10.1021/la3049554

Cicerone, M. T., Tellington, A., Trost, L., & Sokolov, A. (2003). Substanstially improved stability of biological agents in dried form: The role of glassy dynamics in preservation of biopharmaceuticals. *BioProcess International, 1*, 1-9.

Cicerone, M. T., & Douglas, J. F. (2012). ß-relaxation governs protein stability in sugar-glass matrices. *Soft Matter, 8*(10), 2983-2991. doi:10.1039/c2sm06979b

Corradini, M. G., & Ludescher, R. D. (2015). Making sense of luminescence from GRAS optical probes. *Current Opinion in Food Science, 4*, 25-31. doi:10.1016/j.cofs.2015.04.004

Dolenko, T. A., Burikov, S. A., Efitorov, A. O., Plastinin, I. V., Yuzhakov, V. I., Patsaeva, S. V., & Dolenko, S. A. (2015). Raman spectroscopy of water-ethanol solutions: The estimation of hydrogen bonding energy and the appearance of clathrate-like structures in solutions. *Journal of Physical Chemistry A, 119*(44), 10806-10815. doi:10.1021/acs.jpca.5b06678

Draganski, A. R. (2014). *A systematic study of phosphorescent probes in cryosolvents, amorphous solids, and proteins.* (Unpublished Doctoral dissertation). Rutgers, The State University of New Jersey, New Brunswick.

Draganski, A. R., Tiwari, R. S., Sundaresan, K. V., Nack, T. J., You, Y., & Ludescher, R. D. (2010). Photophysical probes of the amorphous solid state of proteins. *Food Biophysics, 5*(4), 337-345. doi:10.1007/s11483-010-9185-9

Dranca, I., Bhattacharya, S., Vyazovkin, S., & Suryanarayanan, R. (2009). Implications of global and local mobility in amorphous sucrose and trehalose as determined by differential scanning calorimetry. *Pharmaceutical Research, 26*(5), 1064-1072. doi:10.1007/s11095-008-9817-7

Fuhrmann, N., Brubach, J., & Dreizler, A. (2013). *Spectral decomposition of phosphorescence decays*

Gao, C., Wang, T., Liu, X., Zhou, G., & Hua, T. (2007). Composition dependence of the Adam–Gibbs cooperative relaxation parameters in glycerol aqueous solutions. *Thermochimica Acta, 456*, 19-24. doi:10.1016/j.tca.2007.02.001

Hayashi, Y., Puzenko, A., & Feldman, Y. (2006). Slow and fast dynamics in glycerol–water mixtures. *Journal of Non-Crystalline Solids, 352*, 4696-4703. doi:10.1016/j.jnoncrysol.2006.01.113

He, X., Fowler, A., & Toner, M. (2006). Water activity and mobility in solutions of glycerol and small molecular weight sugars: Implication for cryo- and lyopreservation. *Journal of Applied Physics, 100*(7), 074702. doi:10.1063/1.2336304

Imamura, K., Sakaura, K., Ohyama, K. -., Fukushima, A., Imanaka, H., Sakiyama, T., & Nakanishi, K. (2006). Temperature scanning FTIR analysis of hydrogen bonding states of various saccharides in amorphous matrixes below and above their glass transition temperatures. *Journal of Physical Chemistry B, 110*(31), 15094-15099. doi:10.1021/jp057527o

Kaminski, K., Kaminska, E., Hensel-Bielowka, S., Chelmecka, E., Paluch, M., Ziolo, J., . . . Ngai, K. L. (2008). Identification of the molecular motions responsible for the slower secondary (ß) relaxation in sucrose. *Journal of Physical Chemistry B, 112*(25), 7662-7668. doi:10.1021/jp711502a

Ludescher, R. D., Shah, N. K., McCaul, C. P., & Simon, K. V. (2001). Beyond tg: Optical luminescence measurements of molecular mobility in amorphous solid foods. *Food Hydrocolloids, 15*(4-6), 331-339. doi:10.1016/S0268-005X(01)00050-9

Menzel, R. (2001). *Photonics
Photonics: Linear and nonlinear interactions of laser light and matter* (1 edition ed.) Springer.

Moore, W. M., McDaniels, J. C., & Hen, J. A. (1977). The photochemistry of riboflavin-vi. the photophysical properties of isoalloxazines. *Photochemistry & Photobiology, 25*(6), 505.

Pastukhov, A. V., Khudyakov, D. V., Vogel, V. R., & Kotelnikov, A. I. (2001). A supercooled glycerol-water mixture: Evidence for the large-scale heterogeneity? *Chemical Physics Letters, 346*(1-2), 61-68. doi:10.1016/S0009-2614(01)00951-4

Penzkofer, A. (2012). Photoluminescence behavior of riboflavin and lumiflavin in liquid solutions and solid films. *Chemical Physics, 400*, 142-153. doi:10.1016/j.chemphys.2012.03.017

Penzkofer, A., Tyagi, A., Slyusareva, E., & Sizykh, A. (2010). Phosphorescence and delayed fluorescence properties of fluorone dyes in bio-related films. *Chemical Physics, 378*(1–3), 58-65. doi:http://dx.doi.org/10.1016/j.chemphys.2010.10.001

Pravinata, L. C., You, Y., & Ludescher, R. D. (2005). Erythrosin B phosphorescence monitors molecular mobility and dynamic site heterogeneity in amorphous sucrose. *Biophysical Journal, 88*(5), 3551-3561. doi:http://dx.doi.org/10.1529/biophysj.104.054825

Richert, R. (1998). Molecular dynamics analyzed in terms of continuous measures of dynamic heterogeneity. *Journal of Non-Crystalline Solids, 235-237*, 41-47.

Richert, R. (2000). Triplet state solvation dynamics: Basics and applications. *Journal of Chemical Physics, 113*(19)

Rodriguez, H. B., San Roman, E., Duarte, P., Machado, I. F., & Ferreira, L. (2012). *Eosin Y triplet state as a probe of spatial heterogeneity in microcrystalline cellulose*

Sahni, E. K., Pikal, M. J., Thakur, M., Chaney, M. A., Sherman, G., & Siegel, D. P. (2015). Dynamics in polysaccharide glasses and their impact on the stability of encapsulated flavors. *Food Biophysics,* , 14p. doi:10.1007/s11483-015-9405-4

Sjöström, J., Mattsson, J., Bergman, R., Johansson, E., Josefsson, K., Svantesson, D., & Swenson, J. (2010). Dielectric secondary relaxation of water in aqueous binary glass-formers. *Physical Chemistry Chemical Physics, 12*(35), 10452-10456. doi:10.1039/c001275k

Steinbach, P. J., Ionescu, R., & Matthews, C. R. (2002). Analysis of kinetics using a hybrid maximum-entropy/nonlinear-least-squares method: Application to protein folding. *Biophysical Journal, 82*, 2244-2255. doi:10.1016/S0006-3495(02)75570-7

Sudo, S., Shimomura, M., Saito, T., Kashiwagi, T., Shinyashiki, N., & Yagihara, S. (2002). Dielectric study on α- and β-processes in supercooled diethyleneglycol– and pentaethyleneglycol–water mixtures. *Journal of Non-Crystalline Solids, 305*(1–3), 197-203. doi:http://dx.doi.org/10.1016/S0022-3093(02)01094-3

Sun, M., Moore, T. A., & Song, P. (1972). Molecular luminescence studies of flavines. I. excited states of flavines. *Journal of American Chemical Society, 94*(5), 1730-1740.

Tiwari, R. S., & Ludescher, R. D. (2010). Vanillin phosphorescence as a probe of molecular mobility in amorphous sucrose. *Journal of Fluorescence, 20*(1), 125.

Trejo González, J. A., Longinotti, M. P., & Corti, H. R. (2011). The viscosity of glycerol-water mixtures including the supercooled region. *Journal of Chemical and Engineering Data, 56*(4), 1397-1406. doi:10.1021/je101164q

You, Y., & Ludescher, R. D. (2010). The effect of molecular size on molecular mobility in amorphous oligosaccharides. *Food Biophysics, 5*(2), 82-93. doi:10.1007/s11483-010-9148-1

Chapter III Investigating Riboflavin Phosphorescence Sensitivity towards Temperature Induced Molecular Mobility in Amorphous Sucrose

Introduction

Amorphous carbohydrates have been widely used as excipients for enzymes, flavors, bioactive compounds and active drug ingredients to achieve desired stability, solubility, and functionality (Cicerone & Douglas, 2012; Dranca, Bhattacharya, Vyazovkin, & Suryanarayanan, 2009; Sahni et al., 2015). The molecular mobility of the carrier materials has a great impact on the formulation design and product quality of labile biological agents. Despite numerous practical applications in pharmaceutical, cosmetics, and food industries, the mechanism of how the rigid glass retards the degradation process is not fully understood.

Earlier studies have suggested glass transition temperature, Tg, as an indicator of mobility, and consequently, stability (Cicerone, Tellington, Trost, & Sokolov, 2003). An amorphous solid is hard and rigid below Tg and it turns into melt above Tg. At Tg, the time scale of structural relaxation, or cooperative α relaxation, becomes shorter than 100s, which gives rise to the global mobility and macroscopic flow of the material. However, more recent studies have shown that degradation of labile ingredients could still happen at temperature as low as 50K below Tg in a glassy carbohydrate matrix and have suggested that the instability was due to local mobility, or secondary relaxations (Bhattacharya & Suryanarayanan, 2011). Although the mechanism through which secondary relaxations affect stability is still not fully understood, the current view on secondary relaxations is that there are two

distinct relaxations, the faster γ relaxation and the slower β relaxation (Cicerone & Douglas, 2012). The γ relaxation happens on a picosecond time scale and is associated with the rotation of the hydroxymethyl groups of carbohydrates; the β relaxation is a universal Johari-Goldstein process in all glass formers that happens on micro- to milli- second timescale and is attributed to the intermolecular motions via glycosidic linkage in sugar glass (Bhattacharya & Suryanarayanan, 2011; Cicerone & Douglas, 2012; Imamura et al., 2006). Recently, Cicerone & Douglas, (2012) have found that secondary relaxations, rather than α relaxations, largely governs the degradation rate of encapsulated labile compounds. A better understanding of secondary relaxations in amorphous carbohydrates would be of invaluable practial importance to the pharmaceutical and food industries.

Our previous work has examined the photophysical properties of triplet riboflavin under cryogenic temperatures in four aqueous solution matrices and our results showed that the phosphorescence lifetime of riboflavin changed in relation to the mobility changes in the matrices.

The goal of this study was to explore the potential of using riboflavin as a phosphorescent probe to monitor molecular mobility in amorphous carbohydrate matrices. This research investigated how the phosphorescence emission spectra and lifetime of riboflavin changed in response to the molecular mobility changes in amorphous sucrose films modulated by temperature. Our results confirmed that both steady state and time-resolved phosphorescence from riboflavin in amorphous

sucrose solid films exhibited sensitivity towards molecular mobility changes over the temperature range from -30 to 100˚C.

Materials and Methods

Sample Preparation: 200μM riboflavin (Sigma-Aldrich, St. Louis, MO, USA) stock solution was prepared in distilled and deionized water. To prepare glassy riboflavin-sucrose films, sucrose (Kodak, Rochester, NY, USA) was added to 1mL of 200μM riboflavin solution to reach a final sucrose concentration of 30wt %. The sucrose concentration was verified using an Atago refractometer (Model N-4E, Bellevue, WA, USA). An approximate riboflavin/sucrose molar ratio of $2{:}10^4$ was reached. The essentially low riboflavin concentration in sucrose films was chosen to avoid probe-probe interaction (Richert, 2000).

Quartz slides that are 30mm long, 13.5mm wide, and 0.6mm thick, custom made by NSG Precision Cells (Farmingdale, NY, USA) were used for amorphous riboflavin-sucrose film preparation. Slides were thoroughly cleaned before use. An aliquot of 24μL riboflavin-sucrose solution was spread on a quartz slide to form a transparent thin layer of amorphous sucrose film. The amorphous films were first dried under room temperature air-flow supplied by a heat gun (Model 201A, Master Appliance Corp., Racine, WI) for 15 min and then stored in a desiccator against DrieRite and P_2O_5 (Fisher Scientific, Fair Lawn, NJ, USA) for at least 96 hours to further reduce water content to ~0%RH before phosphorescence measurement.

The glass transition temperature (Tg) of sucrose was reported to be around 65 ˚C. In this study, Differential Scanning Calorimetry (DSC Q200, TA Instruments, New Catsle, DE, USA) measurements were used to verify the Tg of the sucrose sample.

The midpoint of the glass transition curve was used to quantify Tg and it was determined that the Tg of sucrose used in this study was 57.25˚C.

Phosphorescence Measurements: Phosphorescence measurements were conducted using a Cary Eclipse Spectrophotometer (Agilent Technologies, Santa Clara, CA, USA). Phosphorescence from riboflavin in glassy sucrose films was measured over the temperature range from -30 to 100˚C, at 10˚C interval. Temperature was adjusted using a TLC-50 thermoelectric heating/cooling system (Quantum Northwest, Spokane, WA, USA). Each quartz slide covered with optically clear riboflavin-sucrose glassy film was placed in a 1cm×1cm×3cm quartz cuvette (FireflySci Inc., Brooklyn, NY, USA) for the measurement. The cuvette was capped with a lid and sealed on the sides. To eliminate oxygen and to maintain a low humidity environment during the measurement, a stream of dry nitrogen was introduced into the cuvette through the gas inlet port on the lid. Each cuvette was flushed with dry nitrogen for at least 15 min to create an oxygen-free environment before measurement. A stream of dry air was blown across the cuvette holder to reduce condensation at low temperatures. For all measurements in this study, both monochromator slit widths were set to 20nm to maximize the signal, delay time and gate time set to 0.2 and 5ms, and each dataset was collected from 1 flash.

Steady-State Measurements: Delayed luminescence emission spectra were collected from 480 to 700nm when excited at 440nm. Emission spectra of pure sucrose glassy films were collected under the same conditions. The background spectra were

subtracted from that of riboflavin to eliminate the contribution of light scattering and impurities from sucrose before data analysis.

Delayed luminescence spectra consisted of two peaks: a delayed fluorescence peak located around 515nm and a phosphorescence peak located around 620nm. The log-normal function (III-1) has been shown to adequately describe other phosphorescence emission spectra. However, in the riboflavin doped samples, the delayed fluorescence and phosphorescence peaks were located very close to each other (less than 100nm apart). An open-source spectral analysis program, Fityk version 0.9.8 (http://fityk.nieto.pl/) was used to deconvolute these two peaks (Wojdyr, 2010). A sum of two log-normal functions (III-1) were simultaneously used to fit the overall spectra using the Nelder-Mead Simplex algorithm and the fit was judged based on the weighted sum of squared residuals (Wojdyr, 2010).

$$\mathrm{I}(\nu) = \sum I_{oi} * \exp\{-\ln(2)\left(\frac{\ln\left\{1 + \left[\frac{2\mathrm{b}(\nu_i - \nu_{\mathrm{Pi}})}{\Delta_i}\right]\right\}}{\mathrm{b}_i}\right)^2\} \quad \text{(III-1)}$$

In one log-normal function, I_{0i} corresponds to the peak intensity of emission spectra, ν_P is the wavenumber of maximum emission intensity, Δ_i is the line width parameter, and b_i is an asymmetry parameter. The value of bandwidth Γ_i, which is the full width at half maximum (FWHM) calculated from the line width (Δ_i) and asymmetry parameter (b_i), was directly estimated by Fityk. The subscription *i* indicates whether it is the delayed fluorescence or phosphorescence spectra.

Time-resolved Measurements: Phosphorescence decays were collected at 620nm using a 440nm excitation wavelength. Each measurement was the average of 50 cycles and a total decay time of 1000ms was collected for measurement at each temperature. To analyze the decays, three fitting models were used in this study: stretched exponential, multi-exponential, and Maximum Entropy Method (MEM).

Due to the different relaxation behaviors of phosphorescent probes residing in distinct regions in the glassy matrix, phosphorescence decays cannot be described by a single relaxation function. Two fitting models, stretched exponential and multi-exponential, have been extensively used to describe heterogeneous decays. Yet, the stretched exponential model is sometime insufficient to satisfactorily describe complex data, while multi-exponential function suffers from the difficulty to find the global minimum while minimizing the parameters used. Besides, there is little independence validation of the meaning of the parameters from the multi-exponential model. Therefore, a hybrid algorithm that combines the Maximum Entropy Method with Nonlinear least squares was used to as an alternative probabilistic approach to analyze the data. The free software MemExp, version 4.0, was downloaded through the NIH Center for Molecular Modeling (http://cmm.cit.nih.gov/memexp/). This method uses the MEM to guide a series of discrete NLS fits during the analysis process, which directs a continuous description to evolve and eventually results in an automated and objective approach to solve multiple-minimum problem (Steinbach, Ionescu, & Matthews, 2002).

Analysis of Phosphorescence Decays: To analyze the phosphorescence decays, all negative values were first eliminated to allow for the use of Poisson weight to give more importance to the initial part of decay than the tail of the decay in data analysis. Then, in order to avoid over-fitting of the instrumentation noises at the tail of the decay, the tail was thinned and chopped off on a case-to-case basis. A Mathematica 10.0 (Wolfram Research, Inc., Champaign, IL, USA) routine was programmed to fit the phosphorescence decay with the proposed models and to evaluate their adequacy. The goodness of fit was judged by R^2, a plot of modified residuals ($^{(data-fit)}/_{data^{1/2}}$), and Akaike information criterion (AIC).

The stretched exponential model is presented as (III-2):

	$I(t) = I(0)\times\exp\left[-(^{t}/_{\tau})^{\beta} + c\right]$	(III-2)

where I(0) is the initial intensity at t=0, τ is the fitted stretched lifetime, and β is the stretching exponent factor. The average lifetime was calculated as follow (III-3) using the parameters τ and β from (III-2:

	$\tau_s = \frac{\tau}{\beta}\Gamma(\frac{1}{\beta})$	(III-3)

in which, Γ is the gamma function. In this model, the stretching exponent factor β is a measure of the width of lifetime distribution that varies from 0 to 1. A value of 1 indicates complete homogeneity, whereas a value close to 0 suggests great heterogeneity in the system. This parameter reflects the non-exponential nature of

the decay and describes the distribution of dynamically distinct regions in the amorphous solid.

In the multi-exponential model (Eq. III-4):

	$$I(t) = I(0) * \sum_{n=1}^{n} \alpha_i \exp\left(-\frac{t}{\tau_i}\right)$$	(III-4)

I(0)is the initial intensity at t=0, n is the number of lifetime components, and τ_i and α_i are the lifetime and amplitude of each component. The values of τ_i reflect the molecular mobility of the heterogeneous matrix and the values of α_i represent the distribution of these energetically distinct islands. The average lifetime from multi-exponential model was calculated from the population average (III-5):

	$$\tau_m = \sum_{i}^{n} \alpha_i \tau_i$$	(III-5)

The MEM algorithm utilizes a maximum entropy function and nonlinear least squares method to fit the phosphorescence decays into distributed lifetimes. The lifetimes were calculated from amplitude-weighted average using a program written with Mathematica. Lifetime distributions from three fitting methods were compared and results will be discussed in Results and Discussion section.

Photophysical Rate Constants: The calculated average lifetimes provide a means to calculate the rate constant of triplet state de-excitation (k_P) and consequently the

rate constant of non-radiative decay (k_{TS0}), which is a direct measure of matrix mobility-controlled quenching.

Phosphorescence lifetime is determined by the rate constants of all possible de-excitation pathways (Eq. III-6):

$$\frac{1}{\tau} = k_P = k_{RP} + k_{TS1} + k_{TS0} + k_Q[O_2] \quad \text{(III-6)}$$

the rate constant of radiative decay (k_{RP}), an intrinsic property of the phosphorescent probe; the rate constant of reverse intersystem crossing (k_{TS1}); the rate constant of non-radiative decay (k_{TS0}), a measure of matrix-induced quenching; and the rate constant of collisional quenching with oxygen ($k_Q[O_2]$). In this study, k_{RP} was calculated from the phosphorescence lifetime of riboflavin in glycerol/water mixture (3:1 v/v) at 77K as stated in Chapter I, under the assumption that all the other de-excitation pathways were negligible under this extremely low temperature. The value of k_{TS1} was calculated from the ratio of the intensity of delayed fluorescence and phosphorescence (Parker, 1968):

$$I_{DF}/I_P = \phi_F \left(k_{TS1}/k_{RP}\right) \quad \text{(III-7)}$$

in which ϕ_F is the quantum yield of fluorescence. A value of 0.37 was reported as the quantum yield of riboflavin fluorescence in starch films; this value was used as an estimated ϕ_F in amorphous solid films in the calculation (Penzkofer, 2012). The temperature dependence of rate constant k_{TS1} can be characterized by the Arrhenius equation:

	$k_{TS1}(T) = k^{\circ}_{TS1} \exp\left(-\frac{\Delta E_{TS}}{RT}\right)$	(III-8)

in which k°_{TS1} is the maximum reverse intersystem crossing rate at high temperature, ΔE_{TS} is the activation energy required for reverse intersystem crossing, and R is the universal gas constant of 8.314 J/K·mol (Pravinata et al., 2005; You & Ludescher, 2007). Therefore, Eq. (III-7 can also be written in the following form:

	$I_{DF}/I_P = \left(\frac{\phi_F}{k_{RP}}\right) * [k^{\circ}_{TS1} \exp\left(-\frac{\Delta E_{TS}}{RT}\right)]$	(III-9)

Plotting ln (I_{DF}/I_P) against 1/T results in a linear relationship with an intercept equal to ln$[\left(\frac{\phi_F}{k_{RP}}\right) k^{\circ}_{TS1}]$ and a slope equal to $-\frac{\Delta E_{TS}}{R}$ (Parker, 1968). The activation energy for reverse intersystem crossing ΔE_{TS} and the maximum reverse intersystem crossing rate k°_{TS1} can be approximated and $k_{TS1}(T)$ can be calculated accordingly.

Since nitrogen was purged into the cuvette to create an oxygen-free environment throughout the measurement, $k_Q[O_2]$ was considered negligible. Therefore, the value of k_{TS0} was calculated accordingly. The magnitude of k_{TS0} is a direct measure of matrix-induced quenching modulated by ability of triplet state molecule to dissipate its energy to nearby molecules in the matrix. The temperature dependence of k_{TS0} was analyzed using an Arrhenius plot of ln(k_{TS0}) vs 1/T and the activation energy to quench the triplet molecule within different temperature ranges was calculated from the plot and was associated with relaxation processes in amorphous systems.

Results and Discussions

Delayed Luminescence Emission Spectra: Riboflavin in amorphous sucrose films exhibited two delayed emission peaks at ~515nm and ~620nm (Figure III-1) when excited at 440nm. The long wavelength emission band corresponded to phosphorescence, and the short wavelength emission corresponded to E-type delayed fluorescence. The phosphorescence emission intensity decreased gradually as temperature increased. At temperatures equal or higher than 30°C, the riboflavin phosphorescence spectra overlapped with the delayed fluorescence tail on the blue side. Delayed fluorescence peak first appeared at -20°C and its intensity kept increasing as temperature increased from -20 to 40°C due to the thermally promoted reverse intersystem crossing process. At temperatures higher than 40˚C, i.e., from 50 to 100˚C, the peak intensity of delayed fluorescence decreased. To better understand the data, a non-linear fitting software Fityk that uses a deconvolution procedure allowed for the differentiation of the two peaks and resulted in the extraction of important information from the spectra. The changes in the peak intensity of phosphorescence and delayed fluorescence are summarized in Figure III-2. Two possible reasons might have attributed to the reduction of delayed fluorescence intensity at high temperature (50˚C): 1) a lower concentration of riboflavin caused by increased photo-degradation of riboflavin at elevated temperatures, and 2) higher probability for triplet riboflavin to be quenched via non-radiative decay rather than via reverse intersystem crossing.

The changes of peak frequency and bandwidth from riboflavin phosphorescence emission spectra with temperature are plotted in Figure III-3. The peak energy, reflected by peak frequency, remained relatively constant from -30 to 20˚C and shifted rapidly to longer wavelength from 20 to 50˚C, indicating a decrease in emission energy and an increase in the average extent of matrix dipolar relaxation in the sucrose matrix around the excited triplet riboflavin molecules. The phosphorescence bandwidth increased almost linearly with temperature, suggesting a gradual broadening in the distribution of dynamically distinct environment in the glassy sucrose matrix even below its glass transition temperature.

Figure III-1

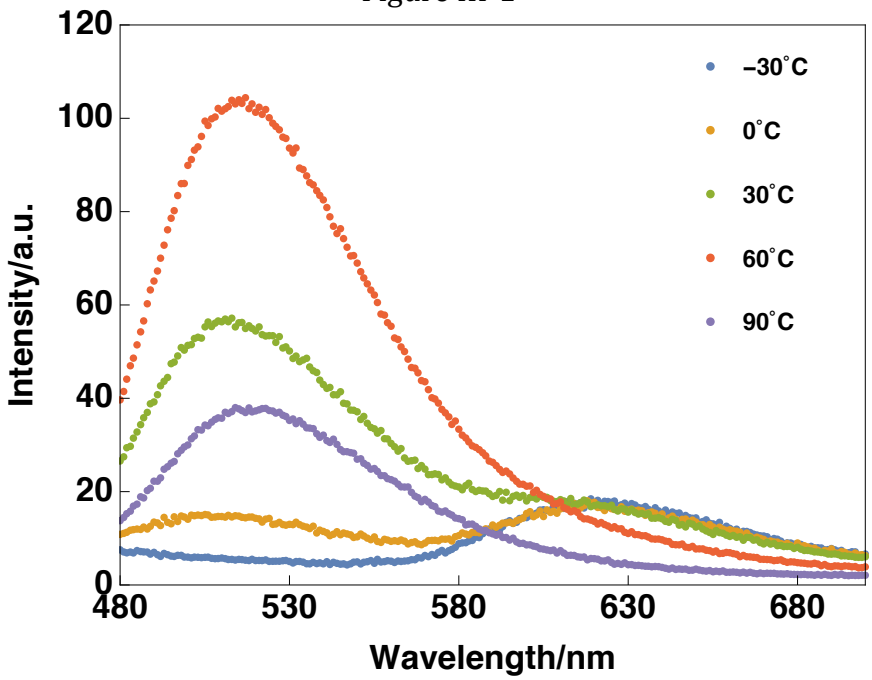

Figure III-1: Delayed luminescence emission spectra of riboflavin in amorphous sucrose films at selected temperatures: -30˚C (blue), 0˚C(yellow), 30˚C (green), 60˚C (red), and 90˚C (purple)

Figure III-2

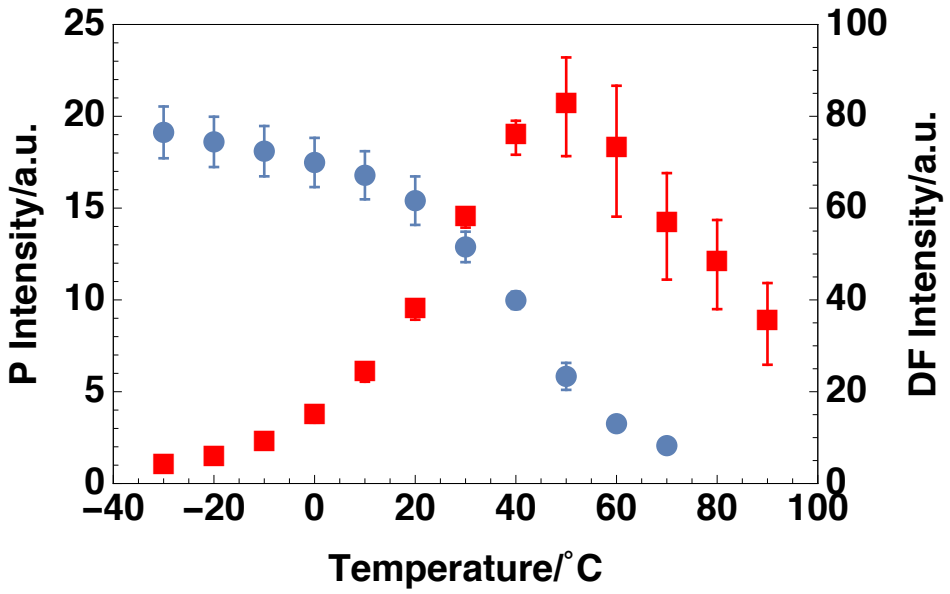

Figure III-2: Phosphorescence (blue circle) and delayed fluorescence (red square) peak intensity as a function of temperature.

Figure III-3

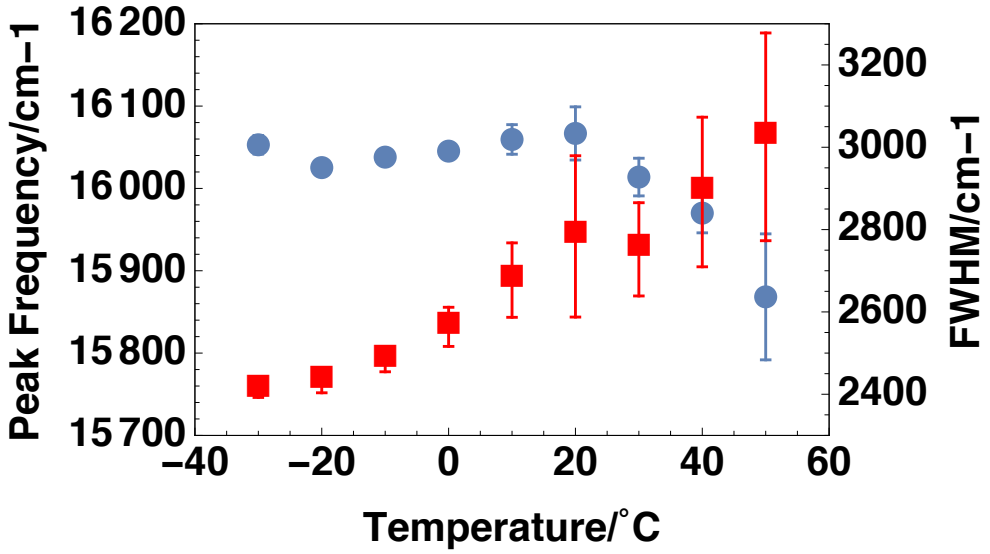

Figure III-3: Peak frequency (blue circle) and FWHM (red square) from riboflavin phosphorescence emission plotted as a function of temperature.

Phosphorescence Decay Kinetics: Time-resolved phosphorescence decays of riboflavin in amorphous sucrose solid film were collected over the temperature range from -30 to 100°C. All decays collected exhibited heterogeneous decay kinetics. Three fitting methods were used to analyze phosphorescence decays from riboflavin in sucrose matrix. Figure III-4 is an example of riboflavin phosphorescence intensity decay collected at 10˚C, along with stretched exponential fit, 2-exponential fit, 3-exponential fit. Although all fits resulted in satisfactory R^2, both the log-linear plot and the plots of modified residuals suggested that 3-exponential model best described the decay kinetics, as the modified residuals for 3-exponential fit varied evenly about zero. The fit using MEM is plotted in Figure III-6. As shown, MEM did not sufficiently fit the entire data range: the initial ~200ms was underestimated but the residuals over the time range 500-1000ms did exhibit uncorrelated pattern about zero. Despite the discrepancy between the fit and the data at the initial of the decay, the lifetime distributions from MEM was analyzed and compared to those from stretched exponential and multi-exponential models. Next, the results from each fitting method will be discussed respectively and suggestions for riboflavin lifetime analysis will be made.

Stretched Exponential Model: Although the plot of modified residuals from stretched exponential did not exhibit excellent random distribution about zero over the initial 100ms od the decay data as shown in Figure III-4, the results from stretched exponential model are discussed because: 1) this model is widely used to describe heterogeneous decays, and 2) the simplicity of this model which only has two

parameters is a big advantage. Decays from -30 to 60˚C were well fitted with the stretched exponential model. Decays collected at temperatures above 60˚C were not adequately fitted by the stretched exponential model and yielded physically meaningless parameters. Both lifetime (τ) and stretching exponent (β) decreased with temperature, as plotted in Figure III-7. In this model, τ reflects the rate of total decay k_P of the triplet state, which is the sum of all de-excitation rates; β is a measure of heterogeneity, originated from the variability of rate constants of non-radiative decay k_{TS0} residing in dynamically different environments in the matrix. Lifetime τ exhibited a relatively linear decrease trend, from ~60ms at -30˚C to ~3ms at 60˚C. The stretching exponent β remained almost constant from -30 to 0˚C and decreased in a rapid manner from 0 to 60˚C.

The decrease in τ with temperature was associated with the increase in the rates of reserve intersystem crossing, k_{TS1}, and non-radiative decay, k_{TS0}. The value of k_{TS1} increased with temperature because reverse intersystem crossing is a thermally activated process. The increase in k_{TS0} was due to increased matrix induced quenching as the temperature increased. Such increase in k_{TS0} was caused by greater ability of excited triplet state riboflavin molecules to undergo intersystem crossing to ground singlet state and to dissipate vibrational energy into the surrounding matrix (Draganski et al., 2010; You & Ludescher, 2010).

The other parameter from stretched exponential model, β, is determined by the shape of each decay curve and corresponds to the non-exponential degree of the relaxation function. The value of β reflects the distribution of dynamically

distinguishable probe environments. A value of 1 indicates zero dynamic heterogeneity and implies that the phosphorescence decay follows a singlet exponential model. The smaller the β value is, the broader the lifetime distribution becomes. The changes in β provide information on the dynamic heterogeneity of the matrix as a function of temperature. As indicated in Figure III-7, the heterogeneity of sucrose amorphous solid changed little as temperature increased from -30˚C to 0˚C but increased remarkably with the temperature from 0 to 60˚C. The stretching exponent β from riboflavin phosphorescence decays demonstrated great sensitivity to matrix heterogeneity much below Tg. In comparison, the value of β obtained from stretched exponential analysis of erythrosine B phosphorescence decays in amorphous sucrose film only exhibited sensitivity to the emergence of α-relaxation around Tg (Pravinata et al., 2005; Shirke & Ludescher, 2005).

Multi-exponential Model: The fit lifetimes and fractional amplitudes estimated from the multi-exponential model are summarized in Figure III-8. At temperatures below 60˚C, three distinct lifetime components were obtained. At temperatures above 60˚C, the value of the long and medium lifetime components (τ_1 and τ_2) became essentially the same, therefore a 2-exponential model was sufficient to describe the decays collected at temperature above 60˚C. As shown in Figure III-8, all fit lifetimes decrease with temperature. The fit lifetimes were 116, 36, and 3ms at -30˚C and the values decreased to 13 and 3ms at 90˚C. At the same temperature, when the reverse intersystem rate constant remained the same throughout the entire matrix, the long triplet lifetime component at -30˚C suggested the presence of rigid glassy regions

where the rate of matrix induced collisional quenching of triplet state (k_{TS0}) was small, while the short triplet lifetime component was an indicator of the presence of less rigid environment, where there was a greater probability for excited riboflavin molecules to dissipate vibrational energy to the matrix. The difference in fit lifetimes also indicated that probes existed in divergent local environments of different k_{TS0} and consequently different molecular mobility.

The fractional amplitude, A_i, of each lifetime component varied systematically as a function of temperature (Figure III-8b). Over the temperature range from -30 to 20˚C, all fractional amplitudes (A_1, A_2, and A_3) remained almost constant, which indicates that the proportion of rigid and flexible environments remained almost the same. From 20˚C onward, the changes in fractional amplitudes became more dramatic: the value of both A_1 and A_2 decreased and the value of A_3 increased with temperature, suggesting that part of the previously rigid environment transformed into less rigid environment and that less rigid matrix environment became more predominant. The changes in fractional amplitudes indicated changes in the distribution of dynamically distinct regions in the matrix, which is in accordance with the trend suggested by β from stretched exponential.

Maximum Entropy Method: In addition to stretched and multi-exponential functions, MEM was also used to characterize riboflavin phosphorescence decays. Figure III-9 shows how MEM lifetime distribution changed with temperature. The resultant MEM lifetime distributions supported the use of three-exponential function over the temperature range from -30 to 50˚C and two-exponential function from 60 to 90˚C:

the MEM lifetime distribution exhibited three peaks at temperatures below 50˚C and two peaks at temperatures above 50˚C. As shown in Figure III-9, the location of the peaks shifted towards short lifetime as the temperature increased. The amplitude of the long lifetime peak decreased while the amplitude of the short lifetime increased.

To take a closer look at the three peaks at -20˚C, we found that the peaks centered at 4.8, 39.2, and 114.1ms, respectively, which were in good accordance with the fit lifetimes from 3-exponential model, at -20˚C the three fit lifetimes from which are 3.7, 33.4, and 109.1ms, respectively. As temperature increased to 60˚C, the MEM lifetime distribution exhibited only two peaks centered at 3.1 and 21.3ms, which correlated well with lifetime components (3.2 and 21.4ms) from 2-exponential model. Again, the good correlation between MEM and multi-exponential model provided good support for the use of multi-exponential model to characterize riboflavin phosphorescence decays in amorphous sucrose.

Amplitude-weighted average lifetime was calculated from MEM distribution and compared with the average lifetimes obtained using both stretched and multi-exponential functions. As shown in Figure III-10, it is obvious that the results from MEM were in good accordance with those from multi-exponential function, while the average lifetime from stretched exponential function yielded deviation from the rest. Therefore, the amplitude-weighted average lifetime calculated from multi-exponential function was used to investigate the rate constant of non-radiative decay and the activation energy to quench triplet riboflavin in the following section.

To further understand how the quenching of triplet state riboflavin molecules might be coupled with the secondary relaxations in sucrose, we compared the time scale of β relaxation measured in amorphous sucrose to the riboflavin phosphorescence lifetime and we found them comparable. Kaminski *et al* (2012) reported the dielectric spectra of glassy sucrose and showed a β relaxation process centered at $\sim 10^{0.9}$Hz, which is about 125ms at 14˚C, and the peak shifted to fast frequencies at higher temperature, while at 46˚C, the β relaxation time was about 10ms. In another study, relaxation time of β relaxation process was determined to be 2.3ms at 25˚C and 0.2ms at 50˚C in lyophilized glassy sucrose (Bhattacharya, Bhardwaj, & Suryanarayanan, 2014). The riboflavin phosphorescence lifetime in sucrose ranged from 32.4ms to 8.4ms over the temperature range from 10 to 50˚C, which is on the same scale as the β relaxation time measured in amorphous sucrose, which suggests that the phosphorescence from riboflavin can be quenched by β relaxation in glassy sucrose.

Figure III-4

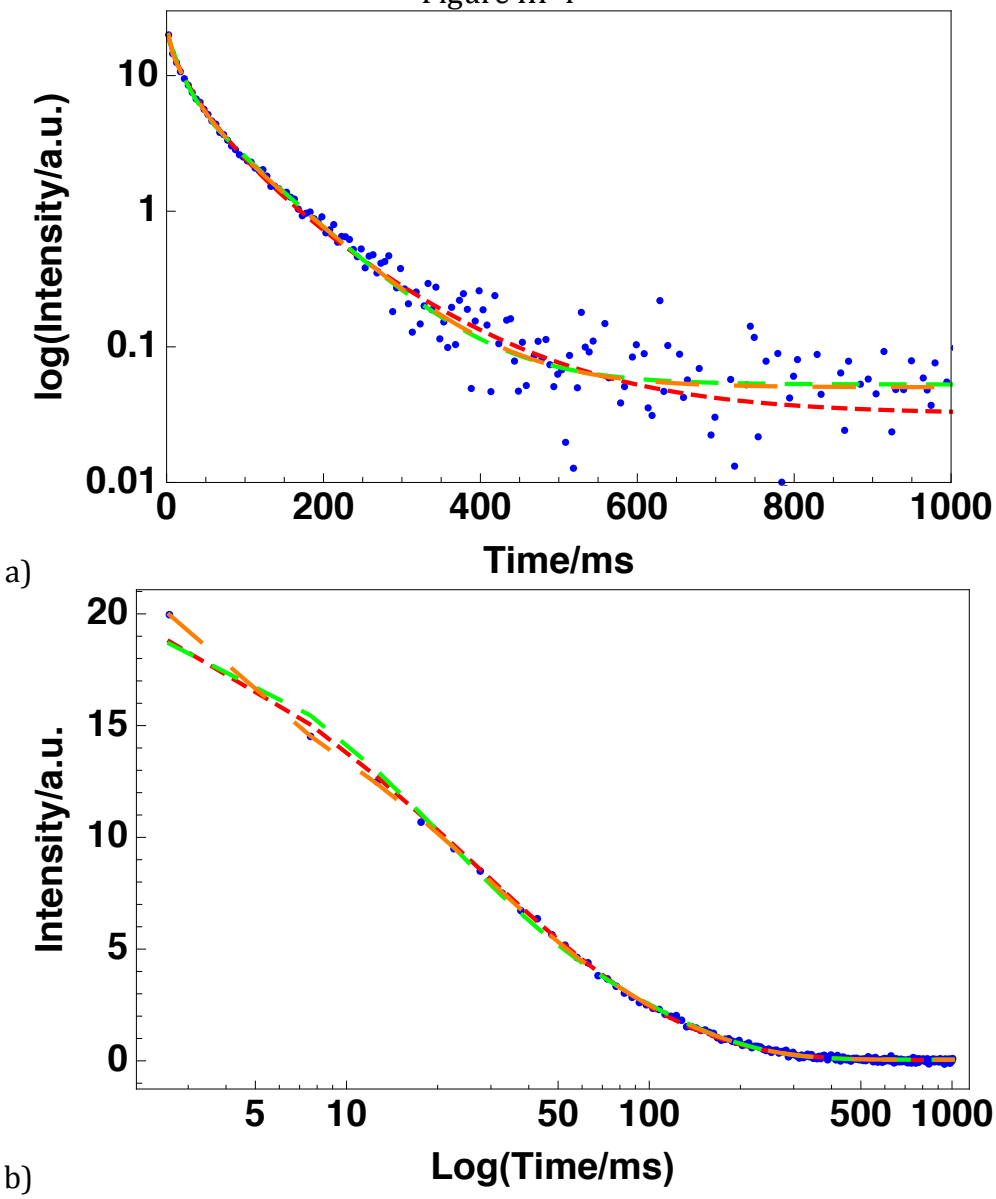

Figure III-4: Phosphorescence decay of riboflavin (blue circles) in an amorphous sucrose matrix at 10˚C. Stretched exponential (red dashed line), two-exponential (green dashed line), and three-exponential fit s(orange dashed line) plotted in a linear-log scale (a) and log-linear coordinates (b).

Figure III-5

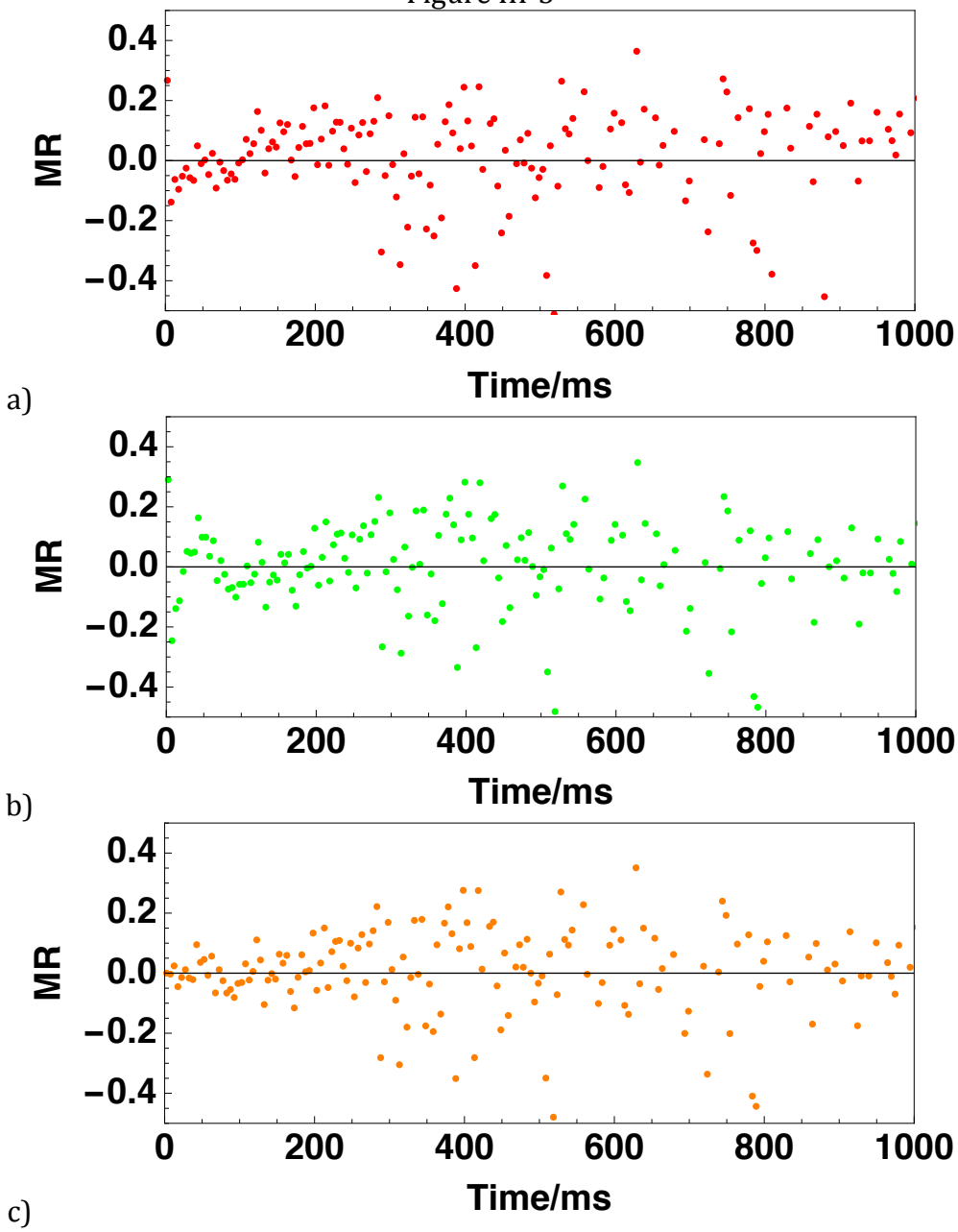

Figure III-5: Modified residuals for the stretched exponential (red), two-exponential (green), and three-exponential fits (orange).

Figure III-6

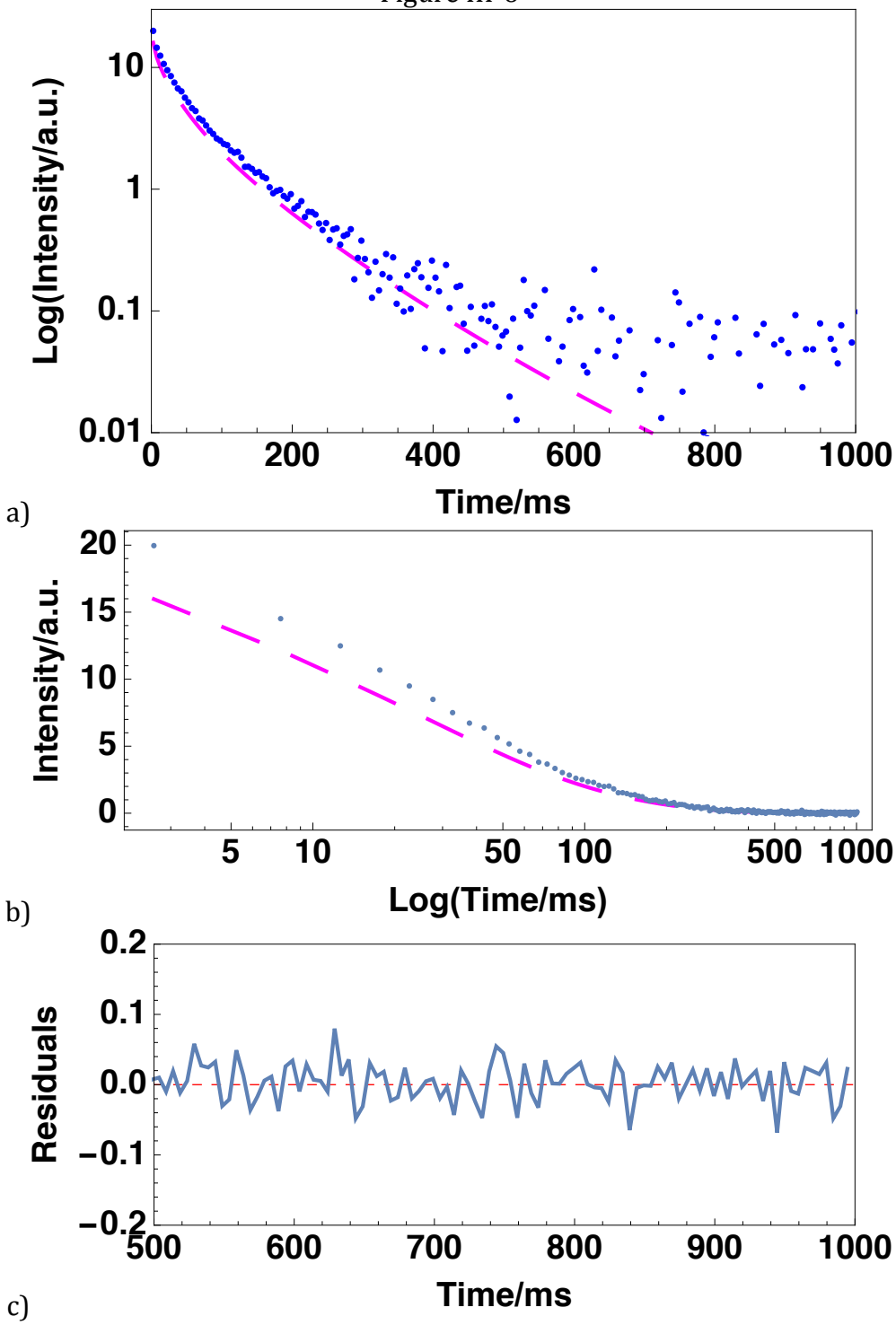

Figure III-6: Phosphorescence decay of riboflavin (blue circles) in an amorphous sucrose film at 10˚C. Estimation using MEM (magenta, dashed line) plotted in a linear-log (a) and a log-linear coordinates (b), and the residuals for the MEM estimation (c).

Figure III-7

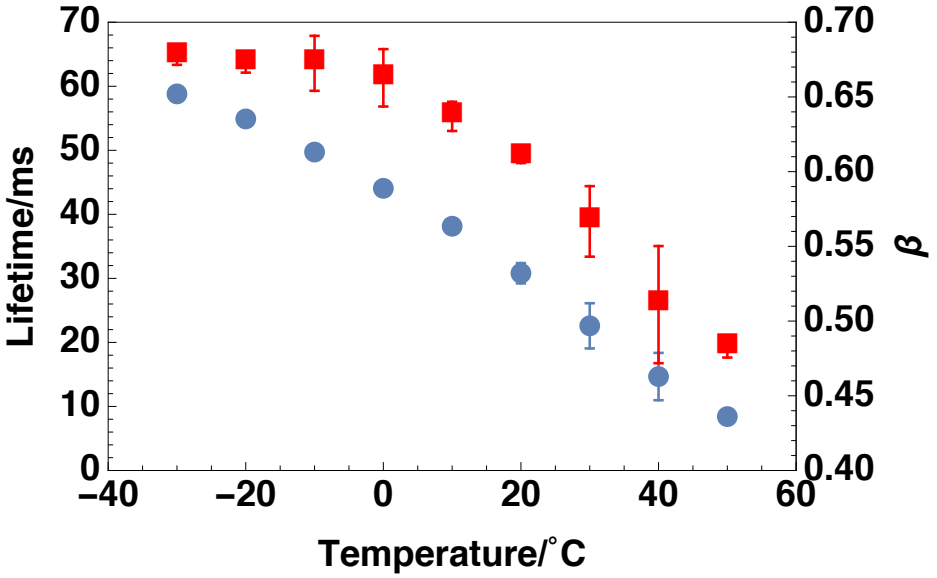

Figure III-7: Average phosphorescence lifetime τ (blue circles) and the stretching exponent β (red squares) of riboflavin phosphorescence intensity decays in sucrose as a function of temperature. The parameters were extracted from the fit to stretched exponetial function.

Figure III-8

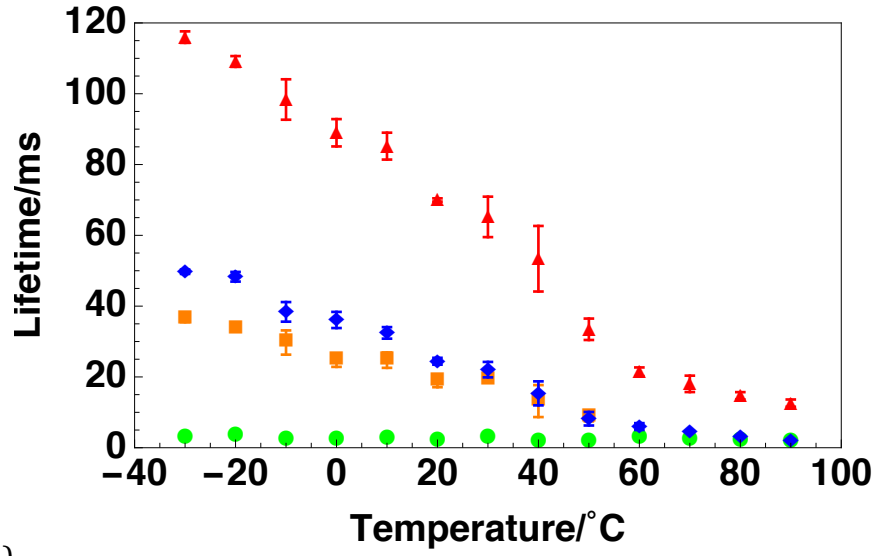

a)

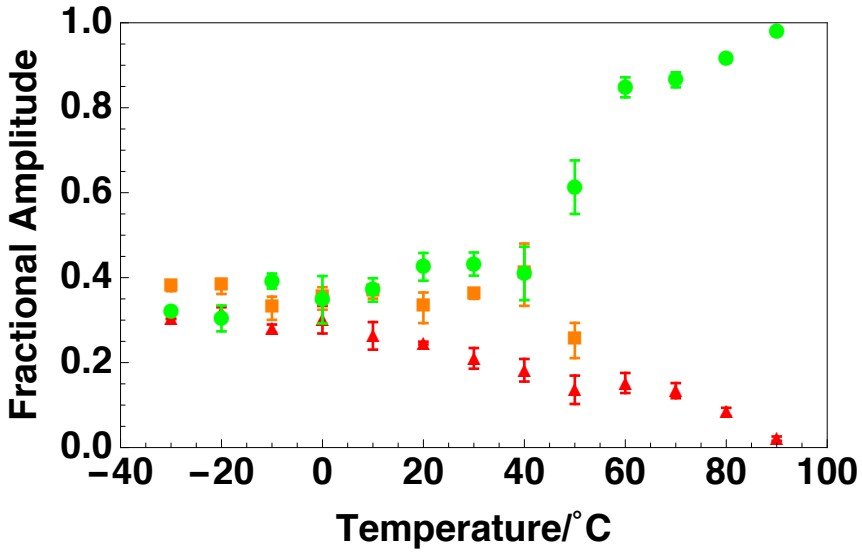

b)

Figure III-8: Lifetimes (a) and fractional amplitudes (b) of phosphorescence decay of riboflavin dispersed in amorphous sucrose film as a function of temperature. Red triangles, orange squares, and green circles denote lifetime component 1, 2, and 3, respectively; blue diamonds correspond to the calculated average lifetimes.

Figure III-9

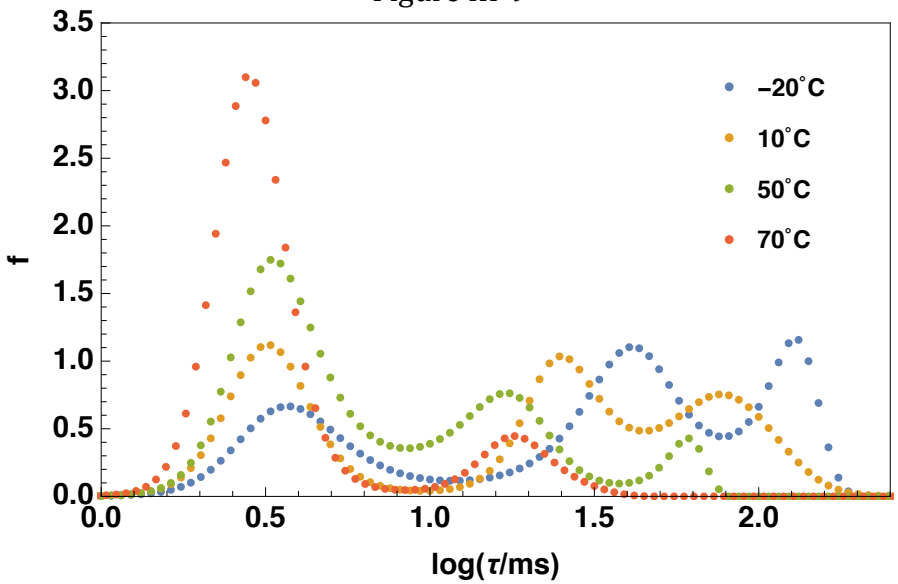

Figure III-9: Riboflavin phosphorescence MEM lifetime distributions at -20 (blue), 30 (orange), 50 (green), and 70˚C (red).

Figure III-10

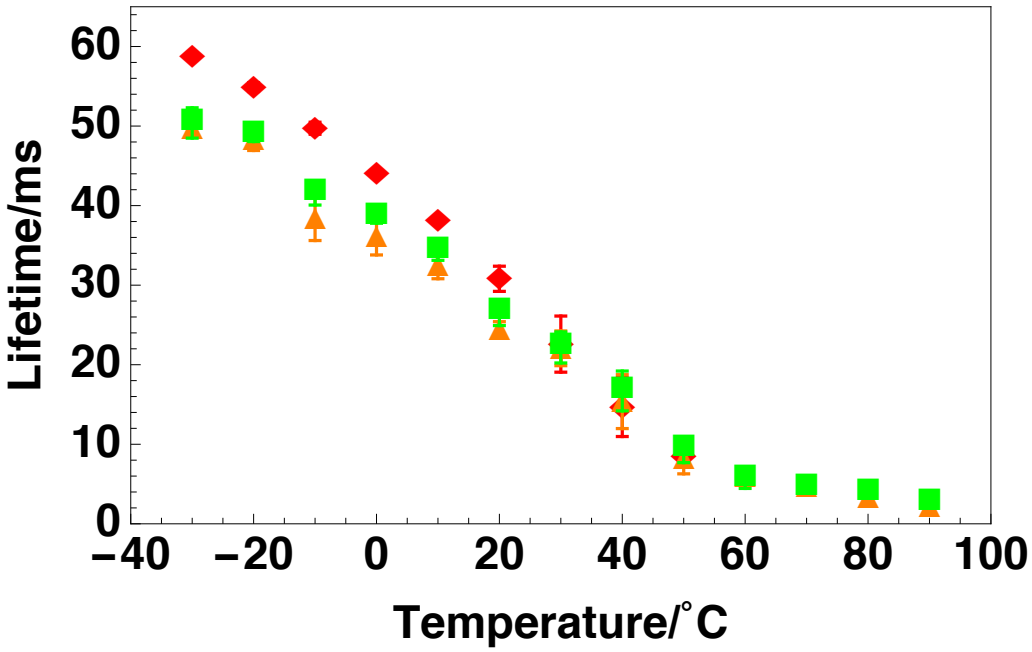

Figure III-10: Average lifetimes calculated from MEM (green squares), multi-exponential function (orange triangles), and stretched exponential function (red diamonds) as a function of temperature.

Non-radiative Decay Rates: The decrease in lifetimes reflected an increase in the rate constant of phosphorescence, k_P ($k_P = 1/\tau$). In order to separate the contribution of riboflavin natural phosphorescence radiative decay and reverse intersystem crossing from the non-radiative decay, the values of k_P and k_{TS1} were first determined. The rate constant of radiative decay was approximated using the riboflavin phosphorescence lifetime measured in glycerol/water (3:1 v/v) mixture at 77K as discussed in great details in the previous chapter, assuming that under this temperature, radiative decay is the only possible deactivation pathway. The longest lifetime was calculated as 170ms and the inverse of it was used as the intrinsic radiative decay rate. The rate constant of reverse intersystem crossing, k_{TS1}, at each temperature point was determined by (III-7 using maximum reverse intersystem crossing rate constant k°_{TS1} and activation energy ΔE_{TS} for reverse intersystem crossing calculated from (III-9. The activation energy ΔE_{TS} was calculated from the slope of the linear plot of ln (I_{DF}/I_P) against 1/T and has a value of 35.47 kJ/mol. This value was in accordance with the value of 32.63kJ/mol previously reported by Chambers and Kearns (Chambers & Kearns, 1969) and was slightly higher than the value of 28.03kJ/mol estimated based on energy separation between excited singlet and triplet states (Gordon-Walker, Penzer, & Radda, 1970). The intercept of linear curve ln (I_{DF}/I_P) against 1/T has a value of ln $[\left(\Phi_F/k_{RP}\right) k^{\circ}_{TS1}]$. A fluorescence quantum yield value of 0.37, measured from riboflavin in starch films, was used as an estimate for Φ_F in the calculation (Penzkofer, 2012). Accordingly, the maximum reverse intersystem crossing rate constant, k°_{TS1}, was estimated to be

$7.78\times10^{7}s^{-1}$. Using this k°_{TS1}value, the calculation of k_{TS0} generated negative values that have no physical meaning. To address this discrepancy, an upper limit value of k°_{TS1} was selected ($3\times10^{7}s^{-1}$) to avoid the generation of physically meaningless negative k_{TS0} values (Pravinata et al., 2005). A literature search did not provide any information on the value of maximum reverse intersystem crossing rate constant. However, when riboflavin was dispersed in starch film at room temperature, a value of $0.93s^{-1}$ was reported for the rate constant of reverse intersystem crossing k_{TS1} (Penzkofer, 2012). In comparison to the value of k_{TS1} in this study at 20˚C ($14.23s^{-1}$), a faster reverse intersystem crossing in the sucrose matrix was suggested by our results. This may be caused by different packing of hosting matrices and/or different calculation methods.

The magnitude of k_{TS0} demonstrates matrix-induced quenching modulated by internal and external factors. The internal factor refers to the ability of excited triplet riboflavin molecules coupling to the highly excited vibrational singlet ground state; the external factor refers to the ability of the singlet ground state to dissipate the vibrational energy to nearby molecules in the matrix (Draganski et al., 2010; You & Ludescher, 2010). The values of k_P, k_{TS0}, and k_{TS1} calculated from the amplitude-weighted average lifetime from the multi-exponential function are plotted as a function of temperature in Figure III-11. The rate of non-radiative decay exhibited a biphasic pattern as a function of temperature: it increased only slightly from -30 to 40˚C and increased exponentially above 40˚C. The fast increase in k_{TS0} at higher

temperature indicates a higher probability for triplet riboflavin molecules to de-excite via collisional quenching under such conditions.

An Arrhenius plot of ln (k_{TS0}) versus 1/T provides information on the activation energy E_A to quench triplet state molecules via non-radiative decay (Figure III-12). The Arrhenius plot exhibited two distinct regimes: low temperature range (-30 to 30˚C), where the activation energy to quench riboflavin was very low (3.43 kJ/mol) and high temperature regime (30 to 50˚C), where the activation energy was approximately 61.54 kJ/mol. The low activation energy over the low temperature range suggested that there was little motion present in the glassy matrix and there was only very slight increase in non-radiative decay. The activation energy measured around from 30˚C to 50˚C fell within the range of reported activation energy for β relaxation of amorphous sucrose from 42kJ/mol to 98kJ/mol (Bhattacharya & Suryanarayanan, 2011; Kaminski et al., 2008; Kaminski et al., 2012). The different measured β relaxation activation energy was partially attributed to the different sample preparation methods used in different studies (Bhattacharya & Suryanarayanan, 2011). The activation energy for β relaxation calculated using the empirical equation derived by Kudlik, was approximately 68kJ/mol, very close to the activation energy to quench triplet riboflavin as we calculated. Some studies have also associated the origin of β relaxation to oscillations via glycosidic bond (Meißner, Einfeldt, & Kwasniewski, 2000) and computer simulations resulted in a value of 76.7kJ/mol for the energy for the rotation of the two rings in sucrose molecule (Kaminski et al., 2008), which is, again, very close to the activation energy

for non-radiative decay calculated in this study. The value of the activation energy measured in this study is also essentially the same as the activation energy of β relaxation (denoted as β1 relaxation by authors) in sucrose measured by dielectric spectroscopy over the temperature range from 30 to 50˚C (Bhattacharya & Suryanarayanan, 2011).

The comparison between activation energy to quench triplet riboflavin molecule and the activation energy for β relaxation in sucrose suggested that the phosphorescence from excited triplet state riboflavin was very likely quenched by β-relaxation in the glassy matrix. Furthermore, the value of 61.54kJ/mol was much smaller than the typical activation energy of α-relaxation, suggesting that phosphorescence from triplet riboflavin exhibited no sensitivity towards α relaxation within the temperature range tested in this study. Additionally, the α relaxation time in glassy sucrose at Tg was reported to be ~4s (Bhattacharya & Suryanarayanan, 2011; Bhugra et al., 2007). Although much faster than the generally accepted α relaxation time of 100s at Tg, the α relaxation time in sucrose is still 1000 times slower than the riboflavin phosphorescence lifetime (6ms) at 60˚C, which is too slow to quench the triplet state riboflavin molecules. Therefore, our results suggested that riboflavin phosphorescence was sensitive to the secondary β relaxation in sucrose and can be used as a sensitive phosphorescent probe to monitor local molecular mobility changes of the matrices induced by secondary relaxations.

Figure III-11

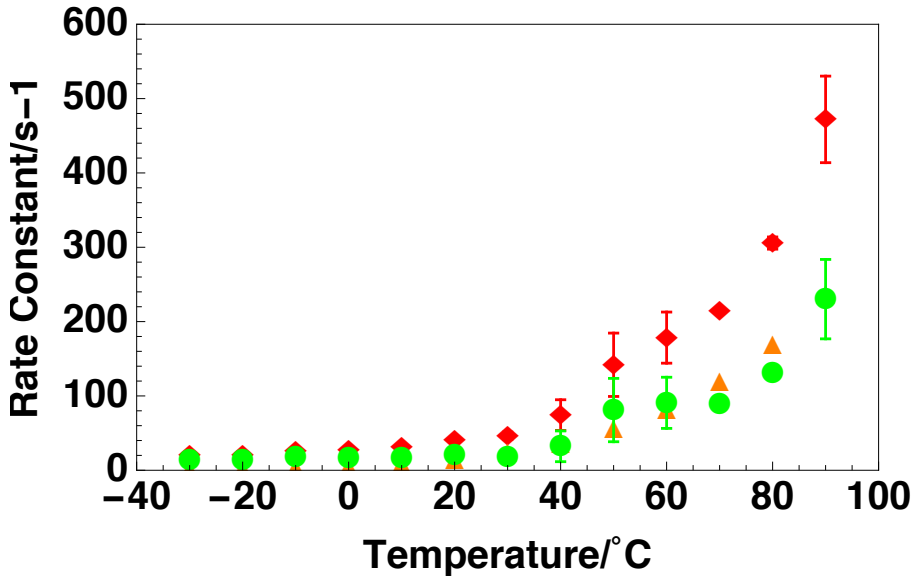

Figure III-11: Rate constants of triplet riboflavin decay processes as a function of temperature. Red diamonds: rate constant of phosphorescence, orange triangles: rate constant of reverse intersystem crossing, and green circle: rate constant of non-radiative decay.

Figure III-12

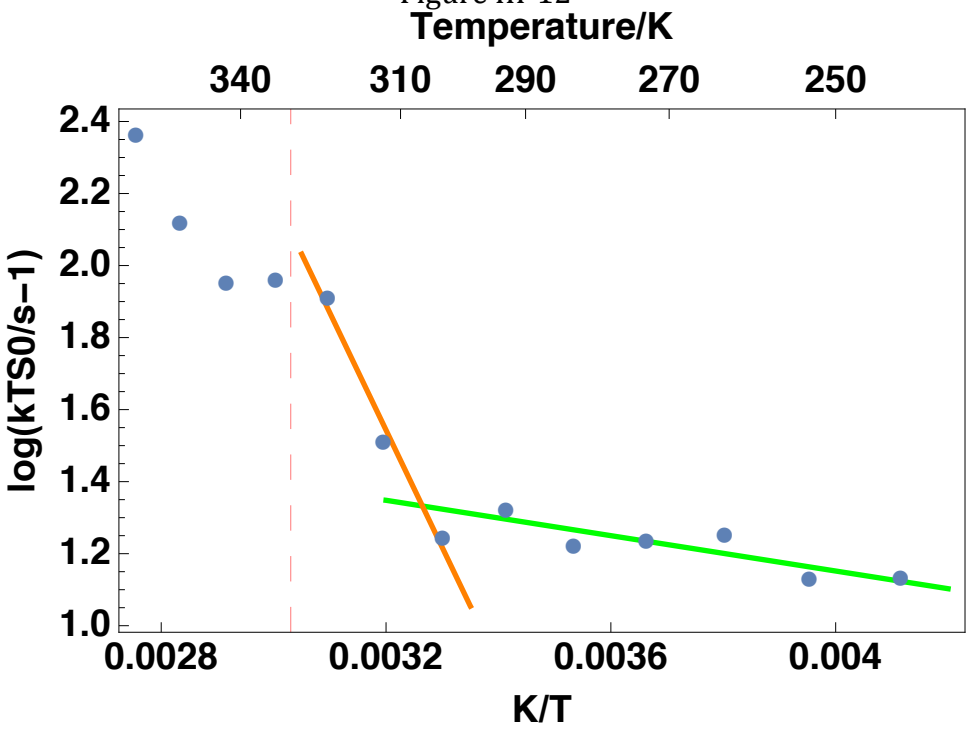

Figure III-12: Arrhenius plot of non-radiative decay rate k_{TS0} calculated from average lifetime from multi exponential fitting of phosphorescence decays of riboflavin dispersed in amorphous sucrose. The red vertical dashed line marks the glass transition temperature of sucrose.

Conclusions

Phosphorescence data from riboflavin in sucrose amorphous films over the temperature range from -30 to 100˚C indicated that riboflavin phosphorescence was sensitive to thermally induced fast secondary relaxation processes in the glassy sucrose matrix. The phosphorescence emission spectra suggested that the dipolar relaxations in the glassy matrix lower the energy of excited triplet riboflavin prior to their de-activation. The phosphorescence decays were fitted using stretched exponential and multi-exponential model, and a MEM approach. A scrutiny of the different fitting methods suggested that the multi-exponential model best characterized the riboflavin phosphorescence decays over -30 to100˚C. The calculated average lifetimes from the multi-exponential model were in good agreement with those from MEM while the estimated average lifetimes from the stretched exponential appeared to be overestimated over low temperature range (-30~20˚C). It was concluded that the multi-exponential model was most suitable to describe the riboflavin decays. Riboflavin phosphorescence lifetime decreased with temperature and the distribution of lifetimes shifted to short lifetime with temperature. The broad distribution of lifetime over two decades indicated that riboflavin molecules resided in various energetically distinct regimes in the sucrose matrix. The Arrhenius study of non-radiative decay rate reveals that the activation energy to quench triplet state riboflavin is essentially close to the activation energy of the β-relaxation in sucrose matrix, which further demonstrates that riboflavin can be used as a phosphorescent probe to study the fast secondary relaxations in glassy materials.

References

Bhattacharya, S., & Suryanarayanan, R. (2011). Molecular motions in sucrose-PVP and sucrose-sorbitol dispersions: I. implications of global and local mobility on stability. *Pharmaceutical Research, 28*(9), 2191-2203. doi:10.1007/s11095-011-0447-0

Bhattacharya, S., Bhardwaj, S. P., & Suryanarayanan, R. (2014). *Molecular motions in sucrose-PVP and sucrose-sorbitol dispersions-II. implications of annealing on secondary relaxations*

Bhattacharya, S., & Suryanarayanan, R. (2009). Local mobility in amorphous pharmaceuticals--characterization and implications on stability. *Journal of Pharmaceutical Sciences, 98*(9), 2935-2953. doi:10.1002/jps.21728

Bhugra, C., Rambhatla, S., Pikal, M. J., Bakri, A., Duddu, S. P., Miller, D. P., & Lechuga-Ballesteros, D. (2007). Prediction of the onset of crystallization of amorphous sucrose below the calorimetric glass transition temperature from correlations with mobility. *Journal of Pharmaceutical Sciences, 96*(5), 1258-1269. doi:10.1002/jps.20918

Capaccioli, S., Paluch, M., Prevosto, D., Wang, L., & Ngai, K. L. (2012). Many-body nature of relaxation processes in glass-forming systems. *The Journal of Physical Chemistry Letters, 3*(6), 735-743. doi:10.1021/jz201634p

Chambers, R. W., & Kearns, D. R. (1969). Triplet states of some common photosensitizing dyes. *Photochemistry & Photobiology, 10*(3), 215.

Cicerone, M. T., Tellington, A., Trost, L., & Sokolov, A. (2003). Substanstially improved stability of biological agents in dried form: The role of glassy dynamics in preservation of biopharmaceuticals. *BioProcess International, 1*, 1-9.

Cicerone, M. T., & Douglas, J. F. (2012). ß-relaxation governs protein stability in sugar-glass matrices. *Soft Matter, 8*(10), 2983-2991. doi:10.1039/c2sm06979b

Cicerone, M. T., Pikal, M. J., & Qian, K. K. (2015). Stabilization of proteins in solid form. *Advanced Drug Delivery Reviews, 93*, 14-24. doi:10.1016/j.addr.2015.05.006

Corradini, M. G., & Ludescher, R. D. (2015). Making sense of luminescence from GRAS optical probes. *Current Opinion in Food Science, 4*, 25-31. doi:10.1016/j.cofs.2015.04.004

Draganski, A. R. (2014). *A systematic study of phosphorescent probes in cryosolvents, amorphous solids, and proteins.* (Unpublished Doctoral dissertation). Rutgers, The State University of New Jersey, New Brunswick.

Draganski, A. R., Tiwari, R. S., Sundaresan, K. V., Nack, T. J., You, Y., & Ludescher, R. D. (2010). Photophysical probes of the amorphous solid state of proteins. *Food Biophysics, 5*(4), 337-345. doi:10.1007/s11483-010-9185-9

Dranca, I., Bhattacharya, S., Vyazovkin, S., & Suryanarayanan, R. (2009). Implications of global and local mobility in amorphous sucrose and trehalose as determined by differential scanning calorimetry. *Pharmaceutical Research, 26*(5), 1064-1072. doi:10.1007/s11095-008-9817-7

Gordon-Walker, A., Penzer, G. R., & Radda, G. K. (1970). Excited states of flavins characterised by absorption, prompt and delayed emission spectra. *European Journal of Biochemistry, 13*(2), 313-321. doi:10.1111/j.1432-1033.1970.tb00933.x

Imamura, K., Sakaura, K., Ohyama, K. -., Fukushima, A., Imanaka, H., Sakiyama, T., & Nakanishi, K. (2006). Temperature scanning FTIR analysis of hydrogen bonding states of various saccharides in amorphous matrixes below and above their glass transition temperatures. *Journal of Physical Chemistry B, 110*(31), 15094-15099. doi:10.1021/jp057527o

Kaminski, K., Adrjanowicz, K., Zakowiecki, D., Kaminska, E., Wlodarczyk, P., Paluch, M., . . . Tarnacka, M. (2012). *Dielectric studies on molecular dynamics of two important disaccharides: Sucrose and trehalose*

Kaminski, K., Kaminska, E., Hensel-Bielowka, S., Chelmecka, E., Paluch, M., Ziolo, J., . . . Ngai, K. L. (2008). Identification of the molecular motions responsible for the slower secondary (ß) relaxation in sucrose. *Journal of Physical Chemistry B, 112*(25), 7662-7668. doi:10.1021/jp711502a

Meißner, D., Einfeldt, J., & Kwasniewski, A. (2000). Contributions to the molecular origin of the dielectric relaxation processes in polysaccharides – the low temperature range. *Journal of Non-Crystalline Solids, 275*(3), 199-209. doi:http://dx.doi.org/10.1016/S0022-3093(00)00248-9

Orford, P. D., Parker, R., Ring, S. G., & Smith, A. C. (1989). Effect of water as a diluent on the glass transition behaviour of malto-oligosaccharides, amylose and amylopectin. *International Journal of Biological Macromolecules, 11*(2), 91-96.

Parker, C. A. (1968). *Photoluminescence of solutions : With applications to photochemistry and analytical chemistry*. Amsterdam: Elsevier.

Penzkofer, A. (2012). Photoluminescence behavior of riboflavin and lumiflavin in liquid solutions and solid films. *Chemical Physics, 400*, 142-153. doi:10.1016/j.chemphys.2012.03.017

Pravinata, L. C., You, Y., & Ludescher, R. D. (2005). Erythrosin B phosphorescence monitors molecular mobility and dynamic site heterogeneity in amorphous sucrose.

Biophysical Journal, 88(5), 3551-3561. doi:http://dx.doi.org/10.1529/biophysj.104.054825

Richert, R. (2000). Triplet state solvation dynamics: Basics and applications. *Journal of Chemical Physics, 113*(19)

Rodriguez, H. B., San Roman, E., Duarte, P., Machado, I. F., & Ferreira, L. (2012). *Eosin Y triplet state as a probe of spatial heterogeneity in microcrystalline cellulose*

Sahni, E. K., Pikal, M. J., Thakur, M., Chaney, M. A., Sherman, G., & Siegel, D. P. (2015). Dynamics in polysaccharide glasses and their impact on the stability of encapsulated flavors. *Food Biophysics,* , 14p. doi:10.1007/s11483-015-9405-4

Steinbach, P. J., Ionescu, R., & Matthews, C. R. (2002). Analysis of kinetics using a hybrid maximum-entropy/nonlinear-least-squares method: Application to protein folding. *Biophysical Journal, 82*, 2244-2255. doi:10.1016/S0006-3495(02)75570-7

Suzuki, T., Komatsu, H., & Miyajima, K. (1996). Effects of glucose and its oligomers on the stability of freeze-dried liposomes. *Biochimica Et Biophysica Acta, 1278*(2), 176-182.

Tiwari, R. S., & Ludescher, R. D. (2010). Vanillin phosphorescence as a probe of molecular mobility in amorphous sucrose. *Journal of Fluorescence, 20*(1), 125.

Wojdyr, M. (2010). Fityk: A general-purpose peak fitting program. *Journal of Applied Crystallography, 43*(5), 1126-1128. doi:10.1107/S0021889810030499

You, Y., & Ludescher, R. D. (2010). The effect of molecular size on molecular mobility in amorphous oligosaccharides. *Food Biophysics, 5*(2), 82-93. doi:10.1007/s11483-010-9148-1

Yu, L. (2001). Amorphous pharmaceutical solids: Preparation, characterization and stabilization. *Advanced Drug Delivery Reviews, 48*(1), 27-42. doi:http://dx.doi.org/10.1016/S0169-409X(01)00098-9

Chapter IV The Use of Riboflavin Phosphorescence to Study the Effects of Molecular Size on Molecular Mobility in a Series of Malto-Oligomers

Introduction

Carbohydrates are a group of widespread natural compounds extensively used in the food and pharmaceutical industries. The use of amorphous carbohydrates for encapsulation has shown to enhance the preservation and stability of biomolecules and to improve poor solubility and the slow dissolution of nutrients and flavors (Cicerone & Douglas, 2012). Although amorphous encapsulation system provides advantages such as high solubility, high dissolution rate, and better compression characteristics compared to their crystalline counterparts, the increased free energy of the amorphous solids inevitably results in decreased physical and chemical stability, which ultimately poses questions on the stability and shelf-life of such amorphous products (Bhattacharya & Suryanarayanan, 2009).

The stability of amorphous carbohydrate systems has been under close scrutiny over the past couple of decades. Some early research associated the ability of glassy carbohydrate systems to stabilize and preserve labile biological agents with sugar vitrification. Vitrification increases the viscosity of sugar by 10^{11}~10^{13} –fold as the sugar melt becomes hard and rigid upon drying and cooling, which largely reduces the potential of molecular aggregation and small molecule diffusion that initiates oxidation and hydrolysis (Yu, 2001). Consequently, the structural relaxation, or α relaxation, as well as the glass transition temperature (Tg), was used as parameters to indicate system stability. It was thought that good stability could be achieved

when active compounds encapsulated in glassy sugar matrix were stored under the Tg of the excipient, when the full molecular mobility is highly restricted (Cicerone & Douglas, 2012). Carbohydrates with high Tg were thus considered as better excipients compared to carbohydrates with low Tg.

Yet, more recently, studies have shown that physical aging, crystallization, and degradation of encapsulated biomaterials could still take place at temperatures 50K below the Tg of the glassy materials and these observations have led to discussion of the validity of using Tg as an indicator of stability (Bhattacharya & Suryanarayanan, 2009; Yu, 2001). These findings suggested that glass transition temperature (Tg) was not sufficient to predict the stability of amorphous solids and raised questions upon how global and local mobility of amorphous carbohydrates affect stability. For example, despite the increase in Tg, the ability of maltodextrins to stabilize liposomes decreased with the increase of glucose units in a series of maltodextrins (Suzuki, Komatsu, & Miyajima, 1996). Moreover, the addition of small molecules such as glycerol to glassy sugar systems that lead to lower Tg has shown to enhance physical stability of the systems and to improve the stability of labile proteins (Bhattacharya & Suryanarayanan, 2011; Cicerone & Douglas, 2012; Cicerone, Pikal, & Qian, 2015). These recent findings suggest that the level of secondary β-and γ-relaxations, rather than α relaxation, determines the stability of encapsulated biomaterials when stored at temperatures below Tg.

The faster secondary relaxation, γ relaxation, has been identified as an inherent feature of all carbohydrates. γ relaxation is thought to originate from rotation of

exocyclic groups and is governed by intramolecular activation energy. The slower relaxation process, β relaxation, also known as a Johari-Goldstein process, is attributed to intermolecular motions associated with the glycosidic linkage (Imamura et al., 2006; Meißner et al., 2000). Both secondary relaxation processes have been found to bear a strong connection to structural α relaxation and are considered as precursors for primary α relaxation (Capaccioli, Paluch, Prevosto, Wang, & Ngai, 2012). In Meißner *et al*'s study, the dielectric spectra of different polysaccharides and their monomer, dimer and oligomer over low temperature range from -150 to -15˚C were investigated to identify the origins of the two secondary relaxations. Their results confirmed that the γ relaxation was attributed to the reorientation of -OH or $-CH_2OH$ side groups, while the β relaxation was originated from the oscillation of glycosidic bond (Meißner et al., 2000). It was also found that the activation energy of the local chain mobility increased in the order of dimer<polymer<pentamer (cellobiose<cellulose<cellopentaose), which was proposed as a result of the number of glycosidic linkages involved in the local chain mobility. This was confirmed through computer simulations that suggest four glycosidic bonds are effectively involved in chain mobility.

In our previous research, it has been demonstrated that the phosphorescence from riboflavin exhibited sensitivity towards molecular mobility changes in amorphous sucrose matrix modulated by the temperature. In particular, its phosphorescence lifetime was very sensitive to β relaxations below the glass transition temperature. Here, we report the use of riboflavin phosphorescence to study molecular mobility modulated by temperature in a series of malto-oligomers. This study is aimed to

investigate the effects of molecular size and Tg on molecular mobility, especially, β relaxation in glassy malto-oligomers and to interpret the observations from the perspective of hydrogen bonding and glycosidic bonds in this series of sugar glasses.

Materials and Methods

Sample Preparation: A series of six malto-oligomers (maltose, G2; maltotriose, G3; maltotetraose, G4; maltopentaose, G5; maltohexaose, G6; maltoheptaose, G7) were used in this study to investigate the effects of molecular size and Tg on molecular mobility in their glassy forms. G2, G3, G4 and G7 were purchased from Sigma-Aldrich (St. Louis, MO, USA) and G5 and G6 were purchased from Supelco (Bellfonte, PA, USA). The molecular mass and measured Tg of these sugars are summarized in (Table IV-1) and the Tg measured with Differential Scanning Calorimetry (Table IV-1-a) was used as a reference in this study. Malto-oligomers were added to 200μM riboflavin (Sigma-Aldrich, St. Louis, MO, USA) solution to reach a final sugar concentration of 30%wt. The sugar concentration in riboflavin solution was verified using an Atago refractometer (Model N-4E, Bellevue, WA, USA). The riboflavin/sugar monomer ratio in the solution was approximately $2{:}10^4$. The riboflavin concentration was essentially low enough that the triplet quenching between riboflavin molecules was avoided.

Table IV-1 Molecular weights and glass transition temperatures of the six malto-oligomers used in this study measured by TS-FTIR and DSC

Sugar	Molecular Weight	Tg/°C (TS-FTIR)[a]	Tg/°C (DSC)
Maltose (G2)	343	90	90[a], 91[b]
Maltotriose (G3)	505	113	110[a], 131[b]
Maltotetraose (G4)	667	133	128[a], 147[b]
Maltopentaose (G5)	829	143	137[a], 165[b]
Maltohexaose (G6)	991	146	145[a], 167[b]
Maltoheptaose (G7)	1153	154	150[a]

a-(Imamura et al., 2006) b-(Orford, Parker, Ring, & Smith, 1989)

Amorphous sugar films were prepared following the procedure previously reported in Chapter III, Materials and Methods: an aliquot of 24μL riboflavin-sugar solution was spread repetitively onto a quartz slide (NSG Precision Cells, Farmingdale, NY) to form a thin and transparent layer of film. The film was first dried with room-temperature airflow supplied by a heat gun (Model 201A, Master Appliance Corp., Racine, WI) for 15min and was further dried by storing in a desiccator against Drierite and P_2O_5 (Fisher Scientific, Fair Lawn, NJ) for at least 72 hours in the dark to reduce the water content to ~0% before phosphorescence measurement.

Phosphorescence Measurements: Steady state and time-resolved phosphorescence measurements were carried out using a Cary Eclipse Fluorescence Spectrophotometer (Agilent Technologies, Santa Clara, CA, USA). Phosphorescence measurements were collected over the temperature range from -30 to 100˚C, at 10˚C interval, for all six sugars studied. Data were collected at least in triplicates. Temperature during phosphorescence measurements was adjusted using a TLC-50 thermoelectric heating/cooling system (Quantum Northwest, Spokane, WA, USA). Samples were equilibrated before measurement for 10 minutes after the Peltier reached a constant reading. Quartz slides covered with amorphous riboflavin-sugar films were placed in a 1cm×1cm×3cm quartz cuvette (FireflySci Inc., Brooklyn, NY, USA) for the measurement. The cuvette was flushed with dry nitrogen throughout the measurement to eliminate oxygen and humidity. In addition, a stream of dry air was introduced across the cuvette holder in the spectrophotometer to reduce condensation during measurements at low temperatures. All measurements were collected using 20nm slits for both excitation and emission to maximize the signal.

Delay time and gate time were set to 0.2ms and 5ms, respectively. Each measurement was collected from 1 excitation flash.

Steady State Measurements: Delayed luminescence emission spectra were collected from 480 to 700nm when excited at 440nm. Emission spectra of pure malto-oligomer glassy films were collected under the same conditions and were subtracted from spectra of riboflavin in glassy sugar films to eliminate the contribution of light scattering and impurities from the sugars.

Delayed luminescence spectra from riboflavin exhibited two peaks: a delayed fluorescence peak located around 515nm and a phosphorescence peak located around 620nm. Previously, we have shown that the use of Fityk (Wojdyr, 2010), an open-source software, allow for adequate separation of these two closely located peaks. Therefore, the same deconvolution procedure was followed here: a sum of two log-normal function (IV-1) was used to simultaneously fit the overall spectra and the fit was judged using the Nelder-Mead Simplex algorithm and the fit was judged based on the weighted sum of squared residuals (Wojdyr, 2010).

$$\mathrm{I}(\nu) = \sum I_{oi} * \exp\left\{-\ln(2)\left(\frac{\ln\left\{1+\left[\frac{2\mathrm{b}(\nu_i-\nu_{\mathrm{Pi}})}{\Delta_i}\right]\right\}}{\mathrm{b}_i}\right)^2\right\} \quad \text{(IV-1)}$$

In one log-normal function, I_{0i} corresponds to the peak intensity of emission spectra, ν_P is the wavenumber of maximum emission intensity, Δ_i is the line width parameter, and b_i is an asymmetry parameter. The value of bandwidth Γ_i, which is the full width at half maximum (FWHM) calculated from the line width (Δ_i) and

asymmetry parameter (b_i), was directly estimated by Fityk. The subscription *i* indicates whether it is the delayed fluorescence or phosphorescence spectra.

Time-resolved Measurements: Phosphorescence intensity decays of riboflavin in glassy sugar films were excited at 440nm and collected at 620nm. A total decay time of 1000ms was collected and each measurement was an average of 50 cycles to smooth the decay curve and to minimize instrument noise. In our previous study, we have shown that 3-exponential model best described the decay kinetics of riboflavin phosphorescence in amorphous sucrose matrix and resulted in evenly distributed modified residuals. Therefore, the 3-exponential model (IV-2) was used in this study to characterize the phosphorescence decay kinetics of riboflavin in the different sugar matrices.

	$$I(t) = I(0) * \sum_{i=1}^{n} \alpha_i \exp\left(-\frac{t}{\tau_i}\right)$$	(IV-2)

In this equation (Eq. IV-2), I(0) is the initial intensity at t=0, n is the number of lifetime components (in this case, 3), and τi and αi are the lifetime and amplitude of each component. The values of τi reflect the molecular mobility of the heterogeneous matrix and the values of αi represent the distribution of these energetically distinct islands. The average lifetime from this model is calculated from population average (Eq.(IV-3):

	$$\tau_m = \sum_{i}^{n} \alpha_i \tau_i$$	(IV-3)

Photophysical Rate Constants: The calculated average lifetime provides a means to calculate the rate constant of triplet state de-excitation (k_P) and consequently the rate constant of non-radiative decay (k_{TS0}), which is a direct measure of matrix mobility-controlled quenching. Phosphorescence lifetime is determined by the rate constants of all possible de-excitation pathways (IV-4):

$$\frac{1}{\tau} = k_P = k_{RP} + k_{TS1} + k_{TS0} + k_Q[O_2] \quad \text{(IV-4)}$$

where k_{RP} is the rate constant of radiative decay, an intrinsic property of the phosphorescent probe; k_{TS1} is the rate constant of reverse intersystem crossing; k_{TS0} is the rate constant of non-radiative decay; $k_Q[O_2]$ is a measure of matrix-induced quenching; and the rate constant of collisional quenching with oxygen. In this study, k_{RP} was approximated using the phosphorescence lifetime of riboflavin in glycerol/water mixture (3:1 v/v) as reported in our previous studies, under the assumption that all the other de-excitation pathways were negligible under this extremely low temperature. The value of k_{TS1} was calculated from the ratio of the intensity of delayed fluorescence and phosphorescence (IV-5) (Parker, 1968):

$$I_{DF}/I_P = \phi_F \left(k_{TS1}/k_{RP}\right) \quad \text{(IV-5)}$$

in which ϕ_F is the quantum yield of fluorescence. A ϕ_F value of 0.37 was reported for riboflavin fluorescence in starch films; this value was used as an estimated ϕ_F in the calculations for amorphous solid films (Penzkofer, 2012). The temperature

dependence of rate constant k_{TS1} can be characterized by the Arrhenius equation (IV-6):

	$k_{TS1}(T) = k^{\circ}_{TS1} \exp\left(-\frac{\Delta E_{TS}}{RT}\right)$	(IV-6)

where k°_{TS1} is the maximum reverse intersystem crossing rate at high temperature, ΔE_{TS} is the activation energy required for reverse intersystem crossing, and R is the universal gas constant of 8.314 J/K·mol (Parker, 1968). Therefore, Eq. (IV-6 can also be written in:

	$I_{DF}/I_P = \left(\frac{\phi_F}{k_{RP}}\right) * [k^{\circ}_{TS1} \exp\left(-\frac{\Delta E_{TS}}{RT}\right)]$	(IV-7)

Plotting ln (I_{DF}/I_P) against 1/T results in a linear relationship with an intercept equal to ln$[\left(\frac{\phi_F}{k_{RP}}\right) k^{\circ}_{TS1}]$ and a slope equal to $-\frac{\Delta E_{TS}}{R}$ (Parker, 1968). The activation energy for reverse intersystem crossing ΔE_{TS} and the maximum reverse intersystem crossing rate k°_{TS1} can be approximated and $k_{TS1}(T)$ can be calculated accordingly. Since nitrogen was purged into the cuvette to create an oxygen-free environment throughout the measurement, $k_Q[O_2]$ was considered negligible. Therefore, the value of k_{TS0} was calculated accordingly. The magnitude of k_{TS0} is a direct measure of matrix-induced quenching modulated by ability of triplet state molecule to dissipate its energy to nearby molecules in the matrix. The temperature dependence of k_{TS0} was analyzed with an Arrhenius plot of ln(k_{TS0}) vs 1/T and the activation energy to

quench the triplet molecule within different temperature ranges was calculated from the plot and was associated with relaxation processes in amorphous systems.

Results and Discussions

Steady state phosphorescence: Delayed luminescence spectra from riboflavin in six malto-oligomers glassy matrices were collected over the temperature range from -30 to 100°C. Riboflavin emission spectra exhibit two peak maxima located around 515nm and 620nm, respectively. The former is delayed fluorescence and the latter is phosphorescence. The emission spectra of riboflavin in maltose (G2) at selected temperatures are plotted in Figure IV-1. As shown, the phosphorescence emission intensity decreased monotonically with temperature, but at temperatures above 50°C the phosphorescence emission overlapped delayed fluorescence on the blue side. The emission intensity of delayed fluorescence, on the other hand, initially increased with temperature from until 60°C and further decreased above 60°C. The E-type delayed fluorescence is a result of thermally promoted reverse intersystem crossing, when triplet riboflavin molecules cross back to the singlet state and emit photons from the exited singlet state (Parker, 1968). The delayed fluorescence emission peak is located in the vicinity of riboflavin fluorescence emission but it happens on a much slower timescale similar to that of phosphorescence emission. The temperature increase from -30 to 60°C contributed to the increase in delayed fluorescence peak intensity over this temperature range. The prominent reverse intersystem crossing process, together with enhanced triplet quenching, as temperature increased, resulted in the decrease in phosphorescence intensity. The decrease of delayed fluorescence peak intensity over 60 to 100°C was likely caused by the enhanced photodegradation of riboflavin at high temperatures and the

promoted rate of non-radiative decay. The same trend was observed in all six malto-oligomers tested in this study. The changes in peak intensity of both phosphorescence and delayed fluorescence from riboflavin emission in glassy maltose films are shown in Figure IV-2 as an example.

The peak frequency (ν_P), a measure of the average emission energy from triplet riboflavin molecules, and the bandwidth (Γ), a measure of the inhomogeneous broadening in the distribution of energetically different regimes in the matrix, were both obtained from fitting the emission spectra with the log-normal function. Figure IV-3 shows how the peak frequency and FWHM of riboflavin phosphorescence emission in amorphous maltose film changed with temperature. As shown, the peak frequency decreased gradually with temperature, indicating a decrease in the average emission energy from triplet riboflavin molecules. This decrease reflected an increase in the dipolar relaxation in the matrix around excited triplet molecules before emission. The value of FWHM is a direct indicator of inhomogeneous broadening. The increase of FWHM reflected an increase in the dynamic heterogeneity due to the broadening in the distribution of local dipolar relaxation rates. Similar trend, i.e. decreasing peak frequency and increasing FWHM with an increase of temperature was observed in all six malto-oligomers used in this study (Data not shown). However, due to the noteworthy distorting effect from the delayed fluorescence emission spectra, parameters from emission spectra were not used as the primary indicators for mobility. Instead, more emphasis was given to the triplet riboflavin decay pattern.

Figure IV-1

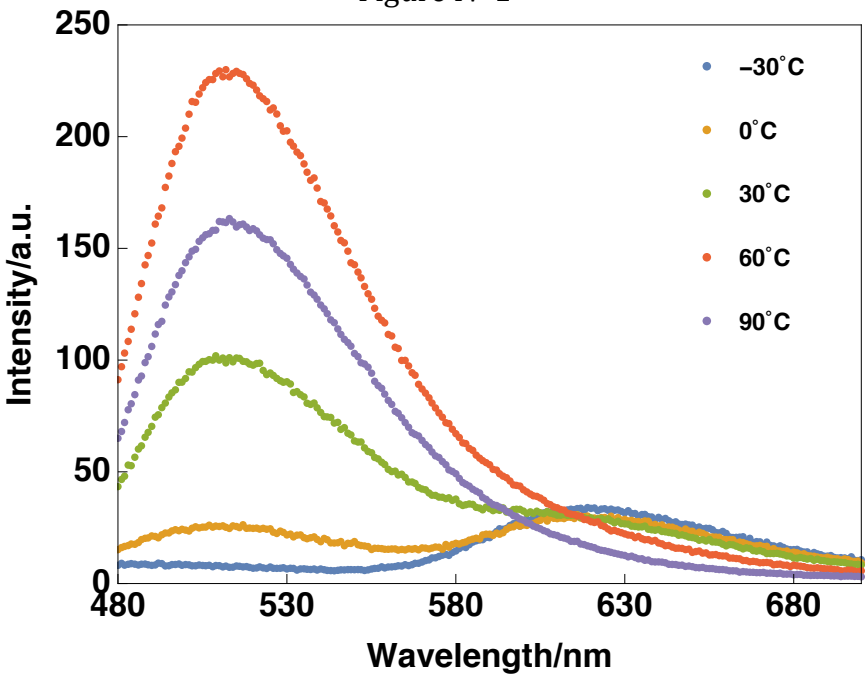

Figure IV-1: Delayed luminescence emission spectra of riboflavin in amorphous maltose film at -30˚C (blue), 0˚C (yellow), 30˚C (green), 60˚C (red), and 90˚C (purple).

Figure IV-2

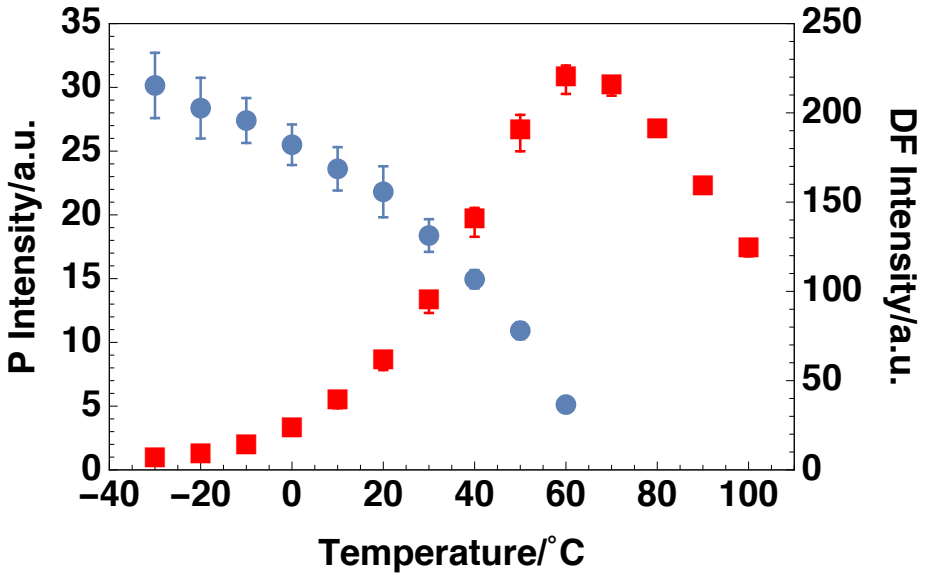

Figure IV-2: Riboflavin delayed luminescence emission in amorphous maltose film: peak intensity of phosphorescence (blue circles) and delayed fluorescence (red squares) as a function of temperature

Figure IV-3

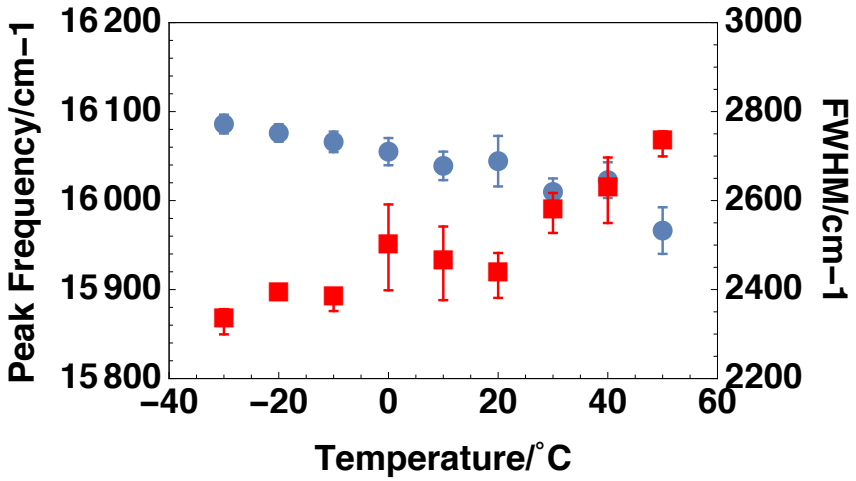

Figure IV-3: Riboflavin delayed luminescence emission in amorphous maltose film: peak frequency (blue circles) and FWHM (red squares) as a function of temperature

Time-resolved phosphorescence: Phosphorescence intensity decays of riboflavin in amorphous malto-oligomers films were collected from -30 to 100˚C at 10˚C intervals. A three-exponential model was used to characterize the decay kinetics. The values of R^2 over the whole temperature range in all six sugars fell within the range of 0.99~1 and the modified residuals distributed evenly about zero. Both suggested that the 3-exponential model was adequate to describe the phosphorescence decays. Figure IV-4 and Figure IV-5 show the phosphorescence intensity decays of riboflavin in the films of maltose (G2) and maltohexaose (G6) fitted using the 3-exponential models at 10˚C, along with the modified residuals from the corresponding fits.

Typical lifetimes and fractional amplitudes from riboflavin decays in glassy maltose film are plotted against temperature in Figure IV-6. The lifetimes (Figure IV-6a) varied largely in magnitudes. The three lifetime components were approximately 130ms, 43ms, and 5ms at -30˚C. At the same temperature, the rate of reverse intersystem crossing remained the same. The lifetime values can thus be considered a rough measure to assess the molecular mobility in the sugar matrix: long lifetime component indicates rigid molecular environment around the triplet molecules while short lifetime component indicates flexible local environment that promotes collisional quenching between the triplet molecules and the matrix. The difference between lifetimes as observed here was an indicator of matrix heterogeneity and suggested that there were local regimes of divergent molecular mobility. All lifetimes decreased monotonically as the temperature increased, but the extent of reduction was most prominent for the longest lifetime, τ_1, which decreased from

130ms at -30˚C to 26ms at 80˚C. The reduction in all lifetimes suggested that there was an overall increase in the matrix mobility as the temperature increased, where the previously rigid regimes gradually became flexible and the previously flexible environment became even more flexible temperature increased. The same lifetime behavior was observed in all six sugars investigated in this study.

The changes in fractional amplitudes of each lifetime component of the riboflavin decays in maltose films as a function of temperature are plotted in Figure IV-6b. As shown, the amplitudes of the long and medium lifetime components decreased while that of short lifetime component increased with increasing temperatures. The same trend was also observed in all six sugars, but the magnitudes of fractional amplitudes differed. The amplitudes reflect the distribution of dynamically distinct regimes in the matrix. Based on the amplitudes, it was speculated that at low temperatures, approximately half of the excited riboflavin molecules resided in the neither too rigid nor too flexible environment and possessed a medium lifetime about 40ms; the remaining half of the population resided almost evenly between the rigid or the flexible environments. As the temperature increased, the population of medium and long lifetime components decreased and the population of short lifetime component increased. This suggested that the previously rigid matrix transformed into less rigid environment and that the flexible regime became predominant in the system. At 80˚C, approximately 80% of the excited population possessed short lifetime, suggesting that most of the excited molecules could easily dissipate the excessive energy to the surrounding environment through non-radiative decay instead of emitting phosphorescence.

The average phosphorescence lifetime was calculated using the population average (IV-3). Figure IV-7 is a summary of the temperature dependence of riboflavin phosphorescence lifetime in the six malto-oligomers investigated. As shown, at the same temperature riboflavin phosphorescence lifetime decreased in the order of: maltose> maltotriose> maltotetraose> maltopentaose≈ maltohexaose≈ maltoheptaose. To take a closer look at the differences in riboflavin phosphorescence lifetimes in these malto-oligomers, we compared the parameters obtained, i.e. lifetimes and amplitudes. Interestingly, we found that at the same temperature, the lifetime varied little among different sugars, as shown in Figure IV-8a. However, the amplitudes of lifetime components vary greatly (Figure IV-8b), indicating that at the same temperature, the dynamic heterogeneity varied among these malto-oligomers. For example, in Figure IV-8b, the fractional amplitudes A_1 from riboflavin decays in maltose, maltotetraose, and maltohexaose varied in the order of maltose>maltotetraose>maltohexaose. Such divergence started to merge as temperature increased above 60˚C. This suggested that under low temperature (<50˚C), the rigid local environment is more prevalent in maltose (smaller molecular size) than in maltohexaose (larger molecular size), but such prevalence became less prominent at high temperatures.

To separate the contribution of Tg and molecular size, the phosphorescence lifetimes are plotted against ΔT=T-Tg, which denotes the distance from glass transition temperature, in Figure IV-9. It is clear that, at the same ΔT, the riboflavin phosphorescence lifetime varied in the order maltose> maltotriose> maltotetraose> maltopentaose≈ maltohexaose≈ maltoheptaose. This indicated that from maltose to

maltotetraose, the addition of glucose unit significantly increased in the molecular mobility; but when the molecular size is larger than maltopentaose, the addition of one glucose unit only marginally increased the molecular mobility the molecular size.

Figure IV-4

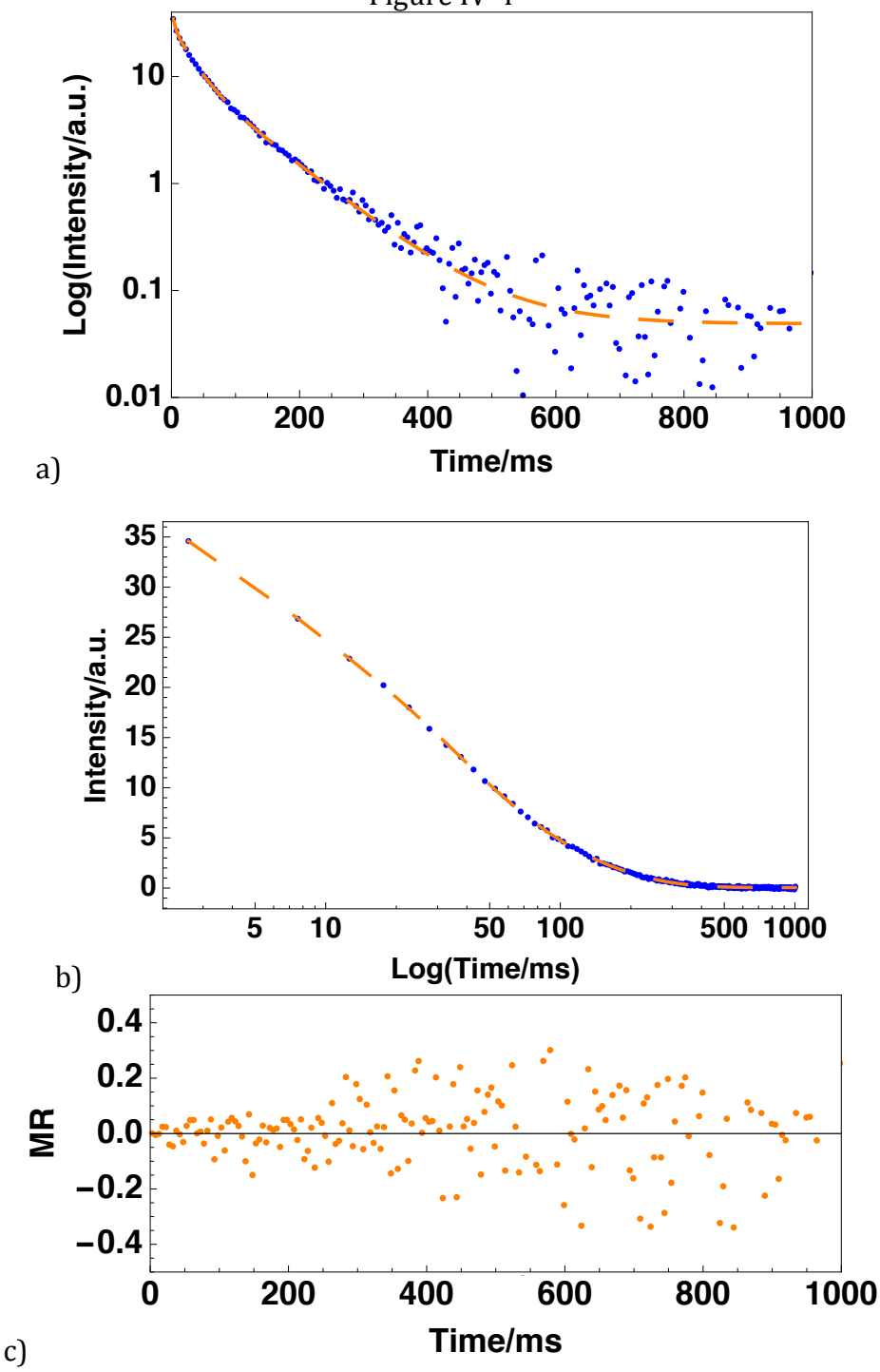

Figure IV-4: Phosphorescence decays of riboflavin (blue circles) in amorphous films of maltose fitted using a 3-exponential model (orange dashed line) plotted in linear-log (a) and log-linear (b) coordinates, and the modified residues (orange circles) from the fit (c).

Figure IV-5

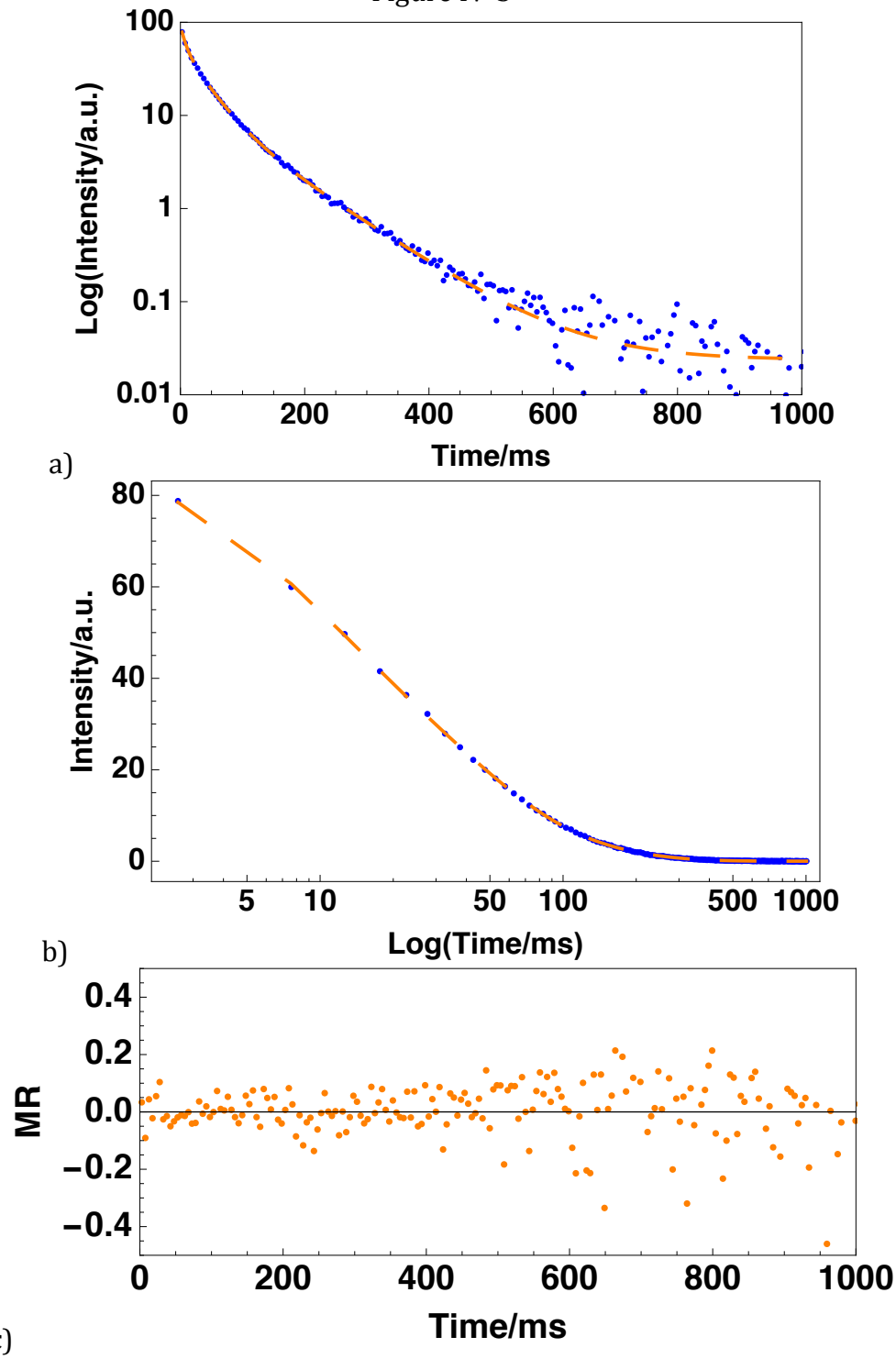

Figure IV-5: Phosphorescence decays of riboflavin (blue circles) in amorphous films of maltohexaose fitted using a 3-exponential model (orange dashed line) plotted in linear-log (a) and log-linear (b) coordinates, and the modified residues (orange circles) from the fit (c).

Figure IV-6

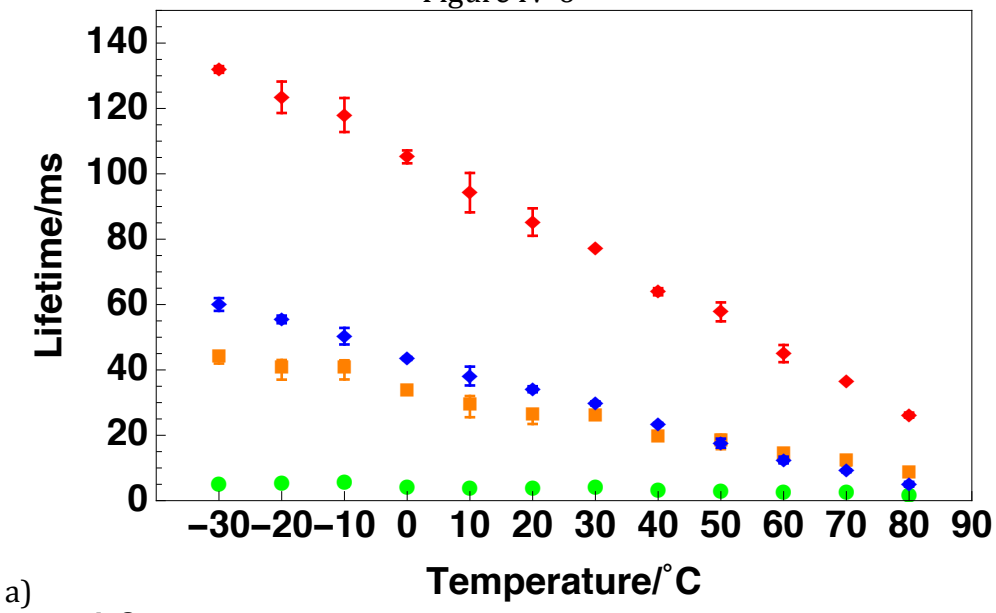

a)

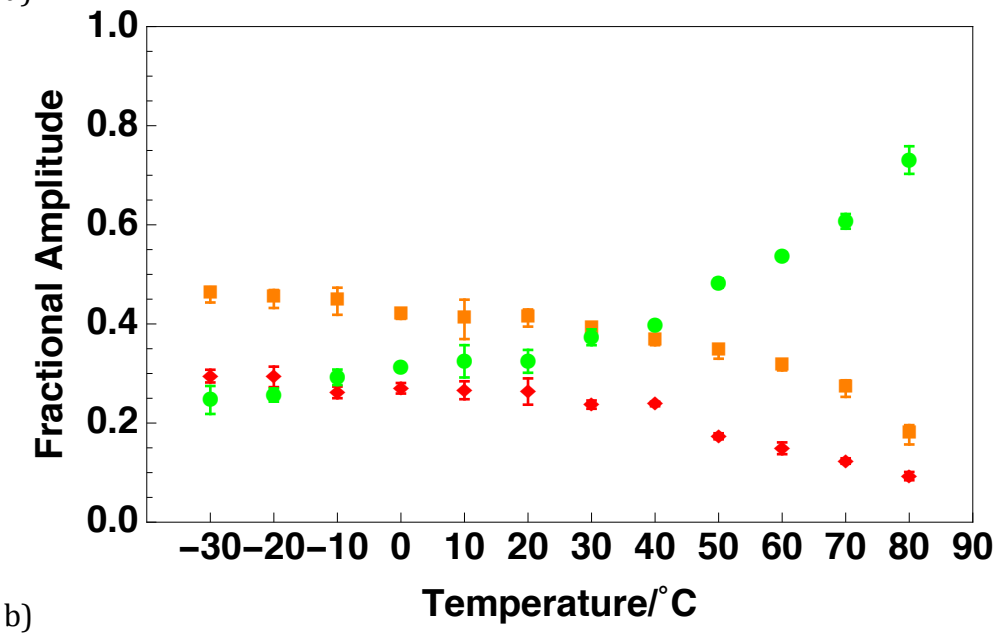

b)

Figure IV-6: a) Lifetimes, τ_1 (red diamonds), τ_2 (orange squares), and τ_3 (green circles) and the average lifetimes (blue diamond) of riboflavin phosphorescence decays in amorphous maltose film as a function of temperature. b) The fractional amplitude α_1 (red diamonds), α_2 (orange squares), and α_3 (green circles) as a function of temperature.

Figure IV-7

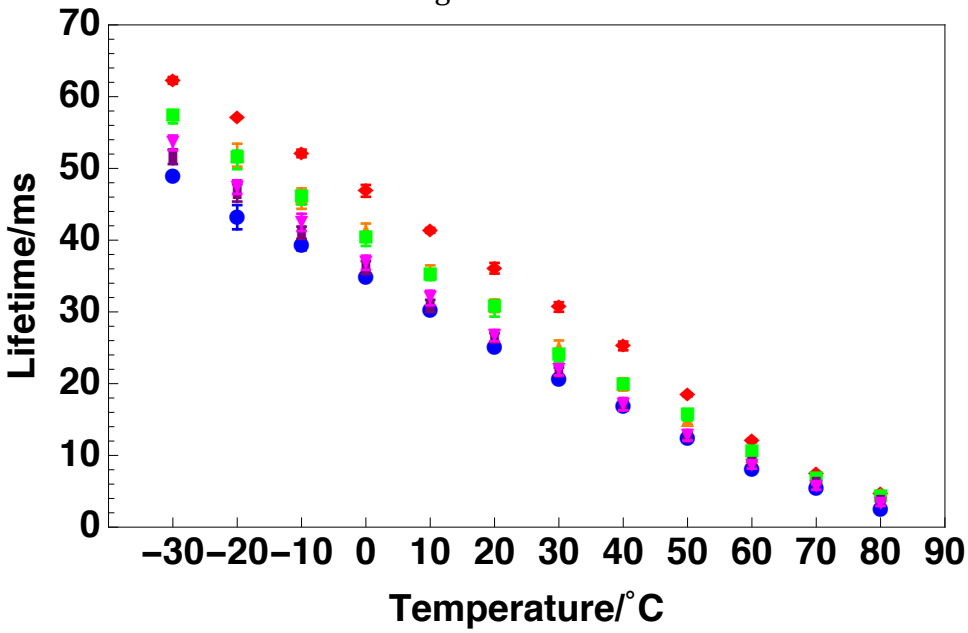

Figure IV-7: Phosphorescence lifetimes of riboflavin in maltose (red diamonds), maltotriose (orange triangles), maltotetraose (green squares), maltopentaose (blue circles), maltohexaose (purple rectangles), and maltoheptaose (magenta down triangles) as a function of temperature.

Figure IV-8

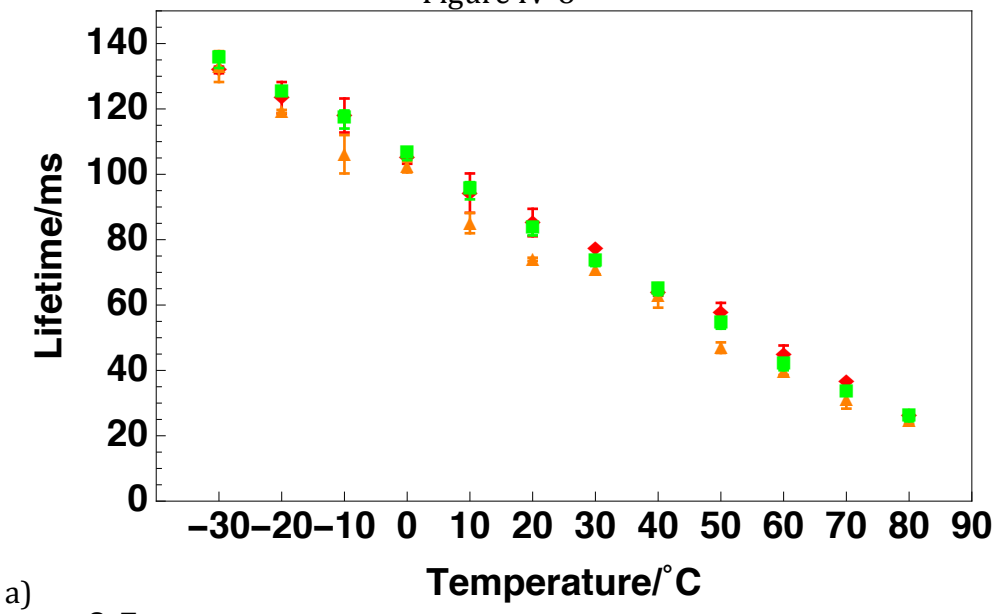

a)

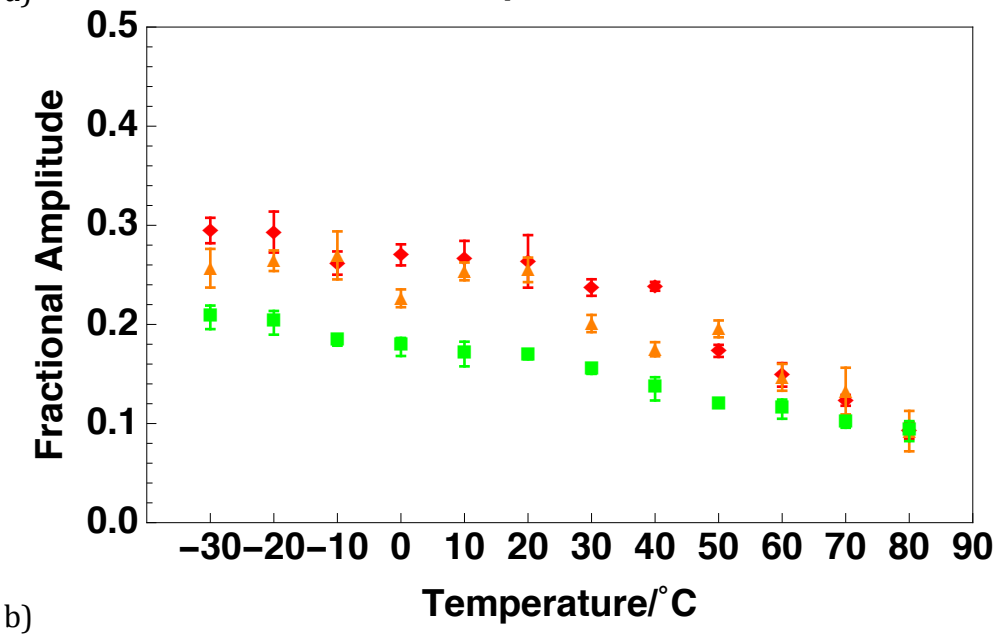

b)

Figure IV-8: a) Lifetime τ_1 and b) fractional amplitude (A_1), of riboflavin phosphorescence decays in amorphous films of maltose (red diamonds), maltotetraose (orange triangles), and maltohexaose (green squares) as a function of temperature.

Figure IV-9

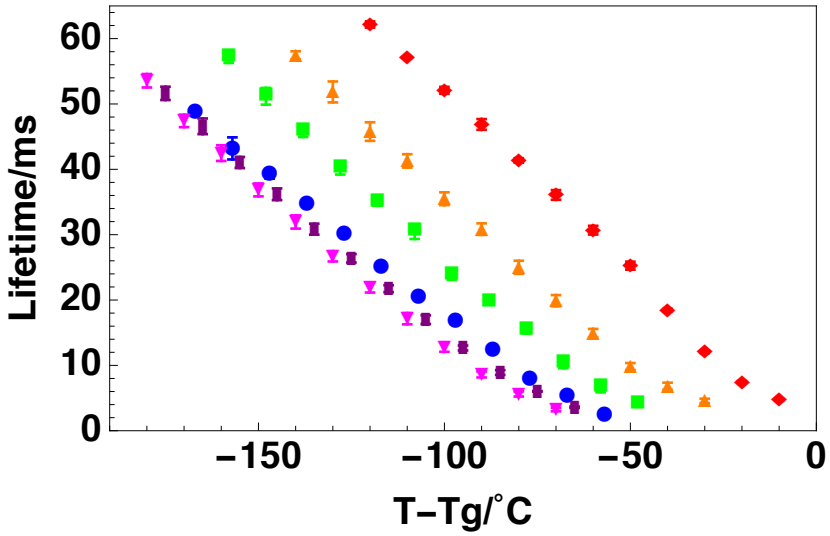

Figure IV-9: Phosphorescence lifetimes of riboflavin in maltose (red diamonds), maltotriose (orange triangles), maltotetraose (green squares), maltopentaose (blue circles), maltohexaose (purple rectangles), and maltoheptaose (magenta down triangles) plotted against ΔT=T-Tg

Non-radiative decay rates: As discussed in Materials and Methods, the overall rate for phosphorescence is the sum of all possible de-excitation pathways (IV-4). The decrease in riboflavin phosphorescence lifetime with increasing temperature reflected an increase in the rate to phosphoresce, which was attributed to the increase in both the rate of reverse intersystem crossing (k_{TS1}) and the rate of non-radiative decay (k_{TS0}), both promoted by thermal energy. The natural phosphorescence lifetime of riboflavin in glycerol-water (3:1 v/v) at 77K has been has been reported in our previous work and the intrinsic phosphorescence rate used in this study is $5.88s^{-1}$. The values of the rate of reverse intersystem crossing (k_{TS1}) were calculated following the procedure described in the Materials and Methods section (IV-5).

In the absence of quenching molecules, the non-radiative decay rate constant was estimated from (IV-4). Figure IV-10 shows the temperature dependence of rate constants, k_P, k_{TS1}, and k_{TS0} of riboflavin phosphorescence decays in an amorphous maltose film. All three rate constants increased gradually over the course from -30 to 30˚C, and from 40˚C onwards, the increase became more dramatic.

The value of k_{TS0} increased with temperature in all six sugars and the increase became more dramatic at higher temperatures (Figure IV-11). In all six malto-oligomers, the increase in k_{TS0} became abrupt when temperature was above 40˚C, regardless of the glass transition temperature. To highlight the influence of physical properties on k_{TS0} and to isolate the influence from Tg, the values of k_{TS0} are plotted against $\Delta T=T-Tg$ (Figure IV-12) and the Arrhenius plots of are plotted against Tg/T

(Figure IV-13). As shown in Figure IV-12, at the same ΔT, the values of k_{TS0} changed in the order of: maltose< maltotriose< maltotetraose<maltopentaose≈ maltohexaose≈ maltoheptaose, suggesting that molecular mobility also increased in the same order. As molecular size increased, molecular mobility increased. Yet such increase became less prominent when the molecular size was larger than five glucose units. This observation was in good agreement with Imamura *et al*'s study, in which Temperature scanning Fourier transform infrared (TS-TFIR) spectroscopy was used to investigate the hydrogen bonding in various amorphous carbohydrates (Imamura et al., 2006). According to their study, hydrogen bonding in malto-oligomers increased in the order of: maltose> maltotriose> maltotetraose≈ maltopentaose≈ maltohexaose≈ maltoheptaose. A greater degree of formation of hydrogen bonds accounts for low molecular mobility in the matrix, which thus echoes with our observation. The clustering of maltopentaose, maltohexaose, and maltoheptaose suggested that the addition of glucose unit above maltotetraose only minimally increased the molecular mobility. This finding is in accordance with what has been proposed by Meißner *et al* (2000). This group used dielectric spectroscopy and computer simulations to study the relaxations of different polysaccharides and their monomers, dimers, and oligomers. In their work, they concluded at low temperatures, the local mobility dominated by small repeating units in amorphous sugars and that the number of monomers involved in the repeating units was between 2-5 (Meißner et al., 2000).

The greater local mobility observed in larger malto-oligomers glassy matrices can also be associated with the free volume theory: when carbohydrates of larger

molecular sizes form glassy matrices, they are more loosely packed compared to their counterparts of smaller molecular size. This results in greater molecular free volume, which consequently leads to a greater degree of freedom to rearrange hydrogen bonds during temperature change (Wolkers, Oliver, Tablin, & Crowe, 2004).

The magnitude of k_{TS0} provides a measurement of matrix-induced quenching. The collisional quenching between the matrix and the excited riboflavin molecules can be attributed to the process of triplet riboflavin coupling with the highly excited vibrational ground state sugar molecules and the ability of these sugar molecules to dissipate the energy from excited triplet riboflavin molecules to nearby molecules in the matrix. The activation energy to quench triplet riboflavin molecules was calculated from the Arrhenius plots of k_{TS0} (Figure IV-14) and the values are summarized in Table IV-2. As shown, at low temperature from -30 to 30˚C, the values of activation energy are overall low across the board, which suggests that there is little motion in the system. The activation energies in six sugars measured over temperature range from 50 to 80˚C are typical of activation energy of β relaxation process, which suggests that the emerging β relaxation quenches triplet state riboflavin molecules.

Figure IV-10

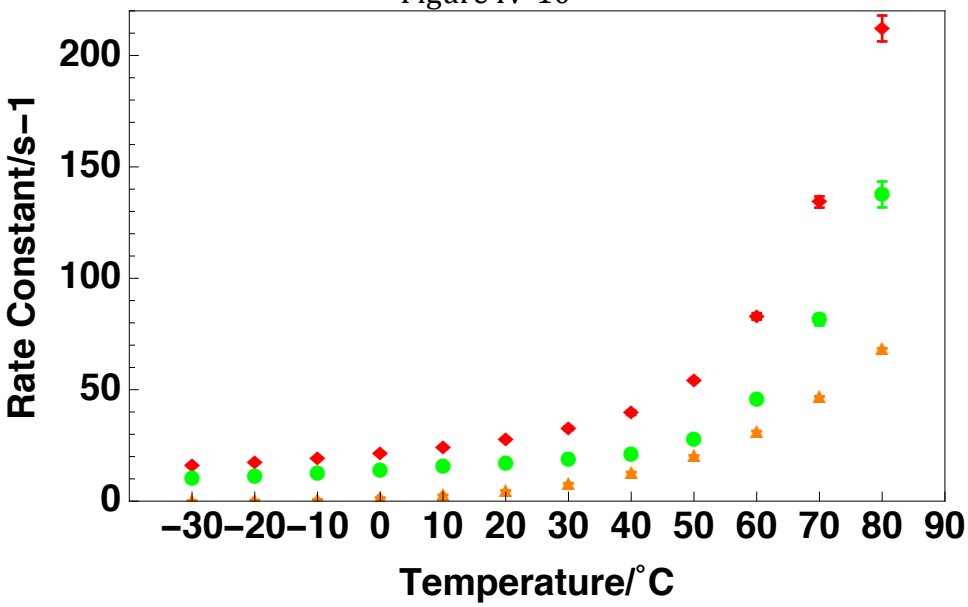

Figure IV-10: Rate constants of triplet riboflavin in amorphous maltose films: rate constant of phosphorescence k_P (red diamonds), rate constant of reverse intersystem crossing k_{TS1} (orange triangles), and rate constant of non-radiative decay k_{TS0} (green circles) as a function of temperature.

Figure IV-11

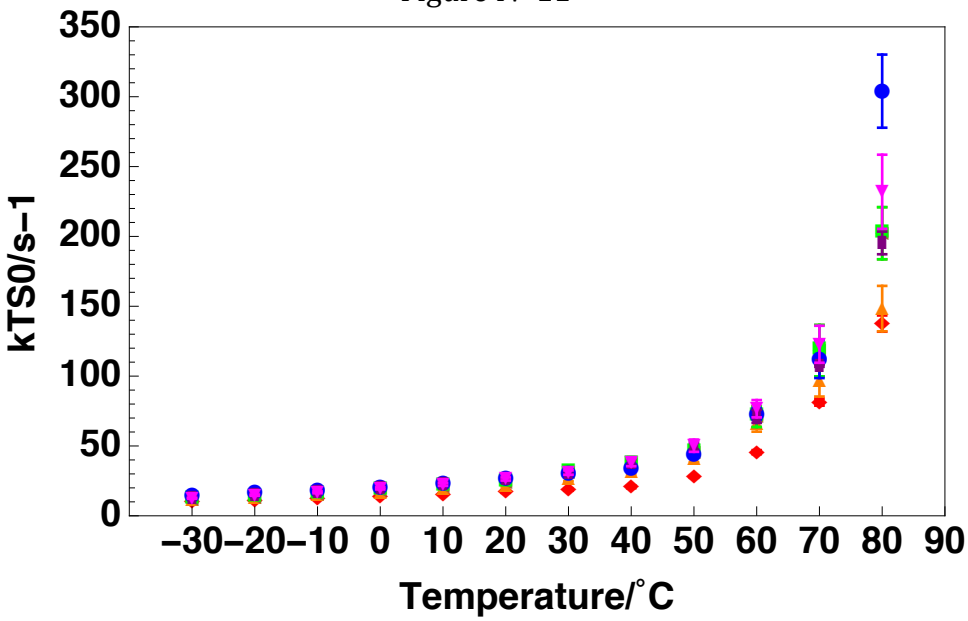

Figure IV-11: Rate of non-radiative decay rate k_{TS0} of riboflavin in amorphous maltose (red diamonds), maltotriose (orange triangles), maltotetraose (green squares), maltopentaose (blue circles), maltohexaose (purple rectangles), and maltoheptaose (magenta down triangles) as a function of temperature.

Figure IV-12

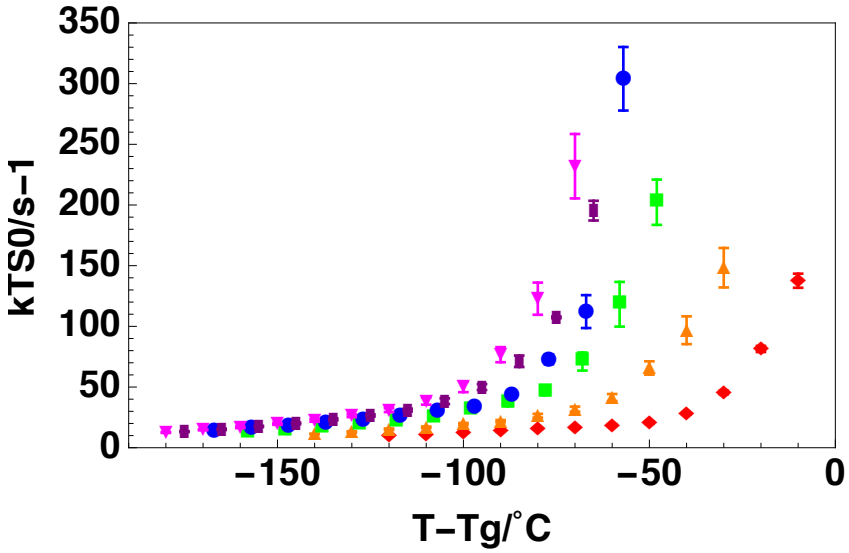

Figure IV-12: Rate of non-radiative decay rate k_{TS0} of riboflavin in in amorphous maltose (red diamonds), maltotriose (orange triangles), maltotetraose (green squares), maltopentaose (blue circles), maltohexaose (purple rectangles), and maltoheptaose (magenta down triangles) plotted against ΔT=T-Tg.

Figure IV-13

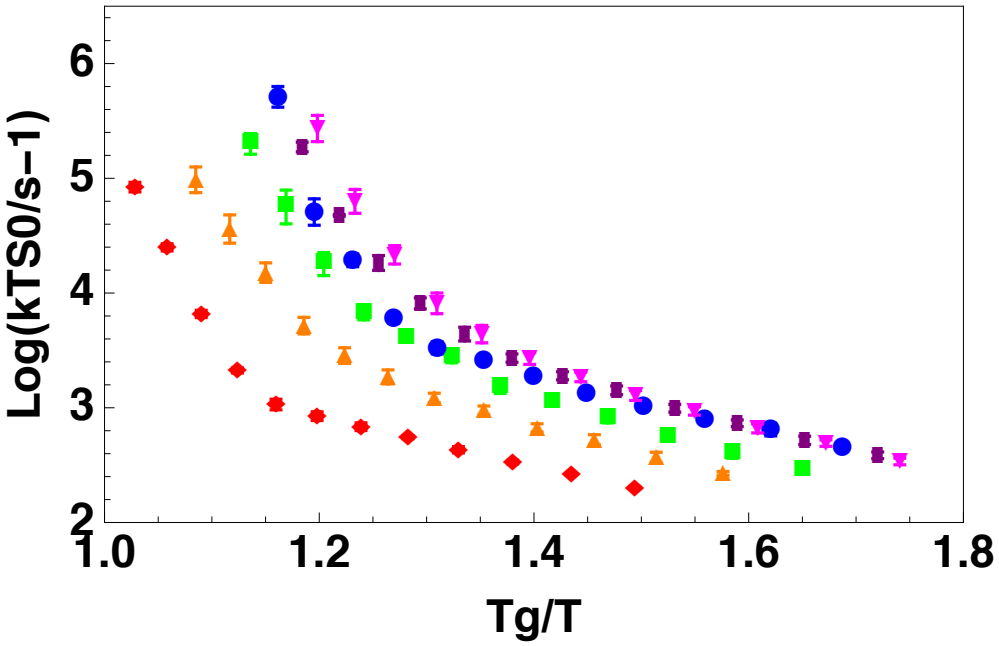

Figure IV-13: Tg-normalized Arrhenius plots of the non-radiative rate constant of triplet riboflavin in amorphous maltose (red diamonds), maltotriose (orange triangles), maltotetraose (green squares), maltopentaose (blue circles), maltohexaose (purple rectangles), and maltoheptaose (magenta down triangles).

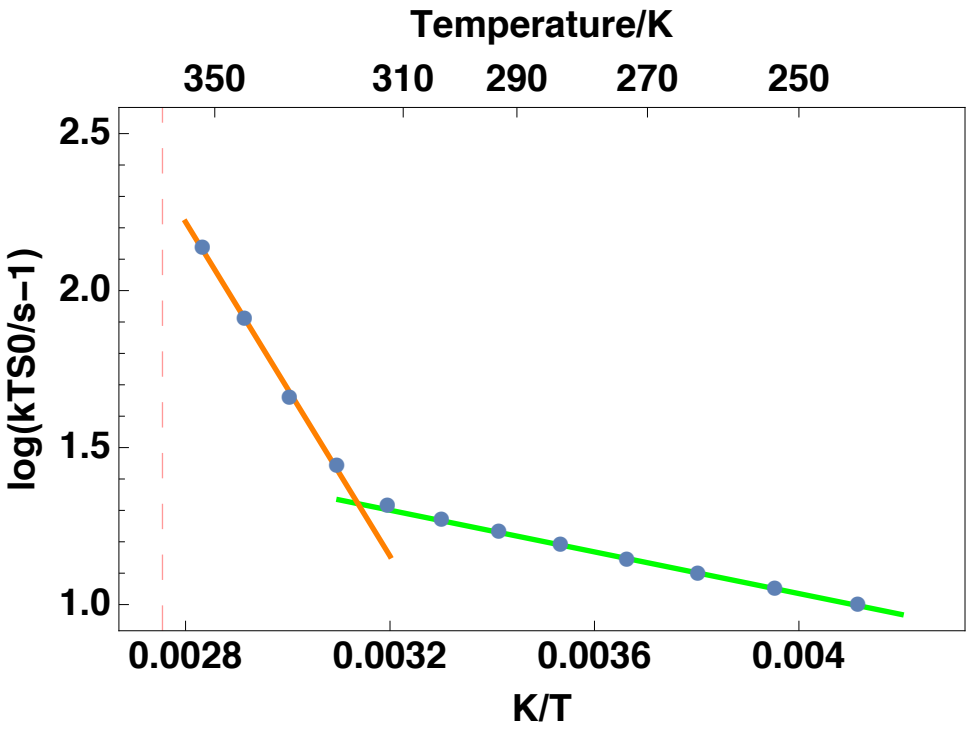

Figure IV-14: Arrhenius plot of non-radiative decay rate k_{TS0} calculated from the average lifetime of the phosphorescence decays of riboflavin dispersed in amorphous maltose. The red vertical dashed line marks the glass transition temperature of maltose.

Table IV-2: Activation energies required to quench triplet riboflavin molecules in amorphous films of maltose (G2), maltotriose (G3), maltotetraose (G4), maltopentaose (G5), maltohexaose (G6), and maltoheptaose (G7)

E_A (kJ/mol)	G2	G3	G4	G5	G6	G7
-30~30˚C	6.55	8.33	8.72	7.44	8.28	8.60
50~80˚C	50.92	40.03	43.90	43.19	42.50	41.21

Conclusion

Phosphorescence responses from riboflavin dispersed in glassy malto-oligomer films measured over the temperature range from -30 to 100˚C showed great sensitivity towards local molecular mobility changes- in particular, β relaxation. The data reported here indicate that the molecular mobility in the six glassy malto-oligomer matrices studied increase with the molecular size, as oligosaccharides with a larger size are more loosely packed and form amorphous matrices with a higher molecular free volume. Our results suggest that high glass transition temperature does not necessarily equals to low molecular mobility and stability. Other factors, such as molecular size and the packing pattern of molecules also play a role in determining the molecular mobility of glassy matrices. Moreover, they also determine the physical and chemical stability of labile biomaterials encapsulated in the amorphous matrices.

References

Bhattacharya, S., & Suryanarayanan, R. (2011). Molecular motions in sucrose-PVP and sucrose-sorbitol dispersions: I. implications of global and local mobility on stability. *Pharmaceutical Research, 28*(9), 2191-2203. doi:10.1007/s11095-011-0447-0

Bhattacharya, S., & Suryanarayanan, R. (2009). Local mobility in amorphous pharmaceuticals--characterization and implications on stability. *Journal of Pharmaceutical Sciences, 98*(9), 2935-2953. doi:10.1002/jps.21728

Capaccioli, S., Paluch, M., Prevosto, D., Wang, L., & Ngai, K. L. (2012). Many-body nature of relaxation processes in glass-forming systems. *The Journal of Physical Chemistry Letters, 3*(6), 735-743. doi:10.1021/jz201634p

Cicerone, M. T., & Douglas, J. F. (2012). ß-relaxation governs protein stability in sugar-glass matrices. *Soft Matter, 8*(10), 2983-2991. doi:10.1039/c2sm06979b

Cicerone, M. T., Pikal, M. J., & Qian, K. K. (2015). Stabilization of proteins in solid form. *Advanced Drug Delivery Reviews, 93*, 14-24. doi:10.1016/j.addr.2015.05.006

Imamura, K., Sakaura, K., Ohyama, K. -., Fukushima, A., Imanaka, H., Sakiyama, T., & Nakanishi, K. (2006). Temperature scanning FTIR analysis of hydrogen bonding states of various saccharides in amorphous matrixes below and above their glass transition temperatures. *Journal of Physical Chemistry B, 110*(31), 15094-15099. doi:10.1021/jp057527o

Meißner, D., Einfeldt, J., & Kwasniewski, A. (2000). Contributions to the molecular origin of the dielectric relaxation processes in polysaccharides – the low temperature range. *Journal of Non-Crystalline Solids, 275*(3), 199-209. doi:http://dx.doi.org/10.1016/S0022-3093(00)00248-9

Orford, P. D., Parker, R., Ring, S. G., & Smith, A. C. (1989). Effect of water as a diluent on the glass transition behaviour of malto-oligosaccharides, amylose and amylopectin. *International Journal of Biological Macromolecules, 11*(2), 91-96.

Parker, C. A. (1968). *Photoluminescence of solutions : With applications to photochemistry and analytical chemistry*. Amsterdam: Elsevier.

Pravinata, L. C., You, Y., & Ludescher, R. D. (2005). Erythrosin B phosphorescence monitors molecular mobility and dynamic site heterogeneity in amorphous sucrose. *Biophysical Journal, 88*(5), 3551-3561. doi:http://dx.doi.org/10.1529/biophysj.104.054825

Suzuki, T., Komatsu, H., & Miyajima, K. (1996). Effects of glucose and its oligomers on the stability of freeze-dried liposomes. *Biochimica Et Biophysica Acta, 1278*(2), 176-182.

Wojdyr, M. (2010). Fityk: A general-purpose peak fitting program. *Journal of Applied Crystallography, 43*(5), 1126-1128. doi:10.1107/S0021889810030499

Wolkers, W. F., Oliver, A. E., Tablin, F., & Crowe, J. H. (2004). A fourier-transform infrared spectroscopy study of sugar glasses. *Carbohydrate Research, 339*(6), 1077-1085. doi:http://dx.doi.org/10.1016/j.carres.2004.01.016

Yu, L. (2001). Amorphous pharmaceutical solids: Preparation, characterization and stabilization. *Advanced Drug Delivery Reviews, 48*(1), 27-42. doi:http://dx.doi.org/10.1016/S0169-409X(01)00098-9

Chapter V Using Riboflavin Phosphorescence as an Optical Probe to Study the Effects of Molecular Size and the Addition of Glycerol on Molecular Mobility in Amorphous Dextran Films

Introduction

Glassy carbohydrates play an important role in pharmaceutical and food industries, as they are widely applied for encapsulation and preservation of bioactive compounds, flavors, antibodies, and enzymes (Cicerone, Tellington, Trost, & Sokolov, 2003). The use of glassy carbohydrates as preservation media allows for the storage of biological agents in a dry format under ambient temperature, as an economic and easy preservation method. The shelf-life and stability of such encapsulated liable products was found to be largely dependent on both the stabilizing effect of the sugar matrix and the physical properties of the encapsulation layer (Cicerone et al., 2003; Imamura et al., 2002). The stabilizing effect is determined by the specific intrinsic properties of sugar and the physical properties are determined by both the intrinsic properties of sugar and environmental factors such as humidity, temperature, and the addition of small molecules.

Historically, carbohydrates with high glass transition temperature (Tg) have often been considered favorable as encapsulation materials for biopreservation. At temperatures near or above Tg, α relaxation process takes place, a rigid glassy matrix becomes soft and transform into rubbery state, and global motions of protein that can lead to denaturation and diffusion of reactive species are prone to occur

(Cicerone et al., 2003). The use of carbohydrates with high Tg thus is effective in suppressing α relaxation at ambient storage temperature. Yet, studies have also shown that Tg is not a sufficient indicator of optimal stability and that degradations of proteins can still occur when stored at temperatures 50˚C below Tg, which is though to be caused by fast secondary relaxation processes (β and γ) (Bhattacharya & Suryanarayanan, 2009). Recently, it has been shown that the addition of small amount of low molecular weight compounds such as glycerol and some disaccharides to a high molecular weight polymeric system can improve the storage stability of encapsulated liable proteins and other liable compounds even though the addition of small molecules ultimately lowers the Tg of the mixture system (Cicerone & Douglas, 2012; Roussenova, Murith, Alam, & Ubbink, 2010; Roussenova, Andrieux, Alam, & Ubbink, 2014; Taylor, 1998). Studies have pointed out that the addition of small molecules is able to slow β relaxation process, to reduce molecular mobility at storage temperature, and eventually to improve the storage stability of encapsulated labile compounds (Cicerone et al., 2003; Cicerone & Douglas, 2012).

Among the small molecules added to enhance storage stability of glassy encapsulation matrices, glycerol is one of the most important and widely studied compounds. In addition to being added to encapsulation materials to improve the barrier properties, glycerol is also frequently added to protein-based or carbohydrate-based biodegradable films to provide desirable mechanical properties and handling characteristics to otherwise rigid and brittle polymeric systems (Domján, Bajdik, & Pintye-Hódi, 2009; Vieira, da Silva, dos Santos, & Beppu, 2011).

The effects of glycerol on the physical properties of glassy matrices have received extensive attention. The addition of 5% (w/w) glycerol was shown to effectively enhance the storage stability of proteins encapsulated in trehalose, maltitol, and lactose, which was suspected to be contributed by the suppression of fast secondary relaxations and the reduction of molecular hole size (Bellavia, Paccou, Guinet, & Hédoux, 2014; Cicerone et al., 2003; Roussenova et al., 2010). Yet, such stabilizing effect did not monotonically increase with glycerol content- a reduction in protein stability was seen when 10% (w/w) glycerol was introduced in the sugar matrices (Cicerone et al., 2003). The phenomenon of plasticization and anti-plasticization is extensively studied in the field of polymer sciences and packaging materials. It is widely accepted that when added at a low concentration, glycerol may act as an anti-plasticizer which results in even stiffer polymers. There is a critical concentration of glycerol that marks the onset of its change in functionality. For example, 2.5% (w/w) glycerol acted as an anti-plasticizer in dry tapioca starch films ($aw \leq 0.22$) (Chang, Abd Karim, & Seow, 2006); glycerol at a concentration lower than 20% (w/w) in malto-oligomers also anti-plasticized the system by reducing the average molecular hole size and modulating the hydrogen bonding in the carbohydrate matrices (Roussenova et al., 2014). Liang *et al* have also reported the use of erythrosine B as a phosphorescent probe to study the effect of glycerol as a plasticizer in various edible matrices including zein and potato starch films and found that glycerol served as an anti-plasticizer at concentrations below 10%(w/w) (Liang et al., 2015; Liang & Ludescher, 2015).

The addition of glycerol also modifies critical properties such as gas permeability of the amorphous matrices. Garcia *et al* (2000) reported that the CO_2 permeability of both corn starch and amylomaize based films were significantly lower in glycerol plasticized films due to hole-filling mechanism. SEM data confirmed that the addition of glycerol inhibited the formation of cracks and pores. However, compared to using sorbitol as a plasticizer, glycerol was less effective in lowering O_2 permeability (García, Martino, & Zaritzky, 2000; McHugh & Krochta, 1994). In zein films plasticized with glycerol, the O_2 permeability was found to decrease significantly with the increase of glycerol content up to 30% (w/w) and this was thought to be a result of decreased oxygen solubility in the plasticized matrix (Liang et al., 2015).

Dextran is a class of polysaccharides that are synthesized by microorganisms. Dextran molecules are made of glucose residues and are connected mainly through α- 1, 6 bond. In the pharmaceutical industry, dextran is widely used as a carrier for therapeutic agents. The use of dextran as an encapsulation layer improves the thermal stability of labile compounds and reduces the toxicity of encapsulated drugs (Pawar et al., 2008). As mentioned before, glycerol is frequently added to polymeric matrices to enhance storage stability of encapsulation excipients and to provide desirable flexibility to rigid polymers. Some studies have observed improved protein stability in glycerol-dextran matrices (Cicerone et al., 2003). Yet, the mechanism and the critical concentration of glycerol at which it changes from anti-plasticizer to plasticizer are not clear.

In previous chapters I have demonstrated that phosphorescence from riboflavin has good sensitivity towards molecular mobility changes, in particular, towards β relaxations in glassy matrices. Here, we report the use of phosphorescence from riboflavin to study the molecular mobility in a series of amorphous dextran of different molecular weights (Mw~6k, 9, and 40k Da) and the effect of the addition of glycerol. The glycerol concentration was varied from 0 to 36% (w/w) in the dry dextran films. The temperature dependence of phosphorescence response and the glass transition temperature of different amorphous dextran solids, as well as glycerol-dextran mixtures were measured. Phosphorescence data were analyzed at different glycerol content, and associated with Tg and mobility change.

Materials and Methods

Sample Preparation: Dextran samples of 6k, 9k, and 40k Da used in this study were purchased from Sigma-Aldrich (St. Louis, MO, USA). Spectrophotometric grade glycerol was purchased from Alfa Aesar (Ward Hill, MA, USA). To prepare riboflavin-dextran amorphous films, 30% w/w dextran solution was mixed with 200μM riboflavin solution to reach a final riboflavin/monomer sugar molar ratio of approximately $1:10^4$. For the glycerol-dextran films, glycerol was added to the riboflavin-dextran (Mr~6k Da) solution to obtain final glycerol mass fractions of 5%, 10%, 22%, and 36% in the dry films.

We followed a similar procedure as discussed in previous chapters to form amorphous films. An aliquot of 24μL mixed solution was spread onto a quartz slide (NSG Precision Cells, Farmingdale, NY, USA) while kept on a heated plate at 30˚C until a transparent film was formed. The film was first dried by room temperature air flow supplied by a heat gun (Model 201A, Master Appliance Corp., Racine, WI, USA) for 15 min and then the film was further dried by storing in a desiccator against DrieRite (W.A. Hammond Drierite Co, Xenia, OH, USA) and P_2O_5 (Sigma-Aldrich, St. Louis, MO, USA) for at least 72 hours in order to reach ~0%RH before phosphorescence measurements. The DrieRite and P_2O_5 were replenished on a regular basis to maintain the dry environment in the desiccator.

Freeze-dried glycerol-dextran samples were prepared for the glass transition temperature measurement using Differential Scanning Calorimetry (DSC). Four dextran solutions of various glycerol contents as mentioned above were prepared

and placed in 50mL sterile centrifuge tubes covered with parafilm and were frozen overnight at -80˚C. The samples were completely solidified after 24 hours. Frozen samples were removed from the freezer and placed in a freeze dryer (Freezone 4.5, Labconco, Kansas City, MO, USA). All moisture was removed after 24hrs and the remaining solid mass was placed in a desiccator against DrieRite and P_2O_5 to prevent moisture absorption before DSC measurements.

Differential Scanning Calorimetry: A Q2000 Differential Scanning Calorimeter (DSC) (TA Instruments, New Castle, DE, USA) was used to measure the glass transition temperature of pure dextran samples of various molecular weights and the freeze-dried glycerol-dextran solids of various glycerol contents. Both pure dextran and freeze-dried glycerol-dextran samples were stored in a desiccator against DrieRite and P_2O_5 before measurements. Approximately 2-5mg of sample was transferred into an aluminum pan (TA Instruments, New Castle, DE, USA) and hermetically sealed prior to the measurement. An empty aluminum pan was used as a reference.

To measure the glass transition temperature of pure dextran, a sample was first pre-cooled to 20˚C and followed by 10˚C/min heating ramp to a temperature that was 10~15˚C higher than the estimated Tg, to eliminate structural enthalpy relaxation and thermal history of the materials (Imamura et al., 2002). The sample was then cooled at 20˚C/min to 20˚C to form glass. Lastly, the sample was reheated to approximately 30~40˚C above Tg to obtain the full thermograms.

Freeze-dried glycerol-dextran samples were subjected to a similar routine for the measurement of Tg with slight modifications: the target temperature during the

cooling process was set to -15˚C instead of 20˚C, as the addition of glycerol lowered the Tg of the mixture. TA analysis software (TA Instruments, New Castle, DE, USA) was used to determine the glass transition temperature, which was computed as the midpoint of heat capacity increase. For the 36% glycerol dextran samples, no prominent transition was observed from the DSC spectra and the estimation of its glass transition temperature is discussed in details below.

To estimate the Tg of 36% glycerol content dextran sample, a modified Couchman-Karasz equation (V-1) was used (Pinal, 2008):

	$$T_g = \frac{x_1 \Delta C_{P1} T_{g1} + x_2 \Delta C_{P2} T_{g2}}{x_1 \Delta C_{P1} + x_2 \Delta C_{P2}}$$	(V-1)

In this equation, x_i and T_{gi} are the mass fraction and glass transition temperature of components. The ΔC_{Pi} is the difference between the heat capacity in the melt and in the glass, which is 1.05J/gK for glycerol (Simon & McKenna, 1997) and 0.55 J/gK for 6k Da dextran (Gidley, Gothard, Darke, & Cooke, 2012). The Tg for glycerol and dextran used in this calculation were 190K and 433K, respectively. The former comes from literature, while the latter was the Tg of 6k Da dextran measured with DSC. In addition, the glass transition temperatures of amorphous glycerol-dextran of 5%, 10%, and 22% glycerol contents was also calculated using this equation to establish a comparison and validate the use of the equation towards the values measured from DSC.

Phosphorescence Measurements and Analysis: Steady state and time-resolved phosphorescence measurements were conducted using a Cary Eclipse Fluorescence

Spectrophotometer (Agilent Technologies, Santa Clara, CA, USA). Temperature during phosphorescence measurements was adjusted using a TLC-50 thermoelectric heating/cooling system (Quantum Northwest, Spokane, WA, USA). A quartz slide covered with amorphous riboflavin-dextran film was placed in a1cm×1cm×3cm quartz cuvette (Firefly Sci, Brooklyn, NY, USA) for phosphorescence measurement. The cuvette was sealed and flushed with dry nitrogen throughout the measurement to eliminate oxygen and humidity. In addition, a stream of dry air was introduced across the cuvette holder in the spectrophotometer to reduce condensation during measurements at low temperatures.

Delayed luminescence emission spectra of riboflavin in amorphous sugar films were collected from 480nm to 700nm when excited at 440nm. Both the excitation and emission slits were set to 20nm to maximize the intensity. Each data set was collected using one flash and a total decay time of 200ms. Phosphorescence decays were excited at 440nm and collected at 620nm with both monochromator slits set to 20nm. Each measurement was an average of 50 cycles, and each cycle was collected from one flash. A total decay time of 1000ms was collected for most of the samples with the delay time and gate time set to 0.2ms and 5ms, respectively. For the phosphorescence intensity decays of riboflavin in 36% glycerol content dextran films, the gate time was set to 2ms to and a total decay time of 500ms was collected. Both steady state and time-resolved measurements were conducted over the temperature range from -30 to 100˚C, at 10˚C interval. Samples were equilibrated

for 10 min after the temperature controller reached a constant reading before measurement.

Steady State Phosphorescence Analysis: The emission spectra of amorphous dextran film were first subtracted from the riboflavin spectra to eliminate the contribution from light scattering and the emission from impurities before analysis. The same analysis procedure using Fityk (Wojdyr, 2010), as discussed in previous chapters, was used in this study, too. Two log-normal functions (V-2) were used to fit the two peaks from both delayed fluorescence and phosphorescence simultaneously.

$$\mathrm{I}(\nu) = \sum I_{oi} * \exp\{-\ln(2)\left(\frac{\ln\left\{1 + \left[\frac{2\mathrm{b}(\nu_i - \nu_{\mathrm{Pi}})}{\Delta_i}\right]\right\}}{\mathrm{b}_i}\right)^2\} \quad \text{(V-2)}$$

In one log-normal function, I_{0i} corresponds to the peak intensity of emission spectra, ν_P is the wavenumber of maximum emission intensity, Δ_i is the line width parameter, and b_i is an asymmetry parameter. The value of bandwidth Γ_i, which is the full width at half maximum (FWHM) calculated from the line width (Δ_i) and asymmetry parameter (b_i), was directly estimated by Fityk. The subscription *i* indicates whether it is the delayed fluorescence or phosphorescence spectra.

Time-resolved Phosphorescence Analysis: Phosphorescence intensity decays of riboflavin in dextran films and glycerol-dextran films were excited at 440nm and collected at 620nm. In our previous study, we have shown that a 3-exponential model best described the decay kinetics of riboflavin phosphorescence in amorphous sucrose matrices and resulted in evenly distributed modified residuals.

In this study, we have also observed that the 3-exponential model was adequate to describe the intensity decay fashion in most samples. Therefore, the 3-exponential model (V-3) was used in this study to characterize the phosphorescence decay kinetics of riboflavin in the different dextran matrices. Under some circumstances, for example, high temperature or high glycerol-content, a 2-exponential function was used as it was sufficient enough to characterize the decays. It should be noted that using a 3-exponential model in these cases resulted in over-fitting of the data.

	$I(t) = I(0) * \sum_{i=1}^{n} \alpha_i \exp\left(-\frac{t}{\tau_i}\right) + \mathrm{c}$	(V-3)

In the 3-exponential model, I(0) is the initial intensity at t=0, n is the number of lifetime components, and τi and αi are the lifetime and amplitude of each component. The values of τi reflect the phosphorescence decay, which is influenced by the molecular mobility of the matrix and the values of αi represent the heterogeneous nature of the amorphous system. The average lifetime was calculated from population average (V-4):

	$\tau_m = \sum_{i}^{n} \alpha_i \tau_i$	(V-4)

Photophysical Rate Constants: The calculated average lifetimes provide a means to calculate the rate constant of triplet state de-excitation (k_P) and consequently the rate constant of non-radiative decay (k_{TS0}), which is a direct measure of matrix mobility-controlled quenching. Phosphorescence lifetime is determined by the rate constants of all possible de-excitation pathways (V-5):

	$\frac{1}{\tau} = k_P = k_{RP} + k_{TS1} + k_{TS0} + k_Q[O_2]$	(V-5)

where k_{RP} is the rate constant of radiative decay, an intrinsic property of the phosphorescent probe; k_{TS1} is the rate constant of reverse intersystem crossing; k_{TS0} is the rate constant of non-radiative decay, a measure of matrix-induced quenching; and $k_Q[O_2]$ is the rate constant of collisional quenching with oxygen. In this study, k_{RP} was approximated using the phosphorescence lifetime of riboflavin in glycerol/water mixture (3:1 v/v) as reported in our previous chapter, under the assumption that all the other de-excitation pathways were negligible under this extremely low temperature. The value of k_{TS1} was calculated from the ratio of the intensity of delayed fluorescence and phosphorescence emission (V-6) (Parker, 1968):

	$I_{DF}/I_P = \phi_F \left(k_{TS1}/k_{RP}\right)$	(V-6)

in which ϕ_F is the quantum yield of fluorescence. A ϕ_F value of 0.37 was reported for riboflavin fluorescence in starch films; this value was used as an estimated ϕ_F in amorphous solid films in the calculation (Penzkofer, 2012). The temperature dependence of rate constant k_{TS1} can be characterized by the Arrhenius equation (V-7):

	$k_{TS1}(T) = k^{\circ}_{TS1} \exp\left(-\frac{\Delta E_{TS}}{RT}\right)$	(V-7)

in which k°_{TS1} is the maximum reverse intersystem crossing rate at high temperature, ΔE_{TS} is the activation energy required for reverse intersystem crossing, and R is the universal gas constant of 8.314 J/K·mol (Parker, 1968). Therefore, Eq. (V-7 can also be written as :

$$I_{DF}/I_P = \left(\frac{\phi_F}{k_{RP}}\right) * [k^{\circ}_{TS1} \exp\left(-\frac{\Delta E_{TS}}{RT}\right)] \quad \text{(V-8)}$$

Plotting ln (I_{DF}/I_P) against 1/T results in a linear relationship with an intercept equal to ln$[\left(\frac{\phi_F}{k_{RP}}\right) k^{\circ}_{TS1}]$ and a slope equal to $-\frac{\Delta E_{TS}}{R}$ (Parker, 1968). The activation energy for reverse intersystem crossing ΔE_{TS} and the maximum reverse intersystem crossing rate k°_{TS1} can be approximated and $k_{TS1}(T)$ can be calculated accordingly.

Since nitrogen was purged into the cuvette to create an oxygen-free environment throughout the measurement, $k_Q[O_2]$ was considered negligible. Therefore, the value of k_{TS0} was calculated accordingly. The magnitude of k_{TS0} is a direct measure of matrix-induced quenching modulated by ability of triplet state molecule to dissipate its energy to nearby molecules in the matrix. The temperature dependence of k_{TS0} was analyzed with an Arrhenius plot of ln(k_{TS0}) vs 1/T and the activation energy to quench the triplet molecule within different temperature ranges was calculated from the plot and was associated with relaxation processes in amorphous systems.

Results

Differential Scanning Calorimetry: Figure V-1 illustrates typical DSC spectra for pure dextran and a freeze-dried 5% glycerol-dextran binary mixture. It can be observed from the DSC curves that the glass transition temperature for 6k Da dextran measured during the first and second heating cycles are significantly different. In contrast, the glass transition temperature for 5% glycerol-dextran mixture during the two heating cycles only show slight variation from one another. For pure dextran samples, the Tg measured during the second heating cycle was used, because the first heating cycle was intended to eliminate previous thermal treatment history and physical ageing during storage.

In this study, the mid-point of glass transition from the DSC curve was determined as the Tg. Table V-1 and Table V-2 summarize the Tg for all dextran and dextran-glycerol mixture samples studied in this chapter. The Tg for 36% glycerol-dextran, as mentioned in the Materials and Methods section, was calculated using the Couchman-Karasz equation (V-1).

Table V-1: Glass transition temperature of dextran of various molecular weights

Dextran Molecular Weight/ Da	6,000	9,000	40,000
Tg/˚C	160±3.02	206.02±1.56	212.28±2.34

Table V-2: Molar and weight ratios of different glycerol-dextran mixtures and their glass transition temperature

Gly% (wt)	5%	10%	22%	36%
Gly:Dex (wt)	1:18	1:9	1:3.5	1:1.8
Gly:Dextran monomer (n)	1:10	1:5	1:2	1:1
Tg/˚C Measured by DSC	121.75±1.02	81.23±1.78	70.17±0.68	\
Tg/ ˚C Calculated using (V-1)	137.6	116.1	73.5	31.6

Figure V-1

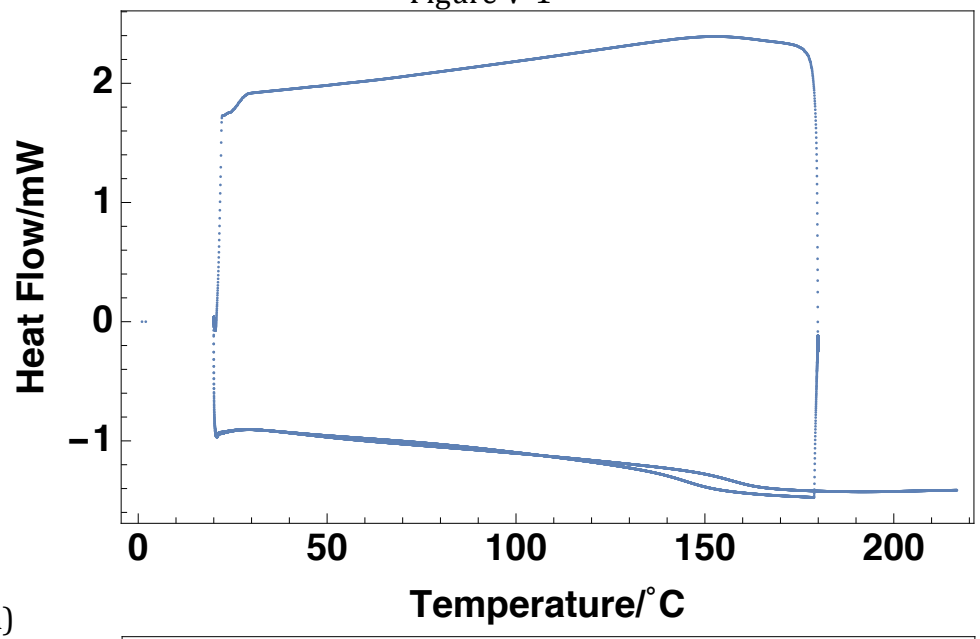

a)

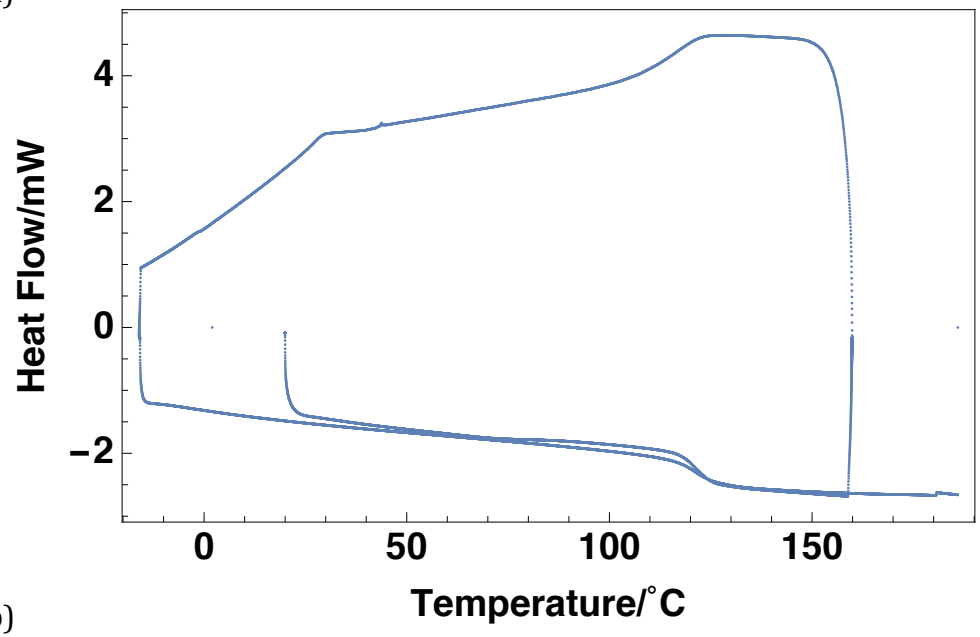

b)

Figure V-1: DSC thermograms for 6k Da dextran (a) and freeze-dried 5% glycerol-dextran (b).

Steady State Phosphorescence Measurements: Riboflavin exhibited two emission peaks- a delayed fluorescence one centered around 515nm and a phosphorescence one centered around 620nm- in amorphous dextran and dextran-glycerol films. The emission spectra exhibited similar patterns as what have been observed when simple sugars like sucrose and malto-oligomers were used as the amorphous hosting matrices. Figure V-2 exemplifies how riboflavin emission spectra in the amorphous 9k Da dextran film changes with the temperature. As shown, the phosphorescence decreased monotonically as the temperature increased. At temperatures above 30˚C, the phosphorescence peak became superimposed by the delayed fluorescence peak. Delayed fluorescence peak gradually appeared as the temperature increased from -30˚C to 0˚C. As the temperature further increased, delayed fluorescence emission intensity kept increasing, until the temperature reached 90˚C. Figure V-2b depicts the intensity of both phosphorescence and delayed fluorescence emission from riboflavin dispersed in 9k Da dextran amorphous film as a function of the temperature. The temperature at which the delayed fluorescence emission intensity stopped increasing was higher in 9k Da dextran films (90˚C) than in sucrose (50˚C) or the malto-oligomers (60~70˚C) amorphous films.

As we have discussed in the previous chapters, the decrease in delayed fluorescence intensity at high temperatures is likely to be a result of 1) higher photodegradation rate promoted by high temperatures and 2) non-radiative quenching triggered by more prominent molecular motions in the sugar matrix that compete with the reverse intersystem crossing process. To single out the dependence of delayed

fluorescence intensity change on the matrix property, in Figure V-3 the intensity change of delayed fluorescence in selected amorphous sugar films is plotted against ΔT=T-Tg. As shown, the critical temperature at which delayed fluorescence starts to decrease varies among these matrices. From disaccharides, sucrose and maltose, to malto-oligomers, maltoheptaose, to polysaccharides, dextran of various molecular weight, it is noticeable that the critical temperature moved further away from Tg as the molecular size of the sugar increased. It is reasonably to assume that the impact of photodegradation remains constant among various sugar films, as all films were optically transparent. Therefore, the more distant the critical temperature is from the Tg, the greater mobility there is in the hosting matrix. In this case, we can also conclude that at the same value of T-Tg, the larger the molecular size, the greater the molecular mobility. Interestingly, when glycerol was added to 6k Da dextran films, the critical temperature at which delayed fluorescence peak starts to decrease is closer to Tg, indicating that the addition of glycerol seems to retard the quenching process between triplet excited riboflavin and the matrices.

Figure V-2

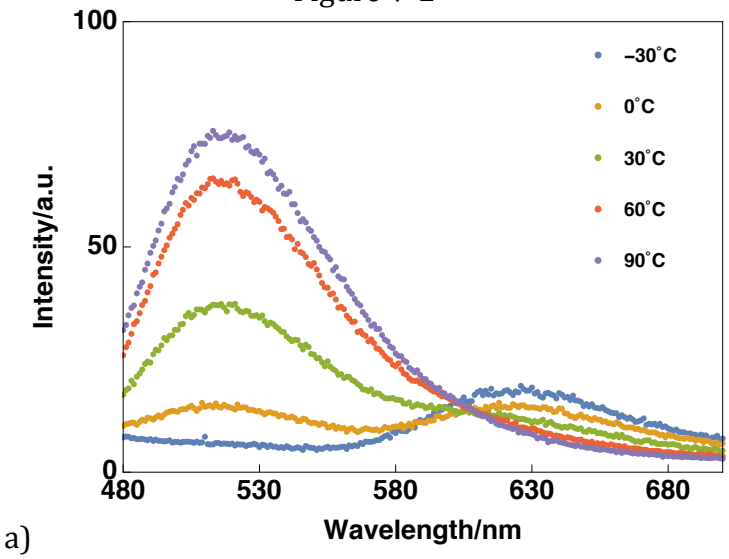

a)

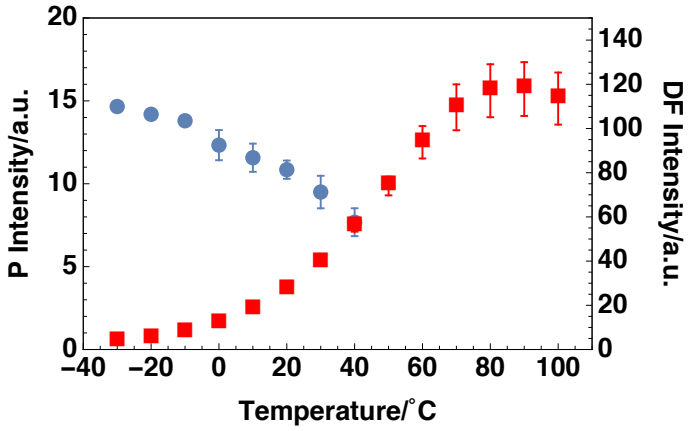

b)

Figure V-2: a) Emission spectra of riboflavin in amorphous dextran (Mw~9,000) films at selected temperatures. b) the phosphorescence (blue circles) and delayed fluorescence (red squares) emission intensity as a function of temperature

Figure V-3

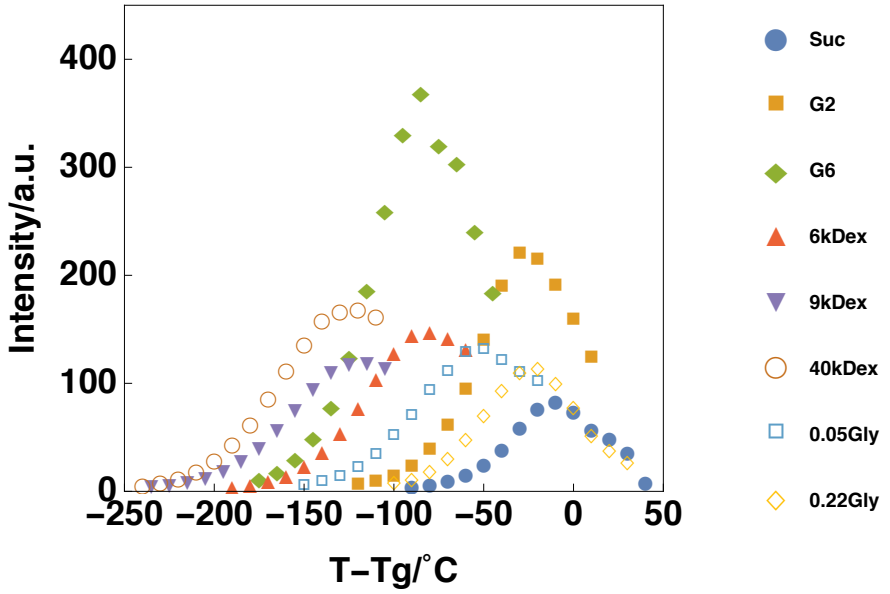

Figure V-3: Delayed fluorescence emission intensity of riboflavin vs T-Tg in amorphous sucrose (blue filled circles), maltose (yellow filled squares), maltoheptaose (green filled diamonds), 6000 dextran (red filled up triangles), 9000 dextran (purple filled down triangles), 40000 dextran (red open circles), 0.05 glycerol content 6000 dextran film (blue open squares), and 0.22 glycerol content 6000 dextran film (yellow open diamonds).

Phosphorescence Intensity Decays: Phosphorescence intensity decays from riboflavin were collected by exciting samples at 440nm and collecting at 620nm over the temperature range from -30 to 100˚C. Most decays were fitted using a three-exponential function. Decays collected from riboflavin in dextran films with 36% glycerol content over the whole temperature range were fitted with two-exponential function. From Figure V-4 to Figure V-7, we present the phosphorescence decays from riboflavin in 9k Da dextran, 40k Da dextran, 10% glycerol-dextran, and 36% glycerol-dextran films, respectively, along with the modified residuals from the fits. As shown, the modified residuals from each fit all varied randomly about zero, suggesting that the fit satisfactorily described the data.

The lifetimes and calculated average lifetime of riboflavin phosphorescence in amorphous films of dextran of various molecular weights and amorphous glycerol-dextran films of various glycerol contents are plotted as a function of temperature in Figure V-8a through Figure V-11a. As shown, all lifetimes and average lifetime decreased monotonically as the temperature increased from -30˚C onwards. According to Eq.(V-5, the phosphorescence lifetime is influenced by two factors: the reverse intersystem crossing rate, k_{TS1}, and non-radiative decay rate k_{TS0}, in the absence of oxygen. Reverse intersystem crossing is a process promoted by thermal energy, i.e., high temperature. At the same temperature, k_{TS1} remains constant throughout the matrix, the differences between the three lifetimes, $\tau 1$, $\tau 2$, and $\tau 3$, were thus a result of different non-radiative decay rates induced by local

environment. We speculate that long lifetime τ1 indicated rigid sugar matrix, where collisional quenching between the triplet riboflavin and the matrix was low, and short lifetimes τ2 and τ3 were signs of environments with greater mobility, where triplet probes were more easily quenched by the interaction with the matrix and through vibrational relaxation. The different values of lifetime components obtained from the multi-exponential function at the same temperature also demonstrated the heterogeneous nature of the amorphous matrix, which will be discussed in more details during the analysis of the amplitude data.

The fractional amplitudes of each lifetime component obtained from the multi-exponential function fitting of riboflavin phosphorescence decays are plotted as a function of temperature in Figure V-8b-11b. As shown, the amplitudes of the long and medium lifetime components, A1 and A2, both decreased as the temperature increased, while the amplitudes of the short lifetime component, A3, increased with the temperature. This trend was observed in all amorphous systems studied here. The changes in the values of fractional amplitudes suggested a continuing evolving heterogeneous environment in all matrices.

The average lifetime was calculated using the population average using (V-4). Figure V-12 and Figure V-13 show the calculated average lifetime of riboflavin phosphorescence as a function of the temperature in a series of dextran of different molecular weights and in a series of dextran films with different glycerol contents. As the molecular weight of the dextran increases from 6k to 9k and 40k Da, the lifetime became shorter at the same temperature, indicating a more mobile

environment in the amorphous films with higher molecular weights. However, at temperatures above 50˚C, the divergence became negligible.

Figure V-13 presents a plot of the calculated average lifetime in amorphous glycerol-dextran films as a function of temperature. When the glycerol content was lower than 10%, the average lifetime of riboflavin was not significantly different from one another. In particular, when the glycerol content was at 10%, the average lifetime of riboflavin was slightly longer than the lifetime measured in non-glycerol dextran films, suggesting that the addition of glycerol may have suppressed some collision between the matrix and the phosphorescent probes. As the glycerol content increased to 22% and 36%, the lifetime became significantly shorter, indicating a more mobile and flexible environment at higher glycerol content. Thus, the role of glycerol changed from anti-plasticizer to plasticizer. The shortened lifetime observed in 22% glycerol dextran films was in accordance with what has been reported by Ramasamy (2012), where the relaxation time measured by dielectric spectroscopy was shorter in 23% glycerol-starch films compared to 9% glycerol-starch films.

To highlight the contribution from the increase in molecular size and the addition of glycerol, the average lifetimes are plotted against $\Delta T=T-Tg$ in Figure V-14. When comparing the data from the three dextran films, over the entire range of ΔT, the lifetime of riboflavin was the longest in 6k Da dextran and the lifetime in 9k Da and 40k Da dextran were approximately the same at the same ΔT. Then we took a look at the data obtained from dextran films with different glycerol contents. As the

glycerol content increased from 0 to 10%, at the same ΔT, riboflavin lifetime increased. When the glycerol content further increased from 10% to 36%, however, the lifetime fluctuated around the value obtained at 10% glycerol. Yet, caution should be taken when interpreting the data, as the lifetime of riboflavin phosphorescence was not only determined by the non-radiative decay rate, but also was influenced by the reverse intersystem crossing. In the discussion below, we will separate the two factors and examine the molecular mobility in these matrices by a more accurate indicator: the non-radiative decay rate.

Figure V-4

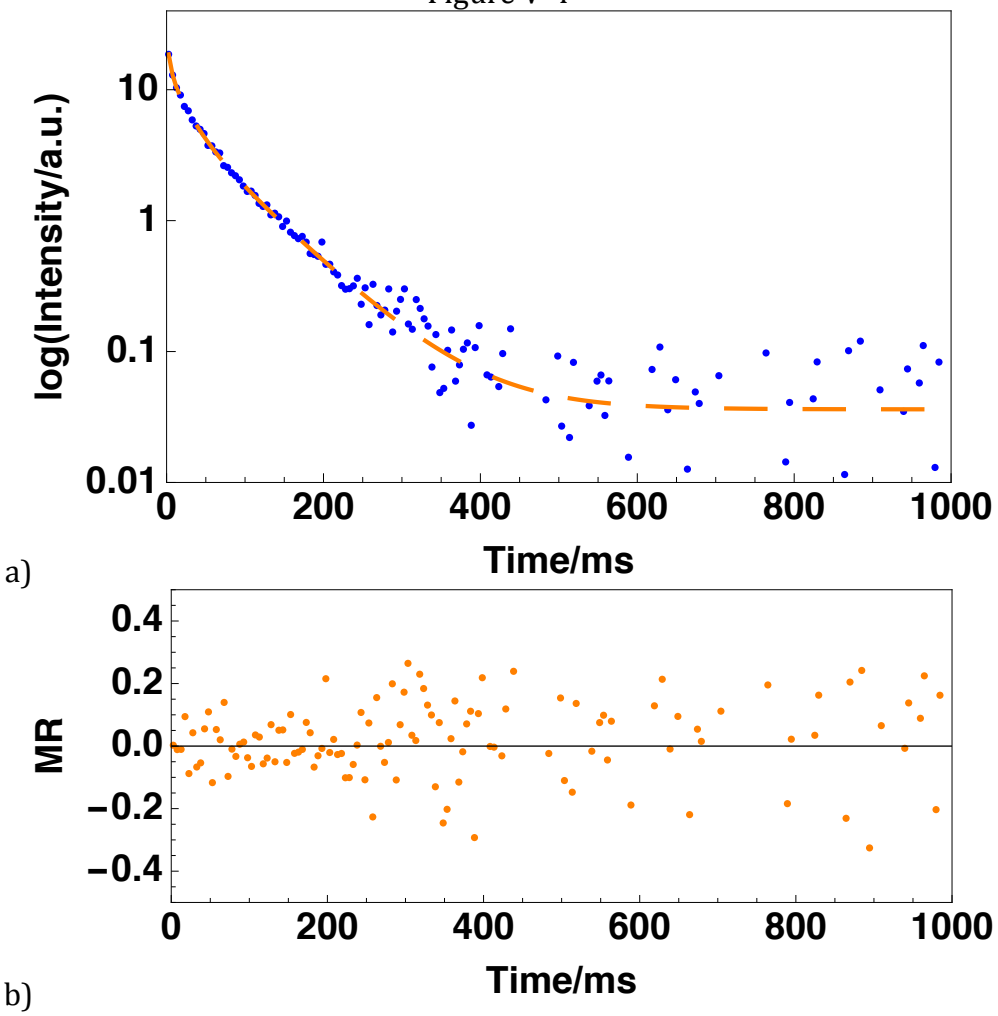

Figure V-4: a) Phosphorescence decay of riboflavin (blue circles) dispersed in 6k Da dextran amorphous film fitted with a 3-exponential model (orange dashed line). b) Modified residuals of the fit(orange circle)

Figure V-5

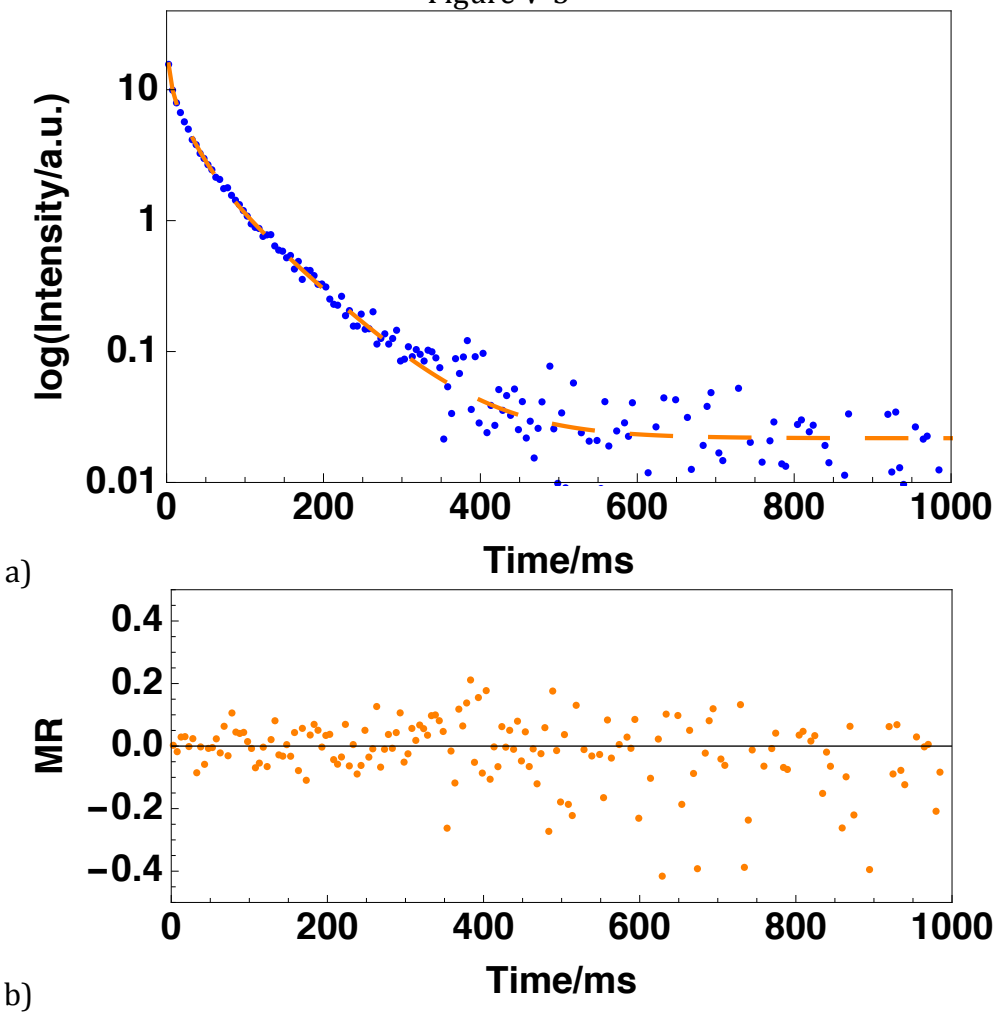

Figure V-5: a) Phosphorescence decay of riboflavin (blue circles) dispersed in 40k Da dextran amorphous film fitted with a 3-exponential model (orange dashed line). b) Modified residuals of the fit (orange circles)

Figure V-6

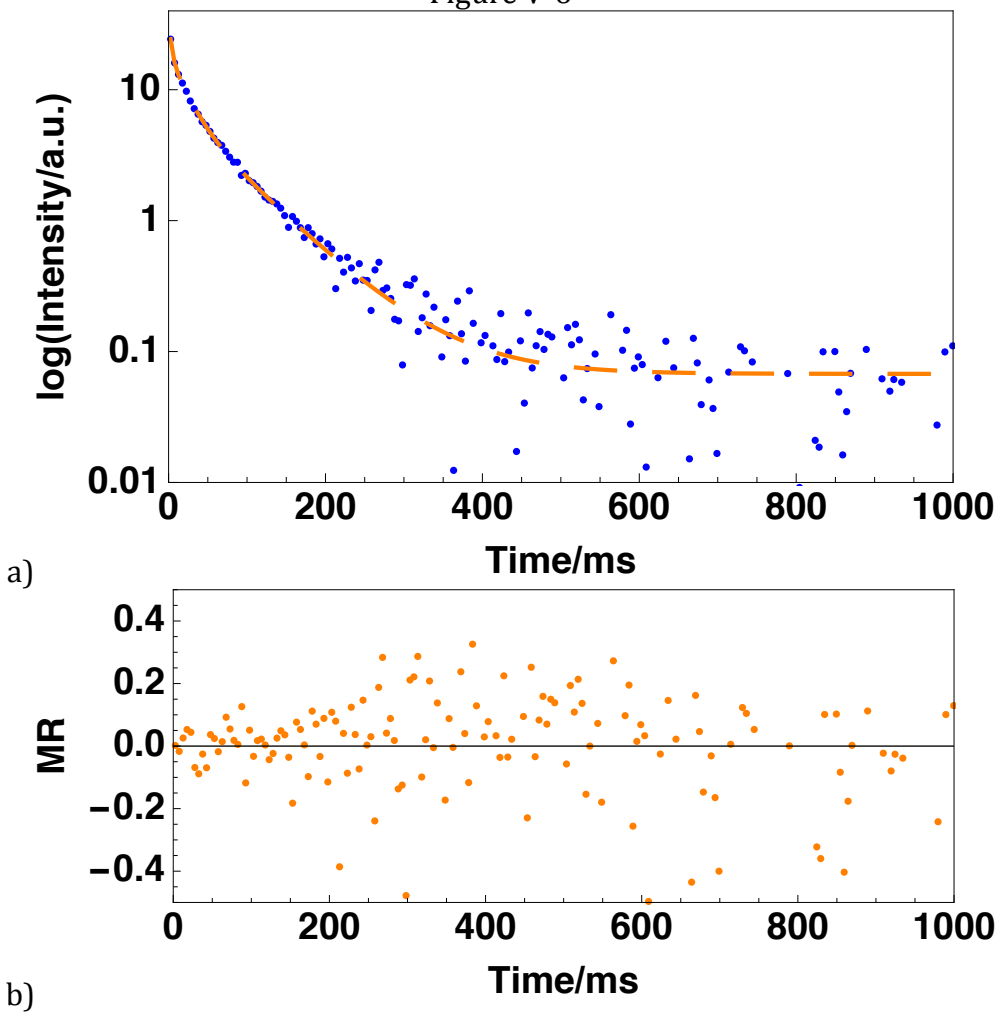

Figure V-6: a) Phosphorescence decay of riboflavin (blue circles) dispersed in 10% glycerol-dextran amorphous film fitted with a 3-exponential model (orange dashed line). b) Modified residuals of the fit (orange circles)

Figure V-7

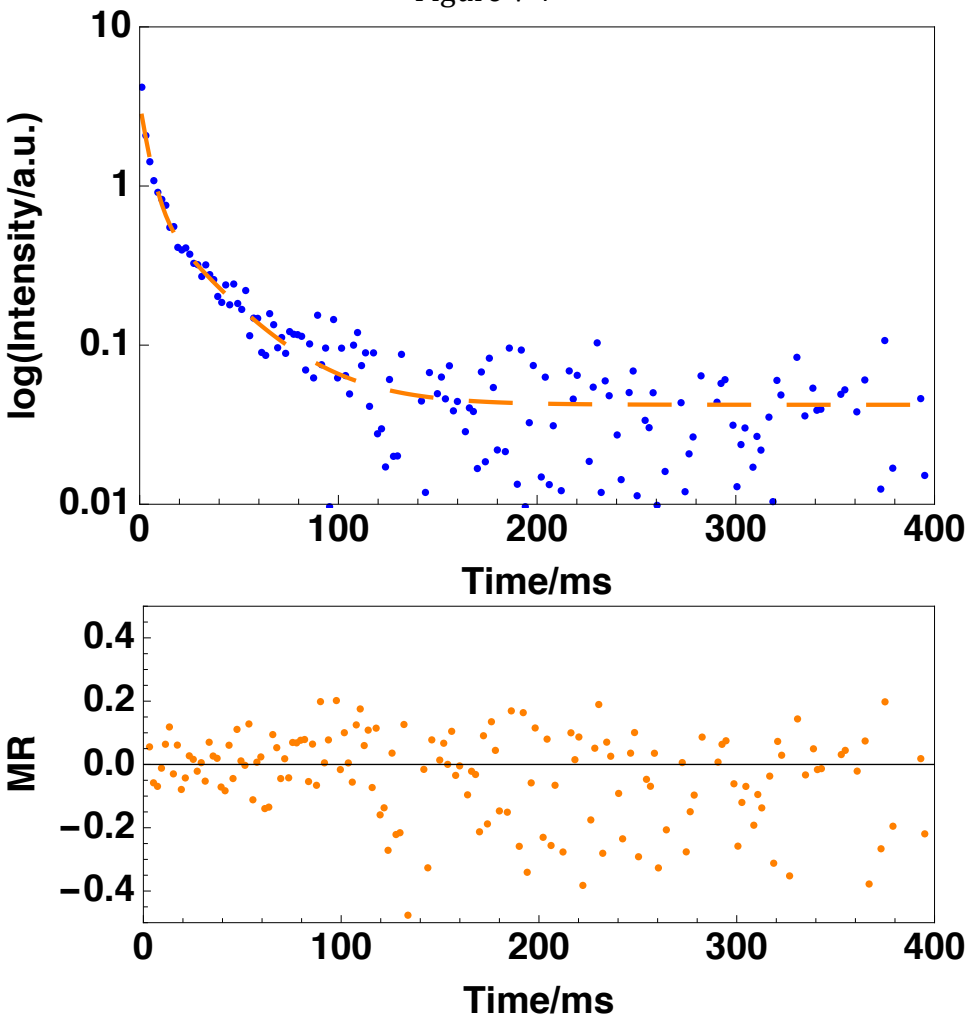

Figure V-7: Phosphorescence decay of riboflavin (blue circles) dispersed in 36% glycerol-dextran amorphous film fitted with a 3-exponential model. b) Modified residuals of the fit (orange circles)

Figure V-8

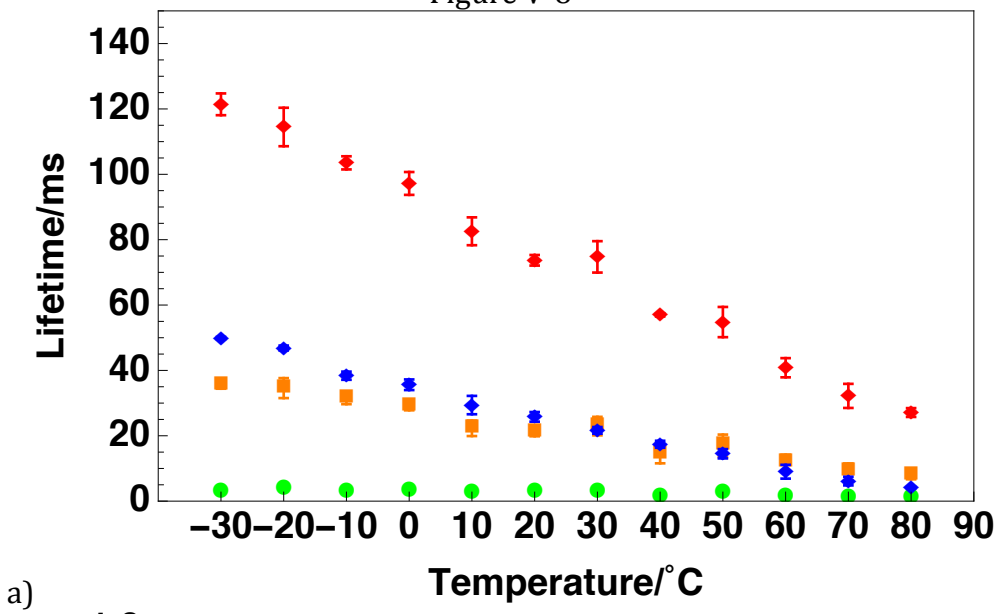

a)

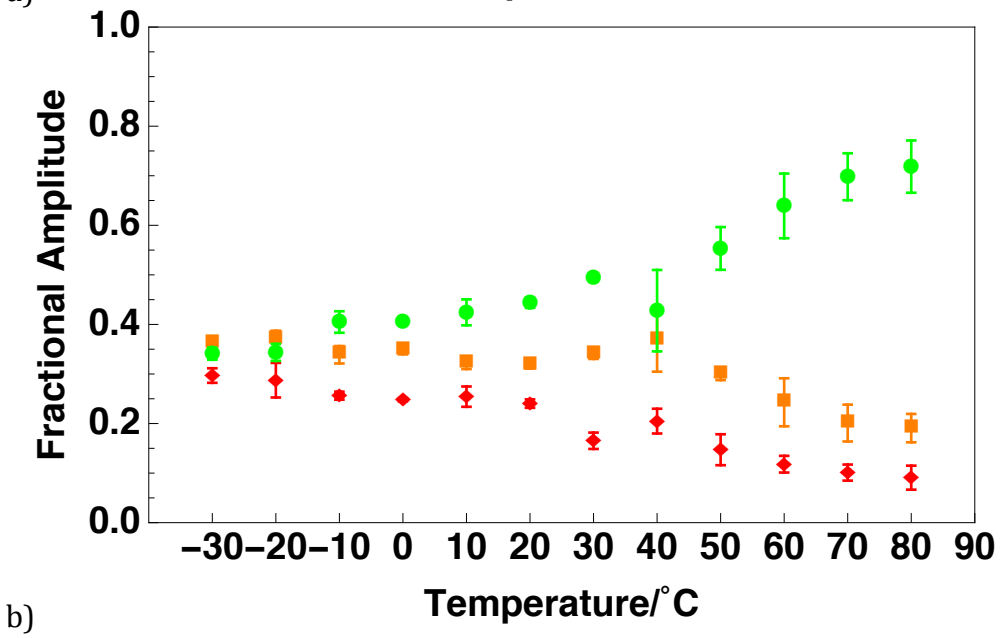

b)

Figure V-8: Lifetimes, τ_1 (red diamonds), τ_2 (orange squares), τ_3 (green circles), and calculated average lifetime (blue diamonds) (a) and fractional amplitudes of each lifetime component, A_1 (red diamonds), A_2 (orange squares), and A_3 (green circles) (b) of riboflavin phosphorescence decays collected when dispersed in amorphous films of 6k Da dextran as a function of temperature

Figure V-9

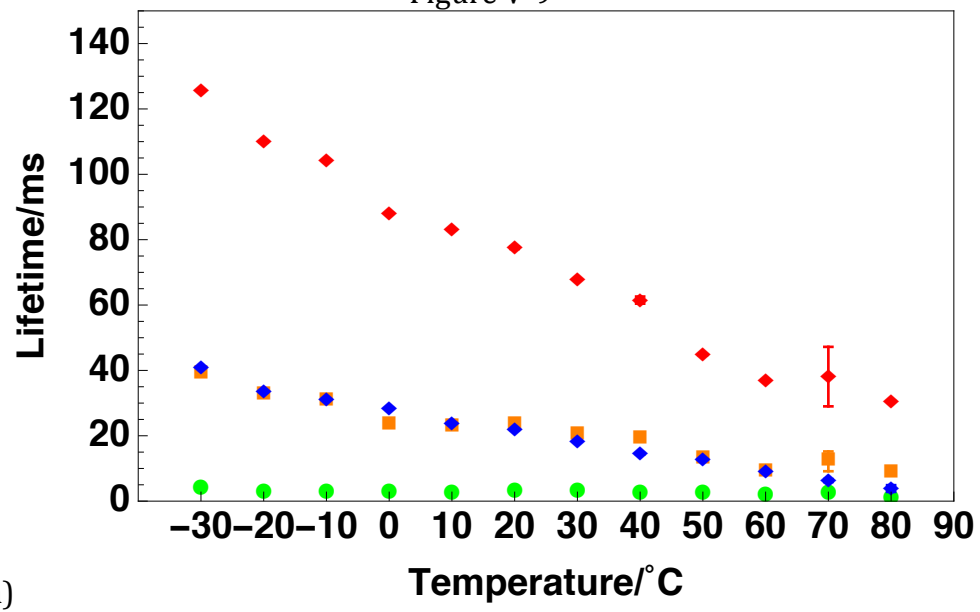

a)

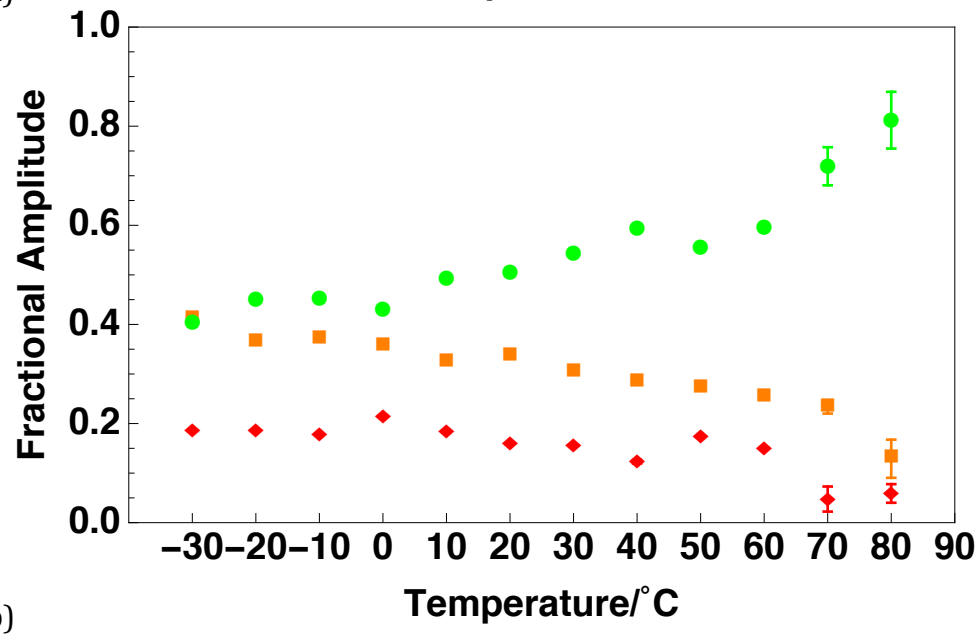

b)

Figure V-9: Lifetimes, τ_1 (red diamonds), τ_2 (orange squares), τ_3 (green circles), and calculated average lifetime (blue diamonds) (a) and fractional amplitudes of each lifetime component, A_1 (red diamonds), A_2 (orange squares), and A_3 (green circles) (b) of riboflavin phosphorescence decays collected when dispersed in amorphous films of 40k Da dextran as a function of temperature

Figure V-10

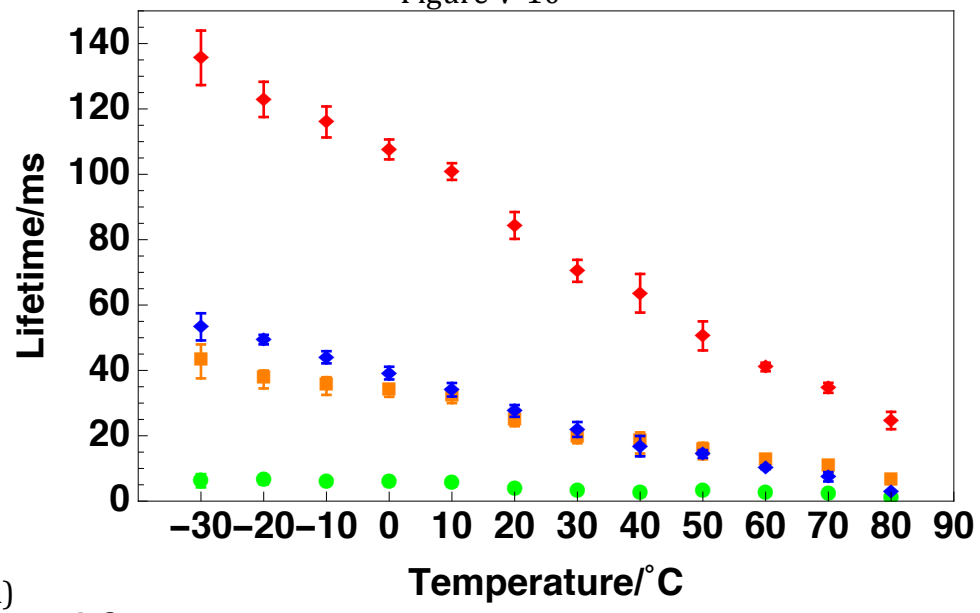

a)

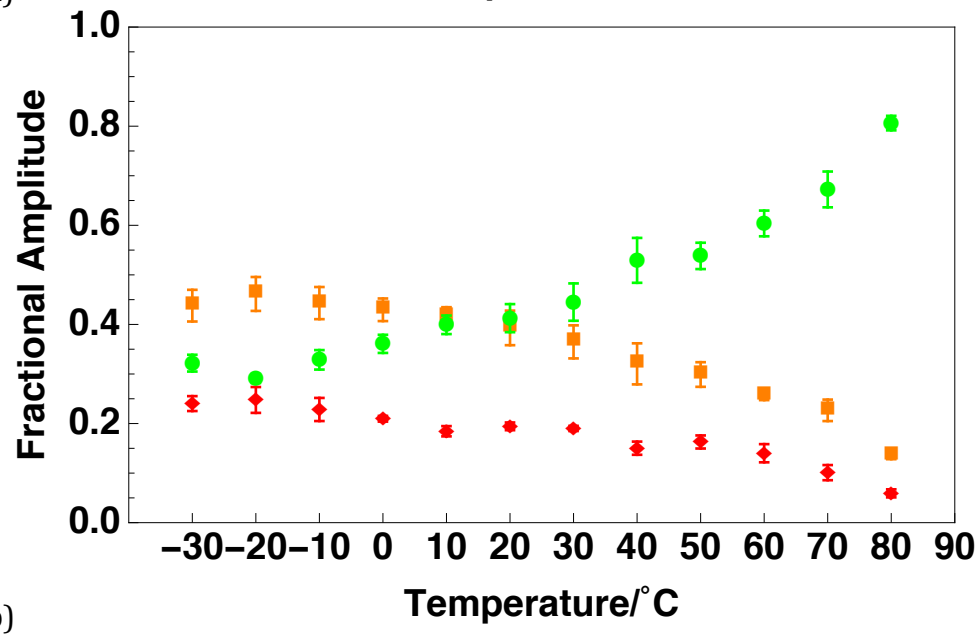

b)

Figure V-10: Lifetimes, τ_1 (red diamonds), τ_2 (orange squares), τ_3 (green circles), calculated average lifetime (blue diamonds) (a) and fractional amplitudes of each lifetime component, A_1 (red diamond), A_2 (orange square), and A_3 (green circle) (b) of riboflavin phosphorescence decays collected when dispersed in amorphous 10% glycerol-dextran film as a function of temperature

Figure V-11

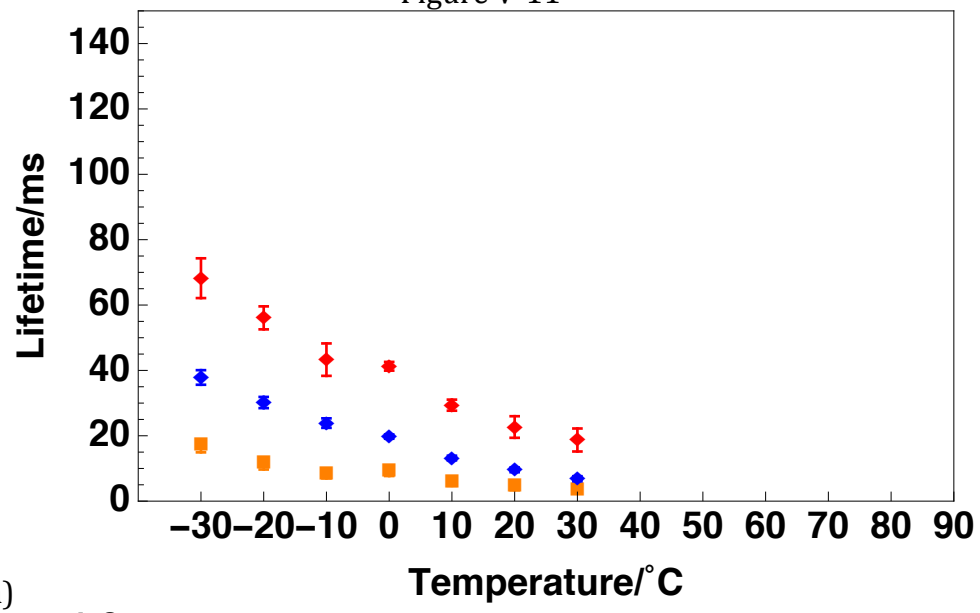

a)

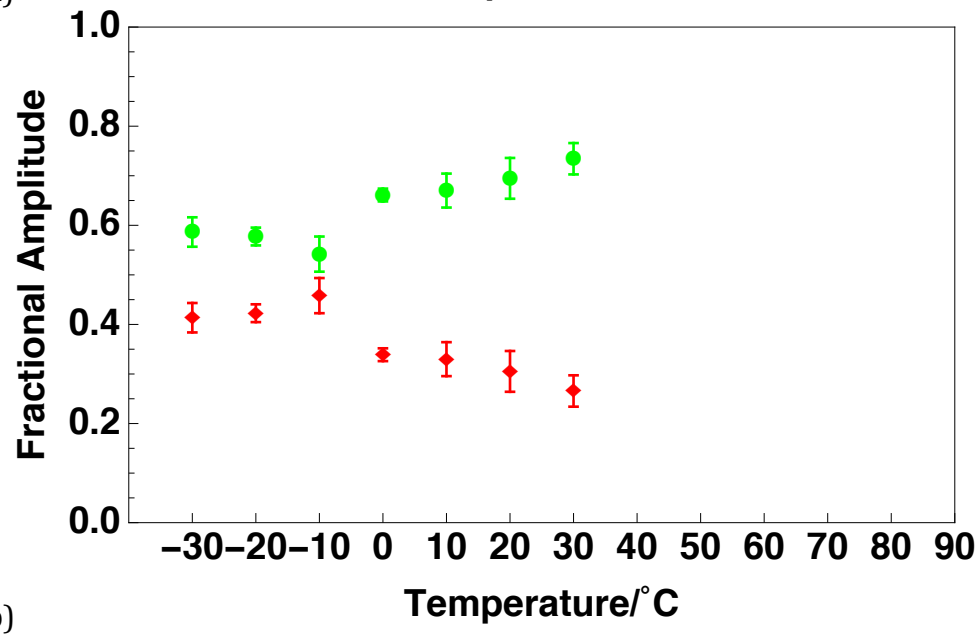

b)

Figure V-11: Lifetimes, τ_1 (red diamonds), τ_2 (orange squares), and calculated average lifetime (blue diamonds) (a) and fractional amplitudes of each lifetime component, A_1 (red diamonds) and A_2 (green circles) (b) of riboflavin phosphorescence decays collected when dispersed in amorphous 36% glycerol-dextran film as a function of temperature

Figure V-12

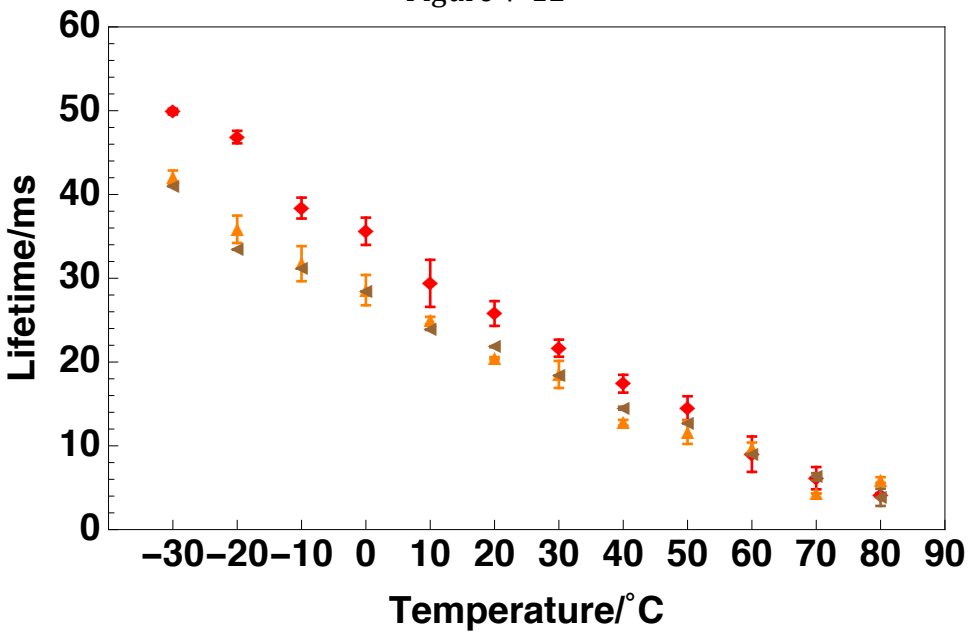

Figure V-12: Calculated average lifetime of phosphorescence decays of riboflavin in amorphous films of 6k Da dextran (red diamonds), 9k Da dextran (orange up triangles), and 40k Da dextran (brown left triangles) as a function of temperature

Figure V-13

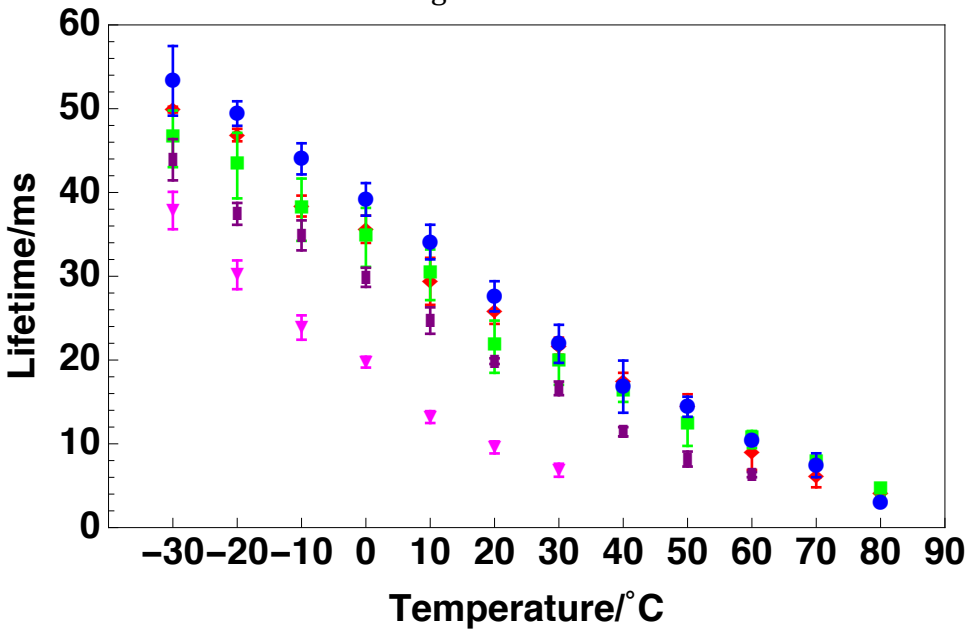

Figure V-13: Calculated average lifetime of phosphorescence decays of riboflavin in amorphous 6k Da dextran films (red diamonds) and amorphous glycerol-dextran films of 5% (green squares), 10% (blue circles), 22% (purple rectangles), and 36% (magenta down triangles) glycerol content (w/w) as a function of temperature

Figure V-14

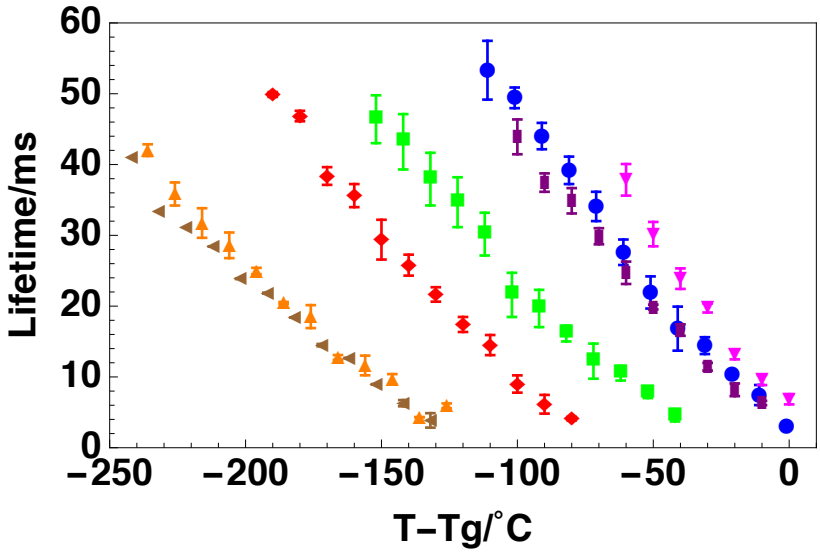

Figure V-14: Calculated average lifetime of phosphorescence decays of riboflavin in amorphous films of 6k Da dextran (red diamonds), 9k Da dextran (orange up triangles), and 40k Da dextran (brown left triangles), and amorphous glycerol-dextran films of 5% (green squares), 10% (blue circles), 22% (purple rectangles), and 36% (magenta down triangles) glycerol content (w/w) against ΔT=T-Tg

Non-radiative Decay Rates: The value of riboflavin phosphorescence lifetime is only a rough indicator of molecular mobility. To better examine the changes in molecular mobility, we calculated the rate constants of individual de-excitation pathways to separate the contributions from reverse intersystem crossing and non-radiative decay processes. As described in the previous chapter, the riboflavin phosphorescence lifetime in glycerol-water (3:1 v/v) at 77K, 170ms, was used as an estimation for the natural phosphorescence lifetime of riboflavin, and the intrinsic phosphorescence rate, k_P, was calculated accordingly. The procedures to calculate the rate of reverse intersystem crossing were detailed in the Materials and Methods section. As discussed in Chapter 2, a value of 3×10^7 s^{-1} was used to approximate the value of k°_{TS1}, and a calculated value of 35.33 kJ/mol was used to approximate the activation energy for reverse intersystem crossing, ΔE_{TS}. The values of non-radiative decay, k_{TS0}, were calculated for all dextran and glycerol-dextran films tested and are plotted as a function of temperature in Figure V-15. As shown, the rate of non-radiative decay in all dextran and glycerol-dextran films studied here increased with the temperature in a biphasic manner: the increase was gradual under low temperatures (-30~30˚C) and drastic at high temperatures (30~90˚C).

The plot was separated into two sections to better capture the effect of increasing molecular weight and the addition of glycerol on molecular mobility. In Figure V-16, the non-radiative decay rates of riboflavin in amorphous films of dextran of molecular weights: 6k, 9k, and 40k Da are presented. When the temperature was below 50˚C, at the same temperature, the rate for non-radiative decay was lower in

the 6k Da dextran films than that in the 9k and 40k Da dextran films, suggesting higher molecular mobility in the matrices dextran of larger molecular weights. At temperatures above 50˚C, the non-radiative decay rates were not significantly different anymore. In Figure V-17, the non-radiative decay rates from 0, 5%, and 10% glycerol dextran films did not vary much from one another, but the values from 22% and 36% glycerol content dextran films were greater at the same temperature. The non-radiative rate was modulated by the physical properties of the matrix and reflects the efficiency of energy dissipation from the probe into the surrounding environment. This suggested that the matrix molecular mobility increased at low (<10%) and decreased at high (>22%) glycerol content. For 0, 5%, and 10% glycerol content dextran films, the critical temperature at which the non-radiative decay rates started to increase more dramatically was around 50-60˚C, while this temperature reduced to 30˚C and 0˚C for 22% and 36% glycerol content dextran films, respectively. This critical temperature marked the onset of prominent molecular motions and high molecular mobility in the matrix. Similar changes were also observed in a study where phosphorescence from erythrosine B was used to monitor the effects of glycerol on molecular mobility in starch matrix (Liang & Ludescher, 2015). The critical temperature at which the non-radiative decay rate of erythrosine b changed dramatically was found to be glycerol content-dependent: the temperature was 70˚C in pure starch and decreased to 40˚C in 30% glycerol starch films.

Re-plotting Figure V-15 versus either $\Delta T=T-Tg$ or Tg/T did not generate an overlaying master curve (shown in Figure V-17). As discussed before, the critical

temperature at which the value of k_{TS0} starts to increase drastically marks the onset of extensive molecular mobility changes in the system. As shown, the increase in molecular weight from 6k to 9k and 40k in dextran moved the critical temperature further away from the glass transition temperature, indicating higher molecular mobility in matrices made with larger sugar molecules at the same ΔT from their Tg. The addition of glycerol at a small amount (<10%) shifted the critical temperature to a value closer to the Tg of the glycerol-dextran blend, suggesting that the small amount of glycerol suppressed molecular motions. A further increase in the amount of glycerol did not lead to changes in the critical temperature in regards to the Tg. Overall, this suggested that the non-radiative decay rate from riboflavin phosphorescence is sensitive to secondary relaxations that happen below Tg, rather than the structural relaxation activated around the Tg.

The Arrhenius plots of non-radiative decay rate of triplet riboflavin for selected matrix are presented in Figure V-18-Figure V-21. For pure dextran films, the Arrhenius plots showed two distinct regimes, while in dextran films with 5%, 10%, and 22% glycerol content, three regimes were observed from the Arrhenius plots. These plots provided information on the activation energy to quench triplet state riboflavin molecules via collisional quenching. The values of activation energy and the critical temperatures that mark the transitions are summarized in Table V-3.

Based on our calculation, the activation energy was around 7~8kJ/mol over the low temperature range. This essentially low activation energy suggested that there was little molecular motion and matrix induced collisional quenching. The activation

energies over the high temperature range varied from 50 to 40kJ/mol in pure dextran films, which was consistent with the values calculated from a series of malto-oligomers (see previous chapter). These calculated activation energies over the high temperature range correlated well with the activation energy, 41kJ/mol, for the relaxation process at high temperatures (70~140˚C) in dry starch reported by Ramasamy (2012). Yet, these values are much smaller compared to the β relaxation activation energy of 82kJ/mol and are closer to the reported 32 kJ/mol activation energy for γ relaxation, calculated from the dielectric spectra of 172k Da dextran (Montès & Cavaillé, 1999). However, the timescale of β relaxation (1.5ms at 280K and 4μs at 310K) is more comparable to the lifetime of riboflavin than that of γ relaxation (0.5ms at 150K and 4μs at 210K). Additionally, the β relaxation process, as a precursor to α relaxation prior to the Tg, is cooperative associated with segment motions of the main chain. It is therefore more reasonable to attribute the activation energy that quenched riboflavin within the high temperature range to emerging β relaxation process rather than γ relaxation.

The addition of glycerol has a complex effect on the matrix. A small amount of glycerol acted as anti-plasticizer and a large amount of glycerol acted as plasticizer. The addition of glycerol at a small amount decreased the activation energy over the low temperature range and increased the activation energy over the high temperature range. In contrast, a higher glycerol content resulted in an increase in the activation energy over low temperatures and a decrease over high temperatures. In addition, when the glycerol content was below 22%, there is an intermediate range, where the activation energy falls around 12~14kJ/mol.

Some previous research has looked into the effect of glycerol in a variety of amorphous matrices including starch, zein, gelatin, and chitosan (Domján et al., 2009; Liang & Ludescher, 2015; Liang et al., 2015; Lukasik & Ludescher, 2006; Ramasamy, 2012). In Ramasamy's study of the effect of glycerol on starch films, this researcher found that the addition of glycerol increased the activation energy for the relaxation process that they observed over the high temperature range (10-50˚C) from ~41kJ/mol in dry starch films to 73kJ/mol (9% glycerol) and 84kJ/mol (23% glycerol). The FTIR data from this research also showed an increase in height in the broad band at 3,345 cm^{-1} in films containing glycerol, which suggested that the addition of glycerol created more hydrogen bonding in the matrix that might account for the increase in activation energy. In Liang *et al*'s two studies, it was reported that glycerol acted as anti-plasticizer that decreased the molecular mobility when added at a level lower than 10% in both starch and zein films. It was concluded that at low glycerol content, the matrix mobility was decreased due to an increase in hydrogen bond strength and enhanced intermolecular interactions. High glycerol content, on the other hand, resulted in increased molecular free volume that enabled thermal activation of vibrational and translational motions, overrode the effect of enhanced hydrogen bond strength, and consequently increased the matrix mobility.

Figure V-15

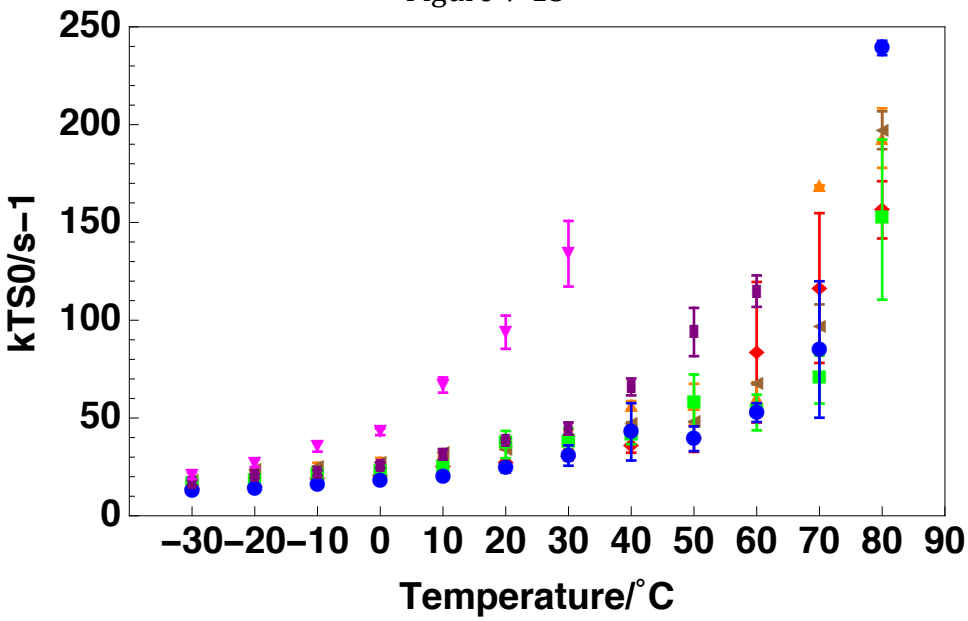

Figure V-15: Rate of non-radiative decay of riboflavin in amorphous films of 6k Da dextran (red diamonds), 9k Da dextran (orange up triangles), and 40k Da dextran (brown left triangles), and amorphous glycerol-dextran films of 5% (green squares), 10% (blue circles), 22% (purple rectangles), and 36% (magenta down triangles) glycerol content (w/w) as a function of temperature

Figure V-16

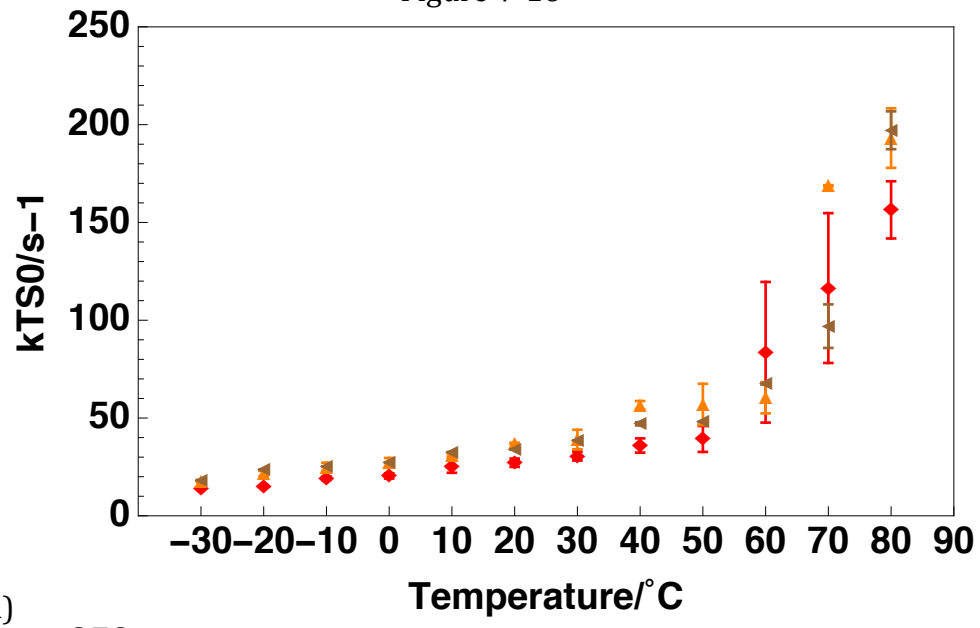

a)

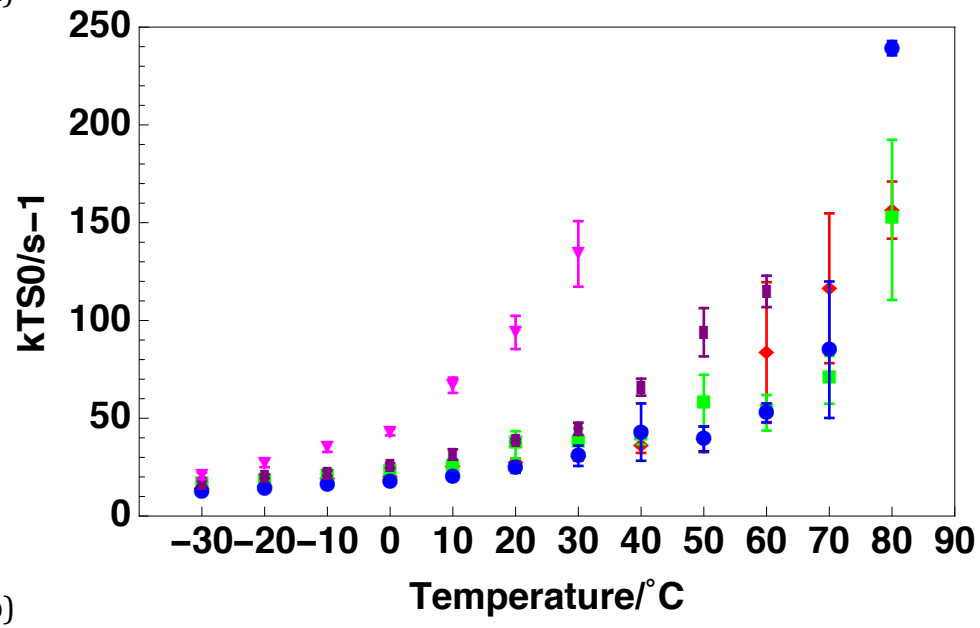

b)

Figure V-16: Rate of non-radiative decay of riboflavin in amorphous films of 6k Da dextran (red diamonds), 9k Da dextran (orange up triangles), and 40k Da dextran (brown left triangles) (a), and amorphous glycerol-dextran films of 5% (green squares), 10% (blue circles), 22% (purple rectangles), and 36% (magenta down triangles) glycerol content (w/w) (b) as a function of temperature

Figure V-17

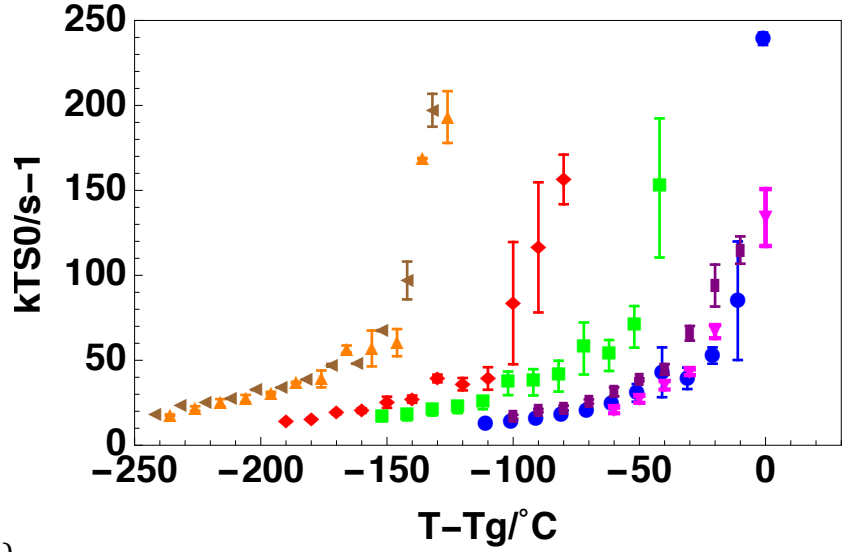

a)

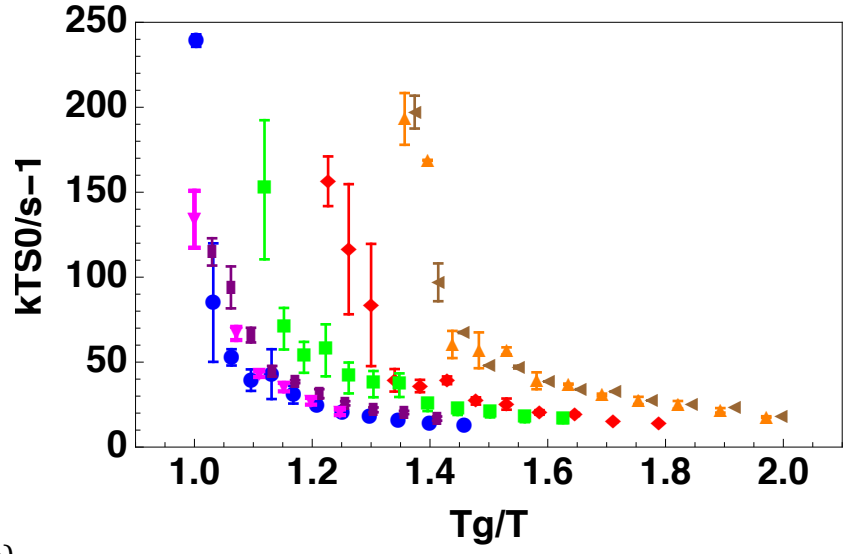

b)

Figure V-17: Rate of non-radiative decay of triplet riboflavin in amorphous films of 6k Da dextran (red diamonds), 9k Da dextran (orange up triangles), and 40k Da dextran (brown left triangles), and amorphous glycerol-dextran films of 5% (green squares), 10% (blue circles), 22% (purple rectangles), and 36% (magenta down triangles) glycerol content (w/w) plotted against T-Tg (a) and Tg/T (b)

Figure V-18

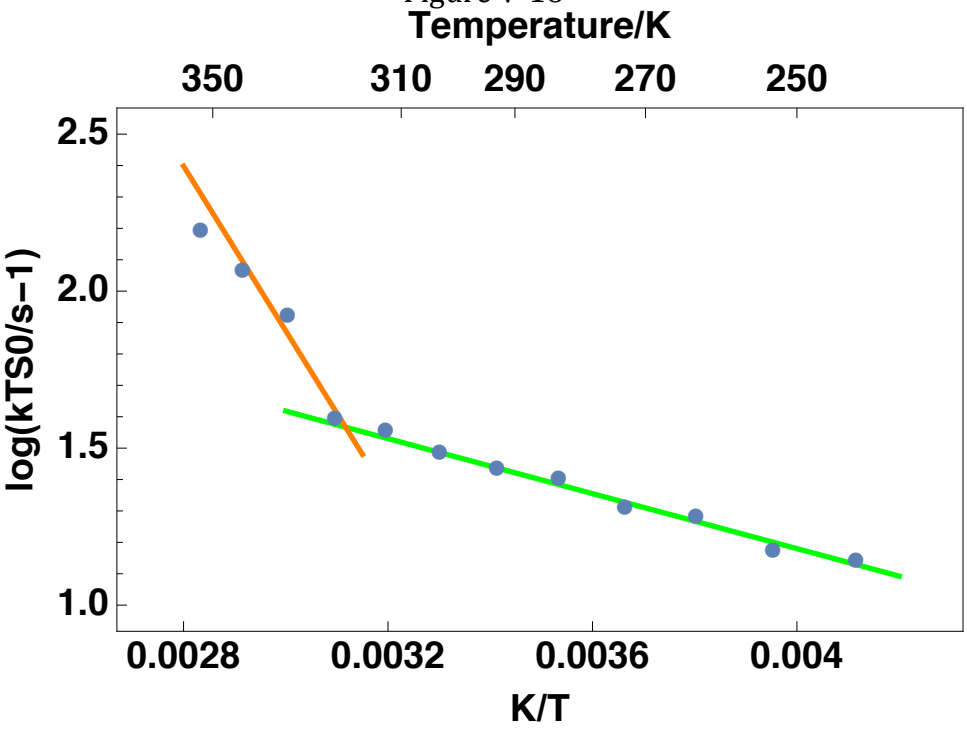

Figure V-18: Arrhenius plots of non-radiative decay rate k_{TS0} for riboflavin dispersed in amorphous 6k Da dextran film.

Figure V-19

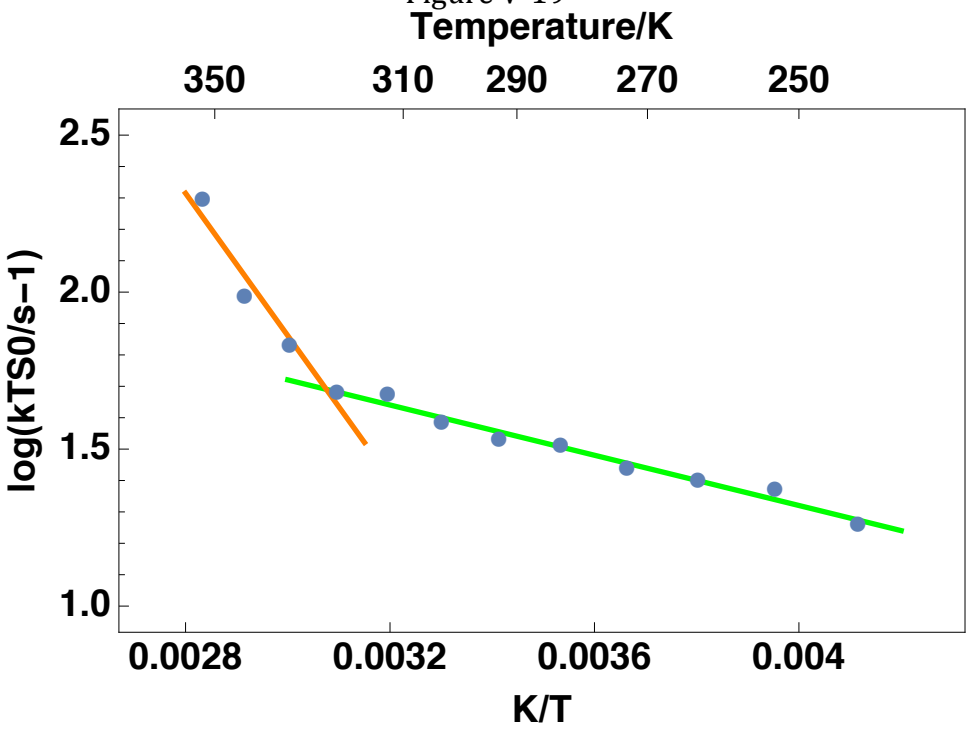

Figure V-19: Arrhenius plots of non-radiative decay rate k_{TS0} for riboflavin dispersed in amorphous 40k Da dextran film.

Figure V-20

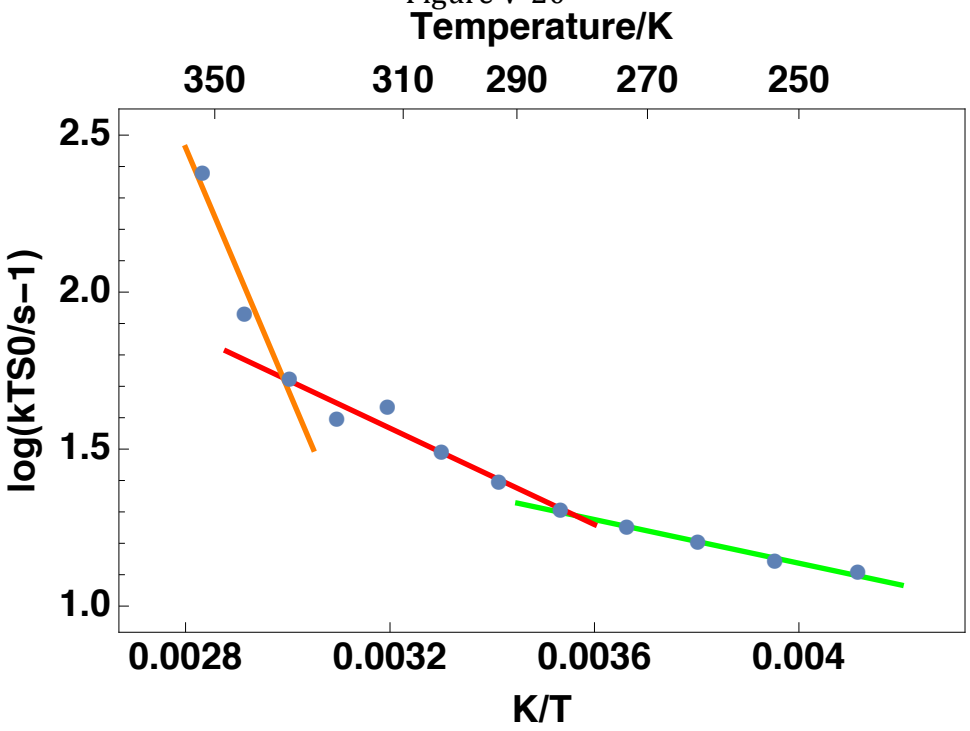

Figure V-20: Arrhenius plots of non-radiative decay rate k_{TS0} for riboflavin dispersed in amorphous 10% glycerol-dextran film.

Figure V-21

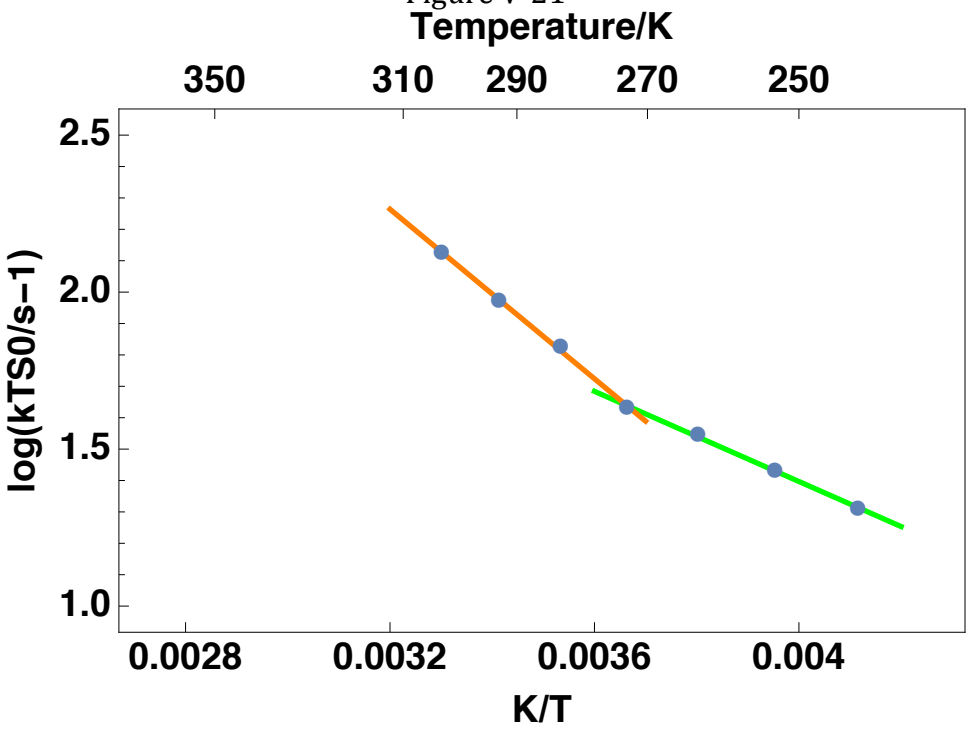

Figure V-21: Arrhenius plots of non-radiative decay rate k_{TS0} for riboflavin dispersed in amorphous 36% glycerol-dextran.

Table V-3: Calculated activation energies, Ea, to quench triplet riboflavin dispersed in 6,000, 9,000, and 40,000 dextran films and dextran films of 5%, 10%, 22%, and 36% glycerol contents, at low, intermediate, and high temperature regimes

Sample	E_A kJ/mol Low Temperature	E_A kJ/mol Intermediate Temperature	E_A kJ/mol High Temperature	Transition Temperature ˚C
6,000 Dex	8.38	\	50.22	50
9,000 Dex	8.04	\	49.58	60
40,000 Dex	7.66	\	43.42	50
5% Gly	6.43	12.49	78.18	10 & 70
10% Gly	6.65	14.69	73.56	10 & 60
22% Gly	7.50	12.75	30.30	0 & 30
36% Gly	13.74	\	25.84	0

Conclusion

Our data indicate that the mobility of the glassy dextran matrix and glassy glycerol-dextran binary systems increased with temperature. In accordance with the results from previous chapter, the increase in molecular size from 6k Da to 9k and 40k Da dextran facilitated the increase in molecular mobility throughout the whole temperature range measured. The effect of the addition of glycerol on molecular mobility exhibited a more complex pattern: at low glycerol content (<10%wt), glycerol acted as an anti-plasticizer and reduced the matrix mobility through enhancing hydrogen bonding and intermolecular interactions in the matrix; while at high glycerol content (>22%), glycerol transitioned into a plasticizer and increased the molecular mobility greatly, by increasing molecular free volume and enabling molecular rearrangements. This work demonstrated that the phosphorescence from riboflavin exhibited good sensitivity to secondary relaxations in glassy polysaccharides and binary glassy glycerol-polysaccharide systems. The effects of molecular size and the addition of glycerol on molecular mobility were studied using phosphorescence from riboflavin and provided insightful implications on the quality and formulation of amorphous food and pharmaceuticals.

References

Bellavia, G., Paccou, L., Guinet, Y., & Hédoux, A. (2014). How does glycerol enhance the bioprotective properties of trehalose? insight from protein-solvent dynamics. *Journal of Physical Chemistry B, 118*(30), 8928-8934. doi:10.1021/jp500673b

Bhattacharya, S., & Suryanarayanan, R. (2009). Local mobility in amorphous pharmaceuticals--characterization and implications on stability. *Journal of Pharmaceutical Sciences, 98*(9), 2935-2953. doi:10.1002/jps.21728

Chang, Y. P., Abd Karim, A., & Seow, C. C. (2006). Interactive plasticizing–antiplasticizing effects of water and glycerol on the tensile properties of tapioca starch films. *Food Hydrocolloids, 20*, 1-8. doi:10.1016/j.foodhyd.2005.02.004

Cicerone, M. T., Tellington, A., Trost, L., & Sokolov, A. (2003). Substanstially improved stability of biological agents in dried form: The role of glassy dynamics in preservation of biopharmaceuticals. *BioProcess International, 1*, 1-9.

Cicerone, M. T., & Douglas, J. F. (2012). ß-relaxation governs protein stability in sugar-glass matrices. *Soft Matter, 8*(10), 2983-2991. doi:10.1039/c2sm06979b

Domján, A., Bajdik, J., & Pintye-Hódi, K. (2009). Understanding of the plasticizing effects of glycerol and PEG 400 on chitosan films using solid-state NMR spectroscopy. *Macromolecules, 42*(13), 4667-4673. doi:10.1021/ma8021234

García, M. A., Martino, M. N., & Zaritzky, N. E. (2000). Microstructural characterization of plasticized starch-based films. *Starch - Stärke, 52*(4), 118-124. doi:10.1002/1521-379X(200006)52:4<118::AID-STAR118>3.0.CO;2-0

Gidley, M., Gothard, M. G., Darke, A. H., & Cooke, D. (2012). Thermal properties of polysaccharides at low moisture: Part 3- comparative behavior of guar gum and dextran. In D. S. Reid (Ed.), *The properties of water in foods ISOPOW 6* (pp. 179)

Imamura, K., Fukushima, A., Sakaura, K., Sugita, T., Sakiyama, T., & Nakanishi, K. (2002). Water sorption and glass transition behaviors of freeze-dried sucrose-dextran mixtures. *Journal of Pharmaceutical Sciences, 91*(10), 2175-2181. doi:10.1002/jps.10218

Liang, J., & Ludescher, R. D. (2015). Effects of glycerol on the molecular mobility and hydrogen bond network in starch matrix. *Carbohydrate Polymers, 115*, 401-407. doi:http://dx.doi.org/10.1016/j.carbpol.2014.08.105

Liang, J., Xia, Q., Wang, S., Li, J., Huang, Q., & Ludescher, R. D. (2015). Influence of glycerol on the molecular mobility, oxygen permeability and microstructure of amorphous zein films. *Food Hydrocolloids, 44*, 94-100. doi:http://dx.doi.org/10.1016/j.foodhyd.2014.09.002

Lukasik, K. V., & Ludescher, R. D. (2006). Effect of plasticizer on dynamic site heterogeneity in cold-cast gelatin films. *Food Hydrocolloids, 20*(1), 88-95. doi:http://dx.doi.org/10.1016/j.foodhyd.2005.03.006

McHugh, T.,Habig, & Krochta, J.,M. (1994). Sorbitol vs glycerol-plasticized whey protein edible films: Integrated oxygen permeability and tensile property evaluation. *Journal of Agricultural and Food Chemistry, 42*(4), 841-845.

Montès, H., & Cavaillé, J. Y. (1999). Secondary dielectric relaxations in dried amorphous cellulose and dextran. *Polymer, 40*, 2649-2657. doi:10.1016/S0032-3861(98)00506-0

Parker, C. A. (1968). *Photoluminescence of solutions : With applications to photochemistry and analytical chemistry*. Amsterdam: Elsevier.

Pawar, R., Jadhav, W., Bhusare, S., Borade, R., Farber, S., Itzkowitz, D., & Domb, A. (2008). 1 - polysaccharides as carriers of bioactive agents for medical applications. In R. L. Reis, N. M. Neves, J. F. Mano, M. E. Gomes, A. P. Marques & H. S. Azevedo (Eds.), *Natural-based polymers for biomedical applications* (pp. 3-53) Woodhead Publishing. doi:http://dx.doi.org/10.1533/9781845694814.1.3

Pinal, R. (2008). Entropy of mixing and the glass transition of amorphous mixtures. *Entropy, 10*(3), 207-223. doi:10.3390/entropy-e10030207

Pravinata, L. C., You, Y., & Ludescher, R. D. (2005). Erythrosin B phosphorescence monitors molecular mobility and dynamic site heterogeneity in amorphous sucrose. *Biophysical Journal, 88*(5), 3551-3561. doi:http://dx.doi.org/10.1529/biophysj.104.054825

Ramasamy, P. (2012). A dielectric relaxation study of starch-water and starch-glycerol films. *Ionics, 18*(4), 413-423. doi:10.1007/s11581-011-0636-1

Roussenova, M., Murith, M., Alam, A., & Ubbink, J. (2010). *Plasticization, antiplasticization, and molecular packing in amorphous carbohydrate-glycerol matrices*

Roussenova, M., Andrieux, J., Alam, M. A., & Ubbink, J. (2014). Hydrogen bonding in maltooligomer–glycerol–water matrices: Relation to physical state and molecular free volume. *Carbohydrate Polymers, 102*, 566-575. doi:10.1016/j.carbpol.2013.12.003

Simon, S. L., & McKenna, G. B. (1997). Interpretation of the dynamic heat capacity observed in glass-forming liquids. *Journal of Chemical Physics, 107*(20), 8678.

Taylor, L. S. (1998). Sugar-polymer hydrogen bond interactions in lyophilized amorphous mixtures. *Journal of Pharmaceutical Sciences, 87*(12), 1615-1621. doi:10.1021/js9800174

Vieira, M. G. A., da Silva, M. A., dos Santos, L. O., & Beppu, M. M. (2011). Natural-based plasticizers and biopolymer films: A review. *European Polymer Journal, 47*(3), 254-263. doi:http://dx.doi.org/10.1016/j.eurpolymj.2010.12.011

Wojdyr, M. (2010). Fityk: A general-purpose peak fitting program. *Journal of Applied Crystallography, 43*(5), 1126-1128. doi:10.1107/S0021889810030499

Chapter VI Riboflavin as a Photosensitizer: Rate of Oxygen Quenching and Singlet Oxygen Generation Efficacy

Introduction

A photosensitizer is a light-sensitive molecule that can absorb energy from light and subsequently transfer the energy to a chemical reaction or to surrounding molecules (Wainwright, 2009). During the process of photosensitization, ground state photosensitizer molecules absorb the energy from photons and jump to the excited singlet state. Some singlet excited state molecules can go through intersystem crossing and become triplet excited state molecules. Some triplet excited state molecules can be quenched by ground state triplet oxygen molecules, which results in the formation of singlet oxygen, a remarkably reactive oxygen species that readily oxidizes lipids, proteins, and nucleic acids and causes damages to living cells.

The mechanism of photosensitization has been successfully applied in photodynamic therapy for treating cancer, macular degeneration, and dermatological conditions (Wainwright, 2009). In recent years, researchers have also demonstrated that photosensitization can be applied to inactivate a wide range of human pathogens, both gram positive and gram negative organisms, including: *Escherichia coli*, *Streptococcus spp.*, *Helicobacter pylori, Staphylococcus aureus, Pseudomonas aeruginosa, Campylobacter rectus, Deinococcus radiodurans, Acinetobacter Baumannii*, and others (Alotaibi & Heaselgrave, 2011; DeRosa & Crutchley, 2002; Kashiwabuchi et al., 2013; Lang, 2008) and that photosensitization

can be used as a novel non-thermal disinfection treatment (Luksiene & Brovko, 2013; Tsai et al., 2011).

Recent food trends have witnessed a strong emphasis on incorporating more fruits and vegetables as part of a healthy diet. Yet, ironically, fresh produce has been increasingly identified as the source of food borne illnesses. Thermal treatment is not applicable for fresh produce and conventional non-thermal disinfection methods such as the use of chlorine and organic acids suffer from insufficient microbial reduction, the risk of development of drug resistant strains, and consumer concerns about mutagenic and carcinogenic residues. Therefore, the increasing prevalence of fresh produce in diet calls for effective novel sanitization method to ensure the food safety of fresh produce. Several studies have evaluated and scrutinized the use of GRAS photosensitizers such as erythrosine B, chlorophyll, and Na-chlorophyllin to photo-inactivate typical foodborne pathogens by incubating pathogens with photosensitizers under controlled light exposure (López-Carballo, Hernández-Muñoz, Gavara, & Ocio, 2008; Luksiene & Brovko, 2013; Tsai et al., 2011).

Riboflavin is known as a good photosensitizer for the formation of singlet oxygen and other reactive oxygen species (Choe & Min, 2006). Foods containing riboflavin, when exposed to light, can experience riboflavin mediated oxidation of unsaturated lipids, proteins, vitamins, phenolic compounds, and carotenoids, which ultimately leads to nutritional losses, the formation of undesirable flavors and colors, and the impairment of food quality and stability (Cardoso, Libardi, & Skibsted, 2012; Choe, Huang, & Min, 2005). Although widely recognized as a photosensitizer that can

initiate photo-oxidation in foods, the potential of riboflavin as a photosensitizer to photo-inactivate food borne pathogens has not been explored.

Studies have verified the high quantum yield of intersystem crossing of riboflavin. In the previous chapters, we have also demonstrated that riboflavin exhibits a relatively long triplet lifetime when immobilized in rigid matrices under room temperature. It is then reasonable to propose that riboflavin has the potential as an environmental friendly and consumer friendly photosensitizer for foodborne pathogen inactivation.

Phosphorescence provides direct information on excited triplet state properties of a molecule, including the interaction between triplet state molecules and ground triplet state oxygen molecules. Therefore, in this chapter, we first report the triplet state properties of riboflavin, in particular, its interaction with ground state oxygen, in various matrices by monitoring the difference in riboflavin phosphorescence in the presence and absence of oxygen. Then, we will discuss the singlet oxygen generation efficacy of riboflavin in comparison to two well-studied photosensitizers, rose bengal and erythrosine B, under various irradiation conditions.

Materials and Methods

PART I: Rate Constant of Oxygen Quenching

Sample Preparation: Three different matrices, amorphous dextran (6k Da, Sigma-Aldrich, St. Louis, MO, USA) films, 5% glycerol-dextran (6k Da), and methyl cellulose (25cP@2% in water, Mw~17,000g/mol, Sigma-Aldrich, St. Louis, MO, USA) were selected and tested to examine the interaction between triplet riboflavin and ground state oxygen. The riboflavin-dextran films were prepared following the same procedure as mentioned in the previous chapter: 200μM riboflavin solution was mixed with 30% wt dextran solution to reach a riboflavin/monomer sugar molar ratio of approximately $1:10^4$. Glycerol was added to the riboflavin-dextran solution to reach 10%wt glycerol in the final dry films. To prepare riboflavin-methylcellulose amorphous films, methylcellulose was first dissolved in ethanol and then mixed with riboflavin solution to reach a riboflavin/methylcellulose monomer ratio of approximately 1:1000.

An aliquot of 24μL mixed solution was spread onto a quartz slide (30mm long, 13.5mm wide, and 0.6mm thick) custom made by NSG Precision Cells (Farmingdale, NY, USA) to form amorphous films as described in previous chapters. Slides were first dried under room temperature air-flow supplied by a heat gun (Model 201A, Master Appliance Corp., Racine, WI, USA) for 15 min and then stored in a desiccator against DrieRite and P_2O_5 (Fisher Scientific, Fair Lawn, NJ, USA) for at least 72 hours to further reduce water content to ~0% RH before each phosphorescence measurement.

Phosphorescence intensity decays from riboflavin in the three different matrices were measured over the temperature range from -30 to 100˚C using a Cary Eclipse Fluorescence Spectrophotometer (Agilent Technologies, Santa Clara, CA, USA). A quartz slide covered with the amorphous film was placed in a 1cm×1cm×3cm cuvette (Firefly Sci, Brooklyn, NY, USA) and positioned with front face geometry for phosphorescence intensity decay measurements. Phosphorescence decays were collected in the absence and presence of oxygen.

Data Analysis: Phosphorescence decays of riboflavin in the three films were collected at 620nm (excited at 440nm). Both the excitation and emission slits were set to 20nm to maximize the intensity. The delay time and gate time were set to 0.2ms and 5ms, respectively. The phosphorescence decay at each temperature was collected as an average of 50 cycles. The phosphorescence decays were fitted using a multi-exponential function (VI-1). The goodness of the fit was judged by the distribution of modified residuals ($^{(data - fit)}/_{data^{1/2}}$) and judged appropriate if the residuals varied randomly about zero. The phosphorescence lifetime was calculated from the population average (VI-2) and used to compare the phosphorescence decays of riboflavin in the absence and presence of oxygen to monitor the oxygen quenching property of riboflavin.

	$I(t) = I(0) * \sum_{i=1}^{n} \alpha_i \exp\left(-\frac{t}{\tau_i}\right)$	(VI-1)

	$\tau_m = \sum_i^n \alpha_i \tau_i$	(VI-2)

The inverse of the phosphorescence lifetime is the rate constant of triplet de-excitation, which is determined by all possible de-excitation pathways (VI-3). At the same temperature, the rate of reverse intersystem crossing and non-radiative decay remain constant and the rate of radiative decay as an intrinsic parameter is independent of environmental factors, therefore the rate constant of oxygen quenching, can thus be calculated using phosphorescence spectroscopy by subtracting k_P in oxygen from k_P in nitrogen.

	$\frac{1}{\tau} = k_P = k_{RP} + k_{TS1} + k_{TS0} + k_Q[O_2]$	(VI-3)

PART II: Quantification of Singlet Oxygen Photosensitized by Riboflavin

Sample Preparation: The singlet oxygen generation efficacy of riboflavin under different irradiation conditions was assessed using a commercially available, water-soluble singlet oxygen sensor, the Singlet Oxygen Sensor Green (SOSG) (Life Technologies, Eugene, OR, USA) and the method was modified from a procedure previously reported by Lin *et al* (2013).

We prepared a 0.25M pH 7.5 phosphate buffer solution (PBS) with monobasic and dibasic potassium phosphate (Sigma-Aldrich, St. Louis, MO, USA). Three photosensitizers were examined in this study: rose bengal, erythrosine B, and riboflavin. Rose bengal was chosen as a reference since it has been widely used as a singlet oxygen generation agent and has a high singlet oxygen quantum yield (0.76); erythrosine B is a Generally Recognized As Safe (GRAS) synthetic dye that has been reported to generate $^1O_2$ under irradiation; riboflavin has a reported $^1O_2$ quantum yield of 0.54. Stock solutions of photosensitizers were prepared with deionized water and further diluted with PBS into solutions ranging from 1μM to 20μM.

The reagent SOSG was used without further purification. This reagent is only weakly fluorescent in its native state, while upon reaction with singlet oxygen, the internal electron transfer is precluded, and fluorescence emission with a peak located at 525nm can be observed. To prepare a ~5mM SOSG stock solution, the contents in one 100μg vial was dissolved in 33μL methanol. The 5mM stock solution was further diluted with deionized water into 1.65mL 100μM SOSG solution. The SOSG solutions were prepared immediately before measurement to avoid degradation of

the reagent. All preparation procedures were carefully conducted under minimal light exposure and samples were stored in the dark before measurements.

Preliminary Zero-Order Reaction Test: A preliminary test was conducted using rose bengal (Acros Organics, New Jersey, USA), a known photosensitizer, to determine the minimal SOSG concentration that allows for zero-order reaction rate. At a fixed rose bengal concentration, the reaction rate of SOSG with $^1O_2$ can be expressed by:

	$r = {}^{d[SOSG-EP]}/_{dt} = k[SOSG]^n[1O2]$	(VI-4)

In which d[SOSG-EP] is the concentration of the complex formed between SOSG and $^1O_2$ that can be measured by the fluorescence emission at 525nm, [SOSG] and [$^1O_2$] are the concentration of SOSG and $^1O_2$, respectively. In the equation, n is the order of reaction with respect to the concentration of SOSG. Only when n equals 0, is the reaction rate only dependent upon [$^1O_2$] and we can use the reaction rate to estimate the [$^1O_2$] generated by photosensitization (Lin et al., 2013). To establish a minimal SOSG concentration for zero-order reaction to use in future study, we monitored the reaction rate between $^1O_2$photosensitized from 1μM rose bengal under 365nm irradiation and SOSG of various concentrations (0.5, 1, 2, 4, 6, 8. 10μM).

Singlet Oxygen Generation Efficacy under Different Irradiation Sources Measured by SOSG: In the preliminary test, it was found that a minimal of 4μM SOSG in the final mixture was required to achieve the zero-order reaction rate between $^1O_2$ photosensitized from 1μM rose bengal and SOSG and this concentration was used in

the following study to measure the $^1O_2$ generation efficacy of various photosensitizers under different irradiation conditions. Absorption spectra of three selected photosensitizers, rose bengal, erythrosine B, and riboflavin were collected using a Cary 60 UV-Vis (Agilent Technologies, Santa Clara, CA, USA). Photosensitizer stock solutions were diluted to 2μM with PBS and stored in the dark at 4˚C before they were used. For each set of tests, three samples, a) photosensitizer and SOSG mixture, b) only SOSG (control 1), and c) only photosensitizer (control 2), were prepared and subjected to irradiation and fluorescence measurement. For the photosensitizer and SOSG mixture, 1.5mL of 2μM photosensitizer solution and 1.5mL of 8μM SOSG solution were mixed in a quartz cuvette (NSG Precision Cells, Farmingdale, NY, USA) to reach a final concentration of 1μM photosensitizer and 4μM SOSG in the solution. SOSG and photosensitizer controls were prepared by mixing 1.5mL 8μM SOSG with 1.5mL PBS and mixing 1.5mL 2μM photosensitizer with 1.5mL deionized water, respectively.

Four irradiation wavelengths were tested in this study. A UV lamp (Spectronics Corporation, Westbury, New York, USA) was used to supply irradiation at 365nm. In addition, a circuit board and a power supply (Arksen DC Power Supply, Model 305D, China) were attached to an array of 6 light emitting diodes (LEDs) (SuperBrightLEDs, St. Louis, MO, USA) to expand the irradiation conditions. The wavelengths of the LEDs were 400, 470, and 524nm.

To photogenerate $^1O_2$, one set of the three samples mentioned above were lined up in front of the irradiation source in a holder on a stirring plate. Each solution was

vigorously stirred throughout the whole irradiation process to ensure a homogenous irradiation treatment and to incorporate as much oxygen into the solution was possible. A Cary Eclipse Fluorescence Spectrophotometer (Agilent Technologies, Santa Clara, CA, USA) was used to monitor the fluorescence emission intensity at 525nm,the characteristic emission wavelength of oxidized SOSG. During fluorescence testing the excitation wavelength was set at 500nm for all samples and the spectra were collected from 515-700nm. Both excitation and emission slits were set at 5nm. Fluorescence measurements were conducted before the irradiation and at 5min intervals during a 30min irradiation process at each selected wavelength, i.e. 365, 400, 470, and 524nm. To analyze the data, fluorescence emission spectra of all samples were plotted using Microsoft Excel (Microsoft Corp., Seattle, WA, USA). The maximum emission intensity at ~525nm was plotted as a function of irradiation time and the slope was used as a measure to compare the $^1O_2$ generation efficacy of the three photosensitizers under different irradiation sources.

Results and Discussions

PART I: Rate Constant of Oxygen Quenching

The phosphorescence decays from riboflavin dispersed in amorphous 6k Da dextran films, 5% glycerol-dextran films, and methylcellulose films were collected in the absence and presence of oxygen over the temperature range from -30 to 80 °C. Figure VI-1-Figure VI-3 are plots showing the phosphorescence decays in different matrices collected at 20 °C with and without oxygen. As shown, there was little difference in phosphorescence decays from riboflavin in both 6,000 dextran films and the dextran films with 5% glycerol content in the absence and presence of oxygen. However, the phosphorescence decays varied dramatically in the amorphous methylcellulose films, where the phosphorescence decay in the presence of oxygen was much faster than the one in the absence of oxygen. To better capture the effect of oxygen and to quantify the oxygen quenching rate, a multi-exponential function was used to characterize the phosphorescence decays and to calculate the average lifetime. Examples of the decays with their corresponding fit and modified residuals are presented in Figure VI-4-Figure VI-6. All modified residuals varied randomly about 0, suggesting that multi-exponential function used here can sufficiently and satisfactorily characterize the decays.

The average phosphorescence lifetimes were calculated from the population average using (VI-2 and the results are shown against temperature in Figure VI-4-Figure VI-6. No significant difference can be observed from riboflavin phosphorescence lifetimes measured with and without oxygen when riboflavin was

dispersed in both 6k Da dextran films and 5% glycerol-dextran films. In contrast, there is a noticeable difference throughout the whole temperature range when the methylcellulose matrix was used. This suggests that the oxygen permeability varies drastically among the three matrices studied here: the oxygen permeability is extremely low in both 6k Da dextran and 5% glycerol-dextran films but relatively high in the methylcellulose films. The addition of 5% glycerol to the dextran film did not increase the oxygen permeability as the glycerol acts as an anti-plasticizer as demonstrated in the previous chapter. Although the addition of glycerol may have slightly increased the oxygen solubility in the matrix, glycerol as an anti-plasticizer increasing the overall molecular mobility and filling up free volume in the dextran matrix is likely to counteract the increase in oxygen solubility by decreasing the oxygen diffusion rate.

According to (VI-3), the difference between the lifetimes measured under nitrogen or oxygen atmosphere is reflected in the value of $k_Q[O_2]$. The value of the oxygen quenching rate $k_Q[O_2]$ is determined by both the efficacy of triplet riboflavin interacting with molecular oxygen and by the concentration of molecular oxygen in the vicinity of triplet riboflavin. The former is an intrinsic property of riboflavin and the latter is determined by the oxygen permeability of the matrix. The calculated oxygen quenching rate, $k_Q[O_2]$, for riboflavin in methylcellulose films as a function of temperature is presented in Figure VI-7. As indicated in the figure, the oxygen quenching rate increased as the temperature increased, which reflects an increase in oxygen permeability caused by increased molecular mobility and thus increased oxygen diffusion rate at elevated temperatures. Miller & Krochta (1997) have shown

that methylcellulose is only a moderate oxygen barrier when used as a packaging material and the reported oxygen permeability was 97 $cm^3 \mu m/m^2 dkPa$, which explains the difference in phosphorescence lifetime of riboflavin dispersed in methylcellulose measured under nitrogen and oxygen-rich environments. The relative large values of oxygen quenching rate of riboflavin in methylcellulose films not only reflected the oxygen permeability of the films, but also indicated that triplet riboflavin can be effectively quenched by ground state oxygen, thus, becoming a potential photosensitizer for singlet oxygen generation.

Figure VI-1

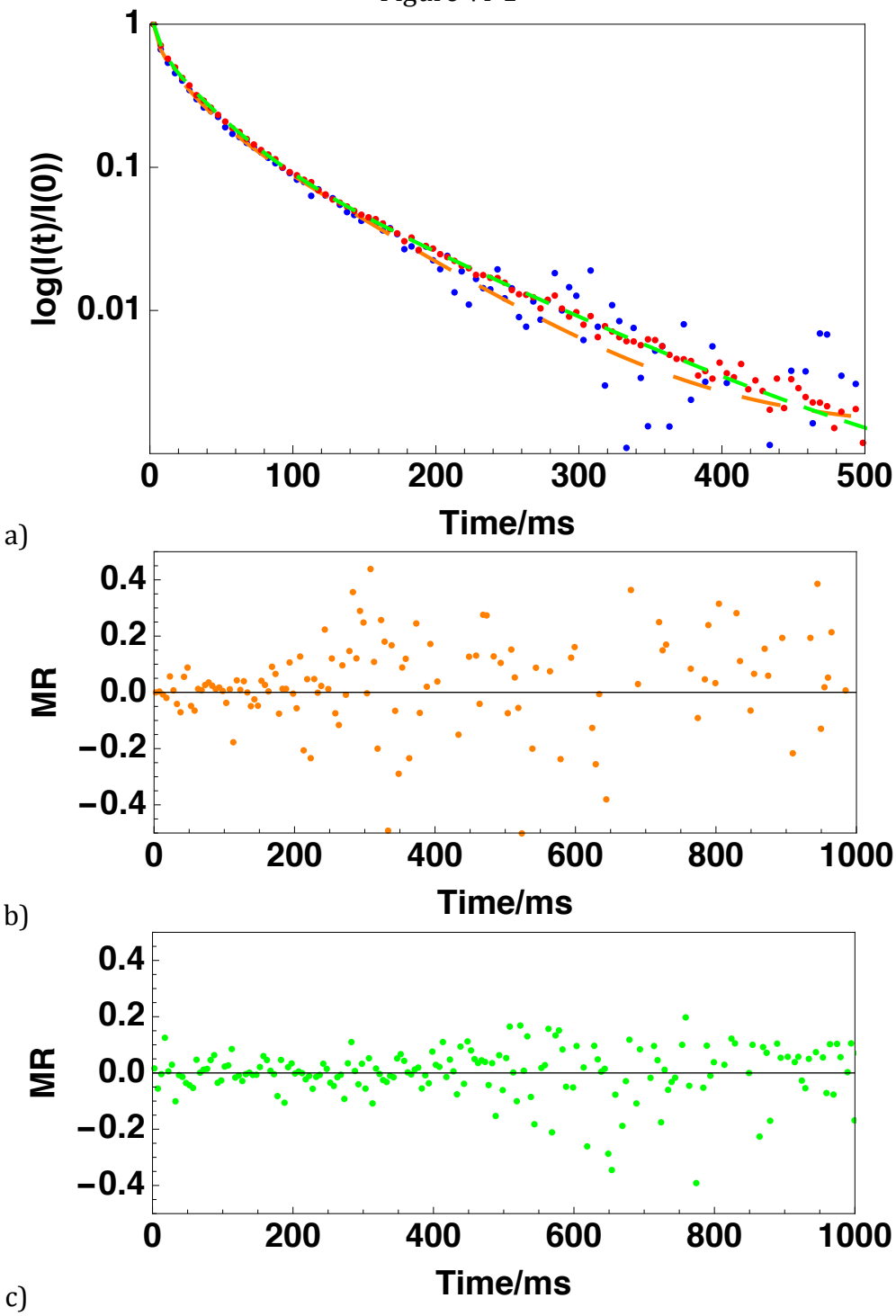

Figure VI-1: a) Phosphorescence decays of riboflavin dispersed in amorphous 6,000 dextran films in the absence (blue circles) and presence (red circles) of oxygen fitted using a three-exponential function in the absence (orange dashed line) and presence of oxygen (green dashed line), respectively. b & c) Modified residuals ((data-fit)/data$^{1/2}$) for each fit.

Figure VI-2

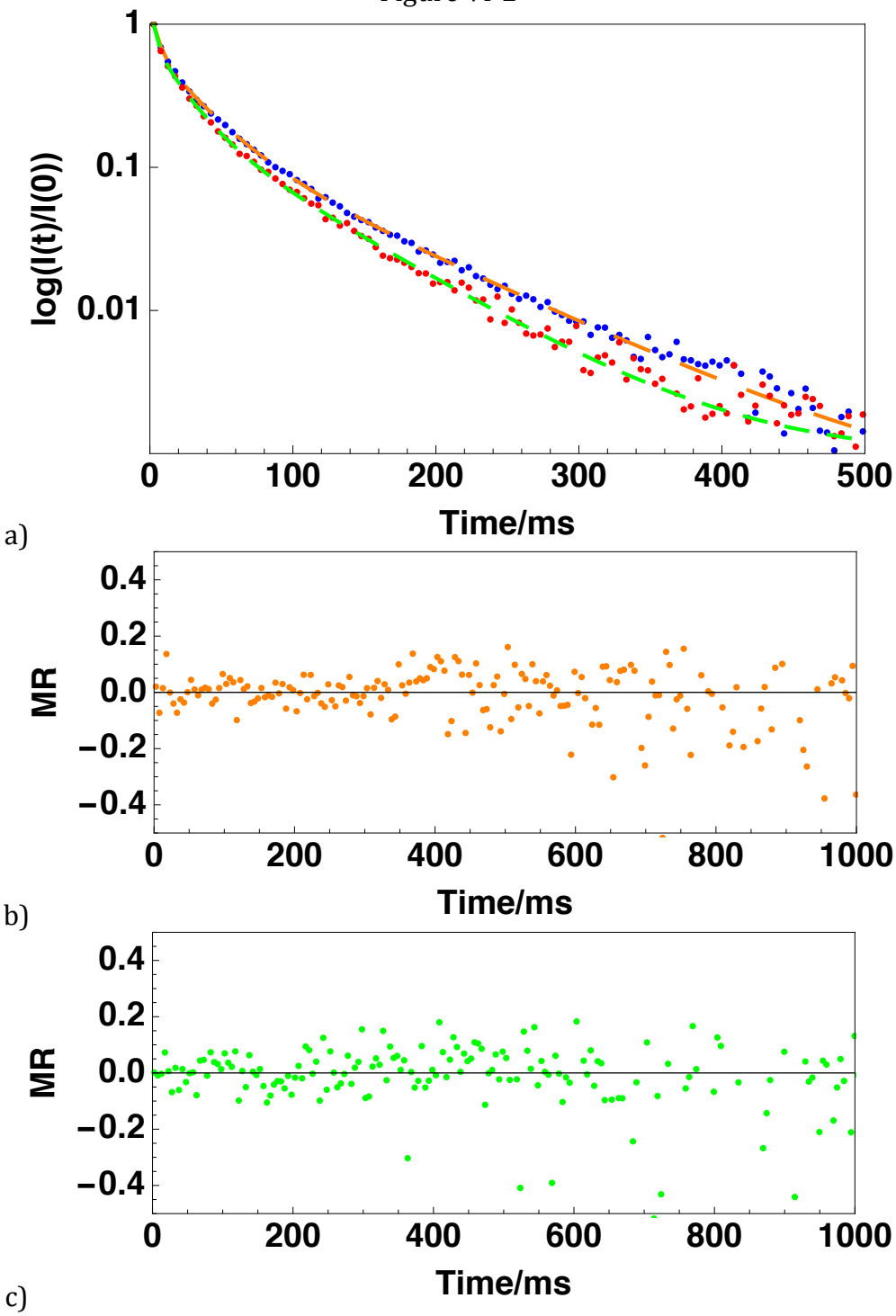

Figure VI-2: a) Phosphorescence decays of riboflavin dispersed in amorphous% glycerol-dextran films in the absence (blue circles) and presence (red circles) of oxygen fitted using a three-exponential function in the absence (orange dashed line) and presence of oxygen (green dashed line), respectively. b & c) Modified residuals ((data-fit)/data$^{1/2}$) for each fit.

Figure VI-3

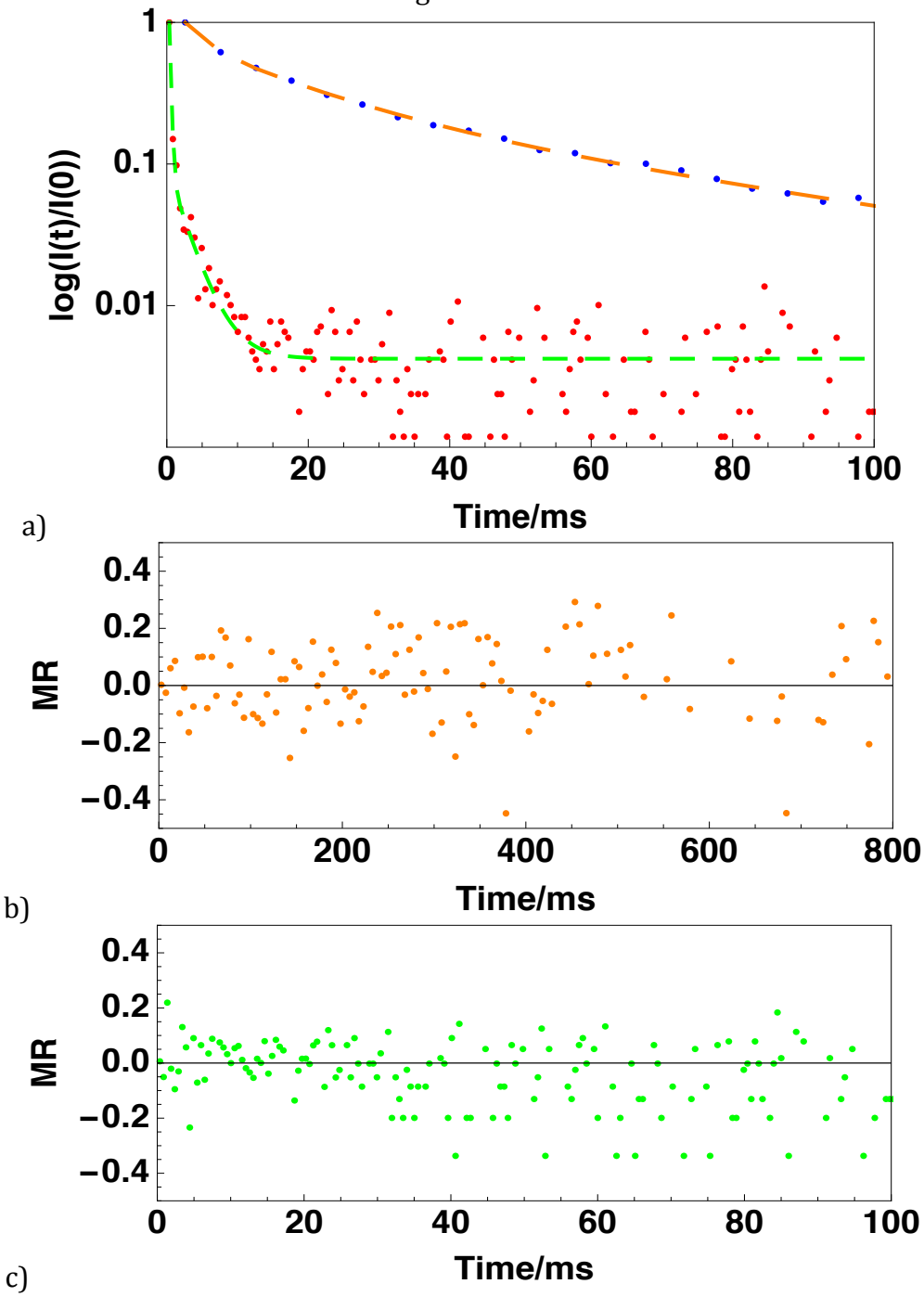

Figure VI-3: a) Phosphorescence decays of riboflavin dispersed in amorphous methylcellulose films in the absence (blue circles) and presence (red circles) of oxygen fitted using a three-exponential function in the absence (orange dashed line) and presence of oxygen (green dashed line), respectively. b & c) Modified residuals ((data-fit)/data$^{1/2}$) for each fit.

Figure VI-4

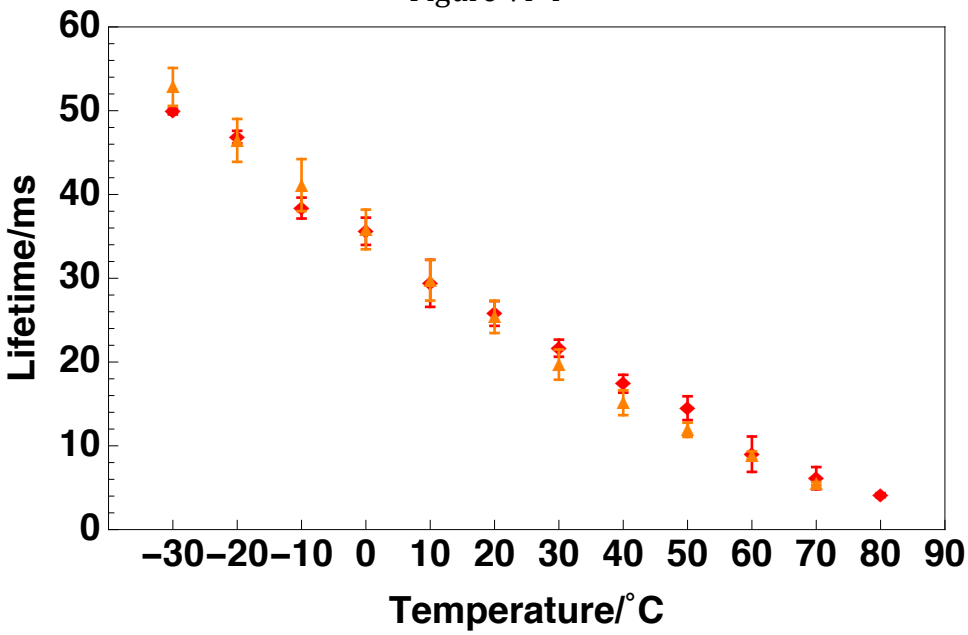

Figure VI-4: Calculated average riboflavin phosphorescence lifetime in 6,000 dextran films in the absence (red diamonds) and presence (orange triangles) of oxygen as a function of temperature.

Figure VI-5

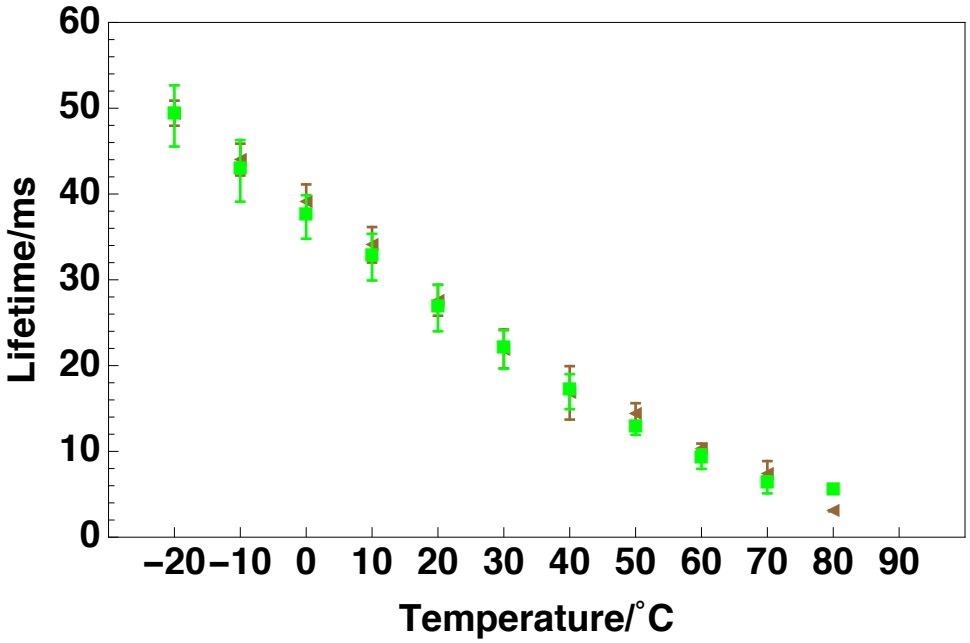

Figure VI-5: Calculated average riboflavin phosphorescence lifetime in 6,000 dextran films with 5% glycerol content in the absence (brown left triangles) and presence (green squares) of oxygen as a function of temperature.

Figure VI-6

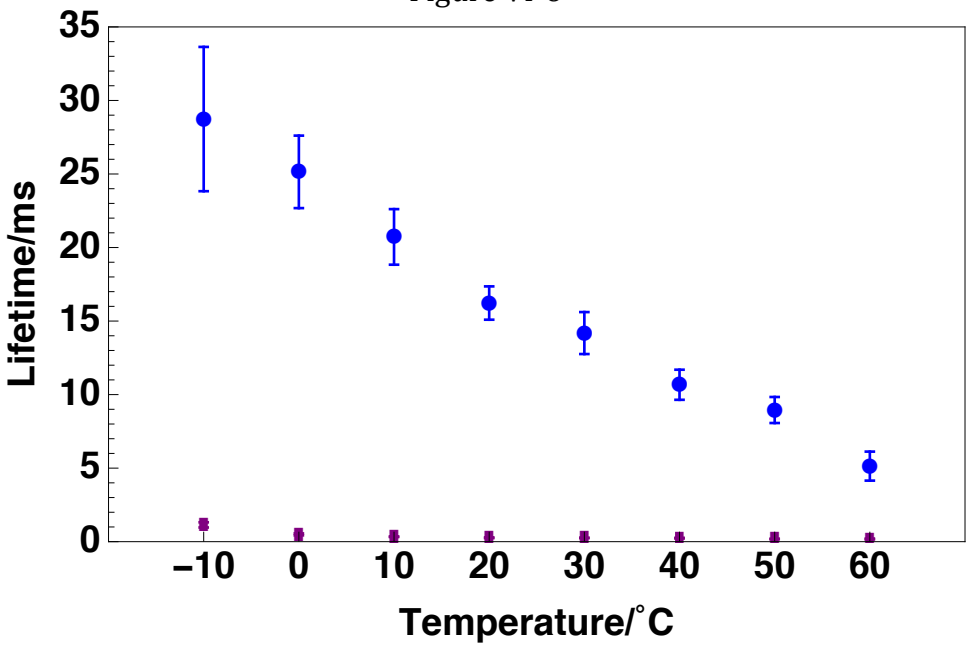

Figure VI-6: Calculated average riboflavin phosphorescence lifetime in methylcellulose films in the absence (blue circles) and presence (purple squares) of oxygen as a function of temperature.

Figure VI-7

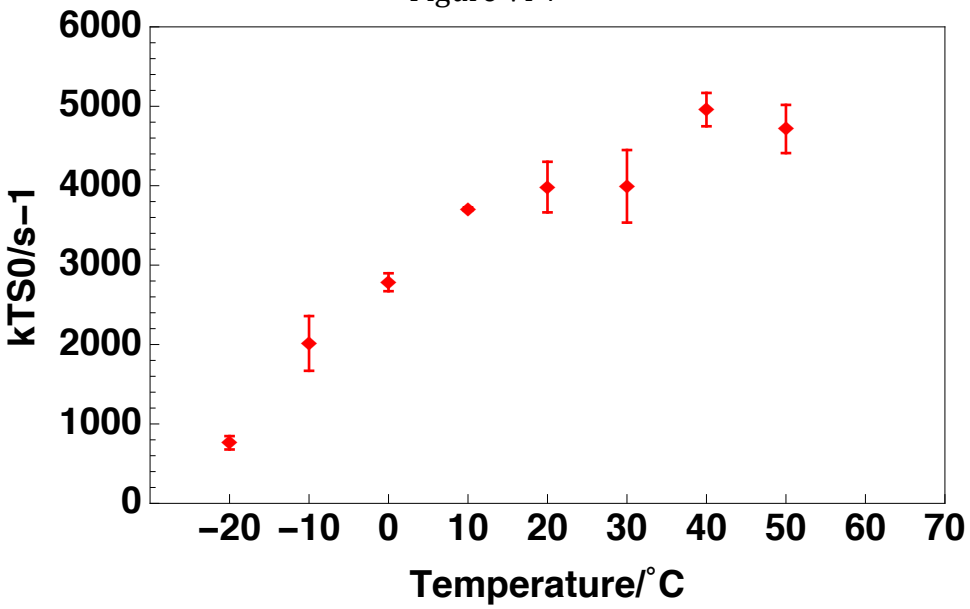

Figure VI-7: Temperature dependence of oxygen quenching rate $k_Q[O_2]$ for riboflavin in amorphous methylcellulose films.

PART II: Singlet Oxygen Generation Measured by SOSG

Zero-Order Reaction Rate Determination: A preliminary study of the minimum SOSG concentration to reach the zero-order reaction rate between SOSG and photogenerated singlet oxygen was conducted between SOSG and rose bengal, a known photosensitizer. SOSG concentrations were varied from 0.5, 1, 2, 4, 6, 8, and 10μM for this study. Figure VI-8 presents the fluorescence emission spectra of SOSG alone (control 1), rose bengal alone (control 2), and the mixture of SOSG and rose bengal when excited at 505nm. As shown, both the mixture and the SOSG control samples exhibit a strong fluorescence emission peak located at 525nm from the oxidized SOSG even before photoirradiation or in the absence of rose bengal in the case of SOSG control. This phenomenon has been previously reported in other studies. They have observed weak fluorescence emission from SOSG in the absence of photosensitizer that is attributed to SOSG's ability to produce singlet oxygen under exposure to UV and visible light (Lin et al., 2013; Ragàs, Jiménez-Banzo, Sánchez-García, Batllori, & Nonell, 2009). Rose bengal exhibits a fluorescence emission maximum at 560nm while its emission at 525nm is negligible compared to that from oxidized SOSG.

To obtain the SOSG concentration that reaches the zero-order reaction rate, we subjected each set of three samples: two controls and a mixture, to photoirradiation at 365nm for 30min and the fluorescence emission spectra of three samples were collected at 5min intervals. Figure VI-9 shows typical fluorescence emission spectra of a mixture of 1μM rose bengal and 4μM SOSG changes after different irradiation

times. The fluorescence intensity at 525nm keeps increasing with the time, reflecting the interaction between SOSG and photosensitized singlet oxygen from rose bengal and the formation of fluorescent oxidized SOSG. Therefore, the changes in maximum intensity with time were used portrait the reaction kinetics between SOSG of various concentrations and 1μM rose bengal under 365nm irradiation condition. Fluorescence emission spectra from SOSG and rose bengal controls were also measured during the irradiation process and the maximum intensity as a function of irradiation time are plotted in Figure VI-10. Although previous research has reported the self-photosensitization ability of SOSG (Ragàs et al., 2009), the increase in the maximum intensity from SOSG control is negligible compared to the increase in the mixture.

By fixing the rose bengal concentration at 1μM and varying the SOSG concentration from 0.5 to 10μM, we determined the critical SOSG concentration at which a zero-order reaction rate was obtained. As shown in Figure VI-11 the measured maximum fluorescence intensity increases linearly with time over the irradiation time 30min in all SOSG concentrations tested. When SOSG concentration was 8μM and 10μM, there is a slight decrease in the first 5 min irradiation: this may be caused by the inner filter effect due to the high concentration of fluorophores (SOSG and RB) in solution. To quantify the reaction rate between SOSG and singlet oxygen, the slopes of the linear curves were calculated (see Figure VI-12). The reaction rate first increases with the increase of SOSG concentration, but a plateau is reached when SOSG concentration is equal to or above 4μM. Moreover, there is a decrease in the reaction rate as the SOSG concentration further increases to 10μM, possibly caused

by inner filter effect. Based on this experiment, we concluded that when the SOSG concentration is equal to or above 4μM, zero order reaction can be reached and the reaction rate is solely dependent on the concentration of singlet oxygen. Additionally, rose bengal is known for having a high singlet oxygen quantum yield. Therefore, this concentration of 4μM was considered sufficient to capture the singlet oxygen generated by riboflavin and erythrosine b, both of which have lower singlet oxygen quantum yield than rose bengal, and was also selected for the following study.

Singlet Oxygen Generation Efficacy of Three Photosensitizers under Various Irradiation Conditions: In the previous section, it was found that 4μM SOSG was sufficient to achieve zero order reaction rate when mixed with 1μM rose bengal, a known photosensitizer with a high singlet oxygen quantum yield of 0.76, so in the following experiments, 4μM SOSG was used to assess the singlet oxygen generation efficacy of three selected photosensitizers, rose bengal, erythrosine B, and riboflavin, under different irradiation conditions. Four irradiation wavelengths were tested: 365, 400, 470, and 524nm, to study the optimal irradiation conditions for singlet oxygen generation by riboflavin. The irradiation wavelengths were selected based on the absorption spectra of the three targeted photosensitizers as shown in Figure VI-13 and on the commercially availability of LEDs. Riboflavin exhibits wide absorption peaks from 350 and 470nm. Both rose bengal and erythrosine B exhibit sharp absorption peaks located around 510-550nm. Therefore, the selected irradiation wavelengths covered the range of intense absorption band of three photosensitizers.

The fluorescence emission intensity from photosensitizer and SOSG mixtures increased as the irradiation time increased (Figure VI-14). Again, the fluorescence maximum intensity was determined from each measured spectrum and used as a proxy for singlet oxygen concentration. The fluorescence emission peak intensity was normalized towards the reading of fluorescence maximum before irradiation. Figure VI-15 summarizes the singlet oxygen generation kinetics from three photosensitizers under different irradiation conditions. The singlet oxygen concentration increases in a linear manner with irradiation time. The slope of the linear curve can be used as a quantifiable indicator to compare the singlet oxygen generation efficacy between different photosensitizers and under different irradiation conditions. As shown, rose bengal exhibit the largest increase in fluorescence intensity when irradiated at the 524nm, followed by 470nm, 365nm, and 400nm, which is supported by its absorption spectra that has an absorption maxima at 550nm. Riboflavin generated the most singlet oxygen when irradiated by 400 and 470nm LEDs. When 524nm LEDs were used as the light source, no fluorescence intensity increase was observed, suggesting that 524nm, in comparison to the other three irradiation wavelengths, does not facilitate singlet oxygen generation from riboflavin. Erythrosine B generated the most singlet oxygen under 524nm irradiation, which is in consistent with its absorption peak at 520nm. The slopes of the linear relationships between fluorescence maximum intensity and time were calculated and summarized in Table VI-1. Based on the singlet oxygen generation rate monitored by the fluorescence intensity increase from oxidized SOSG, we concluded that 400 and 470nm are the optimal irradiation wavelengths

for riboflavin to generate singlet oxygen. In comparison, rose bengal and erythrosine B generated the most singlet oxygen when irradiated with 470 and 524nm light sources.

Figure VI-8

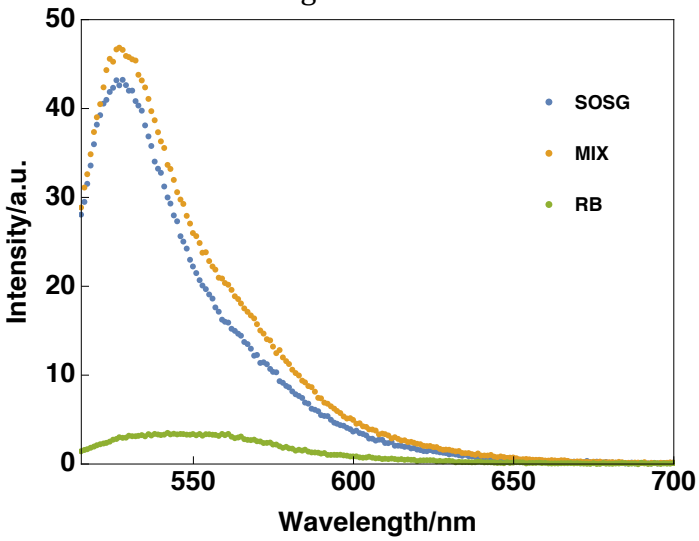

Figure VI-8: Fluorescence emission spectra of 4μM SOSG control (blue), 1μM rose bengal control (green), and a mixture of 4μM SOSG and rose bengal (yellow) before irradiation.

Figure VI-9

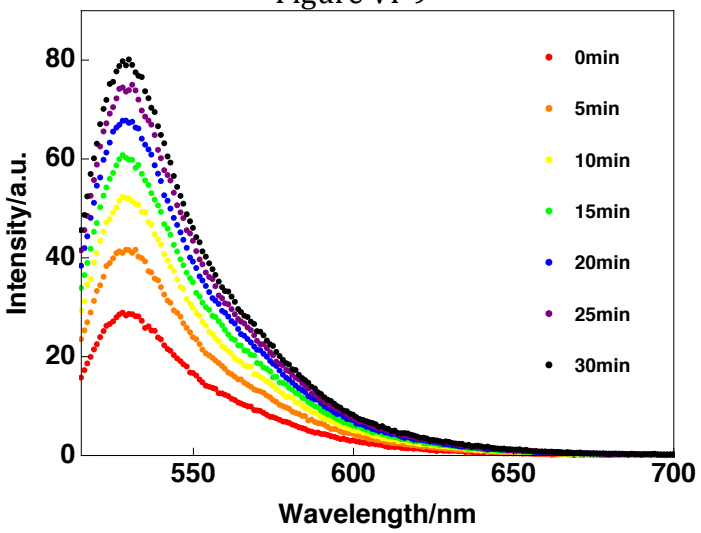

Figure VI-9: Fluorescence emission spectra of 1μM rose bengal mixed with 4μM SOSG excited at 505nm. The samples were irradiated with a 365nm light source during a total period of 30min and fluorescence intensity was measured at the beginning of the irradiation period and at 5min intervals.

Figure VI-10

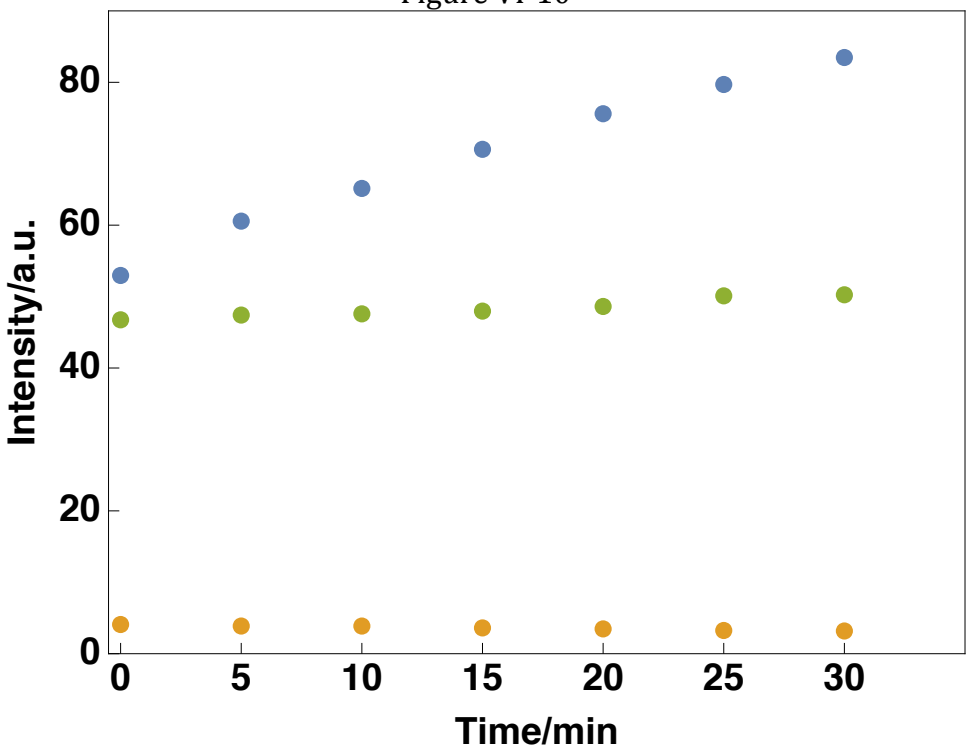

Figure VI-10: Fluorescence maximum intensity of 4μM SOSG control (green), 1μM rose bengal control (yellow), and a mixture of 1μM rose bengal and 4μM SOSG (blue) as a function of time

Figure VI-11

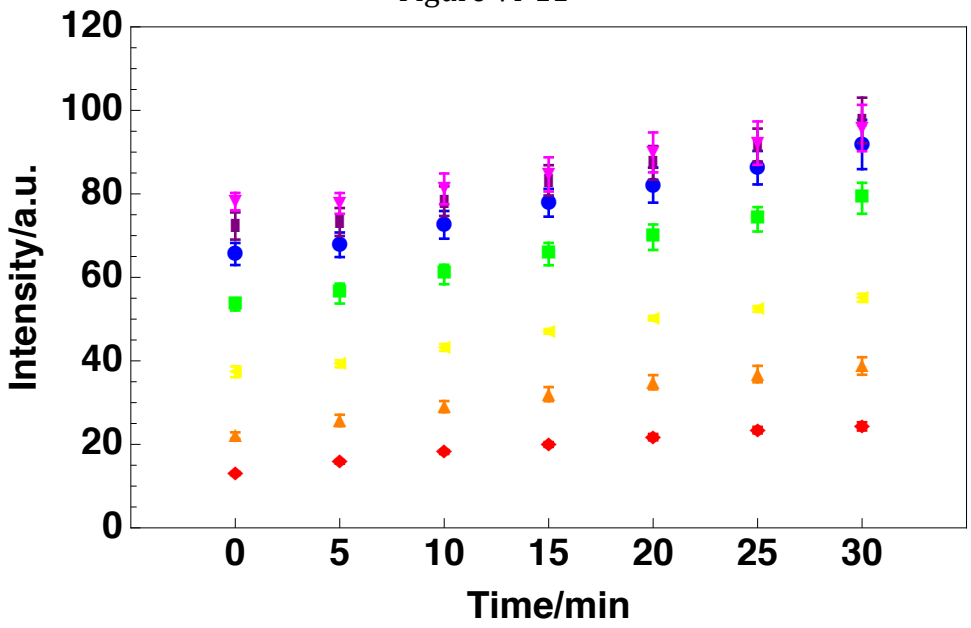

Figure VI-11: Reaction kinetics of singlet oxygen generated by 1μM rose bengal under 365nm irradiation monitored by the fluorescence intensity increase at 525nm. SOSG was used at various concentrations (red, 0.5μM; orange, 1μM; yellow, 2μM, green, 4μM; blue, 6μM; purple, 8μM; and magenta, 10μM).

Figure VI-12

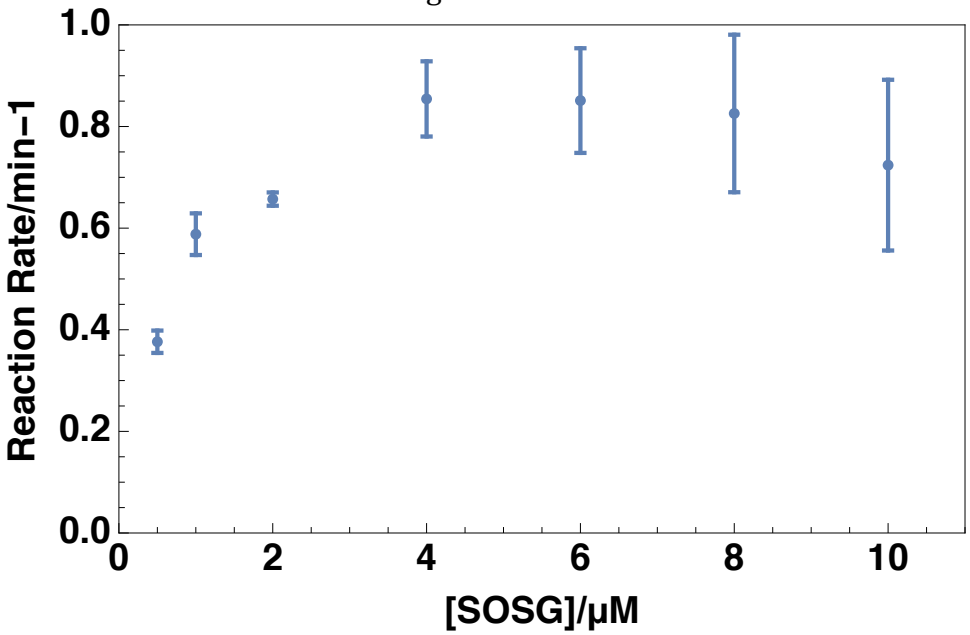

Figure VI-12: Reaction rates plotted against SOSG concentration.

Figure VI-13:

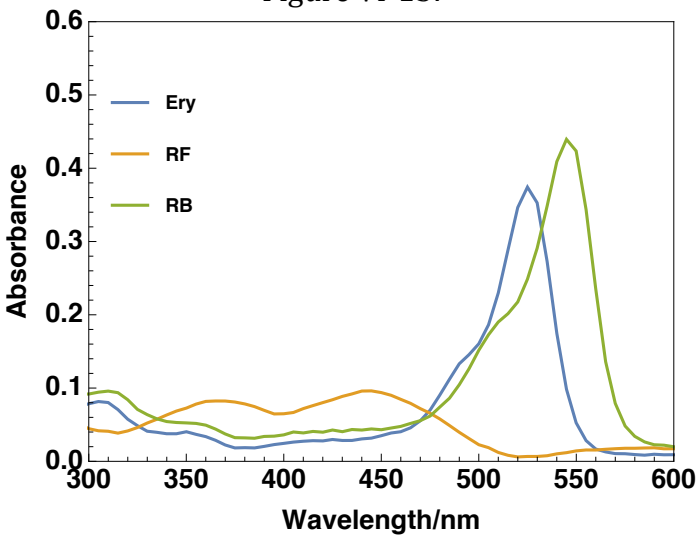

Figure VI-13: Absorption spectra of three photosensitizers: rose bengal (green), riboflavin (yellow), erythrosine B (blue).

Figure VI-14

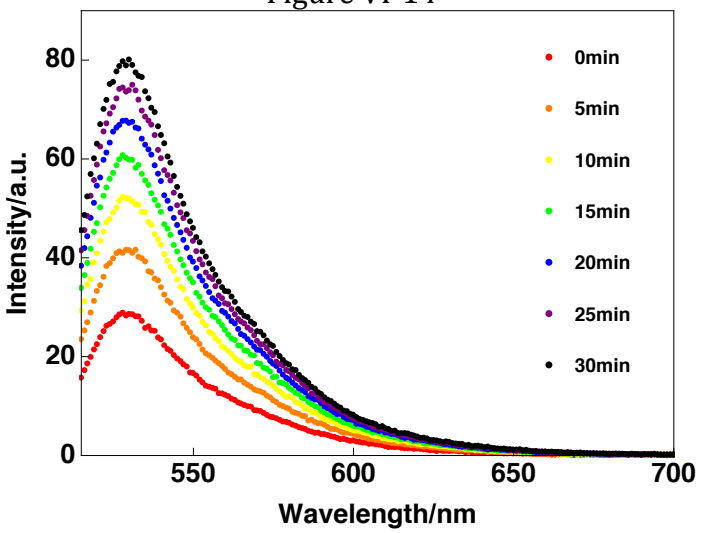

Figure VI-14: Fluorescence emission spectra of 1μM riboflavin mixed with 4μM SOSG excited at 505nm. The samples were irradiated with a 365nm light source during a total period of 30min and fluorescence intensity was measured at the beginning of the irradiation period and at 5min intervals.

Figure VI-15

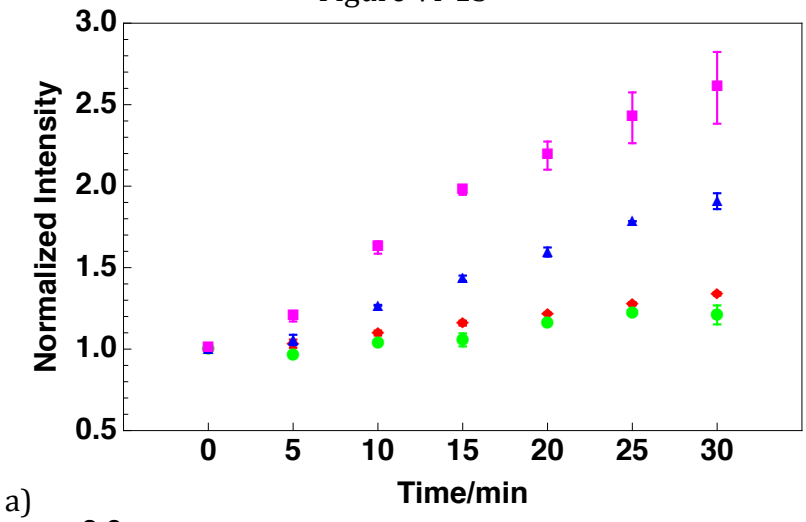

a)

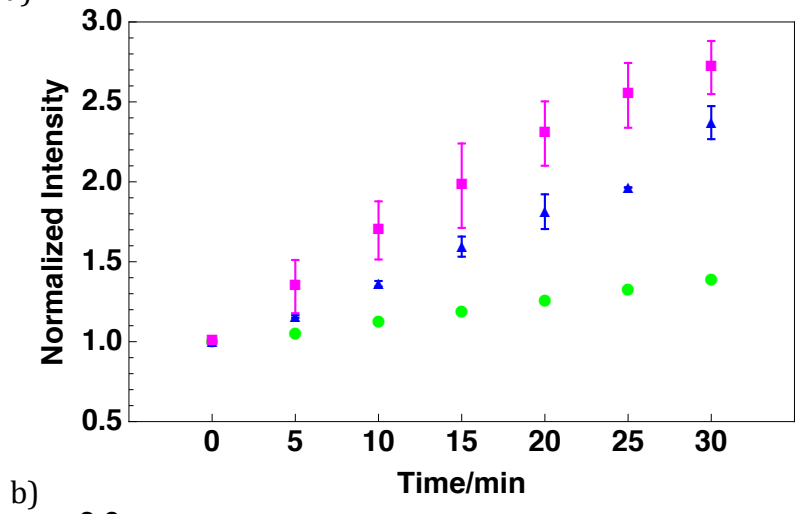

b)

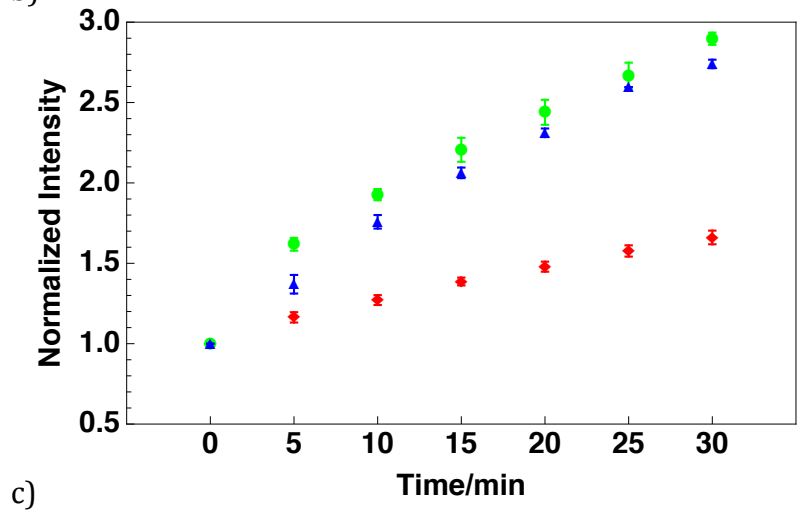

c)

Figure VI-15: Singlet oxygen generation kinetics of three photosensitizers: rose bengal (a), riboflavin (b), and erythrosine B (c) under various irradiation conditions: 365nm (red diamonds), 400nm (green circles), 470nm (blue triangles), and 524nm (magenta squares)

Table VI-1: Singlet oxygen generation rate of three photosensitizers: rose bengal, riboflavin, and erythrosine B, under four irradiation conditions: 365nm, 400nm, 470nm, and 524nm.

Reaction Rate/ min^{-1}				
Photosensitizer	365nm	400nm	470nm	524nm
Rose Bengal	0.012	0.009	0.032	0.056
Riboflavin	0.022	0.059	0.059	\
Erythrosine B	\	0.013	0.044	0.058

Conclusion

In this chapter, we aimed to examine the potential of riboflavin as a photosensitizer. We first investigated the oxygen quenching rate of riboflavin using three different amorphous carbohydrate matrices using the phosphorescence lifetime from riboflavin as an indicator. The results showed that riboflavin phosphorescence lifetime exhibited no significant difference in the absence and presence of oxygen in both 6,000 dextran amorphous films and 6,000 dextran films with 5% glycerol content, which suggests that the oxygen permeability is extremely low in both matrices. On the contrary, methylcellulose exhibited low oxygen permeability and allowed us to calculate the oxygen quenching rate of riboflavin, which 800 to 5000s-1 over the temperature range from -10 to 50°C. This is good evidence that riboflavin can effectively be quenched by oxygen.

To further study its efficacy as a photosensitizer, in this study, we used a commercially available singlet oxygen sensor, SOSG, and compared the singlet oxygen generation efficacy of riboflavin to two known photosensitizers, rose bengal and erythrosine B, under various irradiation conditions. Our results indicate that the singlet oxygen generation rate from riboflavin is the highest when the light source wavelength was 400 and 470nm and by comparing its singlet oxygen generation rate to that of rose bengal and erythrosine B, it was concluded that riboflavin exhibited excellent singlet oxygen generation ability and has potential as a GRAS photosensitizer to inactivate foodborne pathogens. However, more experiments are needed to further study its advantages and limitations as a photosensitizer.

References

Alotaibi, M. A., & Heaselgrave, W. (2011). Solar disinfection of water for inactivation of enteric viruses and its enhancement by riboflavin. *Food and Environmental Virology, 3*(2), 70-73. doi:10.1007/s12560-011-9058-5

Cardoso, D. R., Libardi, S. H., & Skibsted, L. H. (2012). *Riboflavin as a photosensitizer. effects on human health and food quality*

Choe, E., Huang, R., & Min, D. (2005). Chemical reactions and stability of riboflavin in foods. *Journal of Food Science, 70*(1), R28-R36.

Choe, E., & Min, D. (2006). Chemistry and reactions of reactive oxygen species in foods. *Critical Reviews in Food Science & Nutrition, 46*(1), 1.

DeRosa, M. C., & Crutchley, R. J. (2002). Photosensitized singlet oxygen and its applications. *Coordination Chemistry Reviews, 233/234*(2), 351.

Kashiwabuchi, R. T., Carvalho, F. R. S., Khan, Y. A., Hirai, F., Campos, M. S., & McDonnell, P. J. (2013). Assessment of fungal viability after long-wave ultraviolet light irradiation combined with riboflavin administration. *Graefes Archive for Clinical and Experimental Ophthalmology, 251*(2), 521-527. doi:10.1007/s00417-012-2209-z

Lang, A. (2008). In Lang A. (Ed.), *Dyes and pigments: New research* (1st ed.). New York: Nova Science Publishers, Inc.

Lin, H. Y., Shen, Y., Chen, D. F., Lin, L. S., Wilson, B. C., Li, B. H., & Xie, S. S. (2013). *Feasibility study on quantitative measurements of singlet oxygen generation using singlet oxygen sensor green*

López-Carballo, G., Hernández-Muñoz, P., Gavara, R., & Ocio, M. J. (2008). Photoactivated chlorophyllin-based gelatin films and coatings to prevent microbial contamination of food products. *International Journal of Food Microbiology, 126*(1–2), 65-70. doi:http://dx.doi.org/10.1016/j.ijfoodmicro.2008.05.002

Luksiene, Z., & Brovko, L. (2013). Antibacterial photosensitization-based treatment for food safety. *Food Engineering Reviews, 5*(4), 185-199. doi:10.1007/s12393-013-9070-7

Miller, K. S., & Krochta, J. M. (1997). Oxygen and aroma barrier properties of edible films: A review. *Trends in Food Science & Technology, 8*(7), 228-237. doi:http://dx.doi.org/10.1016/S0924-2244(97)01051-0

Ragàs, X., Jiménez-Banzo, A., Sánchez-García, D., Batllori, X., & Nonell, S. (2009). Singlet oxygen photosensitisation by the fluorescent probe singlet oxygen sensor

green. *Chemical Communications (Cambridge, England),* (20), 2920-2922. doi:10.1039/b822776d

Tsai, T., Chien, H., Wang, T., Huang, C., Ker, Y., & Chen, C. (2011). Chitosan augments photodynamic inactivation of gram-positive and gram-negative bacteria. *Antimicrobial Agents and Chemotherapy, 55*(5), 1883-1890. doi:10.1128/AAC.00550-10

Wainwright, M. (2009). *Photosensitizers in biomedicine* (1st ed.). Oxford ; Hoboken, N.J: Wiley-Blackwell.